This is to certify that the

dissertation entitled

MEASUREMENT OF ELECTROMAGNETIC
PROPERTIES OF MATERIALS VIA
COAXIAL PROBE SYSTEMS

presented by

Ching-Lieh Li

has been accepted towards fulfillment
of the requirements for

Ph.D. degree in Electrical Engineering

Major professor

Date 3/9/93

MEASUREMENT OF ELECTROMAGNETIC PROPERTIES OF MATERIALS VIA COAXIAL PROBE SYSTEMS

By

Ching-Lieh Li

A DISSERTATION

Submitted to
Michigan State University
in partial fulfillment of the requirements
for the degree of

DOCTOR OF PHILOSOPHY

Department of Electrical Engineering

1993

ABSTRACT

MEASUREMENT OF ELECTROMAGNETIC PROPERTIES OF MATERIALS VIA COAXIAL PROBE SYSTEMS

by

Ching-Lieh Li

This thesis presents two methods to determine the conductivity, permittivity and permeability of materials via coaxial probe systems. Using a frequency-domain network analyzer, the determination of the complex permittivity and complex permeability over a wide band of frequencies can be achieved simply through two input impedances measurements. In this thesis two coaxial TEM structures operating from 200 MHz to 2 GHz are analyzed.

Two experimental setups of coaxial probe systems were designed to measure the electromagnetic (EM) properties of materials. One is the open-ended coaxial probe system, by which a nondestructive measurement of EM parameters can be easily achieved for various materials in practical applications. The other is called coaxial cavity system, which is suitable for liquid materials or lossy materials of thick dimensions. Experimental results of these two methods are satisfactory and they agree quite well.

In the open-ended coaxial probe system, theoretical analysis predicts the excitation

of surface waves, radiative waves and radial guided waves which can influence the quantification of EM parameters of materials. A careful study on these complex waves was conducted. On the other hand, a resonant phenomenon was observed theoretically and experimentally in the coaxial cavity structure. In order to investigate the effect on the characterization of EM properties near the resonant frequencies, the metallic wall loss of the cavity is calculated using Poynting theorem and perturbation method.

Both methods were studied carefully by full wave analysis. Theoretical approach leads to an integral equation for the electric field at the aperture of the coaxial probe system. The method of moments is applied to transform the integral equation into a set of simultaneous algebraic equations so that the numerical solution for aperture electric field can be obtained. After the aperture E field is obtained, other quantities such as the input impedance and the EM fields inside the material can be calculated. The input impedance of the coaxial probe can then be used to determine the EM parameters of the material.

A series of experiments was conducted to measure the input impedances of the coaxial probe systems, which are in contact with materials, using an HP network analyzer. An inverse algorithm is then used to determine the EM parameters of the materials from the measured input impedances. Various materials, which include low, medium and high permittivity materials, have been measured and the results were found to be satisfactory.

ACKNOWLEDGEMENTS

The author is sincerely grateful to his academic advisor Dr. Kun-Mu Chen who provided much of the guidance, counsel and encouragement throughout the course of this research.

Special thanks are extended to the members of the guidance committee, Dr. E. J. Rothwell and Dr. C. Y. Lo for valuable suggestions, especially to Dr. D. P. Nyquist for his generous and unfailing support during the period of this study.

Special thanks are also extended to Dr. J. Ross and Dr. J. Song for their kindly helps in the experimental and theoretical aspects, respectively.

In addition, it is the author's pleasure to thank his wife, Yuling, who offered thorough understanding, helping and encouragement.

The research reported in this thesis was supported by Michigan Research Excellence Fund and in part by Boeing Airplane Company.

TABLE OF CONTENTS

LIST OF FIGURES

CHAPTER 1
INTRODUCTION

The research described in this thesis deals with the measurement of electromagnetic (EM) properties of materials. Two methods are investigated in this thesis: The first method employs an open-ended coaxial line probe which consists of an open-ended coaxial line terminated on a metallic flange and placed against a material layer. The second method uses a coaxial cavity which is partially filled with material and excited by a coaxial line. The first method offers an easy, nondestructive measurement, and the second method is useful to measure thick lossy materials.

The subject of EM property characterization of materials has attracted interests of many researchers in this field for a long time [1]. In particular, the nondestructive measurement [2]-[4] and simultaneous determination of complex permittivity and permeability [5]-[7] have gained much attention during the last two decades.

The free space methods to achieve nonintrusive measurement employ beams of EM radiation which are directed to pass through the object [8],[9]. These methods possess the advantage that the samples can be easily introduced into the measurement area, but the frequencies employed in these methods are typically in the minimeter wave or quasi-optical range and relatively large material samples are usually necessary. For smaller material samples, the frequency domain transmission line techniques may be suitable, for which the measurement fixture consists of a waveguide or a coaxial transmission line which holds the sample. In particular, the coaxial waveguide structures have been widely

used for EM parameter measurements [1],[10]. Usually the S-parameters of the transmission line are determined and then the EM parameters are calculated. Other structures including stripline [6], microstrip line [11] and closed cavity methods [12] have also been employed. One of the advantages for the setups is that the lower frequency measurement can be achieved with a TEM structure. The disadvantage is that the material samples need to be machined to fit in the fixtures.

To achieve a nondestructive measurement in the frequency range from 0.2 GHz to 2 GHz, an open-ended coaxial probe terminated on a metallic flange is proposed. This geometry possesses the advantage of simplicity and a nondestructive measurement can be achieved easily by placing the probe against the materials. Attempts to measure the EM properties of materials via an open-ended coaxial probe are certainly not new [2]-[4],[13]-[16]. But to our best knowledge, no study has been conducted to characterize both the complex permittivity and permeability of material using an open-ended coaxial probe. And little work has been conducted to investigate the short-circuit case (material layer shorted by a metallic plate) of an open-ended coaxial probe [17]. Also the effect of complex wave excitation upon the characterization of EM parameters has not been addressed before. With the geometry of an open-ended coaxial probe, only a small sample area is illuminated by EM fields in the frequency band of interest; this method is not very sensitive nor suitable for lossy materials of large dimensions.

In order to overcome the weakness of an open-ended coaxial probe scheme, a coaxial cavity method is developed to excite EM fields which penetrate into the material medium. In variation to the conventional cavity method, a single-frequency method to extract the EM parameters from the change in resonant frequency and Q-factor [18],[19], the coaxial cavity is partially filled with material and the reflection coefficient of the

incident wave to the cavity is measured over a wide frequency band. The coaxial cavity structure provides a well-defined reference plane for precision measurement and is suitable for low frequency range. Conceptually, the complex permittivity and permeability of the material can be determined by simply changing the length of the coaxial cavity.

Chapter 2 provides theoretical background of the general waveguide theory. Hertzian potentials, employed to describe the EM fields of guided waves, are reviewed. The orthogonality properties of these guided waves are listed for the subsequent analysis of waveguide discontinuity problems. Also a concise derivation of wave matrices is given to analyze the reflection and transmission of TM waves incident upon a discontinuity interface.

Chapter 3 is devoted to the theoretical and numerical analysis of the open-ended coaxial probe, which consists of an open-ended coaxial line terminated on a large metallic flange and placed against a layer of material. An integral equation for the aperture electric field is established by matching the tangential EM fields across the aperture. The method of moments is then applied to solve the electric field integral equation (EFIE) numerically. The theoretical analysis predicts the excitation of surface waves and radiative waves for the open-circuit case and radial guided waves for the short-circuit case in this structure. The concept of equivalent magnetic surface current was used to replace the aperture E field and an analysis on the radiation of this equivalent surface current in a layered medium is presented. This study offers a check to the study based on the EFIE and also provides some physical pictures relevent to the problem.

Chapter 4 studies the power balance for the open-ended coaxial probe by comparing the total power carried away from the aperture, in the form of surface waves, radiative

waves and radial guided waves, to the transmitted power of the incident wave at the aperture. This provides a solid verification for theoretical and numerical results. The power associated with each complex wave is computed via Poynting vector, of which the EM field components of surface waves and radial guided waves are derived by Cauchy residue theorem, and the far zone field of radiative wave is evaluated by the saddle point method. The EM fields excited inside the material medium are found to be localized around the probe aperture for the frequency band of interest. This finding justifies the assumption of an infinite metallic flange in the analysis.

Chapter 5 is devoted to the theoretical and numerical analysis of the coaxial cavity, which is partially filled with a material and driven by a coaxial line. The matching of the tangential electric and magnetic fields at the probe aperture results in an integral equation for the unknown aperture electric field. The method of moments is then applied to solve the EFIE numerically. It is observed that a resonant phenomenon occurs in this structure, and at the resonant frequencies the determination of the EM parameters of materials becomes ill-conditioned. The metallic wall loss effect of the coaxial cavity near the resonant frequencies is then investigated to help mitigate the ill-conditioned problem.

Chapter 6 presents the experimental results on EM properties of various materials using both methods. The experimental setups and the calibration procedures for conducting accurate experiments are outlined. Two measurements on the probe input impedance are made for each frequency of interest using an HP network analyzer (HP8720B). These measured input impedances are then used to determine the permittivity and permeability by some numerical inverse algorithm. The results on some known materials agree quite well with the published data.

CHAPTER 2

REVIEW OF WAVEGUIDE THEORY

The results of general guided wave theory are outlined in this chapter [21]. Definition of Hertzian potentials is first introduced, and the EM fields of guided waves along an uniform closed-piped system are provided in terms of suitable Hertzian potentials. Then the orthogonality properties for the guided waves confined by a perfectly conducting waveguide are listed, which are useful in the analysis of waveguide excitation and discontinuity problems.

Specifically, the guided waves in coaxial line structures are analyzed in detail in subsequent chapters.

The reflection and transmission of transverse magnetic(TM) waves incident upon a discontinuity interface from the medium of either side are also studied. The concept of wave matrix is then presented to handle the problem of EM wave propagation in a layered material medium systematically.

2.1 Introduction of Hertzian potentials

Hertzian potentials are commonly used to describe electromagnetic (EM) fields in EM theory [22]. And there are in general two types of Hertzian potential, electric type Hertzian potential and magnetic type Hertzian potential.

The electric Hertzian potential, $\vec{\Pi}_e$, is defined such that the electric and magnetic fields in a homogeneous and isotropic medium are derived from it as follows:

$$\vec{H}=\epsilon\frac{\partial}{\partial t}\nabla\times\vec{\Pi}_e$$
$$\vec{E}=\nabla(\nabla\cdot\vec{\Pi}_e)-\mu\epsilon\frac{\partial^2\vec{\Pi}_e}{\partial t^2} \tag{2.1}$$

with

$$\nabla^2\vec{\Pi}_e-\mu\epsilon\frac{\partial^2\vec{\Pi}_e}{\partial t^2}=-\frac{\vec{P}}{\epsilon} \tag{2.2}$$

where $\vec{P}$ is the polarization density vector associated with the sources and defined by

$$\vec{J}=\frac{\partial\vec{P}}{\partial t}, \qquad \rho=-\nabla\cdot\vec{P} \tag{2.3}$$

In the frequency domain and in a source free region, the relations become

$$\vec{E} = k^2\vec{\Pi}_e+\nabla(\nabla\cdot\vec{\Pi}_e) = \nabla\times\nabla\times\vec{\Pi}_e$$
$$\vec{H} = j\omega\epsilon\nabla\times\vec{\Pi}_e \tag{2.4}$$

and

$$\nabla^2\vec{\Pi}_e+k^2\vec{\Pi}_e=0 \tag{2.5}$$

where $k=\omega\sqrt{\mu\epsilon}$ is the wavenumber in the medium.

Similarly the magnetic Hertzian potential, $\vec{\Pi}_h$, is defined such that the electric and magnetic fields in a homogeneous and isotropic medium are derived from it, in frequency domain, as follows:

$$\vec{E} = -j\omega\mu\nabla\times\vec{\Pi}_h$$
$$\vec{H} = k^2\vec{\Pi}_h+\nabla(\nabla\cdot\vec{\Pi}_h)=\nabla\times\nabla\times\vec{\Pi}_h \tag{2.6}$$

and

$$\nabla^2\vec{\Pi}_h+k^2\vec{\Pi}_h=0 \tag{2.7}$$

In studying guided waves along an uniform closed-pipe system, it is common to classify the waves into two basic types as follows [22]:

1. Transverse electric modes (TE modes)

These modes contain magnetic field component but no electric field component in the direction of propagation. They are also referred as H modes and the field components may be derived from a magnetic type Hertzian potential having a single component along the axis of the guide.

2. Transverse magnetic modes (TM modes)

These modes contain electric field component but no magnetic field component in the direction of propagation. They are also referred as E modes and the field components may be derived from an electric type Hertzian potential having a single component along the axis of the guide.

Transverse electric modes ($E_z = 0, H_z \neq 0$)

The TE modes can be derived from a magnetic Hertzian potential by letting $\vec{\Pi}_e = 0$ and $\vec{\Pi}_h = \hat{z}\Pi_h$. The electric field then has transverse components only and can be expressed as follows:

$$\begin{aligned} \vec{E} &= -j\omega\mu\nabla\times\vec{\Pi}_h \\ &= j\omega\mu\hat{z}\times\nabla_t\Pi_h \end{aligned} \tag{2.8}$$

where

$$\nabla_t = \nabla - \hat{z}\frac{\partial}{\partial z} \tag{2.9}$$

Separating variables in Π_h, we write $\Pi_h = \psi_h g(z)$, then the EM fields can be expressed in terms of the wave function ψ_h as

$$
\begin{aligned}
H_z &= k_c^2 \psi_h e^{\mp \Gamma z} \\
\vec{H}_t &= \mp \Gamma \nabla_t \psi_h e^{\mp \Gamma z} \\
\vec{E}_t &= \mp Z_h (\hat{z} \times \vec{H}_t)
\end{aligned}
\tag{2.10}
$$

with

$$
\begin{aligned}
\nabla_t^2 \psi_h + k_c^2 \psi_h &= 0 \\
k_c^2 &= \Gamma^2 + k^2
\end{aligned}
\tag{2.11}
$$

where $Z_h = \dfrac{j\omega\mu}{\Gamma}$ is the TE mode wave impedance.

Transverse magnetic modes ($E_z \neq 0$, $H_z = 0$)

The TM modes can be derived from an electric Hertzian potential by letting $\vec{\Pi}_h = 0$ and $\vec{\Pi}_e = \hat{z}\,\Pi_e$. The magnetic field then has transverse components only and can be expressed as follows:

$$
\begin{aligned}
\vec{H} &= j\omega\epsilon \nabla \times \vec{\Pi}_e \\
&= -j\omega\epsilon \hat{z} \times \nabla_t \Pi_e
\end{aligned}
\tag{2.12}
$$

where

$$
\nabla_t = \nabla - \hat{z}\frac{\partial}{\partial z}
\tag{2.13}
$$

Similarly separating variables in Π_e, we write $\Pi_e = \psi_e g(z)$, the EM fields can be expressed in terms of the wave function ψ_e as

$$
\begin{aligned}
E_z &= k_c^2 \psi_e e^{\mp \Gamma z} \\
\vec{E}_t &= \mp \Gamma \nabla_t \psi_e e^{\mp \Gamma z} \\
\vec{H}_t &= \mp Y_e (\hat{z} \times \vec{E}_t)
\end{aligned}
\tag{2.14}
$$

with

$$
\begin{aligned}
\nabla_t^2 \psi_e + k_c^2 \psi_e &= 0 \\
k_c^2 &= \Gamma^2 + k^2
\end{aligned}
\tag{2.15}
$$

where $Y_e = \dfrac{j\omega\epsilon}{\Gamma}$ is the TM mode wave admittance.

2.2 Orthogonality properties of waveguide modes

Guided-wave modes inside perfectly conducting waveguides possess the following interesting and important mathematical orthogonality properties:

1. Longitudinal field components and/or wave functions of different modes are orthogonal.

2. Transverse field components of different modes are orthogonal.

Mathematical statements of the orthogonality properties are listed here for later developments. Letting ψ_n, ψ_m be the solutions for the n^{th} and m^{th} E mode or H mode with $n \neq m$, then the orthogonality properties are

$$\iint_{C.S.} \psi_n \psi_m \, ds = 0$$
$$\iint_{C.S.} \nabla_t \psi_n \cdot \nabla_t \psi_m \, ds = 0 \tag{2.16}$$

or

$$\iint_{C.S.} H_{zn} H_{zm} \, ds = 0$$
$$\iint_{C.S.} E_{zn} E_{zm} \, ds = 0 \tag{2.17}$$

and

$$\iint_{C.S.} \vec{E}_{tn} \cdot \vec{E}_{tm} \, ds = \iint_{C.S.} \vec{H}_{tn} \cdot \vec{H}_{tm} \, ds = 0$$

... for TE modes or TM modes

$$\iint_{C.S.} \vec{E}_{tn} \cdot \vec{E}_{tm} \, ds = \iint_{C.S.} \vec{H}_{tn} \cdot \vec{H}_{tm} \, ds = 0 \tag{2.18}$$

... for all n,m; mixed TE and TM modes

These orthogonality properties are exceedingly useful because with these a given arbitrary field can be expanded into a series of E and H modes in the analysis of waveguide excitation and discontinuity problems.

2.3 Reflection and transmission at a discontinuity interface for TM modes

In this section the complex amplitudes of the reflected and transmitted waves are studied when a TM wave is incident upon a plane interface surface between two different media. Also the wave matrix is derived for waves incident upon an interface from the medium at either side to handle a general reflection and transmission problem.

A discontinuity interface between two different media is considered first as shown in fig. 2.1. When a TM wave is incident on the interface, it is partially reflected and partially transmitted. The notations $\vec{E}_I, \vec{E}_R$, and $\vec{E}_T$ stand for the electric fields of the incident wave, reflected wave and transmitted wave, respectively, as follows:

$$\begin{aligned}
\vec{E}_I &= [\vec{e}_I(\mu_1,\mu_2) + \hat{z}e_{zI}(\mu_1,\mu_2)]e^{-\Gamma_1 z} \\
\vec{E}_R &= [\vec{e}_R(\mu_1,\mu_2) + \hat{z}e_{zR}(\mu_1,\mu_2)]e^{+\Gamma_1 z} \\
\vec{E}_T &= [\vec{e}_T(\mu_1,\mu_2) + \hat{z}e_{zT}(\mu_1,\mu_2)]e^{-\Gamma_2 z}
\end{aligned} \tag{2.19}$$

where μ_1 and μ_2 are the transverse coordinates.

And the associated magnetic fields are

$$\begin{aligned}
\vec{H}_I &= \vec{h}_I(\mu_1,\mu_2)e^{-\Gamma_1 z} = \vec{\bar{Y}}_1 \cdot \vec{e}_I(\mu_1,\mu_2)e^{-\Gamma_1 z} \\
\vec{H}_R &= \vec{h}_R(\mu_1,\mu_2)e^{+\Gamma_1 z} = -\vec{\bar{Y}}_1 \cdot \vec{e}_R(\mu_1,\mu_2)e^{\Gamma_1 z} \\
\vec{H}_T &= \vec{h}_T(\mu_1,\mu_2)e^{-\Gamma_2 z} = \vec{\bar{Y}}_2 \cdot \vec{e}_T(\mu_1,\mu_2)e^{-\Gamma_2 z}
\end{aligned} \tag{2.20}$$

with

$$\begin{aligned}
\vec{\bar{Y}}_1 &= \frac{j\omega\epsilon_1}{\Gamma_1}(\hat{\mu}_2\hat{\mu}_1 - \hat{\mu}_1\hat{\mu}_2) \equiv Y_{e1}(\hat{\mu}_2\hat{\mu}_1 - \hat{\mu}_1\hat{\mu}_2) \\
\vec{\bar{Y}}_2 &= \frac{j\omega\epsilon_2}{\Gamma_2}(\hat{\mu}_2\hat{\mu}_1 - \hat{\mu}_1\hat{\mu}_2) \equiv Y_{e2}(\hat{\mu}_2\hat{\mu}_1 - \hat{\mu}_1\hat{\mu}_2)
\end{aligned} \tag{2.21}$$

where $\hat{\mu}_1, \hat{\mu}_2$ are the unit vectors of the transverse coordinates.

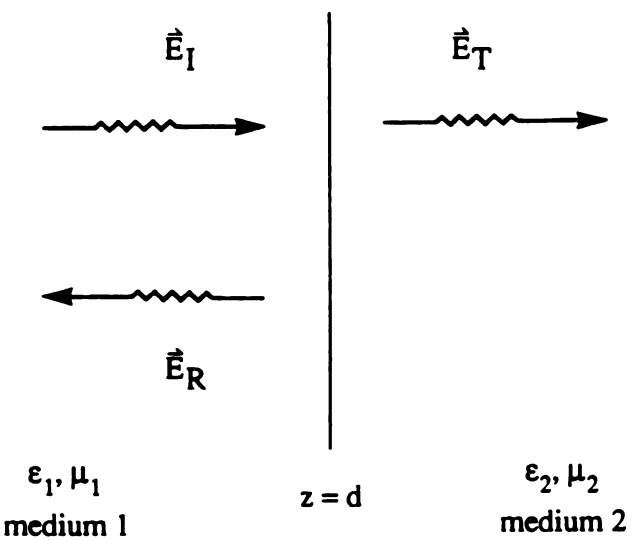

Figure2.1 A discontinuity interface between two different media.

The boundary conditions for tangential E and H fields at the interface are

$$\begin{aligned} \hat{t}\cdot\vec{E}(z=d^-) &= \hat{t}\cdot\vec{E}(z=d^+) \\ \hat{t}\cdot\vec{H}(z=d^-) &= \hat{t}\cdot\vec{H}(z=d^+) \end{aligned} \tag{2.22}$$

Application of the boundary conditions leads to

$$\begin{aligned} \vec{e}_I e^{-\Gamma_1 d} + \vec{e}_R e^{\Gamma_1 d} &= \vec{e}_T e^{-\Gamma_2 d} \\ \vec{\bar{Y}}_1 \cdot (\vec{e}_I e^{-\Gamma_1 d} - \vec{e}_R e^{\Gamma_1 d}) &= \vec{\bar{Y}}_2 \cdot \vec{e}_T e^{-\Gamma_2 d} \end{aligned} \tag{2.23}$$

which can be simplified to

$$\begin{aligned} \vec{e}_I e^{-\Gamma_1 d} + \vec{e}_R e^{\Gamma_1 d} &= \vec{e}_T e^{-\Gamma_2 d} \\ Y_{e1}\vec{e}_I e^{-\Gamma_1 d} - Y_{e1}\vec{e}_R e^{\Gamma_1 d} &= Y_{e2}\vec{e}_T e^{-\Gamma_2 d} \end{aligned} \tag{2.24}$$

Since the boundary conditions on tangential E and H fields must be satisfied at every point of the interface, then clearly $\vec{e}_R$ and $\vec{e}_T$ must have the same transverse functional dependence as $\vec{e}_I$ such that we may define

$$\begin{aligned} \vec{e}_I &= c_1 \vec{e}_o(\mu_1, \mu_2) \\ \vec{e}_R &= b_1 \vec{e}_o(\mu_1, \mu_2) \\ \vec{e}_T &= c_2 \vec{e}_o(\mu_1, \mu_2) \end{aligned} \tag{2.25}$$

Substituting (2.25) into (2.24) gives

$$c_1 e^{-\Gamma_1 d} + b_1 e^{\Gamma_1 d} = c_2 e^{-\Gamma_2 d} \tag{2.26}$$

$$Y_{e1} c_1 e^{-\Gamma_1 d} - Y_{e1} b_1 e^{\Gamma_1 d} = Y_{e2} c_2 e^{-\Gamma_2 d} \tag{2.27}$$

The following operation, (2.26) $*Y_{e2}$ - (2.27), leads to

$$(Y_{e2} - Y_{e1}) c_1 e^{-\Gamma_1 d} + (Y_{e2} + Y_{e1}) b_1 e^{\Gamma_1 d} = 0 \tag{2.28}$$

which is arranged as

$$b_1 = \frac{Y_{e1}-Y_{e2}}{Y_{e1}+Y_{e2}} e^{-2\Gamma_1 d} c_1 \tag{2.29}$$

Defining R to be the ratio of the reflected wave amplitude to the incident wave amplitude, we have

$$R \equiv \frac{b_1}{c_1} = \frac{Y_{e1}-Y_{e2}}{Y_{e1}+Y_{e2}} e^{-2\Gamma_1 d} \tag{2.30}$$

Similarly the following operation, (2.26) $*Y_{e1}$ + (2.27), leads to

$$2 Y_{e1} c_1 e^{-\Gamma_1 d} = (Y_{e1} + Y_{e2}) c_2 e^{-\Gamma_2 d} \tag{2.31}$$

or

$$T \equiv \frac{c_2}{c_1} = \frac{2Y_{e1}}{Y_{e1}+Y_{e2}} e^{(\Gamma_2-\Gamma_1)d} \tag{2.32}$$

where T is the ratio of the transmitted wave amplitude to the incident wave amplitude.

In case $d=0$, then R and T become

$$\begin{aligned} R &= \frac{Y_{e1}-Y_{e2}}{Y_{e1}+Y_{e2}} \equiv R_1 \\ T &= \frac{2Y_{e1}}{Y_{e1}+Y_{e2}} \equiv T_{12} \end{aligned} \tag{2.33}$$

such that the interface reflection coefficient R_1 and transmission coefficient T_{12} have the same forms as those for a transmission line discontinuity as shown in fig. 2.2.

The general reflection and transmission problem must include waves incident upon an interface from either side, which is studied next.

Wave matrices

The wave matrix method is usually employed to handle a general reflection and transmission problem in a systematic way.

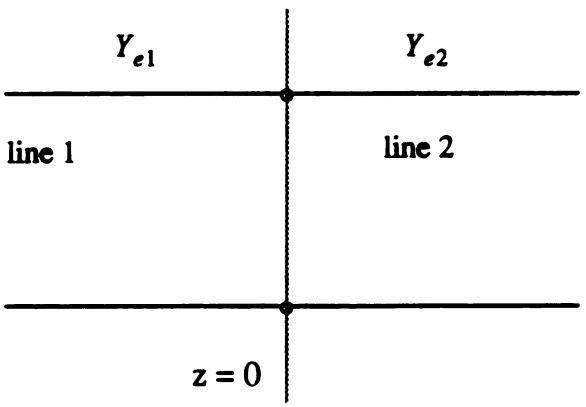

$$R = \frac{Y_{e1} - Y_{e2}}{Y_{e1} + Y_{e2}} \quad , \qquad T = 2\frac{Y_{e1}}{Y_{e1} + Y_{e2}}$$

Figure2.2 The reflection and transmission coefficient of a transmission line discontinuity, where Y_{e1} and Y_{e2} are the characteristic admittance of each line, respectively.

With reference to fig. 2.3, c_i denotes the amplitudes of the waves travelling to the right (i=1,2) and b_i denotes the amplitudes of the waves travelling to the left in either medium. When a TM wave of amplitude c_1 propagates from the left side of the interface, it is partly reflected and partly transmitted, which is also true for a TM wave of amplitude b_2 propagating from the right side of the interface. Therefore in the left side, there is a total reflected wave propagating in negative z direction. And in the right side, there is a total transmitted wave propagating in the positive z direction. Letting b_1 and c_2 be the amplitudes of the latter two waves, respectively, we can write

$$\begin{aligned} b_1 e^{\Gamma_1 d}\vec{e}_o(\mu_1,\mu_2) &= R_1 c_1 e^{-\Gamma_1 d}\vec{e}_o(\mu_1,\mu_2) + T_{21} b_2 e^{\Gamma_2 d}\vec{e}_o(\mu_1,\mu_2) \\ c_2 e^{-\Gamma_2 d}\vec{e}_o(\mu_1,\mu_2) &= R_2 b_2 e^{\Gamma_2 d}\vec{e}_o(\mu_1,\mu_2) + T_{12} c_1 e^{-\Gamma_1 d}\vec{e}_o(\mu_1,\mu_2) \end{aligned} \tag{2.34}$$

or

$$b_1 = R_1 e^{-2\Gamma_1 d} c_1 + T_{21} e^{-(\Gamma_1-\Gamma_2)d} b_2 \tag{2.35}$$

$$c_2 = R_2 e^{2\Gamma_2 d} b_2 + T_{12} e^{-(\Gamma_1-\Gamma_2)d} c_1 \tag{2.36}$$

where

$$R_1 = \frac{Y_{e1} - Y_{e2}}{Y_{e1} + Y_{e2}} = -R_2$$

$$T_{12} = \frac{2Y_{e1}}{Y_{e1} + Y_{e2}} \quad , \quad T_{21} = \frac{2Y_{e2}}{Y_{e2} + Y_{e1}} \tag{2.37}$$

Equation (2.36) can be arranged to be

$$c_1 = \frac{1}{T_{12}} e^{(\Gamma_1-\Gamma_2)d} c_2 - \frac{R_2}{T_{12}} e^{(\Gamma_1+\Gamma_2)d} b_2 \tag{2.38}$$

Substituting (2.38) into (2.35) and after some manipulation, we have

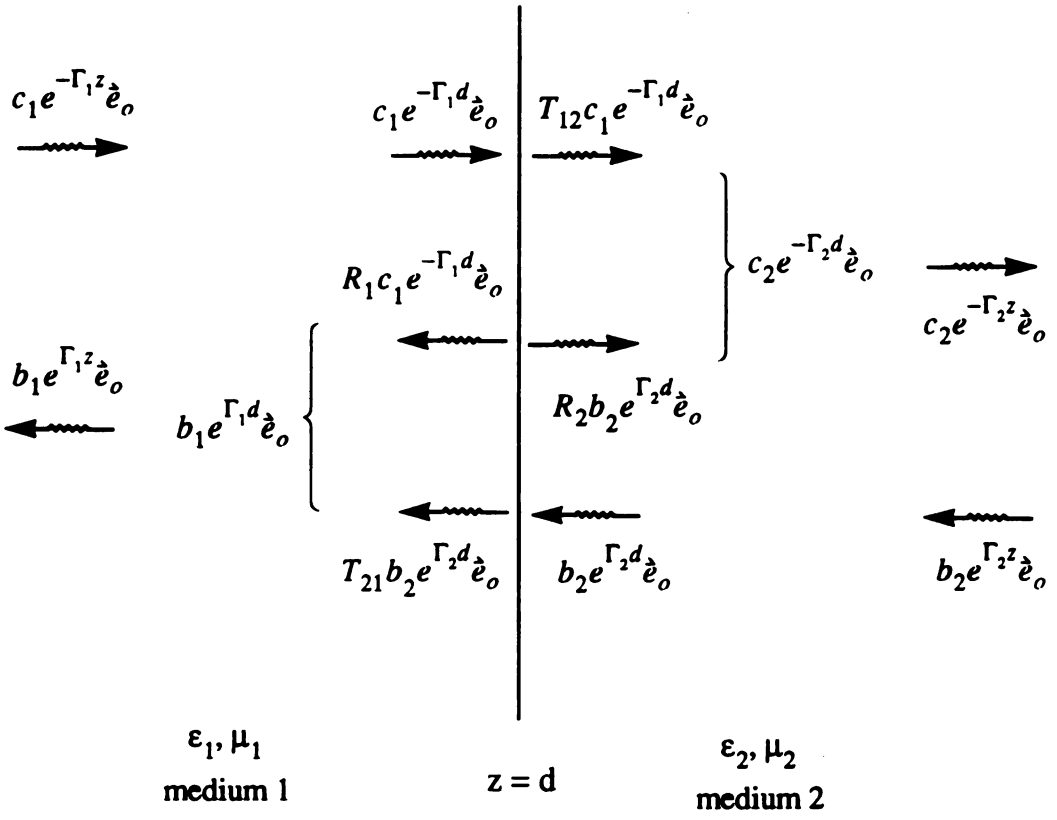

Figure2.3 A discontinuity interface between two different media, where there are TM waves of amplitudes c_1 , b_2 coming from the medium of either side, respectively.

$$b_1 = \frac{R_1}{T_{12}} e^{-(\Gamma_1+\Gamma_2)d} c_2 + \frac{T_{12}T_{21} - R_1R_2}{T_{12}} e^{-(\Gamma_1-\Gamma_2)d} b_2 \tag{2.39}$$

Since using (2.37) it can be shown that $T_{12}T_{21} - R_1R_2 = 1$, then (2.39) becomes

$$b_1 = \frac{R_1}{T_{12}} e^{-(\Gamma_1+\Gamma_2)d} c_2 + \frac{1}{T_{12}} e^{-(\Gamma_1-\Gamma_2)d} b_2 \tag{2.40}$$

Since $R_1 = -R_2$, (2.38) and (2.40) can be written in a matrix form as

$$\begin{bmatrix} c_1 \\ b_1 \end{bmatrix} = \frac{1}{T_{12}} \begin{bmatrix} e^{(\Gamma_1-\Gamma_2)d} & R_1 e^{(\Gamma_1+\Gamma_2)d} \\ R_1 e^{-(\Gamma_1+\Gamma_2)d} & e^{-(\Gamma_1-\Gamma_2)d} \end{bmatrix} \begin{bmatrix} c_2 \\ b_2 \end{bmatrix} \equiv \begin{bmatrix} A_{11} & A_{12} \\ A_{21} & A_{22} \end{bmatrix} \begin{bmatrix} c_2 \\ b_2 \end{bmatrix} \tag{2.41}$$

where [A] is called a wave transmission chain matrix.

With this wave matrix, we can relate the amplitudes of the forward- and backward-propagating waves in the output side to that in the input side such that for a cascade connection of N+1 sections as shown in fig. 2.4 we have

$$\begin{bmatrix} c_1 \\ b_1 \end{bmatrix} = \prod_{j=1}^{N} \frac{1}{T_{j(j+1)}} \begin{bmatrix} e^{(\Gamma_j-\Gamma_{j+1})z_j} & R_j e^{(\Gamma_j+\Gamma_{j+1})z_j} \\ R_j e^{-(\Gamma_j+\Gamma_{j+1})z_j} & e^{-(\Gamma_j-\Gamma_{j+1})z_j} \end{bmatrix} \begin{bmatrix} c_{N+1} \\ b_{N+1} \end{bmatrix} \equiv \begin{bmatrix} A_{11} & A_{12} \\ A_{21} & A_{22} \end{bmatrix} \begin{bmatrix} c_{N+1} \\ b_{N+1} \end{bmatrix} \tag{2.42}$$

Letting R_{bj} be the overall ratio of backward-propagating wave amplitude b_j to the forward-propagating wave amplitude c_j, then R_{b1} can be derived as

$$R_{b1} = \frac{b_1}{c_1} = \frac{A_{21}c_{N+1} + A_{22}b_{N+1}}{A_{11}c_{N+1} + A_{12}b_{N+1}} \tag{2.43}$$

There is an alternative expression for R_{b1} that employs a recursive relationship of R_{bj} as follows [23]:

Since $R_1 = -R_2$, dividing (2.40) by (2.38) leads to

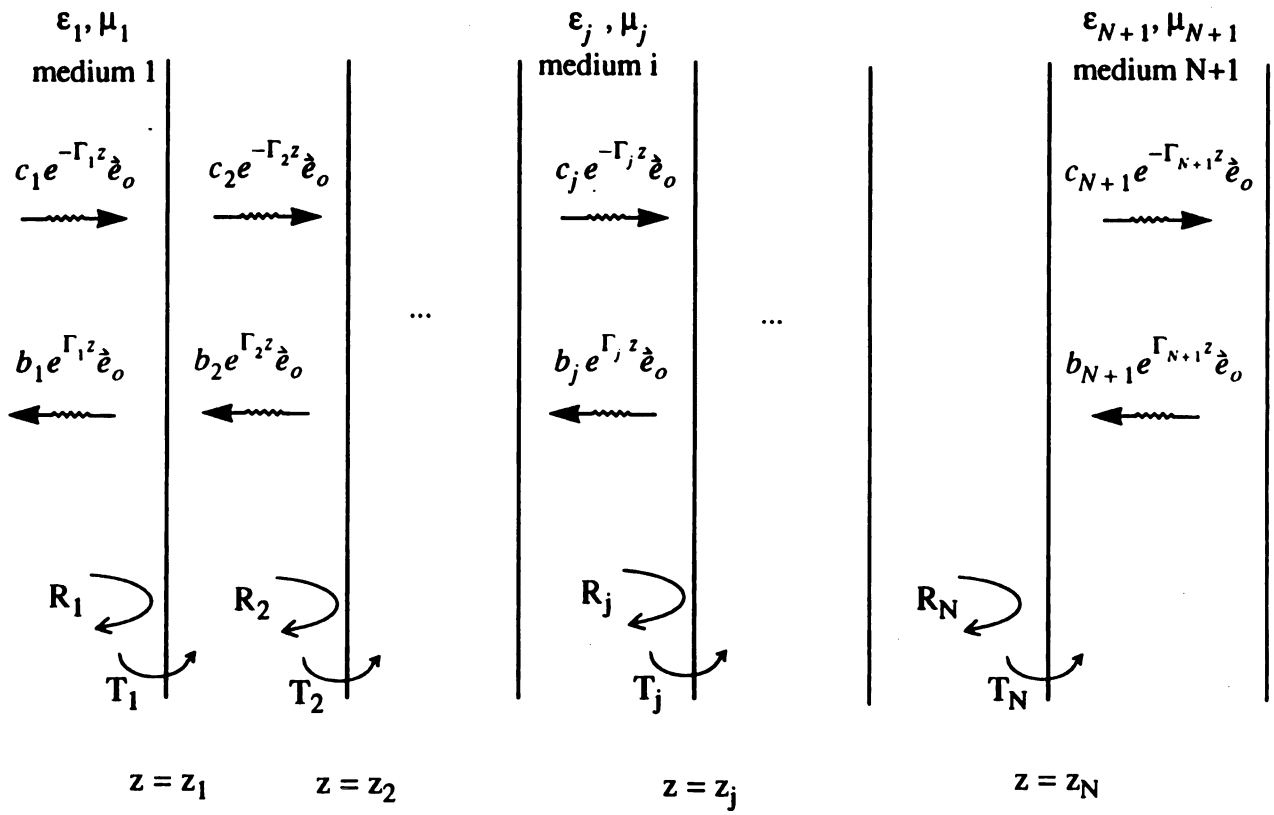

Figure 2.4 A cascade connection of N+1 sections with TM wave incident.

$$\frac{b_1}{c_1} = \frac{R_1 e^{-(\Gamma_1+\Gamma_2)d} c_2 + e^{-(\Gamma_1-\Gamma_2)d} b_2}{e^{(\Gamma_1-\Gamma_2)d} c_2 + R_1 e^{(\Gamma_1+\Gamma_2)d} b_2}$$
$$= e^{-2\Gamma_1 d} \frac{R_1 e^{-\Gamma_2 d} + e^{\Gamma_2 d} b_2/c_2}{e^{-\Gamma_2 d} + R_1 e^{\Gamma_2 d} b_2/c_2} \tag{2.44}$$

which can be written as

$$R_{b1} = e^{-2\Gamma_1 d} \frac{R_1 e^{-\Gamma_2 d} + e^{\Gamma_2 d} R_{b2}}{e^{-\Gamma_2 d} + R_1 e^{\Gamma_2 d} R_{b2}} \tag{2.45}$$

Therefore for a cascade connection of N+1 sections, we have the following recursive relationship (j=1,...,N):

$$R_{bj} = e^{-2\Gamma_j z_j} \frac{R_j e^{-\Gamma_{j+1} z_j} + e^{\Gamma_{j+1} z_j} R_{b(j+1)}}{e^{-\Gamma_{j+1} z_j} + R_j e^{\Gamma_{j+1} z_j} R_{b(j+1)}} \tag{2.46}$$

which offers another approach for computing R_{b1}.

Finally let's verify (2.45) by an example to conclude this section. With reference to fig. 2.5, an open-ended coaxial probe is placed against a dielectric material layer with thickness d, which is investigated in chapter 3 in detail. For each TM mode inside the material and the air, we have

$$R_{b2} = 0 \tag{2.47}$$

and (2.45) reduces to

$$R_{b1} = e^{-2\Gamma_1 d} R_1 = e^{-2\Gamma_1 d} \frac{Y_{e1} - Y_{e2}}{Y_{e1} + Y_{e2}} \tag{2.48}$$

which is exactly the same as (2.30).

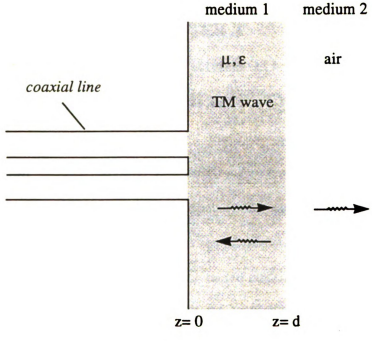

Figure 2.5 An open-ended coaxial probe terminated on a metallic flange placed against a material medium . A TM wave is excited inside the material.

CHAPTER 3

OPEN-ENDED COAXIAL PROBE TO MEASURE THE PERMITTIVITY AND PERMEABILITY OF MATERIAL

3.1 Introduction

In this chapter the analysis of an open-ended coaxial probe system for the measurement of electromagnetic (EM) properties of materials is presented [10,23,24-26].

The geometry of this problem is an open-ended coaxial probe terminated on a large metallic flange placed against a stratified material medium as shown in fig. 3.1, by which a nondestructive measurement of EM parameters can be achieved. The goal is to relate the permittivity ε and permeability μ of the material to the input impedance of the coaxial probe, thus, by measuring the latter the former, ε and μ, can be inversely determined.

Theoretically, this probe is analyzed as follows. An incident TEM mode to the probe is partially reflected by the discontinuity at the aperture and it also excites EM fields in the stratified material medium. Additionally, higher order coaxial waveguide modes are excited near the probe aperture. The EM fields in the coaxial line part and in the material medium can be expressed in terms of modal functions, and the matching of the tangential electric and magnetic fields at the probe aperture will result in an integral equation for the unknown aperture electric field.

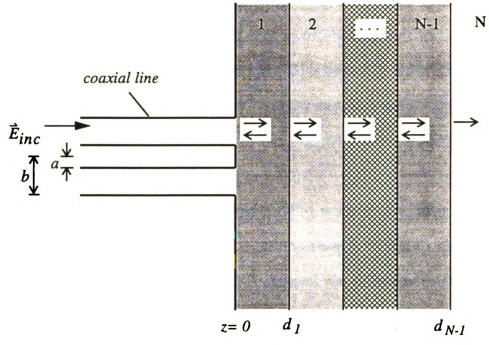

Figure 3.1 Geometry of an open-ended coaxial line terminated on a large metallic flange placed against a stratified isotropic medium.

The electric field integral equation (EFIE) is investigated and it is found that certain singularities may occur in the integrand, which requires a careful analysis before a numerical scheme can be applied to solve this integral equation.

A careful theoretical analysis for the structure of fig. 3.1 leads to the prediction of the excitation of surface waves and radiative waves for the open-circuit case, in which the material is backed by a dielectric (layer N is dielectric, usually air), and radial guided waves for the short-circuit case, in which the material is backed by a metallic plate (layer N is metal). The finding of these complex waves comes from the singularities and/or branch cuts of the integrand in the EFIE and can be identified via deformed contour integration in the complex plane.

To determine the reflection coefficient of TEM mode at the probe aperture, the integral equation for the unknown aperture electric field is solved by the method of moments. After the aperture electric field is obtained, the reflection coefficient of the TEM mode or the input impedance of the probe can be determined in terms of ε and μ of the material medium. Conversely, if the input impedance of the probe is experimentally measured with the help of a network analyzer, ε and μ of the material medium can be inversely determined.

Conceptually, for a simple medium two measurements are required to determine two unknowns ε and μ at each frequency of interest. Therefore by measuring the open-circuit input impedance and the short-circuit input impedance of the probe, the complex ε and μ of the medium can be uniquely determined.

In section 3.2 the results of general guided wave theory are applied to solve the EM fields at both sides of the aperture, and an EFIE is derived by matching the boundary conditions across the aperture. Meanwhile the reflection coefficient of the incident TEM

wave is expressed in terms of the aperture electric field. The identification of complex waves in the structure is also discussed in this section via the Hankel transform representation of EM fields and a deformed complex contour integration.

In section 3.3 the finding of complex waves excitation due to the singularities in integrand of the EFIE is verified using the concept of equivalent magnetic surface current for the aperture field. This offers an independent treatment other than the analysis of section 3.2. Not surprisingly, these results turn out to agree to each other in both sections.

In section 3.4 the method of moments is applied to solve the EFIE. The TM eigenmodes of the coaxial line are chosen to be the basis functions for unknown aperture field and Galerkin's technique is used to convert the integral equation into a set of simultaneous algebraic equations, from which the numerical solution of aperture electric field is obtained and the input admittance at the aperture is resolved. Finally some checkings for the correct numerical implementation are also given in this section.

3.2 Theoretical Study Using Full Wave Analysis

3.2.1 Application of General Waveguide Theory to a Coaxial Structure

In this section the results of guided wave theory in chapter 2 are applied to a coaxial waveguide structure with a geometry as shown in fig. 3.1 [27].

Due to rotational symmetry, only TM modes are excited when a TEM mode is incident to the system. With the help of (2.15) for TM modes, the wave function ψ_e satisfies a two-dimensional Helmholtz equation,

$$\nabla_t^2 \psi_e + k_c^2 \psi_e = 0 \tag{3.1}$$

subject to the boundary conditions of

$$\psi_e(\rho=a)=0$$
$$\psi_e(\rho=b)=0 \tag{3.2}$$

where $k_c^2 = k^2+\Gamma^2$ and ∇_t^2 is the transverse part of the ∇^2 operator.

In cylindrical coordinate ∇_t^2 stands for $\frac{1}{\rho}\frac{\partial}{\partial\rho}(\rho\frac{\partial}{\partial\rho})+\frac{1}{\rho^2}\frac{\partial^2}{\partial\phi^2}$ such that (3.1) becomes

$$\frac{1}{\rho}\frac{\partial}{\partial\rho}\left(\rho\frac{\partial\psi_e}{\partial\rho}\right)+\frac{1}{\rho^2}\frac{\partial^2\psi_e}{\partial\phi^2}+k_c^2\psi_e=0 \tag{3.3}$$

and by the separation of variables method the solution of ψ_e is

$$\psi_{enm}=A_{nm}\left[J_n(k_{cnm}\rho)-\frac{J_n(k_{cnm}a)}{Y_n(k_{cnm}a)}Y_n(k_{cnm}\rho)\right]e^{jn\phi} \tag{3.4}$$

where k_{cnm} satisfies

$$J_n(k_{nm}a)Y_n(k_{nm}b)-J_n(k_{nm}b)Y_n(k_{nm}a)=0 \tag{3.5}$$

With the help of (2.14) the field components of TM modes can be expressed as

$$E_{znm}=k_{cnm}^2\psi_{enm}e^{\mp\Gamma_{nm}z}$$

$$\vec{E}_{tnm}=\mp\Gamma_{nm}\nabla_t\psi_{enm}e^{\mp\Gamma_{nm}z}$$

$$=\mp\Gamma_{nm}A_{nm}\left\{\begin{array}{l}\hat{\rho}\,k_{cnm}\left[J_n'(k_{cnm}\rho)-\frac{J_n(k_{cnm}a)}{Y_n(k_{cnm}a)}Y_n'(k_{cnm}\rho)\right]\\ +\hat{\phi}\frac{jn}{\rho}\left[J_n(k_{cnm}\rho)-\frac{J_n(k_{cnm}a)}{Y_n(k_{cnm}a)}Y_n(k_{cnm}\rho)\right]\end{array}\right\}e^{jn\phi}e^{\mp\Gamma_{nm}z} \tag{3.6}$$

$$\vec{H}_{tnm}=\pm Y_e(\hat{z}\times\vec{E}_t)$$

$$=-j\omega\epsilon A_{nm}\left\{\begin{array}{l}\hat{\phi}\,k_{cnm}\left[J_n'(k_{cnm}\rho)-\frac{J_n(k_{cnm}a)}{Y_n(k_{cnm}a)}Y_n'(k_{cnm}\rho)\right]\\ -\hat{\rho}\frac{jn}{\rho}\left[J_n(k_{cnm}\rho)-\frac{J_n(k_{cnm}a)}{Y_n(k_{cnm}a)}Y_n(k_{cnm}\rho)\right]\end{array}\right\}e^{jn\phi}e^{\mp\Gamma_{nm}z} \tag{3.7}$$

These field components are used to represent the fields inside coaxial line in the next section.

3.2.2 Integral Equation for the Aperture Electric Field

An integral equation for the aperture electric field is derived in this section by matching the tangential EM fields across the aperture. Because of the discontinuity at the aperture, higher order modes are excited near the aperture. The EM fields in both sides can then be expressed as a sum and/or an integration of these higher order modes. For the case of TEM mode excitation, because the fields inside the coaxial line are ϕ-independent and the stratified medium is rotationally symmetric (which is a quite good approximation in practice), the EM fields scattered due to the discontinuity at $z=0$ also exhibit the rotational symmetry. Consequently, only TM modes can be excited, and TE modes can be shown to be zero.

Fields inside the coaxial line

Let's first consider the EM fields in region $z \le 0$ (inside the coaxial line), where there exists incident and reflected TEM mode and backward-propagating higher order TM modes. Letting R be the reflection coefficient of the TEM mode at $z=0$, the field components of TEM mode inside coaxial line can be expressed as follows [27].

$$\begin{aligned} \vec{E}_t &= \hat{\rho} A_o \frac{1}{\rho}(e^{-jk_i z} + R e^{jk_i z}) \\ \vec{H}_t &= \hat{\phi} A_o \frac{1}{\eta_i \rho}(e^{-jk_i z} - R e^{jk_i z}) \end{aligned} \tag{3.8}$$

where A_o is the incident TEM mode amplitude.

For higher order TM modes, only those modes with ϕ-independent property (n=0) are excited as mentioned. By (3.4), (3.6) and (3.7) the TM mode field components are

$$\begin{aligned} E_{zom}^{-} &= k_{com}^2 \psi_{eom} e^{+\Gamma_{om} z} \\ &= A_{om}[J_0(k_{com}\rho) - \frac{J_0(k_{com}a)}{Y_0(k_{com}a)} Y_0(k_{com}\rho)] e^{jo\phi} e^{+\Gamma_{om} z} \\ \vec{E}_{tom}^{-} &= +\Gamma_{om} \nabla_t \psi_{eom} e^{+\Gamma_{om} z} \end{aligned} \tag{3.9}$$

For simplicity, omitting the index o in the above equations leads to

$$\begin{aligned} E_{zm}^{-} &= k_{cm}^2 \psi_{em} e^{+\Gamma_m z} \\ &= A_m[J_0(k_{cm}\rho) - \frac{J_0(k_{cm}a)}{Y_0(k_{cm}a)} Y_0(k_{cm}\rho)] e^{+\Gamma_m z} \\ \vec{E}_{tm}^{-} &= +\Gamma_m \nabla_t \psi_{em} e^{+\Gamma_m z} \end{aligned} \tag{3.10}$$

or more explicitly,

$$\begin{aligned} \vec{E}_{tm}^{-} &= +\Gamma_m A_m \hat{\rho} k_{cm} [J_0'(k_{cm}\rho) - \frac{J_0(k_{cm}a)}{Y_0(k_{cm}a)} Y_0'(k_{cm}\rho)] e^{+\Gamma_m z} \\ \vec{H}_{tm}^{-} &= -j\omega \varepsilon_i A_m \hat{\phi} k_{cm} [J_0'(k_{cm}\rho) - \frac{J_0(k_{cm}a)}{Y_0(k_{cm}a)} Y_0'(k_{cm}\rho)] e^{+\Gamma_m z} \end{aligned} \tag{3.11}$$

Because the eigenvalue k_c, satisfying (3.5), is discrete, the total transverse EM fields in region $z \le 0$ are the sum of the TEM mode and all possible TM modes as follows:

$$\begin{aligned} \vec{E}_t &= \hat{\rho} A_o \frac{1}{\rho} (e^{-jk_i z} + R e^{jk_i z}) + \hat{\rho} \sum_{m=1}^{\infty} A_m \Re_m(\rho) e^{\Gamma_m z} \\ \vec{H}_t &= \hat{\phi} A_o \frac{1}{\eta_i \rho} (e^{-jk_i z} - R e^{jk_i z}) - \hat{\phi} \sum_{m=0}^{\infty} \frac{j\omega \varepsilon_i}{\Gamma_m} A_m \Re_m(\rho) e^{\Gamma_m z} \end{aligned} \tag{3.12}$$

where

$$\Re_m(\rho) = \Gamma_m k_{cm}\left[J_0'(k_{cm}\rho) - \frac{J_0(k_{cm}a)}{Y_0(k_{cm}a)} Y_0'(k_{cm}\rho)\right] \tag{3.13}$$

$$\equiv C_m\left[J_1(k_{cm}\rho)Y_0(k_{cm}a) - J_0(k_{cm}a)Y_1(k_{cm}\rho)\right]$$

Thus the fields at the left hand side of the aperture are obtained by setting $z = 0^-$ in (3.12)

$$\vec{E}_t(z=0^-) = \hat{\rho} A_o \frac{1}{\rho}(1+R) + \hat{\rho} \sum_{m=1}^{\infty} A_m \Re_m(\rho) \tag{3.14}$$

$$\vec{H}_t(z=0^-) = \hat{\phi} A_o \frac{1}{\eta_t \rho}(1-R) - \hat{\phi} \sum_{m=1}^{\infty} \frac{j\omega\epsilon_t}{\Gamma_m} A_m \Re_m(\rho) \tag{3.15}$$

where η_t, ϵ_t are those EM parameters of the material filled in the coaxial line.

Fields inside the material

Next let's consider the EM fields in region $z \geq 0$ (inside the material). As mentioned before the field components exhibit rotational symmetry and only TM modes can be excited inside the material, thus the Helmholtz equation for wave function ψ_e becomes

$$\nabla_t^2 \psi_e + k_c^2 \psi_e = 0 \tag{3.16}$$

subject to $\psi_e(\rho = 0)$ being finite.

The solution of ψ_e can be easily shown to be

$$\psi_e = D J_n(k_c \rho) \quad \text{with } Y_n(k_c\rho) \text{ discarded} \tag{3.17}$$

where $k_c = \sqrt{\Gamma^2 + k_j^2}$ is the continuous eigenvalue and k_j is the wavenumber inside the j^{th} layer of the material.

Again only the rotationally symmetric term (n=0) gives the right solution, therefore with the help of (3.6), (3.7) and (3.17) the field components in the j^{th} layer of material are

$$
\begin{aligned}
E_z^{\pm} &= D_j k_c^2 J_0(k_c\rho) e^{\mp\Gamma_j z} \\
\vec{E}_t^{\pm} &= \pm\Gamma_j D_j k_c \hat{\rho} J_1(k_c\rho) e^{\mp\Gamma_j z} \equiv \pm\hat{\rho} B_j J_1(k_c\rho) e^{\mp\Gamma_j z} \\
\vec{H}_t^{\pm} &= \hat{\phi} Y_{ej} B_j J_1(k_c\rho) e^{\mp\Gamma_j z}
\end{aligned}
\tag{3.18}
$$

where $Y_{ej} = \dfrac{j\omega\epsilon_j}{\Gamma_j}$ is the wave admittance.

Since the eigenvalue k_c is continuous in this case, the total fields should be expressed as an integration (instead of summation) of all the possible solutions. Thus the total transverse field inside the j^{th} layer of the material (including $\pm\hat{z}$ direction) is

$$
\begin{aligned}
\vec{E}_t &= \hat{\rho}\int_0^{\infty} B_j (e^{-\Gamma_j z} + R_{bj} e^{\Gamma_j z}) J_1(k_c\rho) k_c dk_c \\
\vec{H}_t &= \hat{\phi}\int_0^{\infty} Y_{ej} B_j (e^{-\Gamma_j z} - R_{bj} e^{\Gamma_j z}) J_1(k_c\rho) k_c dk_c
\end{aligned}
\tag{3.19}
$$

The quantity R_{bj} is the amplitude ratio of backward wave to forward wave of a TM mode at the interface j (between layer j and $j+1$) and it is shown in chapter 2 that there exists a recursive relationship (2.46) between R_{bj} and R_{bj+1} such that R_{bj} of layer$j$ can be computed from that of neighboring layers.

It can also be checked that the longitudinal component of electric field is

$$
E_z = \int_0^{\infty} \frac{B_j}{\Gamma_j} (e^{-\Gamma_j z} - R_{bj} e^{\Gamma_j z}) J_0(k_c\rho) k_c^2 dk_c \tag{3.20}
$$

The transverse field components at the right hand side of the aperture (inside layer 1) are obtained by setting $z = 0^+$ in (3.19):

$$
\begin{aligned}
\vec{E}_t(z=0^+) &= \hat{\rho}\int_0^{\infty} B_1 (1 + R_{b1}) J_1(k_c\rho) k_c dk_c \\
\vec{H}_t(z=0^+) &= \hat{\phi}\int_0^{\infty} Y_{e1} B_1 (1 - R_{b1}) J_1(k_c\rho) k_c dk_c
\end{aligned}
\tag{3.21}
$$

where R_{b1} of layer 1 can be computed from those of neighboring layers.

Matching the tangential E fields and H fields at z=0, an integral equation can be derived for the unknown aperture E field. Equating (3.14) and (3.21) over the aperture of $a \le \rho \le b$, we have

$$A_o \frac{1}{\rho}(1+R) + \sum_{m=1}^{\infty} A_m \Re_m(\rho) = \int_0^{\infty} B_1(1+R_{b1}) J_1(k_c\rho) k_c dk_c \tag{3.22}$$

and

$$A_o \frac{1}{\eta_i}\frac{1}{\rho}(1-R) - \sum_{m=1}^{\infty} Y_{TM} A_m \Re_m(\rho) = \int_0^{\infty} Y_{e1} B_1(1-R_{b1}) J_1(k_c\rho) k_c dk_c \tag{3.23}$$

where $Y_{TM} = \frac{j\omega\epsilon_i}{\Gamma_m}$ and $Y_{e1} = \frac{j\omega\epsilon_1}{\Gamma_1}$.

Equations (3.22) and (3.23) can be cast into an integral equation for the aperture electric field via orthogonality properties. Let $\mathcal{E}(\rho)$ be the E field at z=0, i.e. $E_\rho(z=0)$, then (3.22) becomes

$$A_o \frac{1}{\rho}(1+R) + \sum_{m=1}^{\infty} A_m \Re_m(\rho) = \mathcal{E}(\rho) = \int_0^{\infty} B_1(1+R_{b1}) J_1(k_c\rho) k_c dk_c \tag{3.24}$$

Employing the orthogonality properties and an identity for the Bessel functions , (3.24) can be solved for the unknown amplitudes A_o, A_m and B_1:

Using

$$\begin{cases} \int_0^{\infty} J_1(k_c\rho) J_1(k_c'\rho)\rho d\rho = \delta(k_c - k_c')/k_c \\ \int_a^b \Re_n(\rho)\Re_m(\rho)\rho d\rho = \delta_{nm} \end{cases} \tag{3.25}$$

we have

$$A_o = \frac{1}{(1+R)\ln(b/a)} \int_a^b \mathcal{E}(\rho)d\rho$$

$$A_m = \int_a^b \mathcal{E}(\rho)\Re_m(\rho)\rho d\rho \tag{3.26}$$

$$B_1(k_c) = \frac{1}{(1+R_{b1})} \int_a^b \mathcal{E}(\rho)J_1(k_c\rho)\rho d\rho$$

Also from A_o we have

$$1+R = \frac{1}{A_0 \ln(\frac{b}{a})} \int_a^b \mathcal{E}(\rho)d\rho$$

$$1-R = 2-\frac{1}{A_0 \ln(\frac{b}{a})} \int_a^b \mathcal{E}(\rho)d\rho \tag{3.27}$$

Substituting these amplitude coefficients into (3.23), an integral equation for $\mathcal{E}(\rho)$ is derived as follows:

$$A_o \frac{1}{\eta_i}\frac{1}{\rho}\left(2-\frac{1}{A_0\ln(\frac{b}{a})}\int_a^b \mathcal{E}(\rho')d\rho'\right) - \sum_{m=1}^{\infty} Y_{TM}\Re_m(\rho)\int_a^b \mathcal{E}(\rho')\Re_m(\rho')\rho' d\rho'$$
$$= \int_0^{\infty} Y_{e1}\frac{(1-R_{b1})}{(1+R_{b1})}\left[\int_a^b \mathcal{E}(\rho')J_1(k_c\rho')\rho' d\rho'\right] J_1(k_c\rho)k_c dk_c \tag{3.28}$$

or

$$A_o \frac{2}{\eta_i}\frac{1}{\rho} = \frac{1}{\eta_i}\frac{1}{\rho}\frac{1}{\ln(\frac{b}{a})}\int_a^b \mathcal{E}(\rho')d\rho' + \sum_{m=1}^{\infty} Y_{TM}\Re_m(\rho)\int_a^b \mathcal{E}(\rho')\Re_m(\rho')\rho' d\rho'$$
$$+ \int_0^{\infty} Y_{e1}\frac{(1-R_{b1})}{(1+R_{b1})}\left[\int_a^b \mathcal{E}(\rho')J_1(k_c\rho')\rho' d\rho'\right] J_1(k_c\rho)k_c dk_c \tag{3.29}$$

Before solving (3.29) for the aperture electric field numerically, it is found that there exists singularities in the integrand of the integral w.r.t. k_c. The understanding of the physical meaning for these singularities requires further study which is presented in subsequent sections.

3.2.3 Identification of Complex Waves

The excitation of surface waves, radiative waves and radial guided waves in the open-ended probe structure is investigated in this section [28]. It is found that there exists singularities in the integrand with respect to k_c of the integral equation (3.29), which correspond to the excitation of surface waves for the open-circuit case and radial guided waves for the short-circuit case. The identification of these complex waves is made by examining the EM field expressions via a deformed complex contour integral and is verified in section 3.3 by using the equivalent source concept for the aperture electric field.

With the help of (3.19) and (3.26) the EM fields in layer 1 of the material are derived as

$$E_\rho = \int_0^\infty \left\{ \frac{(e^{-\Gamma_1 z} + R_{b1} e^{\Gamma_1 z})}{(1+R_{b1})} \left[\int_a^b \mathscr{E}(\rho') J_1(k_c\rho') \rho' d\rho' \right] \right\} J_1(k_c\rho) k_c dk_c$$

$$H_\phi = \int_0^\infty \left\{ Y_{e1} \frac{(e^{-\Gamma_1 z} - R_{b1} e^{\Gamma_1 z})}{(1+R_{b1})} \left[\int_a^b \mathscr{E}(\rho') J_1(k_c\rho') \rho' d\rho' \right] \right\} J_1(k_c\rho) k_c dk_c \qquad (3.30)$$

which can be viewed as the EM field representation via the use of inverse Hankel transform.

By recognizing that the expressions inside the braces of (3.30) are odd functions of k_c, an alternative field representation of EM fields in layer 1 via Hankel function $H_1^{(2)}$ is derived using the following formulas:

$$J_1(\rho) = \frac{H_1^{(1)}(\rho) + H_1^{(2)}(\rho)}{2} \qquad (3.31)$$
$$H_1^{(1)}(\rho) = H_1^{(2)}(-\rho)$$

and for an arbitrary odd function $f(k_c)$ we have

$$\begin{aligned}
&\int_0^{\infty} f(k_c) J_1(k_c\rho) k_c dk_c \\
&= \frac{1}{2}\int_0^{\infty} f(k_c)\,[H_1^{(2)}(-k_c\rho) + H_1^{(2)}(k_c\rho)]\, k_c dk_c \\
&= \left\{ \frac{1}{2}\int_0^{-\infty} f(-u) H_1^{(2)}(u\rho)(-u)(-du) \right. \\
&\qquad \left. + \frac{1}{2}\int_0^{\infty} f(k_c) H_1^{(2)}(k_c\rho) k_c dk_c \right\} \\
&= \frac{1}{2}\int_{-\infty}^{\infty} f(k_c) H_1^{(2)}(k_c\rho) k_c dk_c
\end{aligned} \qquad (3.32)$$

Combining (3.31) and (3.32) gives the field representation in layer 1 as follows:

$$E_\rho = \frac{1}{2}\int_{-\infty}^{\infty} \frac{(e^{-\Gamma_1 z} + R_{b1} e^{\Gamma_1 z})}{(1 + R_{b1})} \left[\int_a^b \mathcal{E}(\rho') J_1(k_c\rho')\rho' d\rho' \right] H_1^{(2)}(k_c\rho) k_c dk_c \qquad (3.33)$$
$$H_\phi = \frac{1}{2}\int_{-\infty}^{\infty} Y_{e1} \frac{(e^{-\Gamma_1 z} - R_{b1} e^{\Gamma_1 z})}{(1 + R_{b1})} \left[\int_a^b \mathcal{E}(\rho') J_1(k_c\rho')\rho' d\rho' \right] H_1^{(2)}(k_c\rho) k_c dk_c$$

With (3.33) it can be verified that the roots of $1 + R_{b1} = 0$ correspond to the surface wave pole singularities for the open-circuit case. This is demonstrated by converting the

real-axis integral to a deformed contour integral with a proper choice of branch cuts as shown in fig. 3.2 [22]. By Cauchy theorem the electric field can be deduced to

$$E_\rho = \frac{1}{2}\oint_{C_p} \frac{(e^{-\Gamma_1 z} + R_{b1} e^{\Gamma_1 z})}{(1+R_{b1})} \left[\int_a^b \mathcal{E}(\rho') J_1(k_c \rho') \rho' d\rho' \right] H_1^{(2)}(k_c \rho) k_c dk_c$$
$$+ \frac{1}{2}\int_{C_b} \frac{(e^{-\Gamma_1 z} + R_{b1} e^{\Gamma_1 z})}{(1+R_{b1})} \left[\int_a^b \mathcal{E}(\rho') J_1(k_c \rho') \rho' d\rho' \right] H_1^{(2)}(k_c \rho) k_c dk_c \tag{3.34}$$

where C_p stands for the contours around the surface wave poles and C_b for the contour along the branch cut.

Also the roots of $1+R_{b1}=0$ correspond to the radial guided wave pole singularities for the short-circuit case, which is depicted in fig. 3.3. For this case the electric field can be deduced to

$$E_\rho = \frac{1}{2}\oint_{C_p} \frac{(e^{-\Gamma_1 z} + R_{b1} e^{\Gamma_1 z})}{(1+R_{b1})} \left[\int_a^b \mathcal{E}(\rho') J_1(k_c \rho') \rho' d\rho' \right] H_1^{(2)}(k_c \rho) k_c dk_c \tag{3.35}$$

where C_p stand for the contours around the radial guided wave poles.

Similar expressions can be derived for magnetic field also. In addition, via the formula of Hankel function $H_1^{(2)}$ the integral equation (3.29) can be rearranged as follows:

$$A_o \frac{2}{\eta_i} \frac{1}{\rho} = \frac{1}{\eta_i} \frac{1}{\rho} \frac{1}{\ln(\frac{b}{a})} \int_a^b \mathcal{E}(\rho') d\rho' + \sum_{m=1}^{\infty} Y_{TM} \Re_m(\rho) \int_a^b \mathcal{E}(\rho') \Re_m(\rho') \rho' d\rho'$$
$$+ \frac{1}{2}\int_{-\infty}^{\infty} Y_{e1} \frac{(1-R_{b1})}{(1+R_{b1})} \left[\int_a^b \mathcal{E}(\rho') J_1(k_c \rho') \rho' d\rho' \right] H_1^{(2)}(k_c \rho) k_c dk_c \tag{3.36}$$

The integral equations (3.29) and (3.36) are in the appropriate form for further development of the numerical solution of aperture electric field $\mathcal{E}(\rho)$, using the real axis integration for (3.29) and the integration along branch cuts for (3.36).

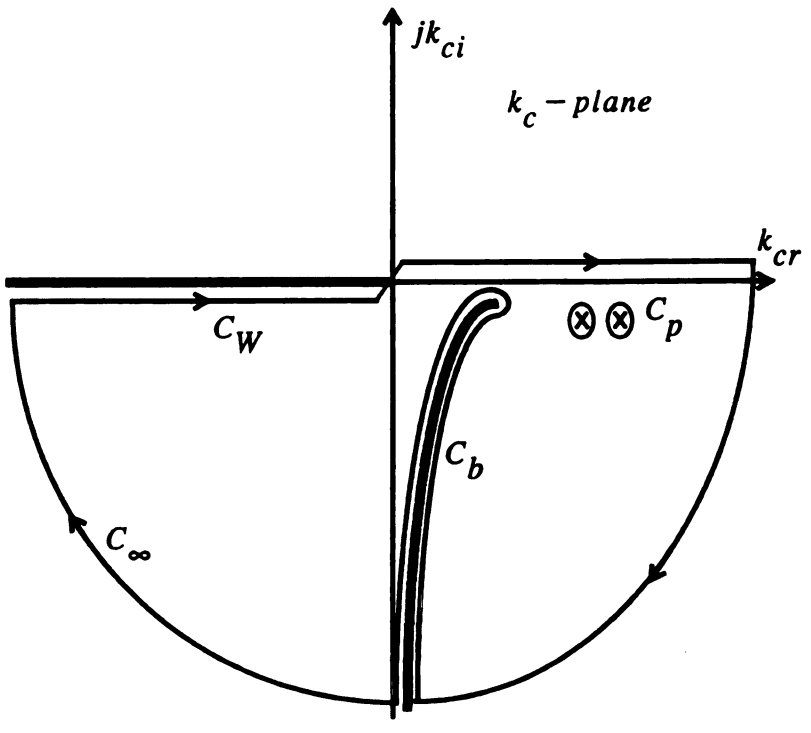

Figure 3.2 Deformed contour integral in complex k_c- plane for open-circuit case.

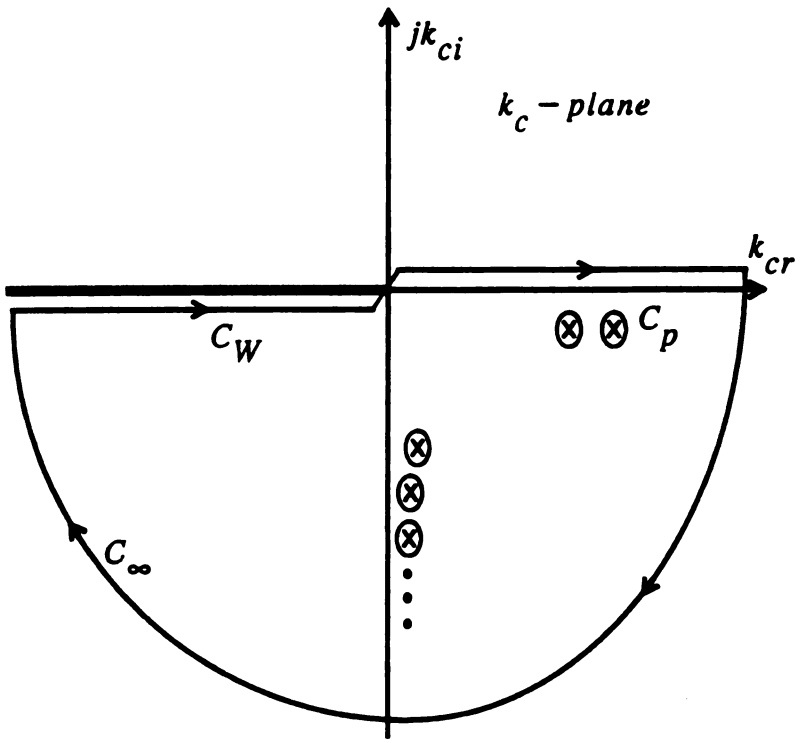

Figure 3.3 Deformed contour integral in complex k_c-plane for short-circuit case.

3.3 Analysis via Equivalent Source Treatment of Aperture Electric Field

In this section the connection between the surface waves/radial guided waves and the singularities in the integrand of the electrical field integral equation (EFIE) for the open-circuit/short-circuit case is studied. The analysis in this section gives an alternative viewpoint and offers another approach to the problem other than the analysis of section 3.2, by which the physical phenomena are revealed clearly.

For the excitation problem of TM modes along a planar dielectric slab waveguide by an annular magnetic current distribution as shown in fig. 3.4, it can be shown that the results do agree with that of the previous section if the aperture electric field is replaced by an equivalent magnetic surface current.

For illustrative purpose an open-circuit case with a 2-layer material is considered in which the excitation of surface waves is well known [21,22]. The analysis of TM mode excitation by a two dimensional surface current source is presented. And by replacing the aperture electric field by an equivalent magnetic surface current, the excited EM fields and the integral equation for the aperture electric field are derived, which are exactly the same as that derived by using a full wave analysis in the previous section. Finally the equation leading to singular points of the integrand in EFIE (3.29) is converted into the exact eigenvalue equation of the surface wave modes.

3.3.1 Wave Equations for EM Field Maintained by Magnetic Current Distribution

In fig. 3.4 a 3-D magnetic current distribution, $\vec{J}_m$, situated over the plane interface between the material and the metallic ground plate is considered. $\vec{J}_m$ is assumed to be rotationally symmetric, and the notation $\vec{E}_1^p$ stands for the primary wave maintained by $\vec{J}_m$ and $\vec{E}_1^s$, $\vec{E}_2^t$ for scattered waves due to contrast between different regions. Only TM

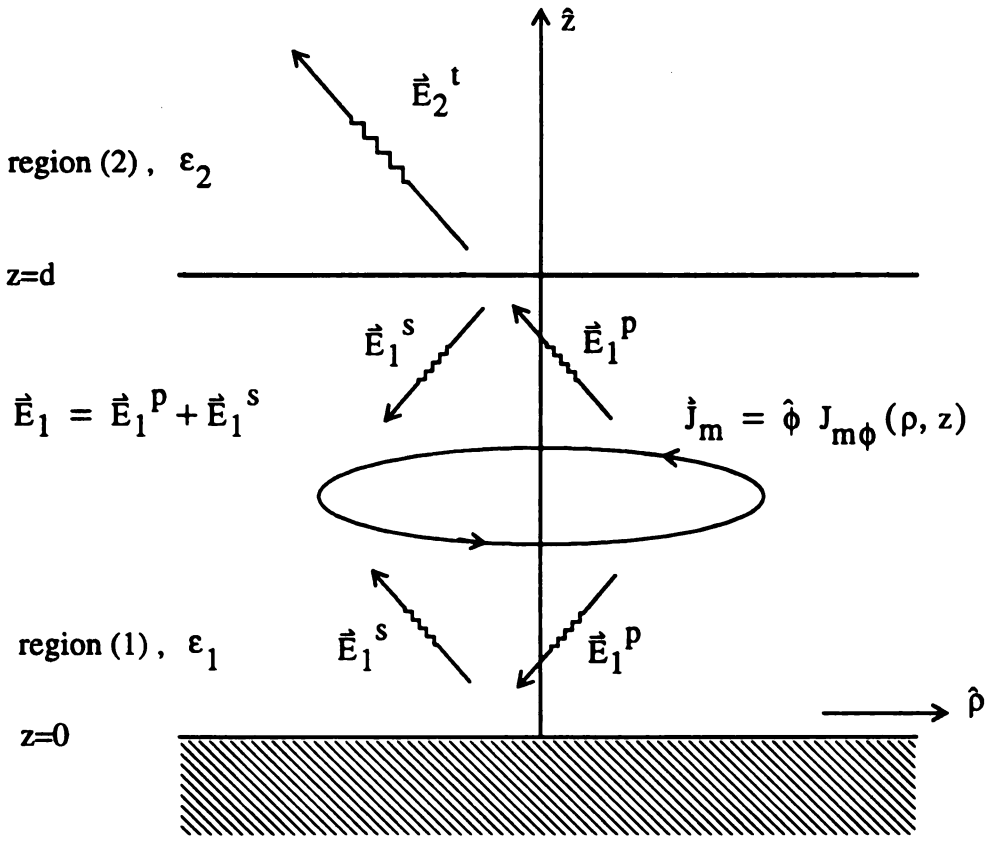

Figure 3.4 Planar waveguide excited by rotationally symmetric magnetic current distribution.

modes with field components E_z, E_ρ and H_ϕ are studied. The wave equations for EM field with magnetic source terms are formulated first in this section, then the solution of the wave equation for magnetic field is derived in next section and the electric field can be deduced from the magnetic field via Ampere's law.

Firstly, let's start with Maxwell's equations for an electric source free region, where $\vec{J}=\rho=0$,

$$\begin{cases} \nabla\bullet\vec{E}=0 \\ \nabla\times\vec{E}=-\vec{J}_m-j\omega\mu\vec{H} \\ \nabla\times\vec{H}=j\omega\epsilon\vec{E} \\ \nabla\bullet\vec{H}=\dfrac{\rho_m}{\mu} \end{cases} \tag{3.37}$$

Taking curl operation on the equation of Ampere's Law leads to

$$\begin{aligned} \nabla\times(\nabla\times\vec{H}) &= j\omega\epsilon\nabla\times\vec{E} \\ \nabla(\nabla\bullet\vec{H})-\nabla^2\vec{H} &= j\omega\epsilon\nabla\times\vec{E} \\ \nabla(\frac{\rho_m}{\mu})-\nabla^2\vec{H} &= -j\omega\epsilon\vec{J}_m+k^2\vec{H} \end{aligned} \tag{3.38}$$

thus the wave equation for $\vec{H}$ is

$$\nabla^2\vec{H}+k^2\vec{H}=\nabla(\frac{\rho_m}{\mu})+j\omega\epsilon\vec{J}_m \tag{3.39}$$

Similarly taking curl operation on the equation of Faraday's Law gives

$$\begin{aligned} \nabla\times(\nabla\times\vec{E}) &= -\nabla\times\vec{J}_m-j\omega\mu\nabla\times\vec{H} \\ \nabla(\nabla\bullet\vec{E})-\nabla^2\vec{E} &= -\nabla\times\vec{J}_m+k^2\vec{E} \end{aligned} \tag{3.40}$$

thus the wave equation for $\vec{E}$ is

$$\nabla^2\vec{E}+k^2\vec{E}=\nabla\times\vec{J}_m \tag{3.41}$$

or

$$\nabla^2\vec{H}+k^2\vec{H}=\nabla(\frac{\rho_m}{\mu})+j\omega\epsilon\vec{J}_m$$
$$\nabla^2\vec{E}+k^2\vec{E}=\nabla\times\vec{J}_m$$

To solve the wave equation (3.39) for H_ϕ, let's first recall the formula of Laplacian operator for a vector field in cylindrical coordinates:

$$\nabla^2\vec{V}=\hat{\rho}(\nabla^2\vec{V})_\rho+\hat{\phi}(\nabla^2\vec{V})_\phi+\hat{z}(\nabla^2\vec{V})_z$$

$$\text{with } (\nabla^2\vec{V})_\rho=\nabla^2V_\rho-\frac{1}{\rho^2}V_\rho-\frac{2}{\rho^2}\frac{\partial V_\phi}{\partial\phi} \tag{3.43}$$

$$(\nabla^2\vec{V})_\phi=\nabla^2V_\phi-\frac{1}{\rho^2}V_\phi+\frac{2}{\rho^2}\frac{\partial V_\rho}{\partial\phi}$$

$$(\nabla^2\vec{V})_z=\nabla^2V_z$$

Secondly, the current is assumed to be $\hat{\phi}J_{m\phi}(\rho,z)$ such that the divergence of $\vec{J}_m$ is zero and the corresponding magnetic charge, ρ_m, is zero. Physically this may happen when the aperture electric field of TM modes in an open-ended coaxial probe is considered and the equivalent source concept is applied. That is, the EM fields at the aperture are

$$\vec{E}(\rho,z)=\hat{\rho}E_\rho+\hat{z}E_z \tag{3.44}$$
$$\vec{H}(\rho,z)=\hat{\phi}H_\phi$$

such that the equivalent sources are

$$\vec{K}_m=-\hat{z}\times\vec{E}|_{z=0}=-\hat{\phi}E_\rho(\rho,0) \tag{3.45}$$
$$\rho_{sm}=-\hat{z}\bullet\vec{H}=0$$

With null magnetic charge and the help of (3.43) the wave equation (3.39) for magnetic field becomes

$$\nabla^2 H_\phi - \frac{1}{\rho^2} H_\phi + k^2 H_\phi = j\omega\epsilon J_{m\phi} \tag{3.46}$$

Due to the rotational symmetry of the structure the Laplacian operator for a scaler field becomes

$$\nabla^2 = \frac{\partial^2}{\partial\rho^2} + \frac{1}{\rho}\frac{\partial}{\partial\rho} + \frac{\partial^2}{\partial z^2} \tag{3.47}$$

Equation (3.46) then becomes

$$\frac{\partial^2}{\partial\rho^2} H_\phi + \frac{1}{\rho}\frac{\partial}{\partial\rho} H_\phi + (k^2 - \frac{1}{\rho^2}) H_\phi + \frac{\partial^2}{\partial z^2} H_\phi = j\omega\epsilon J_{m\phi} \tag{3.48}$$

Wave equation (3.48) can now be solved by exploiting the Hankel transform and the Green's function technique, which is presented in the next section.

3.3.2 Scattered Wave and Primary Wave Solutions of Wave Equation

In this section the complete solutions of the wave equation (3.48) are obtained, which include the homogeneous solutions for the scattered waves with unknown amplitude coefficients and the inhomogeneous solution for the primary wave due to magnetic current source. Then the boundary conditions across the interface of different regions are enforced to determine these unknown amplitudes so that the EM fields are determined, which are shown to be exactly the same as that derived in section 3.2.

Homogeneous solutions for scattered waves

The scattered EM fields due to the contrast of different regions are derived from the homogeneous wave equation via the application of the Hankel transform. Letting $\vec{J}_m = 0$, (3.48) in region (α) becomes,

$$\left[\left(\frac{\partial^2}{\partial\rho^2}+\frac{1}{\rho}\frac{\partial}{\partial\rho}-\frac{1}{\rho^2}\right)+\left(k_a^2+\frac{\partial^2}{\partial z^2}\right)\right]H_\phi=0 \tag{3.49}$$

The integral representation of rotationally symmetric magnetic field via Hankel transform is

$$\begin{cases}\tilde{H}_\phi(\lambda,z)=\int_0^\infty H_\phi(\rho,z)J_1(\lambda\rho)\rho d\rho \\ H_\phi(\rho,z)=\int_0^\infty \tilde{H}_\phi(\lambda,z)J_1(\lambda\rho)\lambda d\lambda\end{cases} \tag{3.50}$$

and the following identity for the Bessel function holds

$$\rho'\int_0^\infty J_1(\lambda\rho)J_1(\lambda\rho')\lambda d\lambda=\delta(\rho-\rho') \tag{3.51}$$

Substituting $H_{a\phi}^s(\rho,z)=\int_0^\infty \tilde{H}_{a\phi}^s(\lambda,z)J_1(\lambda\rho)\lambda d\lambda$ into (3.49) leads to

$$\int_0^\infty\left\{\left(\frac{\partial^2}{\partial\rho^2}+\frac{1}{\rho}\frac{\partial}{\partial\rho}-\frac{1}{\rho^2}\right)J_1(\lambda\rho)\tilde{H}_{a\phi}^s(\lambda,z)+\left(\frac{\partial^2}{\partial z^2}+k_a^2\right)\tilde{H}_{a\phi}^s(\lambda,z)J_1(\lambda\rho)\right\}\lambda d\lambda=0 \tag{3.52}$$

which can be simplified via the definition of $J_1(\lambda\rho)$ to

$$\int_0^\infty\left\{-\lambda^2J_1(\lambda\rho)\tilde{H}_{a\phi}^s(\lambda,z)+\left(\frac{\partial^2}{\partial z^2}+k_a^2\right)\tilde{H}_{a\phi}^s(\lambda,z)J_1(\lambda\rho)\right\}\lambda d\lambda=0 \tag{3.53}$$

or

$$\int_0^\infty\left\{\left(\frac{\partial^2}{\partial z^2}+k_a^2-\lambda^2\right)\tilde{H}_{a\phi}^s(\lambda,z)\right\}J_1(\lambda\rho)\lambda d\lambda=0 \tag{3.54}$$

Equation (3.54) gives

$$\left(\frac{\partial^2}{\partial z^2}-\Gamma_a^2\right)\tilde{H}_{a\phi}^s=0 \tag{3.55}$$

where $-\Gamma_a^2=k_a^2-\lambda^2$.

The solutions of (3.55) are

$$\tilde{H}^s_{\alpha\phi}(\lambda,z) = W^s_\alpha(\lambda) e^{\mp\Gamma_\alpha z} \tag{3.56}$$

With the help of (3.50) and (3.56) the scattered magnetic field in space domain is derived via the inverse Hankel transform,

$$H^s_{\alpha\phi}(\rho,z) = \int_0^\infty W^s_\alpha(\lambda) e^{\mp\Gamma_\alpha z} J_1(\lambda\rho)\lambda d\lambda \tag{3.57}$$

and the electric field can be deduced via Ampere's law as

$$\begin{aligned} E^s_{\alpha\rho} &= -\frac{1}{j\omega\epsilon_\alpha}\frac{\partial}{\partial z} H^s_{\alpha\phi} \\ &= -\frac{1}{j\omega\epsilon_\alpha}\int_0^\infty W^s_\alpha(\lambda)\frac{\partial}{\partial z} e^{\mp\Gamma_\alpha z} J_1(\lambda\rho)\lambda d\lambda \\ &= \pm\int_0^\infty W^s_\alpha(\lambda) Z_\alpha e^{\mp\Gamma_\alpha z} J_1(\lambda\rho)\lambda d\lambda \end{aligned} \tag{3.58}$$

where $Z_\alpha = \Gamma_\alpha / (j\omega\epsilon_\alpha)$ is the wave impedance.

The scattered EM fields are then

$$\boxed{\begin{aligned} E^s_{\alpha\rho} &= \pm\int_0^\infty W^s_\alpha(\lambda) Z_\alpha e^{\mp\Gamma_\alpha z} J_1(\lambda\rho)\lambda d\lambda \\ H^s_{\alpha\phi} &= \int_0^\infty W^s_\alpha(\lambda) e^{\mp\Gamma_\alpha z} J_1(\lambda\rho)\lambda d\lambda \end{aligned}}$$

which are written out explicitly in different regions for further development as follows:

Outgoing transmitted fields in region 2 are

$$\left.\begin{aligned} E^t_{2\rho} &= +\int_0^\infty W^t_2(\lambda) Z_2 e^{-\Gamma_2 z} J_1(\lambda\rho)\lambda d\lambda \\ H^t_{2\phi} &= \int_0^\infty W^t_2(\lambda) e^{-\Gamma_2 z} J_1(\lambda\rho)\lambda d\lambda \end{aligned}\right\} \text{.....} +\hat{z} \text{ direction} \tag{3.60}$$

Outgoing and incoming scattered fields in region 1 are

$$\left.\begin{aligned} E_{1\rho}^{+} &= +\int_0^{\infty} W_1^{+}(\lambda) Z_1 e^{-\Gamma_1 z} J_1(\lambda\rho)\lambda d\lambda \\ H_{1\phi}^{+} &= \int_0^{\infty} W_1^{+}(\lambda) e^{-\Gamma_1 z} J_1(\lambda\rho)\lambda d\lambda \end{aligned}\right\} \text{.....} +\hat{z} \text{ direction}$$

$$\left.\begin{aligned} E_{1\rho}^{-} &= -\int_0^{\infty} W_1^{-}(\lambda) Z_1 e^{+\Gamma_1 z} J_1(\lambda\rho)\lambda d\lambda \\ H_{1\phi}^{-} &= \int_0^{\infty} W_1^{-}(\lambda) e^{+\Gamma_1 z} J_1(\lambda\rho)\lambda d\lambda \end{aligned}\right\} \text{.....} -\hat{z} \text{ direction} \qquad (3.61)$$

Primary wave due to original magnetic current distribution

The Green's function technique is used to solve for the solution of the primary wave. The Green's function for the wave equation due to a ring source is obtained first by the application of Hankel transform and Fourier transform [10,23]. Then the primary magnetic field is deduced from the Green's function by the principle of superposition.

Wave equation (3.48) is rewritten as follows, in region 1,

$$\frac{\partial^2}{\partial\rho^2} H_{1\phi}^{p} + \frac{1}{\rho}\frac{\partial}{\partial\rho} H_{1\phi}^{p} + \left(k_1^2 - \frac{1}{\rho^2}\right) H_{1\phi}^{p} + \frac{\partial^2}{\partial z^2} H_{1\phi}^{p} = j\omega\epsilon J_{m\phi} \qquad (3.62)$$

The Green's function for an unbounded medium 1, due to a ϕ-independent ring source at $\rho=\rho'$, $z=z'$, is defined by

$$\left(\frac{\partial^2}{\partial\rho^2} + \frac{1}{\rho}\frac{\partial}{\partial\rho} + k_1^2 - \frac{1}{\rho^2} + \frac{\partial^2}{\partial z^2}\right) G(\rho,\rho',z,z') = -\frac{\delta(\rho-\rho')\delta(z-z')}{2\pi\rho'} \qquad (3.63)$$

The Hankel transform representation for Green's function and the identity for the Bessel function are

$$\begin{cases} G(\rho,\rho',z) = \int_0^{\infty} \tilde{G}(\lambda,\rho',z) J_1(\lambda\rho)\lambda d\lambda \\ \rho' \int_0^{\infty} J_1(\lambda\rho) J_1(\lambda\rho')\lambda d\lambda = \delta(\rho-\rho') \end{cases} \tag{3.64}$$

Substituting (3.64) into (3.63), we have

$$\begin{aligned} &\int_0^{\infty} \left\{ \left(\frac{\partial^2}{\partial\rho^2} + \frac{1}{\rho}\frac{\partial}{\partial\rho} - \frac{1}{\rho^2}\right) J_1(\lambda\rho)\tilde{G}(\lambda,\rho',z) + \left(\frac{\partial^2}{\partial z^2} + k_1^2\right)\tilde{G}(\lambda,\rho',z) J_1(\lambda\rho) \right\} \lambda d\lambda \\ &\qquad = -\frac{1}{2\pi}\int_0^{\infty} J_1(\lambda\rho) J_1(\lambda\rho')\lambda d\lambda \; \delta(z-z') \end{aligned} \tag{3.65}$$

which can be simplified via the definition of $J_1(\lambda\rho)$ to

$$\begin{aligned} \int_0^{\infty} \Bigg\{ &-\lambda^2 J_1(\lambda\rho)\tilde{G}(\lambda,\rho',z) + \left(\frac{\partial^2}{\partial z^2} + k_1^2\right)\tilde{G}(\lambda,\rho',z) J_1(\lambda\rho) \\ &+ \frac{1}{2\pi}\delta(z-z') J_1(\lambda\rho) J_1(\lambda\rho') \Bigg\} \lambda d\lambda = 0 \end{aligned} \tag{3.66}$$

or

$$\int_0^{\infty} \left\{ \left(\frac{\partial^2}{\partial z^2} + k_1^2 - \lambda^2\right)\tilde{G}(\lambda,\rho',z) + \frac{1}{2\pi}\delta(z-z') J_1(\lambda\rho') \right\} J_1(\lambda\rho)\lambda d\lambda = 0 \tag{3.67}$$

This leads to

$$\begin{aligned} \left(\frac{\partial^2}{\partial z^2} - \Gamma_1^2\right)\tilde{G}(\lambda,\rho',z) &= -\frac{1}{2\pi} J_1(\lambda\rho') \; \delta(z-z') \\ &= -C\,\delta(z-z') \end{aligned} \tag{3.68}$$

where $-\Gamma_1^2 = k_1^2 - \lambda^2$ and $C = \frac{1}{2\pi} J_1(\lambda\rho')$.

Equation (3.68) for $\tilde{G}(\lambda,\rho',z)$ can be solved by exploiting the Fourier transform

$$\mathrm{FT}\{\tilde{G}\} = \int_{-\infty}^{\infty} \tilde{G}(\lambda,\rho',z)e^{-j\eta z}dz$$

$$\tilde{G}(\lambda,\rho',z) = \frac{1}{2\pi}\int_{-\infty}^{\infty} \mathrm{FT}\{\tilde{G}\}e^{j\eta z}d\eta \tag{3.69}$$

and the Cauchy residue theorem of complex analysis.

Skipping the details, the solution of (3.68) can be written as

$$\tilde{G}(\lambda,\rho',z) = \frac{Ce^{-\Gamma_1|z-z'|}}{2\Gamma_1} \tag{3.70}$$

Therefore the Green's function maintained by a ring source is

$$\begin{aligned} G(\rho,\rho',z,z') &= \int_0^{\infty} \frac{Ce^{-\Gamma_1|z-z'|}}{2\Gamma_1} J_1(\lambda\rho)\lambda d\lambda \\ &= \int_0^{\infty} \frac{1}{2\pi}\frac{e^{-\Gamma_1|z-z'|}}{2\Gamma_1} J_1(\lambda\rho')J_1(\lambda\rho)\lambda d\lambda \end{aligned} \tag{3.71}$$

And the primary magnetic field maintained by $J_{m\phi}$ is derived from the Green's function by the principle of superposition as

$$\begin{aligned} H_{1\phi}^{p} &= \iiint_V dv'(-j\omega\epsilon_1 J_{m\phi})\int_0^{\infty} \frac{1}{2\pi}\frac{e^{-\Gamma_1|z-z'|}}{2\Gamma_1} J_1(\lambda\rho')J_1(\lambda\rho)\lambda d\lambda \\ &= \iint d\rho' dz'(-j\omega\epsilon_1 J_{m\phi})\int_0^{\infty} \frac{e^{-\Gamma_1|z-z'|}}{2\Gamma_1}\rho' J_1(\lambda\rho')J_1(\lambda\rho)\lambda d\lambda \end{aligned} \tag{3.72}$$

Also the electric field is deduced via Ampere's law as

$$E_{1\rho}^{p} = \iint d\rho' dz'(-j\omega\epsilon_1 J_{m\phi})\int_0^{\infty} (\pm Z_1)\frac{e^{-\Gamma_1|z-z'|}}{2\Gamma_1}\rho' J_1(\lambda\rho')J_1(\lambda\rho)\lambda d\lambda \tag{3.73}$$

where $\pm Z_1$ in $E_{1\rho}^{p}$ stands for

$$\begin{cases} +Z_1 \text{ ... for primary wave in } +\hat{z} \text{ direction, } z>z' \\ -Z_1 \text{ ... for primary wave in } -\hat{z} \text{ direction, } z<z' \end{cases} \tag{3.74}$$

These results can be specialized for the EM fields maintained by a disk magnetic current $\vec{K}_m = \hat{\phi} K_{m\phi}$ at $z = z''$. The equivalent magnetic surface current at the aperture of an open-ended coaxial probe is a practical example.

If the current is distributed from $\rho = a$ to $\rho = b$, the primary fields maintained by a disk current $K_{m\phi}$ are derived by substitution of $J_{m\phi} = K_{m\phi}(\rho)\delta(z'-z'')$ in (3.72) and (3.73)

$$H_{1\phi}^{p} = \int_a^b d\rho'(-j\omega\epsilon_1 K_{m\phi}) \int_0^\infty \frac{e^{-\Gamma_1|z-z''|}}{2\Gamma_1} \rho' J_1(\lambda\rho') J_1(\lambda\rho)\lambda d\lambda$$

$$E_{1\rho}^{p} = \int_a^b d\rho'(-j\omega\epsilon_1 K_{m\phi}) \int_0^\infty (\pm Z_1) \frac{e^{-\Gamma_1|z-z''|}}{2\Gamma_1} \rho' J_1(\lambda\rho') J_1(\lambda\rho)\lambda d\lambda$$

The summary of scattered fields and primary fields is given below for further development.

Outgoing transmitted fields in region 2 are

$$\left.\begin{aligned} E_{2\rho}^{t} &= +\int_0^\infty W_2^t(\lambda) Z_2 e^{-\Gamma_2 z} J_1(\lambda\rho)\lambda d\lambda \\ H_{2\phi}^{t} &= \int_0^\infty W_2^t(\lambda) e^{-\Gamma_2 z} J_1(\lambda\rho)\lambda d\lambda \end{aligned}\right\} \text{.....} +\hat{z} \text{ direction} \tag{3.76}$$

Outgoing and incoming scattered fields in region 1 are

$$\left.\begin{aligned} E_{1\rho}^{+} &= +\int_0^\infty W_1^+(\lambda) Z_1 e^{-\Gamma_1 z} J_1(\lambda\rho)\lambda d\lambda \\ H_{1\phi}^{+} &= \int_0^\infty W_1^+(\lambda) e^{-\Gamma_1 z} J_1(\lambda\rho)\lambda d\lambda \end{aligned}\right\} \text{.....} +\hat{z} \textit{ direction} \tag{3.77}$$

$$\left.\begin{aligned} E_{1\rho}^{-} &= -\int_0^{\infty} W_1^{-}(\lambda) Z_1 e^{+\Gamma_1 z} J_1(\lambda\rho)\lambda d\lambda \\ H_{1\phi}^{-} &= \int_0^{\infty} W_1^{-}(\lambda) e^{+\Gamma_1 z} J_1(\lambda\rho)\lambda d\lambda \end{aligned}\right\} \text{.....} -\hat{z} \textit{ direction} \qquad (3.78)$$

Primary fields in region 1 are, letting $z'' \to z'$,

$$\begin{aligned} H_{1\phi}^{p} &= \int_a^b d\rho'(-j\omega\epsilon_1 K_{m\phi}) \int_0^{\infty} \frac{e^{-\Gamma_1|z-z'|}}{2\Gamma_1} \rho' J_1(\lambda\rho') J_1(\lambda\rho)\lambda d\lambda \\ E_{1\rho}^{p} &= \int_a^b d\rho'(-j\omega\epsilon_1 K_{m\phi}) \int_0^{\infty} (\pm Z_1) \frac{e^{-\Gamma_1|z-z'|}}{2\Gamma_1} \rho' J_1(\lambda\rho') J_1(\lambda\rho)\lambda d\lambda \end{aligned} \qquad (3.79)$$

Application of Boundary Conditions to Determine W_2^t, W_1^+ **and** W_1^-

The continuity of tangential EM field is applied to determine unknown amplitudes, W_2^t, W_1^+ and W_1^-, of the scattered fields due to the contrast from different regions. The total fields in regions 1 and 2 are

$$\begin{aligned} H_{2\phi} &= H_{2\phi}^{t} \\ E_{2\rho} &= E_{2\rho}^{t} \\ H_{1\phi} &= H_{1\phi}^{p} + H_{1\phi}^{+} + H_{1\phi}^{-} \\ E_{1\rho} &= E_{1\rho}^{p} + E_{1\rho}^{+} + E_{1\rho}^{-} \end{aligned} \qquad (3.80)$$

and the boundary conditions are

B.C. at $z=0$ $\quad E_{1\rho}=0$

B.C. at $z=d$ $\quad E_{2\rho}=E_{1\rho}$ & $H_{2\phi}=H_{1\phi}$

Since there are three unknowns and three boundary conditions, an unique solution is guaranteed. With the help of (3.76) to (3.79), the application of B.C. at $z=0$ leads to

$$\int_a^b d\rho'(-j\omega\epsilon_1 K_{m\phi})\int_0^\infty (-Z_1)\frac{e^{-\Gamma_1 z'}}{2\Gamma_1}\rho' J_1(\lambda\rho')J_1(\lambda\rho)\lambda d\lambda$$

$$+\int_0^\infty W_1^+(\lambda)Z_1 J_1(\lambda\rho)\lambda d\lambda - \int_0^\infty W_1^-(\lambda)Z_1 J_1(\lambda\rho)\lambda d\lambda \tag{3.81}$$

$$=\int_0^\infty \left\{(-Z_1)\left[\int_a^b (-j\omega\epsilon_1 K_{m\phi})\frac{e^{-\Gamma_1 z'}}{2\Gamma_1}\rho' J_1(\lambda\rho')d\rho' - W_1^+(\lambda) - W_1^-(\lambda)\right]\right\} J_1(\lambda\rho)\lambda d\lambda = 0$$

This implies that the integrand of (3.81) is zero, or

$$-W_1^+ + W_1^- = -V_1(0) \tag{3.82}$$

where

$$V_1(0) = \int_a^b (-j\omega\epsilon_1 K_{m\phi})\frac{e^{-\Gamma_1 z'}}{2\Gamma_1}\rho' J_1(\lambda\rho')d\rho' \tag{3.83}$$

With the help of (3.76) to (3.79), the application of B.C. at $z=d$ for the electric field leads to

$$\int_0^\infty W_2^t Z_2 e^{-\Gamma_2 d} J_1(\lambda\rho)\lambda d\lambda = \int_a^b d\rho'(-j\omega\epsilon_1 K_{m\phi})\int_0^\infty (Z_1)\frac{e^{-\Gamma_1(d-z')}}{2\Gamma_1}\rho' J_1(\lambda\rho')J_1(\lambda\rho)\lambda d\lambda \tag{3.84}$$

$$+\int_0^\infty W_1^+(\lambda)Z_1 e^{-\Gamma_1 d} J_1(\lambda\rho)\lambda d\lambda - \int_0^\infty W_1^-(\lambda)Z_1 e^{\Gamma_1 d} J_1(\lambda\rho)\lambda d\lambda$$

or

$$\int_0^\infty \left\{(Z_1)\int_a^b (-j\omega\epsilon_1 K_{m\phi})\frac{e^{-\Gamma_1(d-z')}}{2\Gamma_1}\rho' J_1(\lambda\rho')d\rho'\right. \tag{3.85}$$

$$\left. -W_2^t Z_2 e^{-\Gamma_2 d} + W_1^+(\lambda)Z_1 e^{-\Gamma_1 d} - W_1^-(\lambda)Z_1 e^{+\Gamma_1 d}\right\} J_1(\lambda\rho)\lambda d\lambda = 0$$

and this gives

$$W_1^+\frac{Z_1}{Z_2}e^{-\Gamma_1 d} - W_1^-\frac{Z_1}{Z_2}e^{\Gamma_1 d} - W_2^t e^{-\Gamma_2 d} = -\frac{Z_1}{Z_2}V_1(d) \tag{3.86}$$

where

$$V_1(d) = \int_a^b (-j\omega\epsilon_1 K_{m\phi}) \frac{e^{-\Gamma_1(d-z')}}{2\Gamma_1} \rho' J_1(\lambda\rho') d\rho' \tag{3.87}$$

With the help of (3.76) to (3.79), the application of B.C. at $z=d$ for the magnetic field leads to

$$\begin{aligned} \int_0^\infty W_2^t e^{-\Gamma_2 d} J_1(\lambda\rho)\lambda d\lambda = \int_a^b d\rho' (-j\omega\epsilon_1 K_{m\phi}) \int_0^\infty \frac{e^{-\Gamma_1(d-z')}}{2\Gamma_1} \rho' J_1(\lambda\rho') J_1(\lambda\rho)\lambda d\lambda \\ + \int_0^\infty W_1^+(\lambda) e^{-\Gamma_1 d} J_1(\lambda\rho)\lambda d\lambda + \int_0^\infty W_1^-(\lambda) e^{\Gamma_1 d} J_1(\lambda\rho)\lambda d\lambda \end{aligned} \tag{3.88}$$

or

$$\begin{aligned} \int_0^\infty \Bigg\{ \int_a^b (-j\omega\epsilon_1 K_{m\phi}) \frac{e^{-\Gamma_1(d-z')}}{2\Gamma_1} \rho' J_1(\lambda\rho') d\rho' \\ - W_2^t e^{-\Gamma_2 d} + W_1^+(\lambda) e^{-\Gamma_1 d} + W_1^-(\lambda) e^{+\Gamma_1 d} \Bigg\} J_1(\lambda\rho)\lambda d\lambda = 0 \end{aligned} \tag{3.89}$$

and this leads to

$$-W_1^+ e^{-\Gamma_1 d} - W_1^- e^{\Gamma_1 d} + W_2^t e^{-\Gamma_2 d} = V_1(d) \tag{3.90}$$

Equations (3.82), (3.86) and (3.90) can be used to solve for W_1^+, W_1^-.

Adding (3.86) and (3.90) gives

$$\begin{aligned} (-1+\frac{Z_1}{Z_2}) W_1^+ e^{-\Gamma_1 d} - (1+\frac{Z_1}{Z_2}) W_1^- e^{\Gamma_1 d} = (1-\frac{Z_1}{Z_2}) V_1(d) \\ - \left(\frac{Z_2-Z_1}{Z_2+Z_1}\right) W_1^+ e^{-2\Gamma_1 d} - W_1^- = \frac{Z_2-Z_1}{Z_2+Z_1} e^{-\Gamma_1 d} V_1(d) \end{aligned} \tag{3.91}$$

or

$$-R_{12} W_1^+ e^{-2\Gamma_1 d} - W_1^- = R_{12} e^{-\Gamma_1 d} V_1(d) \tag{3.92}$$

where

$$R_{12} = (Z_2 - Z_1)/(Z_2 + Z_1) \tag{3.93}$$

Adding (3.82) and (3.92) results in

$$-(1 + R_{12} e^{-2\Gamma_1 d}) W_1^+ = -V_1(0) + R_{12} e^{-\Gamma_1 d} V_1(d) \tag{3.94}$$

or

$$W_1^+ = \frac{V_1(0) - R_{12} e^{-\Gamma_1 d} V_1(d)}{1 + R_{12} e^{-2\Gamma_1 d}} \tag{3.95}$$

From (3.86), we have

$$W_1^- = W_1^+ - V_1(0) = \frac{-R_{12} e^{-2\Gamma_1 d} V_1(0) - R_{12} e^{-\Gamma_1 d} V_1(d)}{1 + R_{12} e^{-2\Gamma_1 d}} \tag{3.96}$$

Knowing W_1^+, W_1^-, the EM field expressions in region 1 are now ready to be carried out.

Electromagnetic Fields in region 1

The EM field expressions in region 1 for a general 2-dimensional magnetic disk current $\vec{K}_m = \hat{\phi} K_{m\phi}(\rho)$ are derived here. And the results are specialized to the case of an open-ended coaxial probe when the 2-dimensional magnetic current resides right on the metallic ground plane.

The EM fields in region 1 are the sum of the primary wave and the scattered waves as follows. For the electric field,

$$E_{1\rho} = E_{1\rho}^p + E_{1\rho}^+ + E_{1\rho}^- \tag{3.97}$$

where

$$E_{1\rho}^{p} = \int_{a}^{b} d\rho'(-j\omega\epsilon_1 K_{m\phi}) \int_{0}^{\infty} (\pm Z_1) \frac{e^{-\Gamma_1|z-z'|}}{2\Gamma_1} \rho' J_1(\lambda\rho') J_1(\lambda\rho)\lambda d\lambda$$

$$E_{1\rho}^{+} = \int_{0}^{\infty} \frac{V_1(0) - R_{12}e^{-\Gamma_1 d}V_1(d)}{1 + R_{12}e^{-2\Gamma_1 d}} Z_1 e^{-\Gamma_1 z} J_1(\lambda\rho)\lambda d\lambda \tag{3.98}$$

$$E_{1\rho}^{-} = -\int_{0}^{\infty} \frac{-R_{12}e^{-2\Gamma_1 d}V_1(0) - R_{12}e^{-\Gamma_1 d}V_1(d)}{1 + R_{12}e^{-2\Gamma_1 d}} Z_1 e^{\Gamma_1 z} J_1(\lambda\rho)\lambda d\lambda$$

Substituting $V_1(0)$ and $V_1(d)$ in (3.98), the expressions for $E_{1\rho}^{+}$ and $E_{1\rho}^{-}$ can be arranged in a form similar to $E_{1\rho}^{p}$:

$$\begin{aligned} E_{1\rho}^{+} &= \int_{a}^{b} d\rho'(-j\omega\epsilon_1 K_{m\phi}) \int_{0}^{\infty} \frac{1}{1 + R_{12}e^{-2\Gamma_1 d}} Z_1 \frac{e^{-\Gamma_1(z+z')}}{2\Gamma_1} \rho' J_1(\lambda\rho') J_1(\lambda\rho)\lambda d\lambda \\ &+ \int_{a}^{b} d\rho'(-j\omega\epsilon_1 K_{m\phi}) \int_{0}^{\infty} \frac{-R_{12}e^{-2\Gamma_1 d}}{1 + R_{12}e^{-2\Gamma_1 d}} Z_1 \frac{e^{-\Gamma_1(z-z')}}{2\Gamma_1} \rho' J_1(\lambda\rho') J_1(\lambda\rho)\lambda d\lambda \end{aligned} \tag{3.99}$$

and

$$\begin{aligned} E_{1\rho}^{-} &= \int_{a}^{b} d\rho'(-j\omega\epsilon_1 K_{m\phi}) \int_{0}^{\infty} \frac{R_{12}e^{-2\Gamma_1 d}}{1 + R_{12}e^{-2\Gamma_1 d}} Z_1 \frac{e^{\Gamma_1(z-z')}}{2\Gamma_1} \rho' J_1(\lambda\rho') J_1(\lambda\rho)\lambda d\lambda \\ &+ \int_{a}^{b} d\rho'(-j\omega\epsilon_1 K_{m\phi}) \int_{0}^{\infty} \frac{R_{12}e^{-2\Gamma_1 d}}{1 + R_{12}e^{-2\Gamma_1 d}} Z_1 \frac{e^{\Gamma_1(z+z')}}{2\Gamma_1} \rho' J_1(\lambda\rho') J_1(\lambda\rho)\lambda d\lambda \end{aligned} \tag{3.100}$$

Similarly the magnetic field in region 1 can be expressed as the sum of the primary wave and the scattered waves as follows

$$H_{1\phi} = H_{1\phi}^{p} + H_{1\phi}^{+} + H_{1\phi}^{-} \tag{3.101}$$

where

$$H_{1\phi}^{p}=\int_{a}^{b}d\rho'(-j\omega\varepsilon_1 K_{m\phi})\int_{0}^{\infty}\frac{e^{-\Gamma_1|z-z'|}}{2\Gamma_1}\rho' J_1(\lambda\rho')J_1(\lambda\rho)\lambda d\lambda$$

$$H_{1\phi}^{+}=\int_{0}^{\infty}\frac{V_1(0)-R_{12}e^{-\Gamma_1 d}V_1(d)}{1+R_{12}e^{-2\Gamma_1 d}}e^{-\Gamma_1 z}J_1(\lambda\rho)\lambda d\lambda \qquad (3.102)$$

$$H_{1\phi}^{-}=\int_{0}^{\infty}\frac{-R_{12}e^{-2\Gamma_1 d}V_1(0)-R_{12}e^{-\Gamma_1 d}V_1(d)}{1+R_{12}e^{-2\Gamma_1 d}}e^{\Gamma_1 z}J_1(\lambda\rho)\lambda d\lambda$$

Substituting $V_1(0)$ and $V_1(d)$ in (3.102), the expressions for $H_{1\phi}^{+}$ and $H_{1\phi}^{-}$ can be arranged in a form similar to $H_{1\phi}^{p}$,

$$\begin{aligned}H_{1\phi}^{+}=&\int_{a}^{b}d\rho'(-j\omega\varepsilon_1 K_{m\phi})\int_{0}^{\infty}\frac{1}{1+R_{12}e^{-2\Gamma_1 d}}\frac{e^{-\Gamma_1(z+z')}}{2\Gamma_1}\rho' J_1(\lambda\rho')J_1(\lambda\rho)\lambda d\lambda\\&+\int_{a}^{b}d\rho'(-j\omega\varepsilon_1 K_{m\phi})\int_{0}^{\infty}\frac{-R_{12}e^{-2\Gamma_1 d}}{1+R_{12}e^{-2\Gamma_1 d}}\frac{e^{-\Gamma_1(z-z')}}{2\Gamma_1}\rho' J_1(\lambda\rho')J_1(\lambda\rho)\lambda d\lambda\end{aligned} \qquad (3.103)$$

and

$$\begin{aligned}H_{1\phi}^{-}=&\int_{a}^{b}d\rho'(-j\omega\varepsilon_1 K_{m\phi})\int_{0}^{\infty}\frac{-R_{12}e^{-2\Gamma_1 d}}{1+R_{12}e^{-2\Gamma_1 d}}\frac{e^{\Gamma_1(z-z')}}{2\Gamma_1}\rho' J_1(\lambda\rho')J_1(\lambda\rho)\lambda d\lambda\\&+\int_{a}^{b}d\rho'(-j\omega\varepsilon_1 K_{m\phi})\int_{0}^{\infty}\frac{-R_{12}e^{-2\Gamma_1 d}}{1+R_{12}e^{-2\Gamma_1 d}}\frac{e^{\Gamma_1(z+z')}}{2\Gamma_1}\rho' J_1(\lambda\rho')J_1(\lambda\rho)\lambda d\lambda\end{aligned} \qquad (3.104)$$

To utilize the above results for the EM fields of an open-ended coaxial probe $z'=0$, $z>0$ is assumed such that

$$\begin{aligned}V_1(0)&=\int_a^b(-j\omega\varepsilon_1 K_{m\phi})\frac{1}{2\Gamma_1}\rho' J_1(\lambda\rho')d\rho'\\V_1(d)&=\int_a^b(-j\omega\varepsilon_1 K_{m\phi})\frac{e^{-\Gamma_1 d}}{2\Gamma_1}\rho' J_1(\lambda\rho')d\rho'\end{aligned} \qquad (3.105)$$

From (3.97) to (3.100), the electric fields can then be expressed as

$$E_{1\rho}^{p} = \int_a^b d\rho'(-j\omega\epsilon_1 K_{m\phi}) \int_0^\infty Z_1 \frac{e^{-\Gamma_1 z}}{2\Gamma_1} \rho' J_1(\lambda\rho') J_1(\lambda\rho) \lambda d\lambda$$

$$E_{1\rho}^{+} = \int_a^b d\rho'(-j\omega\epsilon_1 K_{m\phi}) \int_0^\infty \frac{1 - R_{12} e^{-2\Gamma_1 d}}{1 + R_{12} e^{-2\Gamma_1 d}} Z_1 \frac{e^{-\Gamma_1 z}}{2\Gamma_1} \rho' J_1(\lambda\rho') J_1(\lambda\rho) \lambda d\lambda \qquad (3.106)$$

$$E_{1\rho}^{-} = \int_a^b d\rho'(-j\omega\epsilon_1 K_{m\phi}) \int_0^\infty \frac{2R_{12} e^{-2\Gamma_1 d}}{1 + R_{12} e^{-2\Gamma_1 d}} Z_1 \frac{e^{\Gamma_1 z}}{2\Gamma_1} \rho' J_1(\lambda\rho') J_1(\lambda\rho) \lambda d\lambda$$

Letting R_{b1} be $R_{12} e^{-2\Gamma_1 d}$, the total transverse electric field then becomes

$$\begin{aligned} E_{1\rho} &= E_{1\rho}^{p} + E_{1\rho}^{+} + E_{1\rho}^{-} \\ &= \int_a^b d\rho'(-j\omega\epsilon_1 K_{m\phi}) \int_0^\infty \frac{2}{1 + R_{b1}} Z_1 \frac{e^{-\Gamma_1 z}}{2\Gamma_1} \rho' J_1(\lambda\rho') J_1(\lambda\rho) \lambda d\lambda \\ &\quad + \int_a^b d\rho'(-j\omega\epsilon_1 K_{m\phi}) \int_0^\infty \frac{2R_{b1}}{1 + R_{b1}} Z_1 \frac{e^{\Gamma_1 z}}{2\Gamma_1} \rho' J_1(\lambda\rho') J_1(\lambda\rho) \lambda d\lambda \qquad (3.107) \\ &= \int_a^b d\rho'\left(-\frac{j\omega\epsilon_1}{\Gamma_1} Z_1 K_{m\phi}\right) \int_0^\infty \frac{e^{-\Gamma_1 z} + R_{b1} e^{\Gamma_1 z}}{1 + R_{b1}} \rho' J_1(\lambda\rho') J_1(\lambda\rho) \lambda d\lambda \\ &= \int_a^b d\rho'(-K_{m\phi}) \int_0^\infty \frac{e^{-\Gamma_1 z} + R_{b1} e^{\Gamma_1 z}}{1 + R_{b1}} \rho' J_1(\lambda\rho') J_1(\lambda\rho) \lambda d\lambda \end{aligned}$$

Replacing the aperture electric field by an equivalent surface current, that is $E_{1\rho}(z=o^{+}) = -K_{m\phi}$, the electric field for an open-ended coaxial probe is derived as

$$E_{1\rho} = \int_a^b d\rho' E_{1\rho}(z=0^{+}) \int_0^\infty \frac{e^{-\Gamma_1 z} + R_{b1} e^{\Gamma_1 z}}{1 + R_{b1}} \rho' J_1(\lambda\rho') J_1(\lambda\rho) \lambda d\lambda \qquad (3.108)$$

$$= \int_0^\infty \frac{e^{-\Gamma_1 z} + R_{b1} e^{\Gamma_1 z}}{1 + R_{b1}} \left(\int_a^b E_{1\rho}(z=0^{+}) J_1(\lambda\rho') \rho' d\rho' \right) J_1(\lambda\rho) \lambda d\lambda$$

Equation (3.108) is exactly the same as (3.30), which was derived by the previous approach, if the dummy variable λ is changed to k_c.

Similarly from (3.101) to (3.104), letting $z' = 0$ the magnetic fields can be expressed as

$$
\begin{aligned}
H_{1\phi}^{p} &= \int_a^b d\rho'(-j\omega\varepsilon_1 K_{m\phi}) \int_0^\infty \frac{e^{-\Gamma_1 z}}{2\Gamma_1} \rho' J_1(\lambda\rho') J_1(\lambda\rho)\lambda d\lambda \\
H_{1\phi}^{+} &= \int_a^b d\rho'(-j\omega\varepsilon_1 K_{m\phi}) \int_0^\infty \frac{1-R_{12}e^{-2\Gamma_1 d}}{1+R_{12}e^{-2\Gamma_1 d}} \frac{e^{-\Gamma_1 z}}{2\Gamma_1} \rho' J_1(\lambda\rho') J_1(\lambda\rho)\lambda d\lambda \\
H_{1\phi}^{-} &= \int_a^b d\rho'(-j\omega\varepsilon_1 K_{m\phi}) \int_0^\infty \frac{-2R_{12}e^{-2\Gamma_1 d}}{1+R_{12}e^{-2\Gamma_1 d}} \frac{e^{\Gamma_1 z}}{2\Gamma_1} \rho' J_1(\lambda\rho') J_1(\lambda\rho)\lambda d\lambda
\end{aligned}
\tag{3.109}
$$

Since R_{bl} is $R_{12}e^{-2\Gamma_1 d}$, the total transverse magnetic field becomes

$$
\begin{aligned}
H_{1\phi} &= H_{1\phi}^{p} + H_{1\phi}^{+} + H_{1\phi}^{-} \\
&= \int_a^b d\rho'(-j\omega\varepsilon_1 K_{m\phi}) \int_0^\infty \frac{2}{1+R_{bl}} \frac{e^{-\Gamma_1 z}}{2\Gamma_1} \rho' J_1(\lambda\rho') J_1(\lambda\rho)\lambda d\lambda \\
&\quad + \int_a^b d\rho'(-j\omega\varepsilon_1 K_{m\phi}) \int_0^\infty \frac{-2R_{bl}}{1+R_{bl}} \frac{e^{\Gamma_1 z}}{2\Gamma_1} \rho' J_1(\lambda\rho') J_1(\lambda\rho)\lambda d\lambda \\
&= \int_a^b d\rho'(-Y_{e1} K_{m\phi}) \int_0^\infty \frac{e^{-\Gamma_1 z} - R_{bl}e^{\Gamma_1 z}}{1+R_{bl}} \rho' J_1(\lambda\rho') J_1(\lambda\rho)\lambda d\lambda
\end{aligned}
\tag{3.110}
$$

where $Y_{e1} = \dfrac{j\omega\varepsilon_1}{\Gamma_1}$ is the wave admittance.

Replacing the aperture electric field by an equivalent surface current, that is $E_{1\rho}(z=o^+) = -K_{m\phi}$, the magnetic field for an open-ended coaxial probe is derived as

$$H_{1\phi} = \int_a^b d\rho' Y_{e1} E_{1\rho}(z=0^+) \int_0^\infty \frac{e^{-\Gamma_1 z} - R_{b1} e^{\Gamma_1 z}}{1+R_{b1}} \rho' J_1(\lambda\rho') J_1(\lambda\rho)\lambda d\lambda$$
$$= \int_0^\infty Y_{e1} \frac{e^{-\Gamma_1 z} - R_{b1} e^{\Gamma_1 z}}{1+R_{b1}} \left(\int_a^b E_{1\rho}(z=0^+) J_1(\lambda\rho')\rho' d\rho' \right) J_1(\lambda\rho)\lambda d\lambda \tag{3.111}$$

Equation (3.111) is exactly the same as (3.30), which was derived previously, if dummy variable λ is changed to k_c.

It has been shown that the same EM fields are excited when the aperture electric field is replaced by an equivalent surface current. Consequently, the same integral equation for the aperture electric field can be derived. What is left to be verified is that the roots of $1+R_{b1}=0$ correspond to the surface wave pole singularities in this TM open-circuit case with a 2-layer medium.

With the help of (3.93) and the definition of R_{b1}, R_{b1} is shown to be

$$e^{-2\Gamma_1 d} \frac{\Gamma_2/\Gamma_1 - \epsilon_2/\epsilon_1}{\Gamma_2/\Gamma_1 + \epsilon_2/\epsilon_1} \tag{3.112}$$

where $\Gamma_i = (k_c^2 - k_i^2)^{1/2}$, $i=1,2$.

The relation of $1+R_{b1}=0$ can be rewritten as

$$1+R_{b1} = 1+e^{-2\Gamma_1 d} \frac{\Gamma_2/\Gamma_1 - \epsilon_2/\epsilon_1}{\Gamma_2/\Gamma_1 + \epsilon_2/\epsilon_1} = 0 \tag{3.113}$$

which can be arranged to be

$$\frac{1-e^{-2\Gamma_1 d}}{1+e^{-2\Gamma_1 d}} = -\frac{\Gamma_2}{\Gamma_1}\frac{\epsilon_1}{\epsilon_2} \tag{3.114}$$

It can be easily check that the roots exist only in range of $k_2 \le k_c \le k_1$. Thus letting

$$\Gamma_1 = jK_1 = j(k_1^2 - k_c^2)^{\frac{1}{2}} \tag{3.115}$$

then (3.114) becomes

$$\frac{1-e^{-2jK_1d}}{1+e^{-2jK_1d}} = -\frac{\Gamma_2}{jK_1}\frac{e_1}{e_2} \tag{3.116}$$

The left hand side is equivalent to $j\tan(K_1 d)$ so that

$$\tan(K_1 d) = \frac{\Gamma_2}{K_1}\frac{e_1}{e_2} \tag{3.117}$$

Equation (3.117) is the well known eigenvalue equation of TM surface wave modes for a dielectric slab waveguide.

3.4 Numerical Simulation - Method of Moments

In this section the method of moments is employed to solve the EFIE (3.29) [29]. The TM eigenmodes of the coaxial line are chosen to be the basis functions for the unknown aperture field and Galerkin's technique is used to convert the integral equation into a set of simultaneous algebraic equations, from which the numerical solution of aperture electric field is obtained and the input admittance at the aperture is resolved. Finally some verifications of the correct numerical implementation are also shown in this section.

The unknown aperture electric field is expanded into a finite sum of TM eigenmodes of the coaxial probe as follows:

$$\mathcal{E}(\rho) = \sum_{i=0}^{S} V_i \mathcal{R}_i(\rho) \tag{3.118}$$

where

$$\mathcal{R}_i(\rho) = \begin{cases} C_i\left[J_1(k_{ci}\rho)Y_0(k_{ci}a) - J_0(k_{ci}a)Y_1(k_{ci}\rho)\right] & \cdots i \neq 0 \\ \dfrac{1}{\rho} & \cdots i = 0 \end{cases} \tag{3.119}$$

and k_{ci} satisfies the following eigenvalue equation [30]

$$J_o(k_{ci}a)Y_o(k_{ci}b)-J_o(k_{ci}b)Y_o(k_{ci}a)=0 \tag{3.120}$$

Substituting (3.118) in the integral equation (3.29) leads to (from now on let $\eta_i \to \eta_o$ for simplicity),

$$\begin{aligned} A_o\frac{2}{\eta_o}\frac{1}{\rho} &= \frac{1}{\eta_o}\frac{1}{\rho}\frac{1}{\ln(\frac{b}{a})}\int_a^b\sum_{i=0}^{S}V_i\Re_i(\rho')d\rho' \\ &+ \sum_{m=1}^{\infty}Y_{TM}\Re_m(\rho)\int_a^b\sum_{i=0}^{S}V_i\,\Re_i(\rho')\Re_m(\rho')\rho'd\rho' \\ &+ \int_0^{\infty}Y_{el}\frac{(1-R_{bl})}{(1+R_{bl})}\left[\int_a^b\sum_{i=0}^{S}V_i\,\Re_i(\rho')J_1(k_c\rho')\rho'd\rho'\right]J_1(k_c\rho)k_cdk_c \end{aligned} \tag{3.121}$$

which is rearranged to be

$$\begin{aligned} A_o\frac{2}{\eta_o}\frac{1}{\rho} &= \sum_{i=0}^{S}V_i\frac{1}{\eta_o}\frac{1}{\rho}\frac{1}{\ln(\frac{b}{a})}\int_a^b\Re_i(\rho')d\rho' \\ &+ \sum_{i=0}^{S}V_i\sum_{m=1}^{\infty}Y_{TM}\Re_m(\rho)\int_a^b\Re_i(\rho')\Re_m(\rho')\rho'd\rho' \\ &+ \sum_{i=0}^{S}V_i\int_0^{\infty}Y_{el}\frac{(1-R_{bl})}{(1+R_{bl})}\left[\int_a^b\Re_i(\rho')J_1(k_c\rho')\rho'd\rho'\right]J_1(k_c\rho)k_cdk_c \end{aligned} \tag{3.122}$$

Galerkin's method

Galerkin's method suggests using basis functions $\Re_j(\rho)$ as testing functions and does the following operation:

Operating

$$\int_a^b (3.122)*\Re_j(\rho)\rho d\rho \qquad ,j=0,\cdots,S$$

a system of linear equations is derived as follows:

$$
\begin{aligned}
& A_0 \frac{2}{\eta_o} \int_a^b \Re_j(\rho) d\rho \\
& = \sum_{i=0}^{S} V_i \frac{1}{\eta_o} \frac{1}{\ln(\frac{b}{a})} \int_a^b \Re_j(\rho) d\rho \int_a^b \Re_i(\rho') d\rho' \\
& + \sum_{i=0}^{S} V_i \sum_{m=1}^{\infty} Y_{TM} \int_a^b \Re_j(\rho) \Re_m(\rho) d\rho \int_a^b \Re_i(\rho') \Re_m(\rho') \rho' d\rho' \\
& + \sum_{i=0}^{S} V_i \int_0^{\infty} Y_{el} \frac{(1-R_{bl})}{(1+R_{bl})} \left[\int_a^b \Re_j(\rho) J_1(k_c \rho) d\rho \right] \left[\int_a^b \Re_i(\rho') J_1(k_c \rho') \rho' d\rho' \right] k_c dk_c
\end{aligned}
\tag{3.123}
$$

with j = 1,...,S.

Via orthogonality properties, (3.123) is simplified to be

$$
\begin{aligned}
& A_0 \frac{2}{\eta_o} \delta_{j0} \ln(\frac{b}{a}) \\
& = \sum_{i=0}^{S} V_i \frac{1}{\eta_o} \frac{1}{\ln(\frac{b}{a})} \delta_{j0} \ln(\frac{b}{a}) \delta_{i0} \ln(\frac{b}{a}) \\
& + \sum_{i=0}^{S} V_i \sum_{m=1}^{\infty} Y_{TM} \delta_{jm} \delta_{im} \\
& + \sum_{i=0}^{S} V_i \int_0^{\infty} Y_{el} \frac{(1-R_{bl})}{(1+R_{bl})} \left[\int_a^b \Re_j(\rho) J_1(k_c \rho) d\rho \right] \left[\int_a^b \Re_i(\rho') J_1(k_c \rho') \rho' d\rho' \right] k_c dk_c
\end{aligned}
\tag{3.124}
$$

with j = 1,...,S.

These simultaneous algebraic equations can be expressed as

$$
A_o[I] = \{[Y^c] + [Y^b] + [Y^a]\}[V] \tag{3.125}
$$

with the matrix elements as

$$
\begin{aligned}
I_j &= \frac{2}{\eta_o}\ln(\frac{b}{a})\,\delta_{j0} \\
Y_{ji}^{c} &= \frac{1}{\eta_o}\ln(\frac{b}{a})\,\delta_{j0}\,\delta_{i0} \\
Y_{ji}^{b} &= \sum_{m=1}^{\infty} Y_{TM}\,\delta_{jm}\,\delta_{im} \\
Y_{ji}^{a} &= \int_0^{\infty} Y_{el}\frac{(1-R_{bl})}{(1+R_{bl})}\left[\int_a^b \Re_j(\rho)J_1(k_c\rho)d\rho\right]\left[\int_a^b \Re_i(\rho')J_1(k_c\rho')\rho' d\rho'\right]k_c dk_c
\end{aligned}
\tag{3.126}
$$

Equation (3.125) can then be solved by a standard numerical subroutine for linear equations [31].

After solving $\mathscr{E}(\rho)$ from (3.125), the normalized input admittance can be related to $\mathscr{E}(\rho)$ with the help of (3.27) [32,33],

$$
y_{in} = \frac{1-R}{1+R} = \frac{2 - \dfrac{1}{A_o \ln(b/a)}\displaystyle\int_a^b \mathscr{E}(\rho)d\rho}{\dfrac{1}{A_o \ln(b/a)}\displaystyle\int_a^b \mathscr{E}(\rho)\,d\rho} \tag{3.127}
$$

Since $\mathscr{E}(\rho)$ is proportional to A_o, A_o will be canceled in the expression of normalized input admittance. Setting A_o to 1 leads to

$$
y_{in} = \frac{2 - \dfrac{1}{A_o \ln(b/a)}\displaystyle\int_a^b \mathscr{E}(\rho)\,d\rho}{\dfrac{1}{A_o \ln(b/a)}\displaystyle\int_a^b \mathscr{E}(\rho)\,d\rho} = \frac{2\ln(\frac{b}{a}) - \displaystyle\int_a^b \mathscr{E}(\rho)\,d\rho}{\displaystyle\int_a^b \mathscr{E}(\rho)\,d\rho} \tag{3.128}
$$

Before presenting some results of the numerical simulation for (3.125) some aspects about evaluation of the matrix elements are addressed next.

Evaluation of the matrix elements

The computation for the elements of matrices Y^c and Y^b is trivial. However the evaluation for the elements of matrix Y^a, involving an infinite integration w.r.t. k_c, need more care due to the slow convergence and oscillatory behavior of Bessel functions.

Fast convergence of the integration w.r.t. k_c can be achieved by the technique of adding and subtracting an asymptotic term to the integrand [34]. By observing $\Gamma_1 \to k_c$ & $R_{bl} \to 0$ when $k_c \to \infty$, we can rewrite Y_{ji}^a as

$$\begin{aligned}\frac{Y_{ji}^a}{j\omega\varepsilon_1} &= \int_0^\infty \left(\frac{1}{\Gamma_1}\frac{(1-R_{bl})}{(1+R_{bl})} - \frac{1}{k_c}\right)\left[\int_a^b \Re_j(\rho) J_1(k_c\rho)\rho d\rho\right]\left[\int_a^b \Re_i(\rho') J_1(k_c\rho')\rho' d\rho'\right] k_c dk_c \\ &\quad + \int_0^\infty \left[\int_a^b \Re_j(\rho) J_1(k_c\rho)\rho d\rho\right]\left[\int_a^b \Re_i(\rho') J_1(k_c\rho')\rho' d\rho'\right] dk_c \\ &\equiv Y_{ji}^{a-} + \overline{asym}\end{aligned} \tag{3.129}$$

The integrand of Y_{ji}^{a-} is now proportional to k_c^{-2} despite of the decaying factor of Bessel functions. Furthermore, Y_{ji}^{a-} involving a double integral can be reduced to a single integral by employing the following formula [20].

$$\int Z_\nu(\alpha\rho) J_\nu(\beta\rho)\rho d\rho = \frac{\rho}{\alpha^2-\beta^2}\left[\beta Z_\nu(\alpha\rho) J_{\nu-1}(\beta\rho) - \alpha Z_{\nu-1}(\alpha\rho) J_\nu(\beta\rho)\right] \tag{3.130}$$

with $\alpha \neq \beta$ and Z_ν denoting J_ν and Y_ν.

The fast convergent integral Y_{ji}^{a-} can now be evaluated numerically and the infinite integral range can be truncated at a reasonable value according to a preset accuracy.

It may save many efforts if the asymptotic term $\overline{asym}$, a double integral with a slow convergence and oscillatory behavior, can be cast into some kind of closed form. Unfortunately $\overline{asym}$ need to be evaluated numerically.

Using the following formula the time consuming form for $\overline{asym}$ in (3.129) can be converted into a hypergeometric function with an integral range only from 0 to 1 instead of from 0 to infinity [48]:

$$\begin{aligned}\int_0^{\infty} J_1(k_c\rho')J_1(k_c\rho)dk_c &= \frac{\rho'}{\rho^2}\frac{\Gamma(3/2)}{\Gamma(1/2)}F[\frac{1}{2},\frac{3}{2};2;(\frac{\rho'}{\rho})^2] \\ &= \frac{\rho'}{2\rho^2}\frac{\Gamma(2)}{\Gamma(3/2)\Gamma(1/2)}\int_0^1 \frac{\sqrt{t}}{\sqrt{1-t}\sqrt{1-(\rho'/\rho)^2 t}}dt \\ &\equiv K(\rho',\rho)\end{aligned} \tag{3.131}$$

with $\rho'<\rho$.

Therefore, $\overline{asym}$ becomes

$$\overline{asym} = \int_a^b\int_a^b \left\{ \begin{array}{l} K(\rho',\rho) \text{ if } \rho'<\rho \\ K(\rho,\rho') \text{ if } \rho'>\rho \end{array} \right\} \Re_j(\rho)\Re_i(\rho')\rho\,\rho' d\rho\,\rho' \tag{3.132}$$

Using the following change of variables,

$$\begin{aligned} x &= (\rho+\rho')/\sqrt{2} \\ y &= (-\rho+\rho')/\sqrt{2} \end{aligned} \tag{3.133}$$

and with $dxdy = d\rho d\rho'$, $\overline{asym}$ becomes

$$\begin{aligned}\overline{asym} = \int_{\sqrt{2}a}^{(\sqrt{2}a+\sqrt{2}b)/2} &\left[\int_0^{x-\sqrt{2}a} K(\rho',\rho)\Re_j(\rho)\Re_i(\rho')\rho\,\rho' dy \right. \\ &\left. + \int_{-x+\sqrt{2}a}^{0} K(\rho,\rho')\Re_j(\rho)\Re_i(\rho')\rho\,\rho' dy\right] dx \\ + \int_{(\sqrt{2}a+\sqrt{2}b)/2}^{\sqrt{2}b} &\left[\int_0^{-x+\sqrt{2}b} K(\rho',\rho)\Re_j(\rho)\Re_i(\rho')\rho\,\rho' dy \right. \\ &\left. + \int_{x-\sqrt{2}b}^{0} K(\rho,\rho')\Re_j(\rho)\Re_i(\rho')\rho\,\rho' dy\right] dx\end{aligned} \tag{3.134}$$

where $\rho' = (x+y)/\sqrt{2}$ and $\rho = (x-y)/\sqrt{2}$.

Equation (3.134) is now ready for numerical evaluation. Although $\overline{asym}$ involves a triple integral, the improper integral from 0 to infinity no longer exists. Furthermore the evaluation of the asymptotic term can be performed once for all cases because it only depends on the dimensions of the coaxial line.

After all these considerations about the evaluation of the matrix elements, (3.125) can now be calculated numerically by any kind of computer code.

Computer program and numerical results

A fortran computer program was written for the numerical evaluation of (3.125) and (3.126) such that the aperture electric field and other quantities can be calculated when μ,ϵ of the material are given. The validity of the computer program is verified by computing the reflection coefficient of a SR-7 type coaxial line radiating into a homogeneous material medium of complex permittivity at 3 GHz, the geometry in the study by D. K. Misra [35] and J. R. Mosig [36]. The reflection coefficient as a function of $\epsilon=\epsilon'-j\epsilon''$, the material permittivity, is computed for various permittivities along the constant ϵ' and constant ϵ'' lines. Our numerical results as shown in fig. 3.5 compare quite well with the existing ones.

So far the "forward problem" has been solved correctly and the "inverse problem", the final goal, for determining μ and ϵ of the material via measurements of the input impedance of the coaxial probe will be addressed in chapter 6.

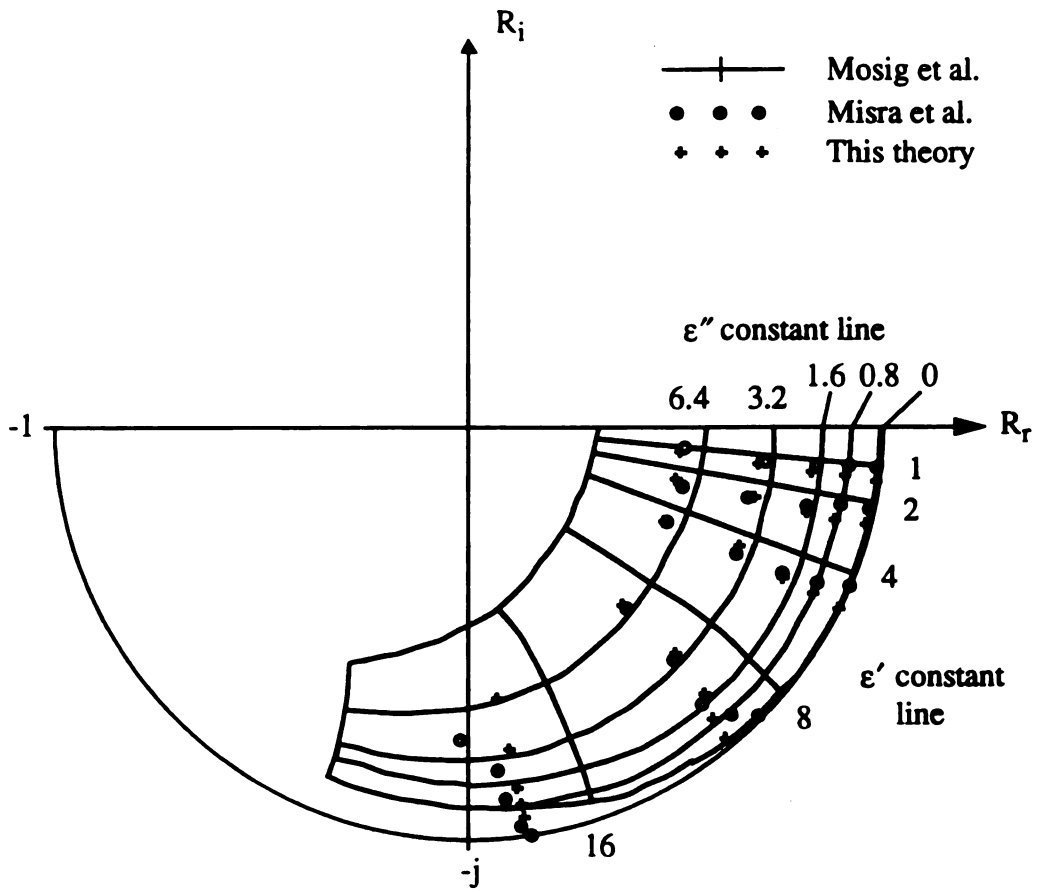

Figure 3.5 Reflection coefficient of an SR-7 type coaxial line placed against various homogeneous materials, frequency is 3 GHz.

CHAPTER 4

POWER BALANCE FOR COMPLEX WAVE EXCITATION IN OPEN-ENDED COAXIAL PROBE STRUCTURE

4.1 Introduction

The power balance is verified in this chapter for an open-ended coaxial probe system by comparing the total power carried away from the aperture to the transmitted power of the incident wave at the aperture [38]. Also the EM fields excited inside the material medium are found to be localized around the probe aperture when the frequency is lower than 2 GHz.

With the complex wave excitation for an open-ended coaxial probe identified in chapter 3, it is possible to identify various contributors to the total power carried away from the aperture. The power contributors are surface waves and radiative waves for the open-circuit case and radial guided waves for the short-circuit case. The power carried by each wave can be expressed in a concise form using Cauchy residue theorem or saddle point method so that it can be evaluated more efficiently [39]. In addition, the excitation of the complex wave is found to be strongly dependent on the frequency.

In section 4.2 the surface wave power of the open-circuit case is evaluated. The EM field components of each surface wave mode are derived. The associated power carried in the radial direction can be calculated using the Poynting theorem.

In section 4.3 the radiative wave power of the open-circuit case is evaluated. Since the wave is directed into the half space, the radiative wave power can be computed over the surface of a hemisphere in the far zone. The far zone fields are derived and then simplified using the saddle point method so that the associated power can be computed more efficiently.

In section 4.4 the radial guided wave power of the short-circuit case is evaluated. The EM field components of each radial guided wave are derived using a deformed contour integral. The radial guided wave poles are investigated and it is found that there exists propagating and evanescent radial guided waves. The power of the propagating wave is then computed using the Poynting theorem.

4.2 Surface Wave Power for Open-Circuit Case

In this section the total power of the surface waves excited by an open-ended coaxial probe system in the material layer is studied while the power of radiative wave through the material layer is investigated in the next section.

For illustrative purpose we consider fig. 4.1, an open-ended coaxial probe placed against a two-layer lossless medium. Since the surface wave modes are orthogonal [21], the total power of surface waves is the sum of the power associated with each surface wave mode.

The surface wave is known to propagate laterally, therefore no real power is carried away in positive z direction, and the power is directed in radial direction in both regions 1 and 2. The EM field components of each surface wave mode inside the material layers are computed first using a deformed contour integral, and then the associated power is evaluated numerically.

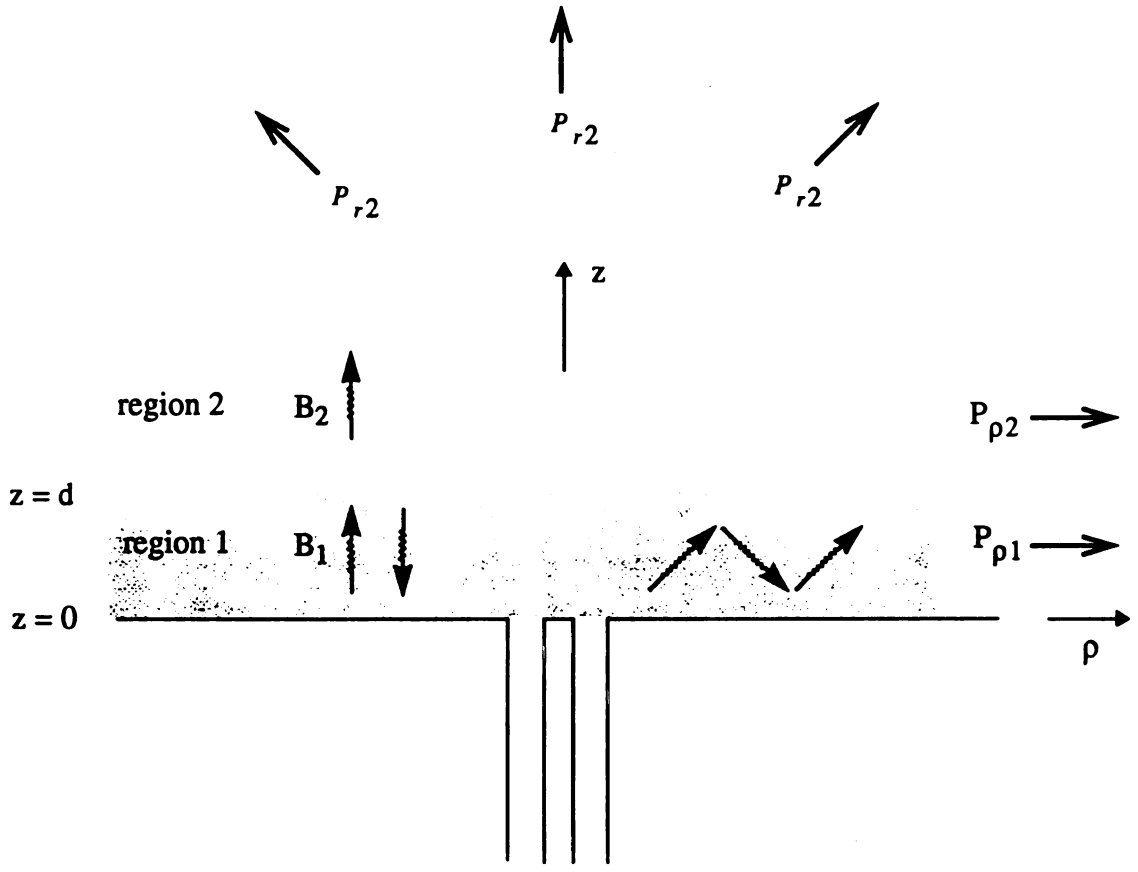

Figure 4.1 Surface waves and radiative wave excitation in the open-circuit case of an open-ended coaxial line probe placed against a material layer.

4.2.1 Derivation of Surface Wave Field Expressions

Surface Wave Fields in Region 1

With the help of (3.19), (3.20) and (3.26), the EM field components in region 1 of the material medium can be expressed as

$$\vec{E}_t = \hat{\rho} E_\rho = \hat{\rho} \int_0^\infty \frac{1}{1+R_{b1}} \left(\int_a^b \mathscr{E}(\rho') J_1(k_c \rho') \rho' d\rho' \right) (e^{-\Gamma_1 z} + R_{b1} e^{\Gamma_1 z}) J_1(k_c \rho) k_c dk_c$$

$$\vec{H}_t = \hat{\phi} H_\phi = \hat{\phi} \int_0^\infty Y_{e1} \frac{1}{1+R_{b1}} \left(\int_a^b \mathscr{E}(\rho') J_1(k_c \rho') \rho' d\rho' \right) (e^{-\Gamma_1 z} - R_{b1} e^{\Gamma_1 z}) J_1(k_c \rho) k_c dk_c \quad (4.1)$$

$$E_z = \int_0^\infty \frac{1}{\Gamma_1} \frac{1}{(1+R_{b1})} \left(\int_a^b \mathscr{E}(\rho') J_1(k_c \rho') \rho' d\rho' \right) (e^{-\Gamma_1 z} - R_{b1} e^{\Gamma_1 z}) J_o(k_c \rho) k_c^2 dk_c$$

In order to identify the surface wave fields, the EM field components in (4.1) are rewritten, with the help of (3.30) and (3.31), as follows:

$$E_{\rho 1} = \frac{1}{2} \int_{-\infty}^\infty \frac{1}{1+R_{b1}} \left(\int_a^b \mathscr{E}(\rho') J_1(k_c \rho') \rho' d\rho' \right) (e^{-\Gamma_1 z} + R_{b1} e^{\Gamma_1 z}) H_1^{(2)}(k_c \rho) k_c dk_c$$

$$H_{\phi 1} = \frac{1}{2} \int_{-\infty}^\infty Y_{e1} \frac{1}{1+R_{b1}} \left(\int_a^b \mathscr{E}(\rho') J_1(k_c \rho') \rho' d\rho' \right) (e^{-\Gamma_1 z} - R_{b1} e^{\Gamma_1 z}) H_1^{(2)}(k_c \rho) k_c dk_c \quad (4.2)$$

$$E_{z1} = \frac{1}{2} \int_{-\infty}^\infty \frac{1}{\Gamma_1} \frac{1}{1+R_{b1}} \left(\int_a^b \mathscr{E}(\rho') J_1(k_c \rho') \rho' d\rho' \right) (e^{-\Gamma_1 z} - R_{b1} e^{\Gamma_1 z}) H_0^{(2)}(k_c \rho) k_c^2 dk_c$$

It was proved in chapter 3 that the surface wave poles satisfy

$$1 + R_{b1} = 1 + e^{-2\Gamma_1 d} \frac{\Gamma_2/\Gamma_1 - \varepsilon_2/\varepsilon_1}{\Gamma_2/\Gamma_1 + \varepsilon_2/\varepsilon_1} = 0 \quad (4.3)$$

With reference to fig. 3.2, it is shown that using the deformed contour integral with proper choice of branch cut, $E_{\rho 1}$ in (4.2) becomes

$$E_{\rho 1}=\frac{1}{2}\oint_{C_p}\frac{(e^{-\Gamma_1 z}+R_{b1}e^{\Gamma_1 z})}{(1+R_{b1})}\left[\int_a^b \mathcal{E}(\rho')J_1(k_c\rho')\rho' d\rho'\right]H_1^{(2)}(k_c\rho)k_c dk_c$$
$$+\frac{1}{2}\int_{C_b}\frac{(e^{-\Gamma_1 z}+R_{b1}e^{\Gamma_1 z})}{(1+R_{b1})}\left[\int_a^b \mathcal{E}(\rho')J_1(k_c\rho')\rho' d\rho'\right]H_1^{(2)}(k_c\rho)k_c dk_c \tag{4.4}$$

where C_p stands for the contour around the surface wave poles and C_b for the contour along the branch cut.

Similar expressions can be derived for $H_{\phi 1}$ and E_{z1} also.

It is found that the surface wave poles are simple poles. Thus by letting k_{cpm} denote the m^{th} surface wave pole, the surface wave field component E_ρ in region 1 can be derived by the residue evaluation of the first integrand in (4.4) as following

$$E_{\rho 1}=-\pi j\left(\int_a^b \mathcal{E}(\rho')J_1(k_{cpm}\rho')\rho' d\rho'\right)(e^{-\Gamma_1 z}+R_{b1}e^{\Gamma_1 z})H_1^{(2)}(k_{cpm}\rho)k_{cpm}$$
$$\lim_{k_c\to k_{cpm}}\left[\frac{1}{1+R_{b2}}\right][k_c-k_{cpm}] \tag{4.5}$$

Similarly the surface wave field components for H_ϕ and E_z in region 1 are

$$H_{\phi 1}=-\pi j Y_{e1}\left(\int_a^b \mathcal{E}(\rho')J_1(k_{cpm}\rho')\rho' d\rho'\right)(e^{-\Gamma_1 z}-R_{b1}e^{\Gamma_1 z})H_1^{(2)}(k_{cpm}\rho)k_{cpm}$$
$$\lim_{k_c\to k_{cpm}}\frac{1}{1+R_{b1}}[k_c-k_{cpm}]$$
$$E_{z1}=-\pi j\frac{1}{\Gamma_1}\left(\int_a^b \mathcal{E}(\rho')J_1(k_{cpm}\rho')\rho' d\rho'\right)(e^{-\Gamma_1 z}-R_{b1}e^{\Gamma_1 z})H_0^{(2)}(k_{cpm}\rho)k_{cpm}^2 \tag{4.6}$$
$$\lim_{k_c\to k_{cpm}}\frac{1}{1+R_{b1}}[k_c-k_{cpm}]$$

Introducing notations Q and L, (4.5) and (4.6) are written as following,

$$E_{\rho 1} = -\pi j Q L k_{cpm} (e^{-\Gamma_1 z} + R_{b1} e^{\Gamma_1 z}) H_1^{(2)}(k_{cpm}\rho)$$

$$H_{\phi 1} = -\pi j Y_{e1} Q L k_{cpm} (e^{-\Gamma_1 z} - R_{b1} e^{\Gamma_1 z}) H_1^{(2)}(k_{cpm}\rho) \qquad (4.7)$$

$$E_{z1} = -\pi j \frac{1}{\Gamma_1} Q L k_{cpm}^2 (e^{-\Gamma_1 z} - R_{b1} e^{\Gamma_1 z}) H_0^{(2)}(k_{cpm}\rho)$$

where

$$Q \equiv \int_b^a \mathscr{E}(\rho') J_1(k_{cpm}\rho') \rho' d\rho'$$

$$L \equiv \lim_{k_c \to k_{cpm}} \frac{1}{1 + R_{b1}} (k_c - k_{cpm}) \qquad (4.8)$$

Surface Wave Fields in region 2

With the help of (3.19), (3.20) and letting R_{b2}=0, the EM field components in region 2 are

$$\vec{E}_t = \hat{\rho} E_{\rho 2} = \hat{\rho} \int_0^\infty B_2 e^{-\Gamma_2 z} J_1(k_c\rho) k_c dk_c$$

$$\vec{H}_t = \hat{\phi} H_{\phi 2} = \hat{\phi} \int_0^\infty Y_{e2} B_2 e^{-\Gamma_2 z} J_1(k_c\rho) k_c dk_c \qquad (4.9)$$

$$E_{z2} = \int_0^\infty \frac{1}{\Gamma_2} B_2 e^{-\Gamma_2 z} J_o(k_c\rho) k_c^2 dk_c$$

where B_2 is the unknown amplitude of each TM mode.

With the help of (2.32), we have

$$\frac{B_2}{B_1} = \frac{2 Y_{e1}}{Y_{e1} + Y_{e2}} e^{(\Gamma_2 - \Gamma_1)d} \equiv T \qquad (4.10)$$

where B_1 is expressed in (3.26) as

$$B_1(k_c) = \frac{1}{(1 + R_{b1})} \int_a^b \mathscr{E}(\rho) J_1(k_c\rho) \rho d\rho \qquad (4.11)$$

Equation (4.9) then leads to

$$E_{\rho 2} = \int_0^{\infty} \frac{1}{1+R_{b1}} \left(\int_a^b \mathcal{E}(\rho') J_1(k_c \rho') \rho' d\rho' \right) T e^{-\Gamma_2 z} J_1(k_c \rho) k_c dk_c \tag{4.12}$$

$$\begin{aligned} H_{\phi 2} &= \int_0^{\infty} Y_{e2} \frac{1}{1+R_{b1}} \left(\int_a^b \mathcal{E}(\rho') J_1(k_c \rho') \rho' d\rho' \right) T e^{-\Gamma_2 z} J_1(k_c \rho) k_c dk_c \\ E_{z2} &= \int_0^{\infty} \frac{1}{\Gamma_2} \frac{1}{1+R_{b1}} \left(\int_a^b \mathcal{E}(\rho') J_1(k_c \rho') \rho' d\rho' \right) T e^{-\Gamma_2 z} J_o(k_c \rho) k_c^2 dk_c \end{aligned} \tag{4.13}$$

In order to identify the surface wave fields, the EM field components in (4.12) and (4.13) are rewritten, with the help of (3.30) and (3.31), as

$$\begin{aligned} E_{\rho 2} &= \frac{1}{2} \int_{-\infty}^{\infty} \frac{1}{1+R_{b1}} \left(\int_a^b \mathcal{E}(\rho') J_1(k_c \rho') \rho' d\rho' \right) T e^{-\Gamma_2 z} H_1^{(2)}(k_c \rho) k_c dk_c \\ H_{\phi 2} &= \frac{1}{2} \int_{-\infty}^{\infty} Y_{e2} \frac{1}{1+R_{b1}} \left(\int_a^b \mathcal{E}(\rho') J_1(k_c \rho') \rho' d\rho' \right) T e^{-\Gamma_2 z} H_1^{(2)}(k_c \rho) k_c dk_c \\ E_{z2} &= \frac{1}{2} \int_{-\infty}^{\infty} \frac{1}{\Gamma_2} \frac{1}{1+R_{b1}} \left(\int_a^b \mathcal{E}(\rho') J_1(k_c \rho') \rho' d\rho' \right) T e^{-\Gamma_2 z} H_o^{(2)}(k_c \rho) k_c^2 dk_c \end{aligned} \tag{4.14}$$

The surface wave field components $E_{\rho 2}, H_{\phi 2}$ and E_{z2} can then be derived in a similar way as in region 1. By the residue evaluation of integrand in (4.14), we have

$$\begin{aligned} E_{\rho 2} &= -\pi j \int_a^b \mathcal{E}(\rho') J_1(k_{cpm} \rho') \rho' d\rho' T e^{-\Gamma_2 z} H_1^{(2)}(k_{cpm} \rho) k_{cpm} \lim_{k_c \to k_{cpm}} \frac{k_c - k_{cpm}}{1+R_{b1}} \\ H_{\phi 2} &= -\pi j Y_{e2} \int_a^b \mathcal{E}(\rho') J_1(k_{cpm} \rho') \rho' d\rho' T e^{-\Gamma_2 z} H_1^{(2)}(k_{cpm} \rho) k_{cpm} \lim_{k_c \to k_{cpm}} \frac{k_c - k_{cpm}}{1+R_{b1}} \\ E_{z2} &= -\pi j \frac{1}{\Gamma_2} \int_a^b \mathcal{E}(\rho') J_1(k_{cpm} \rho') \rho' d\rho' T e^{-\Gamma_2 z} H_0^{(2)}(k_{cpm} \rho) k_{cpm}^2 \lim_{k_c \to k_{cpm}} \frac{k_c - k_{cpm}}{1+R_{b1}} \end{aligned} \tag{4.15}$$

or

$$E_{\rho 2} = -\pi j Q L T k_{cpm} e^{-\Gamma_2 z} H_1^{(2)}(k_{cpm}\rho)$$

$$H_{\phi 2} = -\pi j Y_{e2} Q L T k_{cpm} e^{-\Gamma_2 z} H_1^{(2)}(k_{cpm}\rho) \tag{4.16}$$

$$E_{z2} = -\pi j \frac{1}{\Gamma_2} Q L T k_{cpm}^2 e^{-\Gamma_2 z} H_o^{(2)}(k_{cpm}\rho)$$

where Q and L have been defined in (4.8).

With the field components in both regions, as given in (4.7) and (4.16), for each individual surface wave mode, the associated power is calculated next.

4.2.2 Calculation of Surface Wave Power

To calculate the power associated with each surface wave mode, the following relationship is used,

$$P = \int_S \frac{1}{2} R_e[\vec{E} \times \vec{H}^*] \cdot d\vec{s} \tag{4.17}$$

Since $\vec{H}$ has only H_ϕ component while $\vec{E}$ has E_ρ and E_z components, we have

$$P = \frac{1}{2} \iint_S R_e\left[\hat{z} E_\rho H_\phi^* - \hat{\rho} E_z H_\phi^*\right] \cdot d\vec{s} \tag{4.18}$$

With the help of (4.7) and (4.16), it is found that $E_\rho H_\phi^*$ is pure imaginary in both regions, therefore the real power flows only in the ρ direction, which is consistent with the characteristic of the surface wave. Equation (4.18) then becomes

$$\begin{aligned} P &= \frac{1}{2} \int_0^\infty \int_0^{2\pi} R_e[-E_z H_\phi^*] \rho \, d\phi \, dz \\ &= \frac{1}{2} \int_0^d \int_0^{2\pi} R_e[-E_{z1} H_{\phi 1}^*] \rho \, d\phi \, dz + \frac{1}{2} \int_d^\infty \int_0^{2\pi} R_e[-E_{z2} H_{\phi 2}^*] \rho \, d\phi \, dz \\ &\equiv P_{\rho 1} + P_{\rho 2} \end{aligned} \tag{4.19}$$

where $P_{\rho 1}$ and $P_{\rho 2}$ are the radial power flows in regions 1 and 2, respectively.

Let's compute the radial power flow in region 2 first. Since the surface wave poles k_{cpm} exist in the range of $[k_2, k_1]$, Γ_2 in (4.16) is real and the surface wave fields can be expressed as

$$\begin{aligned} H_{\phi 2}^{*} &= \pi j\, Y_{e2}^{*}\, Q^{*}\, L^{*}\, T^{*}\, k_{cpm}^{*}\, e^{-\Gamma_2 z}\, H_1^{(2)^{*}}(k_{cpm}\rho) \\ E_{z2} &= -\pi j \frac{1}{\Gamma_2} Q\, L\, T\, k_{cpm}^{2}\, e^{-\Gamma_2 z}\, H_o^{(2)}(k_{cpm}\rho) \end{aligned} \tag{4.20}$$

where $Y_{e2}=j\omega\epsilon_2/\Gamma_2$.

Therefore we have

$$E_{z2}\, H_{\phi 2}^{*} = \pi^2 \frac{-j\omega\epsilon_2}{|\Gamma_2|^2} |Q\, L\, T\, k_{cpm}|^2 k_{cpm}\, e^{-2\Gamma_2 z}\, H_o^{(2)}(k_{cpm}\rho) H_1^{(2)^{*}}(k_{cpm}\rho) \tag{4.21}$$

Using the following Wronskin,

$$J_\nu(z) Y_\nu'(z) - Y_\nu(z) J_\nu'(z) = \frac{2}{\pi z} \tag{4.22}$$

the product of the two Hankel functions in (4.21) can be reduced to

$$\begin{aligned} & j H_0^{(2)}(k_{cpm}\rho)\; H_1^{(2)^{*}}(k_{cpm}\rho) \\ &= j\left[J_0(k_{cpm}\rho) - jY_0(k_{cpm}\rho)\right]\left[J_1(k_{cpm}\rho) + jY_1(k_{cpm}\rho)\right] \\ &= \left[J_1(k_{cpm}\rho) Y_0(k_{cpm}\rho) - J_0(k_{cpm}\rho) Y_1(k_{cpm}\rho)\right] + j[\,.....\,] \\ &= \frac{2}{\pi k_{cpm}\rho} + j[.....] \end{aligned} \tag{4.23}$$

where the imaginary part [...] doesn't contribute to the real power.

With (4.21) and (4.23), we have

$$R_e\left[E_{z2} H_{\phi 2}^{*}\right] = -2\pi \frac{\omega\epsilon_2}{|\Gamma_2|^2} |QLTk_{cpm}|^2 \frac{e^{-2\Gamma_2 z}}{\rho} \tag{4.24}$$

With (4.24) $P_{\rho 2}$ becomes

$$P_{\rho 2} = \frac{1}{2}\int_0^{2\pi} 2\pi \frac{\omega \epsilon_2}{|\Gamma_2|^2} |QLTk_{cpm}|^2 \left(\int_d^{\infty} e^{-2\Gamma_2 z} dz\right) d\phi$$
$$= \frac{\pi^2}{\Gamma_2} \frac{\omega \epsilon_2}{|\Gamma_2|^2} |QLTk_{cpm}|^2 e^{-2\Gamma_2 d} \tag{4.25}$$

Next, let's compute the radial power flow of the surface wave in region 1. With $\Gamma_1 \equiv j\beta_1$ in (4.7) the surface wave fields become

$$H_{\phi 1}^* = \pi j Y_{e1}^* Q^* L^* k_{cpm}^* \left(e^{-j\beta_1 z} - R_{b1} e^{j\beta_1 z}\right)^* H_1^{(2)^*}(k_{cpm}\rho)$$
$$E_{z1} = -\pi j \frac{1}{j\beta_1} QLk_{cpm}^2 \left(e^{-j\beta_1 z} - R_{b1} e^{j\beta_1 z}\right) H_0^{(2)}(k_{cpm}\rho) \tag{4.26}$$

where β_1 is real and R_{b1} has been derived in (2.48) as

$$R_{b1} = e^{-2\Gamma_1 d} \frac{Y_{e1} - Y_{e2}}{Y_{e1} + Y_{e2}} = e^{-2j\beta_1 d} \frac{\Gamma_2/\beta_1 - j\epsilon_2/\epsilon_1}{\Gamma_2/\beta_1 + j\epsilon_2/\epsilon_1} \equiv e^{-2j\beta_1 d} \frac{\upsilon - jK_r^2}{\upsilon + jK_r^2} \tag{4.27}$$

where Γ_2 is real, $\upsilon = \Gamma_2/\beta_1$ and $K_r^2 = \epsilon_2/\epsilon_1$.

Using (4.27), we have

$$e^{-j\beta_1 z} - R_{b1} e^{j\beta_1 z}$$
$$= e^{-j\beta_1 z} - e^{-2j\beta_1 d} \frac{\upsilon - jK_r^2}{\upsilon + jK_r^2} e^{j\beta_1 z}$$
$$= 2j \frac{e^{-j\beta_1 d}}{\upsilon + jK_r^2} \left[K_r^2 \cos\beta_1(d-z) - \upsilon \sin\beta_1(d-z)\right] \tag{4.28}$$

The substitution of (4.28) in (4.26) leads to

$$E_{z1} H_{\phi 1}^* = 4\pi^2 \frac{-j\omega\epsilon_1}{\beta_1^2} |QLk_{cpm}|^2 k_{cpm} \frac{1}{\upsilon^2 + K_r^4}$$
$$\left[K_r^2 \cos\beta_1(d-z) - \upsilon \sin\beta_1(d-z)\right]^2 H_o^{(2)}(k_{cpm}\rho) H_1^{(2)^*}(k_{cpm}\rho) \tag{4.29}$$

With the product of the two Hankel functions being simplified, as in (4.23), equation (4.29) leads to

$$R_e\left[E_{z1}H_{\phi 1}^*\right]=-8\pi\frac{\omega\varepsilon_1}{\beta_1^2}\left|QLk_{cpm}\right|^2\frac{1}{\upsilon^2+K_r^4}\left[K_r^2\cos\beta_1(d-z)-\upsilon\sin\beta_1(d-z)\right]^2\frac{1}{\rho} \tag{4.30}$$

Therefore, $P_{\rho 1}$ becomes

$$P_{\rho 1}=\frac{1}{2}\int_0^{2\pi}8\pi\frac{\omega\varepsilon_1}{\beta_1^2}\left|QLk_{cpm}\right|^2\frac{1}{\upsilon^2+K_r^4}\int_0^d\left[K_r^2\cos\beta_1(d-z)-\upsilon\sin\beta_1(d-z)\right]^2dzd\phi \tag{4.31}$$

After some manipulation, the integral with respect to z in (4.31) can be expressed as

$$\begin{aligned}&\int_0^d\left[K_r^2\cos\beta_1(z-d)-\upsilon\sin\beta_1(z-d)\right]^2dz\\&=K_r^4\frac{d}{2}\left[1+\cos\beta_1 d\frac{\sin\beta_1 d}{\beta_1 d}\right]+\upsilon^2\frac{d}{2}\left[1-\cos\beta_1 d\frac{\sin\beta_1 d}{\beta_1 d}\right]+K_r^4\upsilon d\frac{1-\cos 2\beta_1 d}{2\beta_1 d}\\&\equiv f(d)\end{aligned} \tag{4.32}$$

Equation (4.31) then becomes

$$P_{\rho 1}=\frac{8\pi^2\omega\varepsilon_1}{\beta_1}\frac{\left|QLk_{cpm}\right|^2}{\upsilon^2+K_r^4}f(d) \tag{4.33}$$

Note that with (4.25) and (4.33), it is clear that P_ρ is independent of ρ. This is consistent with the fact that surface waves excited in this structure are cylindrical waves.

Combining (4.25) and (4.33), the radial power flow associated with each surface wave mode is

$$\begin{aligned}P_\rho&=P_{\rho 1}+P_{\rho 2}\\&=\frac{8\pi^2\omega\varepsilon_1}{\beta_1}\frac{\left|QLk_{cpm}\right|^2}{\upsilon^2+K_r^4}f(d)+\frac{\pi^2}{\Gamma_2}\frac{\omega\varepsilon_2}{\left|\Gamma_2\right|^2}\left|QLTk_{cpm}\right|^2e^{-2\Gamma_2 d}\end{aligned} \tag{4.34}$$

with

$$\Gamma_2=\sqrt{k_{cpm}^2-k_2^2}$$

$$\beta_1=\sqrt{k_1^2-k_{cpm}^2}$$

$$L=\lim_{k_c-k_{cpm}}\frac{1}{1+R_{bl}}(k_c-k_{cpm})$$

$$\upsilon=\frac{\Gamma_2}{\beta_1} \tag{4.35}$$

$$K_r^2=\frac{\epsilon_2}{\epsilon_1}$$

$$Q=\int_a^b \mathscr{E}(\rho')J_1(k_{cpm}\rho')\rho' d\rho'$$

and $f(d)$ is defined in (4.32).

Finally it is noted that the numerical computation of Q requires the information of aperture electric field $\mathscr{E}(\rho)$. The numerical solution of $\mathscr{E}(\rho)$ can be obtained by eigenmode expansion as presented in section 3.4. From (3.118) and (3.119), we have

$$\mathscr{E}(\rho)=\sum_{i=0}^{S} V_i \Re_i(\rho) \tag{4.36}$$

where $\Re_i(\rho)$ is defined in (3.119).

Then after some manipulation, the quantity Q in (4.35) can be expressed as

$$\begin{aligned} Q&=\int_a^b \mathscr{E}(\rho')J_1(k_{cpm}\rho')\rho' d\rho' \\ &=\sum_{i=1}^{s} V_i \int_a^b \Re_i(\rho')J_1(k_{cpm}\rho')\rho' d\rho' + V_0\int_a^b J_1(k_{cpm}\rho')d\rho' \\ &=\sum_{i=1}^{s} V_i \frac{C_i k_{cpm}}{(k_{ci}^2-k_{cpm}^2)k_{ci}}\frac{2}{\pi}\{J_0(k_{cpm}b)\frac{J_0(k_{ci}a)}{J_0(k_{ci}b)}-J_0(k_{cpm}a)\} \\ &\quad + V_0\frac{1}{k_{cpm}}[J_0(k_{cpm}a)-J_0(k_{cpm}b)] \end{aligned} \tag{4.37}$$

The total surface wave power is the sum of the power of individual surface wave mode, as given in (4.34). The other contributor to the total power carried away from the aperture is the radiative wave which is considered next.

4.3 Radiated Power for Open-Circuit Case

In this section, the radiated power contribution of the open-circuit case for an open-ended coaxial probe is studied.

With reference to fig. 4.1 in the previous section, the total power carried away from the aperture consists of the surface wave power and the radiative wave power. Because of the orthogonality relationship between the surface wave and radiative wave [21,37], the total power can be expressed as the sum of the surface wave power and the radiative wave power, the former has been presented in the previous section. To compute the radiative wave power, the radiative wave should be evaluated along the branch cut for the sake of consistency. But for simplicity and computational efficiency, the far zone fields is evaluated via the saddle point method instead, since it can be shown that the far zone fields can be approximated by the radiative wave fields [40].

4.3.1 Power Relation in Spherical Coordinates

As given by (4.14) in previous section, the EM fields in region 2 are

$$
\begin{aligned}
E_{\rho 2} &= \frac{1}{2}\int_{-\infty}^{\infty} \frac{1}{1+R_{b1}} \left(\int_a^b \mathcal{E}(\rho') J_1(k_c\rho')\rho' d\rho' \right) T e^{-\Gamma_2 z} H_1^{(2)}(k_c\rho) k_c dk_c \\
H_{\phi 2} &= \frac{1}{2}\int_{-\infty}^{\infty} Y_{e2} \frac{1}{1+R_{b1}} \left(\int_a^b \mathcal{E}(\rho') J_1(k_c\rho')\rho' d\rho' \right) T e^{-\Gamma_2 z} H_1^{(2)}(k_c\rho) k_c dk_c \\
E_{z2} &= \frac{1}{2}\int_{-\infty}^{\infty} \frac{1}{\Gamma_2} \frac{1}{1+R_{b1}} \left(\int_a^b \mathcal{E}(\rho') J_1(k_c\rho')\rho' d\rho' \right) T e^{-\Gamma_2 z} H_o^{(2)}(k_c\rho) k_c^2 dk_c
\end{aligned}
\tag{4.38}
$$

With reference to fig. 4.2, the total radiative wave power carried away from the aperture is computed as follows:

$$P_r = P_{r1} + P_{r2} = \int_S \frac{1}{2} R_e\left[\vec{E} \times \vec{H}^*\right] \cdot d\vec{s} = \int_S \frac{1}{2} R_e\left[\vec{r} \cdot (\vec{E} \times \vec{H}^*)\right] ds \tag{4.39}$$

where S is the surface of the hemisphere with radius r and P_{ri} is the radiated power in region i, i=1,2.

Because the material is assumed to be lossless, the total power is independent of the spherical radius r. In order to compute the power more efficiently, the radiative wave at great distance is considered, where r is sufficiently large.

When $r \to \infty$, it is clear that P_{r1} is zero. This leads to

$$P_r = P_{r2} = \frac{1}{2} \int_0^{\frac{\pi}{2}} \int_0^{2\pi} R_e\left[\hat{r} \cdot (\vec{E}_2 \times \vec{H}_2^*)\right] r^2 \sin\theta \, d\phi \, d\theta \tag{4.40}$$

The electric field in region 2 has z and ρ components as

$$\vec{E}_2 = \hat{\rho} E_{\rho 2} + \hat{z} E_{z2} \tag{4.41}$$

Using the following relationship between different coordinates

$$\begin{aligned} \hat{\rho} &= \sin\theta \, \hat{r} + \cos\theta \, \hat{\theta} \\ \hat{z} &= \cos\theta \, \hat{r} - \sin\theta \, \hat{\theta} \end{aligned} \tag{4.42}$$

the electric field in (4.41) becomes

$$\vec{E}_2 = \hat{r} E_{r2} + \hat{\theta} E_{\theta 2} \tag{4.43}$$

where

$$\begin{aligned} E_{r2} &= E_{\rho 2} \sin\theta + E_{z2} \cos\theta \\ E_{\theta 2} &= E_{\rho 2} \cos\theta - E_{z2} \sin\theta \end{aligned} \tag{4.44}$$

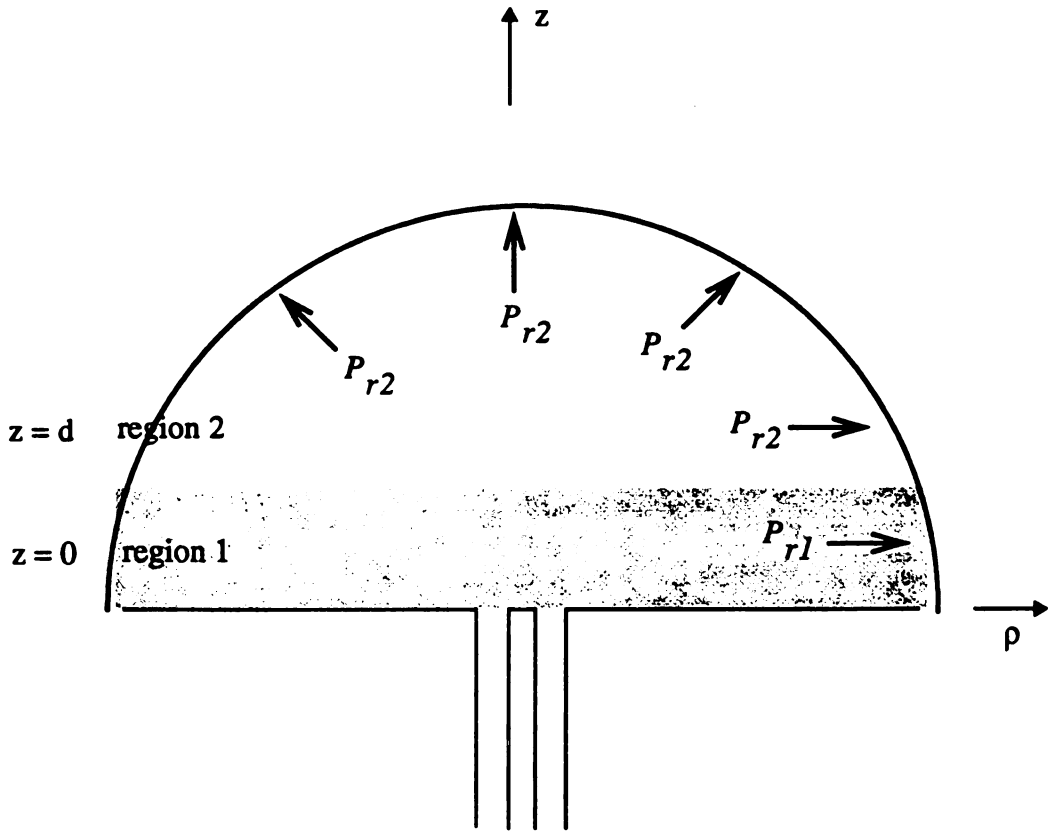

Figure 4.2 The power radiated into the material medium is evaluated over the surface of a hemisphere for an open-ended coaxial probe.

With $\vec{H}_2 = \hat{\phi} H_{\phi 2}$, the substitution of (4.44) in (4.40) leads to

$$P_r = \frac{1}{2}\int_0^{\frac{\pi}{2}}\int_0^{2\pi} R_e\left[E_{\theta 2} H_{\phi 2}^*\right] r^2 \sin\theta \, d\phi \, d\theta$$
$$= \pi \int_0^{\frac{\pi}{2}} R_e\left[-r^2 \sin^2\theta E_{z2} H_{\phi 2}^* + r^2 \sin\theta \cos\theta E_{\rho 2} H_{\phi 2}^*\right] d\theta \tag{4.45}$$

With $\rho = r\sin\theta$, if r approaches infinity at far zone with $\theta \neq 0$, then ρ approached infinity also. This leads to

$$H_1^{(2)}(k_c\rho) \approx \sqrt{\frac{2}{\pi k_c \rho}}\, e^{-j\left(k_c\rho - \frac{3}{4}\pi\right)}$$
$$H_o^{(2)}(k_c\rho) \approx \sqrt{\frac{2}{\pi k_c \rho}}\, e^{-j\left(k_c\rho - \frac{\pi}{4}\right)} \tag{4.46}$$

Substituting (4.46) in (4.38), the EM fields at the far zone can be expressed as

$$E_{\rho 2} = \int_{-\infty}^{\infty} h_1(k_c)\, e^{-\Gamma_2 z}\, e^{-jk_c\rho} dk_c$$
$$E_{z2} = \int_{-\infty}^{\infty} h_2(k_c)\, e^{-\Gamma_2 z}\, e^{-jk_c\rho} dk_c \tag{4.47}$$
$$H_{\phi 2} = \int_{-\infty}^{\infty} h_3(k_c)\, e^{-\Gamma_2 z}\, e^{-jk_c\rho} dk_c$$

where

$$h_1(k_c) = \sqrt{\frac{k_c}{2\pi\rho}}\, e^{j\frac{3}{4}\pi} \frac{T}{1+R_{b1}} \int_a^b \mathcal{E}(\rho') J_1(k_c\rho')\rho' d\rho'$$
$$h_2(k_c) = \sqrt{\frac{k_c^3}{2\pi\rho}}\, e^{j\frac{\pi}{4}} \frac{1}{\Gamma_2} \frac{T}{1+R_{b1}} \int_a^b \mathcal{E}(\rho') J_1(k_c\rho')\rho' d\rho' \tag{4.48}$$
$$h_3(k_c) = \sqrt{\frac{k_c}{2\pi\rho}}\, e^{j\frac{3}{4}\pi} Y_{e2} \frac{T}{1+R_{b1}} \int_a^b \mathcal{E}(\rho') J_1(k_c\rho')\rho' d\rho'$$

The far zone fields in (4.47) can be evaluated more efficiently using the saddle point method (also known as the method of steep decent). It is observed that the far zone fields

in (4.47) take a form of a generic integral as

$$I(k_c) = \int_{-\infty}^{\infty} h_i(k_c)\, e^{-\Gamma_2 z} e^{-jk_c\rho} dk_c \tag{4.49}$$

where $h_i(k_c)$, i=1 to 3, is defined in (4.48).

4.3.2 Far Zone Field Derivation via Saddle Point Method [21,39]

To apply the saddle point method, the integral of (4.49) must be first placed in an appropriate form as follow:

With $\Gamma_2 \equiv j\beta$, we can transform the (ρ,z) and (k_c,β) planes to spherical coordinates. With reference to fig. 4.3, we have

$$\begin{aligned} \rho &= r\sin\theta \\ z &= r\cos\theta \end{aligned} \tag{4.50}$$

and

$$\begin{aligned} k_c &= k_2 \sin\psi \\ \beta &= k_2 \cos\psi \end{aligned} \tag{4.51}$$

with

$$\begin{aligned} \psi &= \sigma + j\eta \\ dk_c &= k_2 \cos\psi\, d\psi \end{aligned} \tag{4.52}$$

This leads to

$$\begin{aligned} \beta z + k_c\rho &= k_2 r\cos\theta\cos\psi + k_2 r\sin\theta\sin\psi \\ &= k_2 r\cos(\psi-\theta) \end{aligned} \tag{4.53}$$

Equation (4.51) represents a mapping of complex k_c plane into a strip of the complex ψ plane. The two Riemann sheets in k_c plane are mapped into a connected strip with 2π along the σ axis as follows:

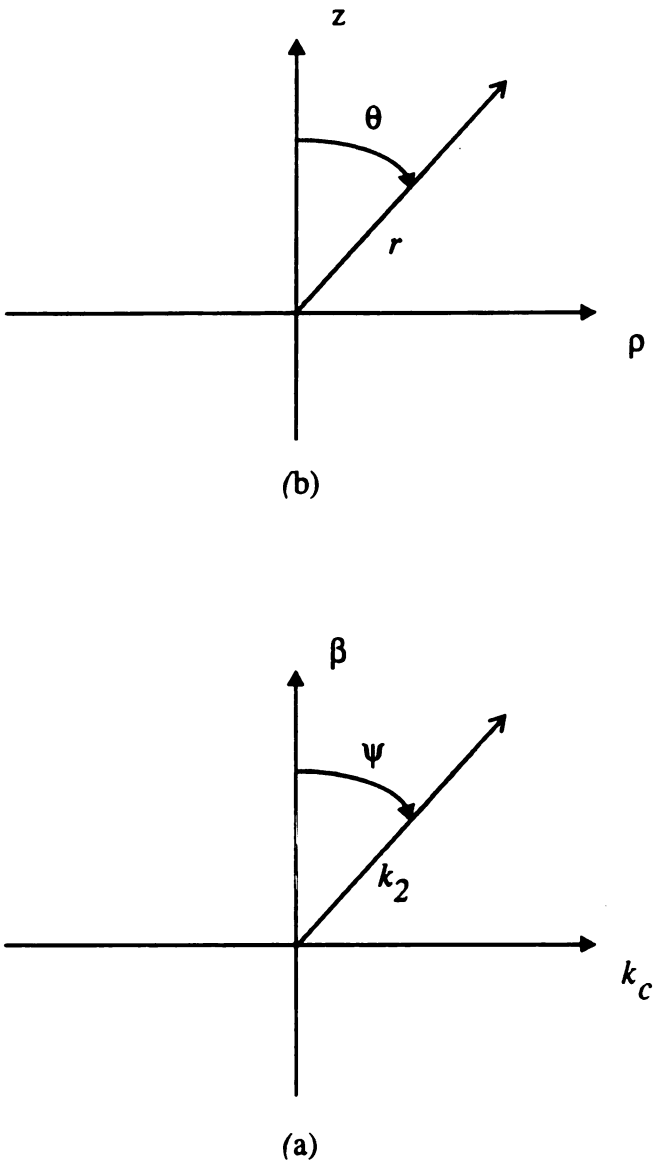

Figure 4.3 Transformation to spherical coordinates, (a) in k_c -β plane (b) in ρ–z plane.

With (4.51), we have

$$\begin{aligned}\Gamma_2 &= j\beta = jk_2\cos(\sigma + j\eta) \\ &= k_2 \sin\sigma \sinh\eta + jk_2 \cos\sigma \cosh\eta\end{aligned} \tag{4.54}$$

On the proper sheet of the Riemann surface, we have $R_e\{\Gamma_2\}>0$ and hence

$$\sin\sigma \sinh\eta > 0 \tag{4.55}$$

which corresponds to the range of

$$\begin{cases}\sigma:[-\pi,0] , & \eta<0 \\ \sigma:[0,\pi] , & \eta>0\end{cases} \tag{4.56}$$

Similarly for the improper sheet of the Riemann surface, we have

$$\begin{cases}\sigma:[-\pi,0] , & \eta>0 \\ \sigma:[0,\pi] , & \eta<0\end{cases} \tag{4.57}$$

This mapping is illustrated in fig. 4.4 where the shaded regions are the proper Riemann sheet.

Also with (4.51), we have

$$\begin{aligned}k_c &= k_2 \sin\psi \\ &= k_2 \sin\sigma \cosh\eta + jk_2 \cos\sigma \sinh\eta\end{aligned} \tag{4.58}$$

or

$$\begin{aligned}R_e\{k_c\} &= k_2 \sin\sigma \cosh\eta \\ I_m\{k_c\} &= k_2 \cos\sigma \sinh\eta\end{aligned} \tag{4.59}$$

With (4.59), the four quadrants of the proper Riemann sheet on k_c plane are mapped into the regions designated by P_i, i=1,...,4, as shown in fig. 4.4.

Also the real axis of k_c plane is mapped into the contour, denoted by C, passing from $(-\pi/2,-\infty)$ to $(\pi/2,\infty)$ in the ψ plane.

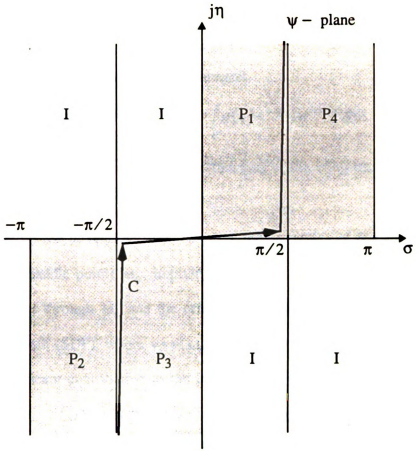

Figure 4.4 Mapping of two Riemann sheets of the k_c plane onto a stripe of the $\psi = \sigma + j\eta$ plane.

With (4.52) and (4.53), the generic integral (4.49) can be rewritten in spherical coordinates as

$$I(\psi)=\int_C h(\psi)e^{-jk_2 r\cos(\psi-\theta)}\,k_2\cos\psi\,d\psi \tag{4.60}$$

Let's consider the following general integral,

$$I(\alpha)=\int_C g(\omega)e^{\alpha f(\omega)}d\omega=\int_C g(\omega)e^{\alpha u(\omega)}e^{j\alpha v(\omega)}d\omega \tag{4.61}$$

in which $f(\omega)=u(\omega)+jv(\omega)$ is a complex function of the complex variable ω and α is a large positive number.

This integral can be approximated based on the properties of $f(\omega)$ at the stationary point (or called saddle point) ω_0, implying $f'(\omega_0)=0$. The concept is to deform the contour C to pass through ω_0 and the orientation of the contour is directed along the steepest decent path (SDP), where $v=v(\omega_0)$ is constant and $u(\omega_0)$ is maximum.

Then significant contribution to the integral comes from this steepest decent path near ω_0, because $\alpha u(\omega)$ decrease rapidly away from ω_0 along the SDP and destructive oscillation is avoided due to the constant phase $v(\omega_0)$.

By Taylor's series expansion about the saddle point, we have

$$\begin{aligned} f(\omega) &\approx f(\omega_0)+\frac{1}{2}f''(\omega_0)(\omega-\omega_0)^2 \\ &= f(\omega_0)+\frac{1}{2}FR^2e^{j(\xi+2\delta)} \end{aligned} \tag{4.62}$$

where

$$\begin{aligned} f''(\omega_0) &= Fe^{j\xi} \\ (\omega-\omega_0) &= Re^{j\delta} \end{aligned} \tag{4.63}$$

This leads to

$$u(\omega) \approx u(\omega_0) + \frac{1}{2} FR^2 \cos(\xi + 2\delta)$$
$$v(\omega) \approx v(\omega_0) + \frac{1}{2} FR^2 \sin(\xi + 2\delta) \tag{4.64}$$

Along the path

$$\xi + 2\delta = \pm \pi \tag{4.65}$$

we have

$$u(\omega) = u(\omega_0) - \frac{1}{2} FR^2$$
$$v(\omega) = v(\omega_0) \tag{4.66}$$

and

$$e^{\alpha f(\omega)} = e^{\alpha f(\omega_0)} e^{-\frac{\alpha FR^2}{2}} \tag{4.67}$$

It is clear that $e^{\alpha f(\omega)}$ in (4.67) has a constant phase, in addition, it has a maximum at ω_0, $(R=0)$, and decreases exponentially away from ω_0. Therefore (4.65) defines the steepest decent path about the saddle point ω_0. Hence we have

$$\delta = \frac{-\xi}{2} \pm \frac{\pi}{2} \tag{4.68}$$

With the change of variable in (4.63) and assuming δ unchanged, we have $d\omega = e^{j\delta} dR$ and (4.61) becomes,

$$I(\alpha) \approx e^{\alpha f(\omega_0)} e^{j\delta} \int_{SDP} g(\omega_0 + Re^{j\delta}) e^{-\frac{\alpha}{2} FR^2} dR \tag{4.69}$$

where SDP is the steepest decent path.

For a sufficient large α, the contribution to the integral in (4.69) mainly comes from the SDP near the saddle point ω_0 since $e^{-\frac{\alpha}{2} FR^2}$ decreases rapidly away from ω_0. This argument prevails even on the limiting case, where α approaches infinity, such that $e^{-\frac{\alpha}{2} FR^2}$ is extremely small for $R \neq 0$, then we have

$$I(\alpha) = g(\omega_0) e^{\alpha f(\omega_0)} e^{j\delta} \int_{-\infty}^{\infty} e^{-\frac{\alpha}{2} F R^2} dR$$
$$= \sqrt{\frac{2\pi}{\alpha F}}\, g(\omega_0) e^{\alpha f(\omega_0)} e^{j\delta} \tag{4.70}$$

The generic integral (4.60) in spherical coordinates can now be converted into a closed form using (4.70). Comparing (4.60) to (4.61), we have

$$\begin{aligned} \alpha &= k_2 r \\ g(\psi) &= k_2 h_i(\psi) \cos\psi \\ f(\psi) &= -j\cos(\psi - \theta) = u(\psi) + jv(\psi) \end{aligned} \tag{4.71}$$

This leads to

$$\begin{aligned} u(\psi) &= -\sin(\sigma - \theta)\sinh\eta \\ v(\psi) &= -\cos(\sigma - \theta)\cosh\eta \end{aligned} \tag{4.72}$$

and

$$\begin{aligned} f'(\psi) &= j\sin(\psi - \theta) \\ f''(\psi) &= j\cos(\psi - \theta) \end{aligned} \tag{4.73}$$

The saddle point is obtained from $f'(\psi_o) = 0$, then we have

$$\psi_o = \theta \tag{4.74}$$

This gives

$$\begin{aligned} f''(\psi_o) &= j \\ F &= 1 \\ \xi &= \frac{\pi}{2} \\ \delta &= -\frac{\pi}{4} \pm \frac{\pi}{2} \end{aligned} \tag{4.75}$$

and

$$f(\psi_o) = -j$$
$$u(\psi_o) = 0 \tag{4.76}$$
$$v(\psi_o) = -1$$

The steepest decent path is determined by equating $v(\psi)$ to $v(\psi_0)$ in (4.72) and (4.76) as

$$\cos(\sigma - \theta)\cosh\eta = 1 \tag{4.77}$$

The SDP is depicted in fig. 4.5 and it is clear that $\delta = \frac{\pi}{4}$ should be chosen. Therefore, with (4.70) the generic integral in (4.60) becomes

$$I(r) = \sqrt{\frac{2\pi}{k_2 r}}\, h_i(k_c) k_2 \cos\theta\, e^{-jk_2 r} e^{j\frac{\pi}{4}} \tag{4.78}$$

where $h_i(k_c)$, i=1 to 3, is given in (4.48) with

$$k_c = k_2 \sin\theta$$
$$\Gamma_2 = j\beta = jk_2\cos\theta \tag{4.79}$$
$$\Gamma_1 = \sqrt{k_c^2 - k_1^2} = \sqrt{k_2^2\sin^2\theta - k_1^2}$$

Thus the EM fields in (4.47) becomes

$$E_{\rho 2} = \sqrt{\frac{2\pi}{k_2 r}}\, h_1(k_c) k_2 \cos\theta\, e^{-jk_2 r} e^{j\frac{\pi}{4}}$$
$$E_{z2} = \sqrt{\frac{2\pi}{k_2 r}}\, h_2(k_c) k_2 \cos\theta\, e^{-jk_2 r} e^{j\frac{\pi}{4}} \tag{4.80}$$
$$H_{\phi 2} = \sqrt{\frac{2\pi}{k_2 r}}\, h_3(k_c) k_2 \cos\theta\, e^{-jk_2 r} e^{j\frac{\pi}{4}}$$

with $h_i(k_c)$, i=1 to 3, defined in (4.48).

Hence, using the saddle point method, we are able to derive the far zone fields in (4.80) by deforming the contour C to SDP. However in deforming the contour, some of

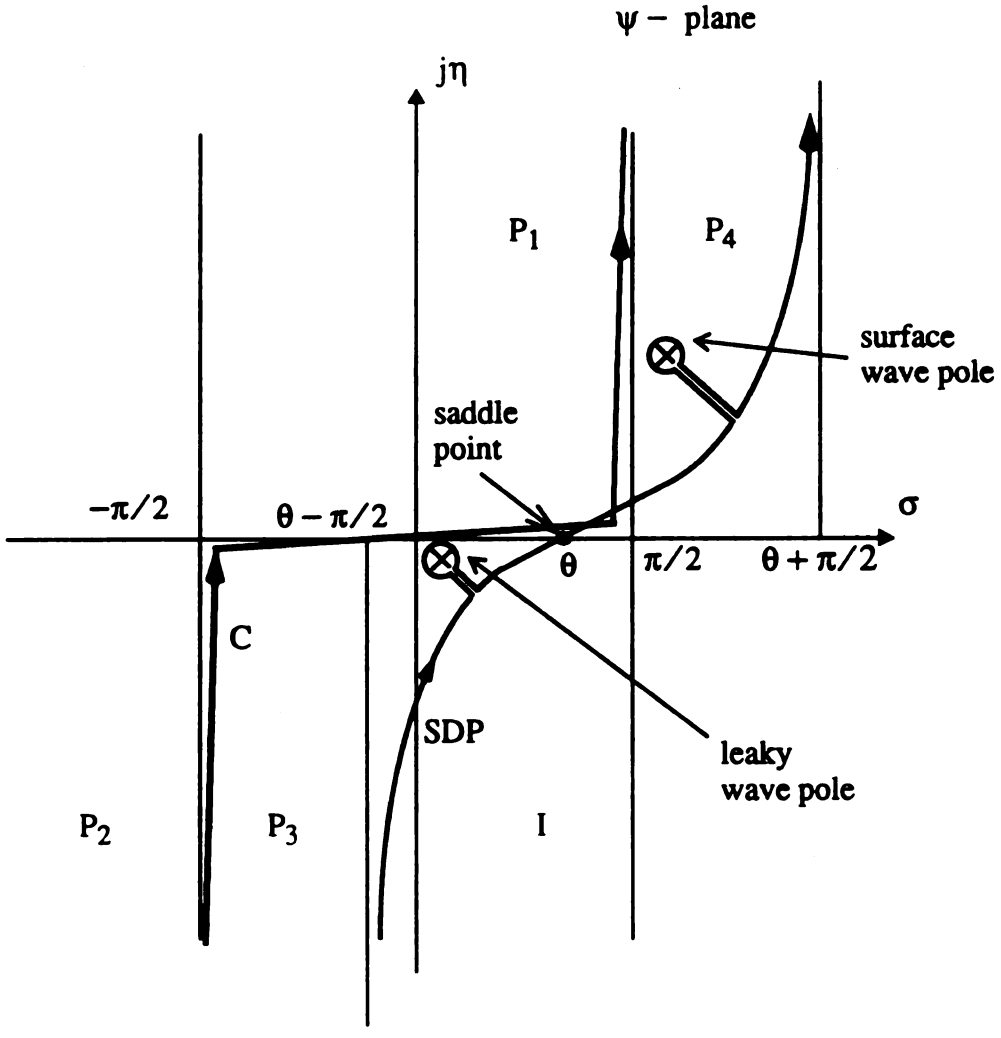

Figure 4.5 Deformation of contour C into steepest decent path SDP.

the poles in $h_t(k_c)$ may be encountered. When this happens, the contour should be warped as in fig. 4.5. Thus the contribution to the far zone fields from the integration around these poles need to be included

There are two kinds of poles, the surface wave poles and the leaky wave poles, the former locates on the proper Riemann sheet and the latter on the improper Riemann sheet.

From fig. 4.5, it is shown that these poles are encountered only for a range of θ greater than some critical angle θ_c. Also even when these poles are encountered, it can be shown that the contribution from either surface waves or leaky waves decays exponentially as $r \to \infty$. Therefore the far zone fields can be approximated by the radiative wave fields.

Substituting (4.80) and (4.48) in (4.45), it can be verified that the radiative wave power is independent of r. Therefore by letting $r \to \infty$, the evaluation of the far zone fields via saddle point method becomes exact, not just approximate, and the accuracy of the power evaluation can be preserved.

Power Balance Verification

The total power P_T carried away from the aperture is the sum of the surface wave power and the radiative wave power as mentioned before. Physically, P_T should be equal to the transmitted power of the incident TEM wave, which is shown as follows:

The TEM wave in its transverse dependence can be expressed as

$$\vec{E} = \hat{\rho}\,\frac{1}{\rho}$$
$$\vec{H} = \hat{\phi}\,\frac{1}{\rho\eta} \tag{4.81}$$

and the incident power of the TEM wave is obtained as

$$P_i = \frac{1}{2}\int_0^{2\pi}\int_a^b R_e[E_\rho H_\phi^*]\rho\, d\rho\, d\phi$$
$$= \frac{\pi}{\eta}\ln\left(\frac{b}{a}\right) \tag{4.82}$$

Since R is the reflection coefficient of the TEM wave at the aperture, the transmitted power P_t is

$$P_t = (1 - |R|^2)P_i \tag{4.83}$$

By solving the simultaneous algebraic equations (3.125), the numerical aperture electric field is determined and the reflection coefficient is obtained. Then the transmitted power P_t can be computed using (4.83) and the total power P_T carried away from the aperture can be computed using (4.34) and (4.45).

The quantity P_T is compared to P_t as shown in fig. 4.6, where a=0.3102cm, b=0.7145cm, d=1cm, $\varepsilon_1=3\varepsilon_o$ and $\varepsilon_2=\varepsilon_o$ are assumed. They are almost equal as expected.

Also it is found that the excitation of surface waves and radiative waves is strongly dependent on the frequency. Especially at the low frequency range, less than 2 GHz in this case, the transmitted power is so small that the EM fields excited inside the material media are localized around the probe aperture. This finding justifies the assumption of the infinite metallic plate in the full wave analysis, and provides a physical reason for the validity of the quasi-static analysis [14,35].

Similar phenomenon is observed for the short-circuit case in next section.

4.4 Radial Guided Wave Power for Short-Circuit Case

In this section the total power contribution due to radial guided waves excited in the short-circuit case of an open-ended coaxial probe system is studied.

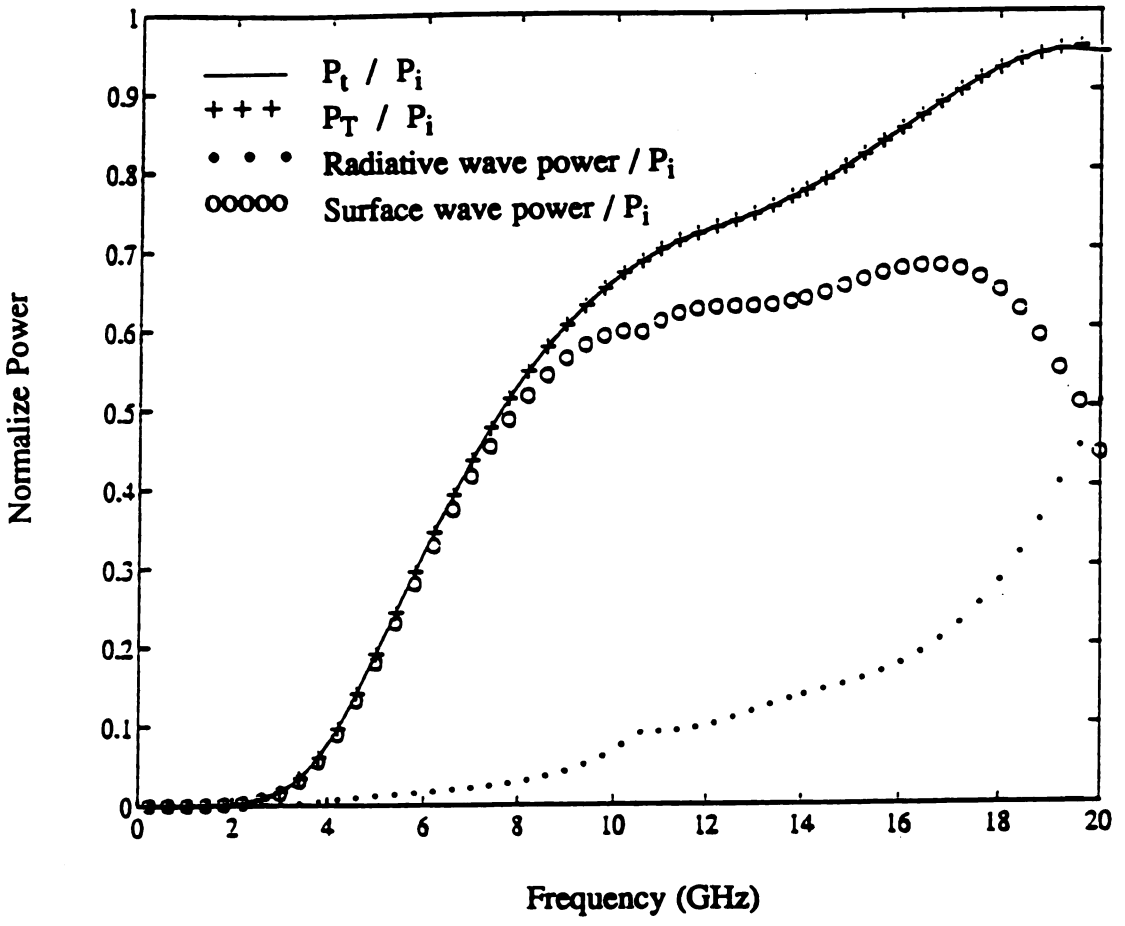

Figure 4.6 The power balance verification for open-circuit case. The total power carried away from the aperture and the transmitted power of the incident wave, both normalized by the input power, agree quite well.

For illustrative purpose, we consider an open-ended coaxial probe placed against a single layer lossless material medium as shown in fig. 4.7. Since the radial guided waves are orthogonal, the total power carried by radial guided waves can be computed by summing up the power associated with each individual mode.

The radial guided wave poles are studied and it is found that there exists propagating and evanescent radial guided waves. It's obvious that the power is carried away in radial direction. The EM fields for each radial guided wave are derived first using a deformed contour integral, after that the power of a propagating wave can be evaluated numerically.

4.4.1 Radial Guided Waves inside Material Medium

The general field expression (4.2) in region 1 is valid for either open- or short-circuit case:

$$E_{\rho 1} = \frac{1}{2}\int_{-\infty}^{\infty} \frac{1}{1+R_{b1}} \left(\int_a^b \mathcal{E}(\rho') J_1(k_c\rho')\rho' d\rho' \right) (e^{-\Gamma_1 z} + R_{b1} e^{\Gamma_1 z}) H_1^{(2)}(k_c\rho) k_c dk_c$$

$$H_{\phi 1} = \frac{1}{2}\int_{-\infty}^{\infty} \frac{j\omega\epsilon_1}{\Gamma_1} \frac{1}{1+R_{b1}} \left(\int_a^b \mathcal{E}(\rho') J_1(k_c\rho')\rho' d\rho' \right) (e^{-\Gamma_1 z} - R_{b1} e^{\Gamma_1 z}) H_1^{(2)}(k_c\rho) k_c dk_c \quad (4.84)$$

$$E_{z1} = \frac{1}{2}\int_{-\infty}^{\infty} \frac{1}{\Gamma_1} \frac{1}{1+R_{b1}} \left(\int_a^b \mathcal{E}(\rho') J_1(k_c\rho')\rho' d\rho' \right) (e^{-\Gamma_1 z} - R_{b1} e^{\Gamma_1 z}) H_0^{(2)}(k_c\rho) k_c^2 dk_c$$

For short-circuit case, R_{b1} satisfies the boundary condition of tangential electric field being zero at z=d. That is,

$$e^{-\Gamma_1 d} + R_{b1} e^{\Gamma_1 d} = 0 \quad (4.85)$$

where $\Gamma_1 = \sqrt{k_c^2 - k_1^2}$.

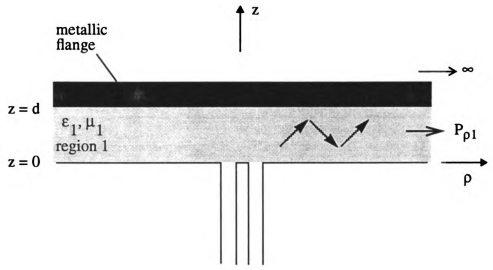

Figure 4.7 The radial guided waves are excited in the short-circuit case of an open-ended coaxial probe placed against a layered material medium, where $P_{\rho 1}$ stands for the power flow in region 1.

This leads to

$$R_{b1} = -e^{-2\Gamma_1 d} \tag{4.86}$$

It is found that the radial guided wave poles satisfy

$$1 + R_{b1} = 1 - e^{-2\Gamma_1 d} = 0 \tag{4.87}$$

Letting $\Gamma_1 = j\beta_1$, we have $\beta_1 = \sqrt{k_1^2 - k_c^2} > 0$. Equation (4.87) then becomes

$$1 - e^{-j2\beta_1 d} = e^{j2m\pi} - e^{-j2\beta_1 d} = 0 \tag{4.88}$$

or

$$\beta_1 = \beta_{1m} = \frac{m\pi}{d} \tag{4.89}$$

where $m = 0, 1, 2, 3, \ldots.$

It is found that the propagating radial guided wave poles exist in the range of $[0, k_1]$ such that from (4.89) we have

$$k_{cpm} = \sqrt{k_1^2 - \beta_{1m}^2} = \sqrt{k_1^2 - (\frac{m\pi}{d})^2} \tag{4.90}$$

where k_{cpm} is the m^{th} radial guided wave pole and m goes from 0 up to $M < k_1 d/\pi$.

Also there are evanescent radial guided waves when k_{cpm} locates along the negative imaginary axis, which decay exponentially in ρ direction and carry no real power flow at all.

With reference to fig. 3.3, it is shown that using a deformed contour integral $E_{\rho 1}$ in (4.84) becomes

$$E_{\rho 1} = \frac{1}{2}\oint_{C_p} \frac{(e^{-\Gamma_1 z} + R_{b1} e^{\Gamma_1 z})}{(1 + R_{b1})} \left[\int_a^b \mathcal{G}(\rho') J_1(k_c \rho') \rho' d\rho' \right] H_1^{(2)}(k_c \rho) k_c dk_c \tag{4.91}$$

where C_p stands for the contour around the radial guided wave poles.

Similar expressions can be derived for $H_{\phi 1}$ and E_{z1}, also.

It can be shown that the propagating radial guided wave poles are simple poles. Therefore the radial guided wave field $E_{\rho 1}$ can be derived by the residue evaluation of the integrand in (4.91) as

$$E_{\rho 1} = -\pi j \left(\int_a^b \mathscr{E}(\rho') J_1(k_{cpm}\rho') \rho' d\rho' \right) (e^{-\Gamma_1 z} + R_{b1} e^{\Gamma_1 z}) H_1^{(2)}(k_{cpm}\rho) k_{cpm} \lim_{k_c \to k_{cpm}} \frac{1}{1 + R_{b1}} [k_c - k_{cpm}] \tag{4.92}$$

Introducing notations Q and L_s, (4.92) becomes

$$E_{\rho 1} = -\pi j \Gamma_1 Q L_s k_{cpm} (e^{-\Gamma_1 z} + R_{b1} e^{\Gamma_1 z}) H_1^{(2)}(k_{cpm}\rho) \tag{4.93}$$

where Q has been defined in (4.8) and L_s is

$$L_s = \lim_{k_c \to k_{cpm}} \frac{1}{\Gamma_1} \frac{1}{1 + R_{b1}} (k_c - k_{cpm}) \tag{4.94}$$

Similarly the field components $H_{\phi 1}$ and E_{z1} of a radial guided wave are

$$\begin{aligned} H_{\phi 1} &= -\pi j (j\omega \epsilon_1) Q L_s k_{cpm} (e^{-\Gamma_1 z} - R_{b1} e^{\Gamma_1 z}) H_1^{(2)}(k_{cpm}) \\ E_{z1} &= -\pi j Q L_s k_{cpm}^2 (e^{-\Gamma_1 z} - R_{b1} e^{\Gamma_1 z}) H_o^{(2)}(k_{cpm}) \end{aligned} \tag{4.95}$$

4.4.2 Calculation of Radial Guided Wave Power

The power associated with each radial guided wave is computed using (4.18). Since the power is directed in radial direction only, $P_{\rho 1}$ is calculated from (4.19) as

$$P_\rho = P_{\rho 1} = \frac{1}{2} \int_0^d \int_0^{2\pi} R_e[-E_{z1} H_{\phi 1}^*] \rho \, d\phi \, dz \tag{4.96}$$

With $\Gamma_1 = j\beta_1$ and (4.95), the field components of the radial guided wave become

$$H_{\phi 1}^{*} = \pi j(-j\omega \epsilon_1) Q^{*} L_s^{*} k_{cpm}^{*} \left(e^{-j\beta_1 z} - R_{b1} e^{j\beta_1 z}\right)^{*} H_1^{(2)^{*}}(k_{cpm})$$
$$E_{z1} = -\pi j Q L_s k_{cpm}^2 \left(e^{-j\beta_1 z} - R_{b1} e^{j\beta_1 z}\right) H_o^{(2)}(k_{cpm}) \tag{4.97}$$

After some manipulation, we have

$$e^{-j\beta_1 z} - R_{b1} e^{j\beta_1 z} = e^{-j\beta_1 z} + e^{-2j\beta_1 d} e^{j\beta_1 z} = e^{-2j\beta_1 d} 2\cos\beta_1(d-z) \tag{4.98}$$

Substitution of (4.98) in (4.97) leads to

$$E_{z1} H_{\phi 1}^{*} = 4\pi^2(-j\omega \epsilon_1) \left|Q L_s k_{cpm}\right|^2 k_{cpm} \cos^2\beta_1(d-z) H_0^{(2)}(k_{cpm}\rho) H_1^{(2)^{*}}(k_{cpm}\rho) \tag{4.99}$$

With the product of the two Hankel functions as simplified in (4.23), (4.99) gives

$$R_e[E_{z1} H_{\phi 1}^{*}] = -8\pi\omega\epsilon_1 \left|Q L_s k_{cpm}\right|^2 \cos^2\beta_1(d-z) \frac{1}{\rho} \tag{4.100}$$

Substituting (4.100) in (4.96) results in

$$P_\rho = \frac{1}{2} \int_0^{2\pi} 8\pi\omega\epsilon_1 \left|Q L_s k_{cpm}\right|^2 \int_0^{d} \cos^2\beta_1(d-z) dz d\phi \tag{4.101}$$

Note that $P_{\rho 1}$ in (4.101) is independent of ρ, which is consistent with the fact that radial guided wave is a cylindrical wave.

After some manipulation, the integral with respect to z in (4.101) can be expressed as

$$g(d) = \int_0^{d} \cos^2\beta_1(d-z) dz$$
$$= \begin{cases} d, & \text{if } \beta_1 = 0 \\ \dfrac{d}{2}, & \text{if } \beta_1 \neq 0 \end{cases} \tag{4.102}$$

Therefore (4.101) becomes

$$P_\rho = 8\pi^2\omega\epsilon_1 \left|Q L_s k_{cpm}\right|^2 g(d) \tag{4.103}$$

with

$$\beta_1 = \sqrt{k_1^2 - k_{cpm}^2}$$

$$L_s = \lim_{k_c \to k_{cpm}} \frac{1}{\Gamma_1} \frac{1}{1 + R_{b1}} (k_c - k_{cpm}) \qquad (4.104)$$

$$Q = \int_a^b \mathcal{E}(\rho') J_1(k_{cpm}\rho') \rho' d\rho'$$

Also the quantity Q can be computed numerically using (4.37).

With (4.103), the total power carried away by radial guided waves is the sum of the power of each individual propagating wave:

$$P_{r.g.w} = \sum_{m=0}^{M} 8\pi^2 \omega \varepsilon_1 |Q L_s k_{cpm}|^2 g(d) \qquad (4.105)$$

Power Balance Verification

The radial guided wave power $P_{r.g.w.}$ is the total power carried away from the aperture, which should be equal to the transmitted power of the incident wave due to power conservation. The total radial guided wave power $P_{r.g.w.}$ in (4.105) is compared to the transmitted power P_t of (4.83) as shown in fig. 4.8, where a=0.3102cm, b=0.7145cm, d=1cm and $\varepsilon=3\varepsilon_0$ are assumed. They are almost equal as expected.

Also in fig. 4.8 the excitation of radial guided waves is shown to be strongly dependent on the frequency. The kinks in the figure correspond to the occurance of the next high order radial guided wave mode. It is noted that in the low frequency range, less than 2 GHz in this case, the transmitted power is so small that the EM fields excited inside the material medium are localized around the probe aperture, as in the open-circuit case.

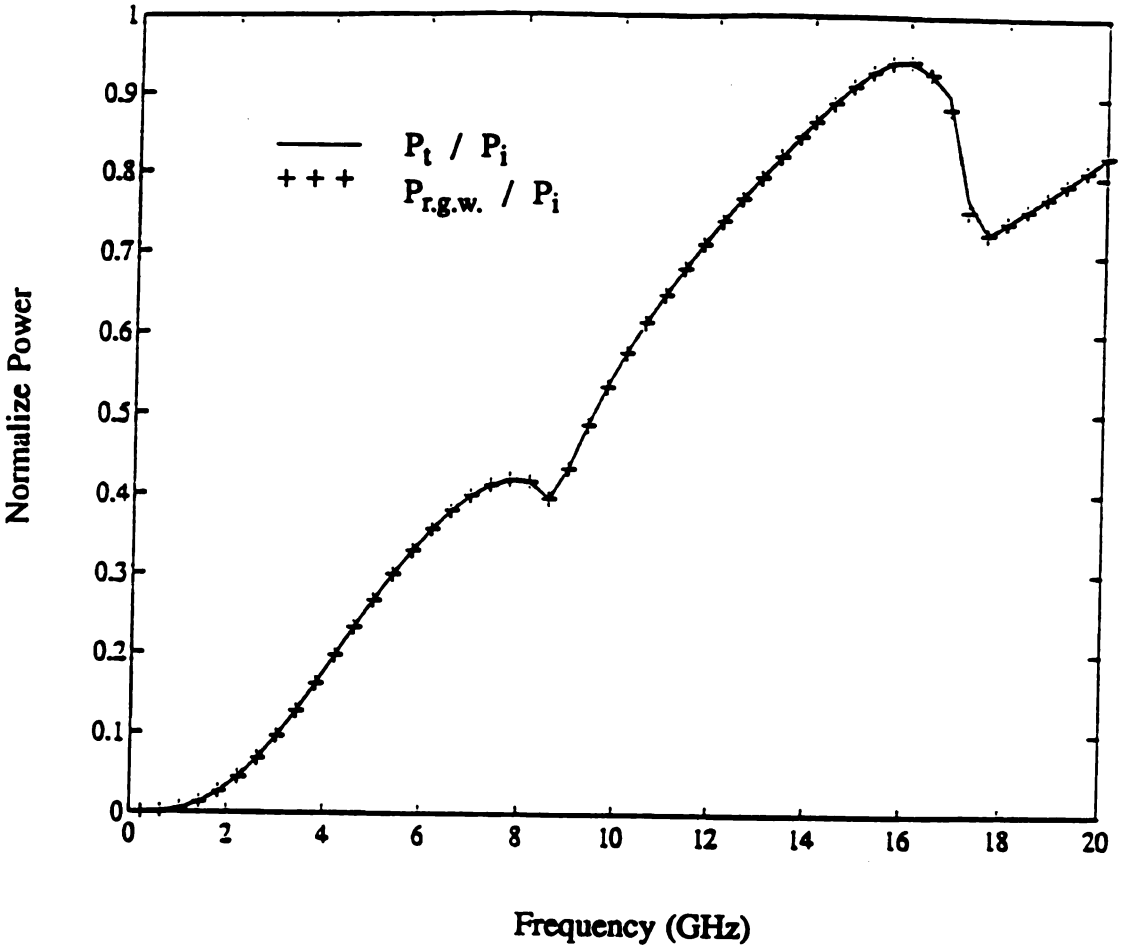

Figure 4.8 The power balance verification for short-circuit case of an open-ended coaxial probe. The radial guided wave power and the transmitted power of the incident wave, both normalized by the input power, agree quite well.

Therefore when an open-ended coaxial probe is used to measure the EM properties of a thick material layer at the low frequency range, the scheme of using open-circuit input impedance and short-circuit input impedance to quantify both complex permittivity ε and permeability μ fails , because these two impedances are almost identical.

To overcome this difficulty we can either prepare two samples of the same material with different thicknesses, or use a coaxial cavity structure to contain the material, which is studied in chapter 5. With these schemes the complex permittivity ε and permeability μ can be uniquely determined as long as two different input impedances of the probe can be measured for the same material.

CHAPTER 5
COAXIAL CAVITY SYSTEM TO MEASURE THE PERMITTIVITY AND PERMEABILITY OF MATERIAL

5.1 Introduction

In this chapter the analysis of a coaxial cavity system for the measurement of electromagnetic (EM) properties of materials is presented [21].

As mentioned in chapter 4, when an open-ended coaxial probe is used to measure the EM properties of a thick material layer, the EM fields excited inside the material layer are localized around the probe aperture. Thus, the scheme of using open-circuit input impedance and short-circuit input impedance to quantify both complex permittivity ε and permeability μ will fail, because these two impedances are almost identical.

One method to overcome this difficulty is to let the center conductor of the coaxial probe extend into the material medium so that the EM fields are extended deep into the materials. To accommodate this arrangement, a coaxial line is terminated on a coaxial cavity with a movable backwall as shown in fig. 5.1. When the cavity is partially filled with a material, two input impedances of the coaxial line can be measured by setting the cavity backwall at two different locations. From these two input impedances the complex permittivity ε and permeability μ of the material can be determined.

Theoretically this cavity system is analyzed as follows. An incident TEM mode to the probe is partially reflected by the discontinuity at the aperture and it also excites EM

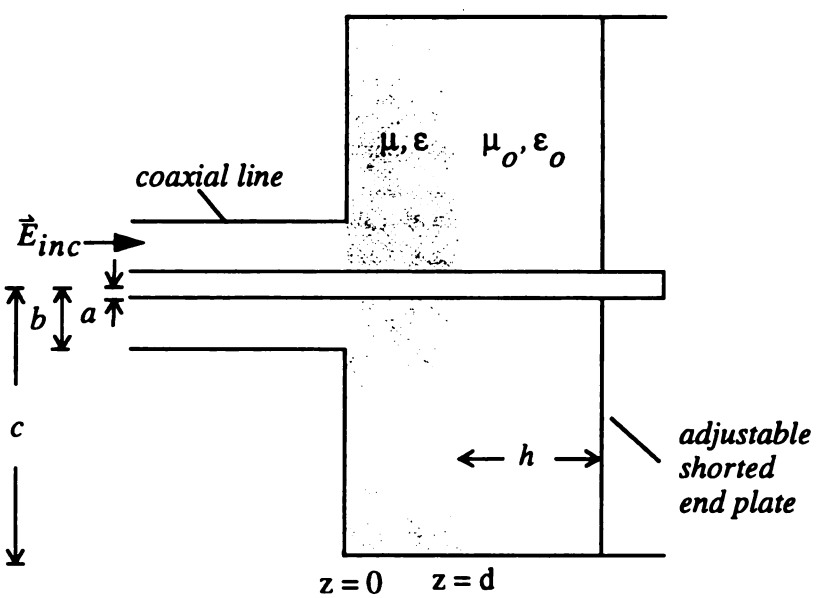

Figure 5.1 Geometry of a coaxial line terminated on a coaxial cavity which accommodates an isotropic material layer medium.

fields in the material layer medium inside the cavity. Additionally, the higher order coaxial modes are excited near the probe aperture. The EM fields in the coaxial line part and in the material medium inside the cavity can be expressed in terms of modal functions. The matching of the tangential electric and magnetic fields at the probe aperture will lead to an integral equation for the unknown aperture electric field.

To determine the reflection coefficient of TEM mode at the probe aperture, the integral equation for the unknown aperture electric field is solved by the method of moments. After the aperture electric field is obtained, the reflection coefficient of the TEM mode or the input impedance of the coaxial line can be determined in terms of ε and μ of the material medium. Conversely, if the input impedances of the coaxial line are experimentally measured with the help of a network analyzer, ε and μ of the material medium can be inversely determined.

It can be observed that a resonant phenomenon occurs in this structure, and at these resonant frequencies the determination of μ and ε of materials becomes ill-conditioned. The metallic wall loss effect of the coaxial cavity near the resonance frequencies is then investigated to help mitigate the ill-conditioned problem.

In section 5.2 the results of general guided wave theory are applied to solve the EM fields at both sides of the aperture, and an EFIE is derived by matching the boundary conditions across the aperture. Meanwhile the reflection coefficient of the incident TEM wave is expressed in terms of the aperture electric field.

In section 5.3 an equivalent circuit concept for a coaxial line discontinuity is presented, by which the physical meaning of input impedance at the aperture of the probe is clearly revealed [41,42]. Also, the validity of the results based on full wave analysis is verified by comparison with that of equivalent circuit concept.

In section 5.4 the method of moments is applied to solve the EFIE. The TM eigenmodes of the coaxial line are chosen to be the basis functions for the unknown aperture field. Galerkin's technique is used to convert the integral equation into a set of simultaneous algebraic equations. After the numerical solution of aperture electric field is obtained, the input admittance at the aperture is resolved.

In section 5.5 the power loss due to a non-perfectly conducting cavity wall is studied and several numerical results are presented. The analysis is based on the energy conservation (complex Poynting theorem) and perturbation approach. In general, this analysis can be applied to a cavity of any shape.

5.2 Theoretical Study Using Full Wave Analysis

Integral Equation for Aperture Electric Field

An integral equation for the aperture electric field is derived in this section by matching the tangential EM fields across the aperture. Because of the discontinuity at the aperture, higher-order modes are excited in the coaxial line near the aperture in addition to the incident TEM mode. In addition, the EM fields excited inside the cavity can be expressed as a sum of coaxial cavity modes. For the case of TEM mode excitation, because the fields inside the coaxial line are ϕ-independent and the coaxial cavity with materials is rotationally symmetric the fields excited due to the discontinuity at $z=0$ also exhibit the rotational symmetry. Consequently, only TM modes are excited, and TE modes can be shown to be zero.

With the total transverse EM fields inside the coaxial line in (3.12), and the fields at the left hand side of the aperture $z=0^-$ already given in (3.14) and (3.15), only the EM fields inside the coaxial cavity need to be solved.

Fields inside coaxial cavity

For the fields in region $z \geq 0$ (inside the cavity and material), the field components exhibit rotational symmetry as mentioned before and only TM modes can be excited in the cavity.

For the α^{th} TM mode the field components in the j^{th} layer of material are derived from (3.6) and (3.7) in the form of (3.11).

By letting $m \rightarrow \alpha$, we have

$$\vec{E}_{t\alpha}^{\pm} = \mp\Gamma_{j\alpha} D_{j\alpha} \hat{\rho}\, k_{c\alpha} [J_0'(k_{c\alpha}\rho) - \frac{J_0(k_{c\alpha}a)}{Y_0(k_{c\alpha}a)} Y_0'(k_{c\alpha}\rho)] e^{\mp\Gamma_{j\alpha} z}$$
$$\vec{H}_{t\alpha}^{\pm} = -j\omega\epsilon_j D_{j\alpha} \hat{\phi}\, k_{c\alpha} [J_0'(k_{c\alpha}\rho) - \frac{J_0(k_{c\alpha}a)}{Y_0(k_{c\alpha}a)} Y_0'(k_{c\alpha}\rho)] e^{\mp\Gamma_{j\alpha} z} \tag{5.1}$$

Combining the forward and backward waves in the z-direction leads to

$$\vec{E}_{t\alpha} = \hat{\rho} B_{j\alpha} (e^{-\Gamma_{j\alpha} z} + R_{bj\alpha} e^{\Gamma_{j\alpha} z}) \Re_\alpha(\rho)$$
$$\vec{H}_{t\alpha} = \hat{\phi} \frac{j\omega\epsilon_j}{\Gamma_{j\alpha}} B_{j\alpha} (e^{-\Gamma_{j\alpha} z} - R_{bj\alpha} e^{\Gamma_{j\alpha} z}) \Re_\alpha(\rho) \tag{5.2}$$

where

$$\Re_\alpha(\rho) = N_\alpha [J_1(k_{c\alpha}\rho) Y_0(k_{c\alpha}a) - J_0(k_{c\alpha}a) Y_1(k_{c\alpha}\rho)] \tag{5.3}$$

with $k_{c\alpha}$ satisfies

$$J_0(k_{c\alpha}a) Y_0(k_{c\alpha}c) - J_0(k_{c\alpha}c) Y_0(k_{c\alpha}a) = 0 \tag{5.4}$$

The quantity $R_{bj\alpha}$ is the amplitude ratio of backward wave to forward wave of the α^{th} TM mode at interface j (between layers j and $j+1$). It is shown in chapter 2 that there exists a recursive relationship (2.46) between $R_{bj\alpha}$ and $R_{b(j+1)\alpha}$ such that $R_{bj\alpha}$ of layer j can be computed from that of neighboring layers.

For the TEM mode the field components in the j^{th} layer of material are

$$\vec{E}_t = \hat{\rho} B_{jo} \frac{1}{\rho} (e^{-jk_j z} + R_{bjo} e^{jk_j z})$$
$$\vec{H}_t = \hat{\phi} B_{jo} \frac{1}{\eta_j \rho} (e^{-jk_j z} - R_{bjo} e^{jk_j z}) \tag{5.5}$$

where $\eta_j = \sqrt{\mu_j / \epsilon_j}$ and $k_j = \omega\sqrt{\mu_j \epsilon_j}$ and R_{bjo} is the amplitude ratio of backward wave to forward wave of the TEM mode at the interface j.

The total transverse fields in the j^{th} layer are the sum of TEM mode and all the possible TM modes. For layer 1 the expressions are

$$\vec{E}_t = \hat{\rho} \left\{ B_{1o} \frac{1}{\rho} (e^{-jk_1 z} + R_{b1o} e^{jk_1 z}) + \sum_{\alpha=1}^{\infty} B_{1\alpha} (e^{-\Gamma_{1\alpha} z} + R_{b1\alpha} e^{\Gamma_{1\alpha} z}) \Re_\alpha(\rho) \right\}$$
$$\vec{H}_t = \hat{\phi} \left\{ \frac{B_{1o}}{\eta_1} \frac{1}{\rho} (e^{-jk_1 z} - R_{b1o} e^{jk_1 z}) + j\omega\epsilon_1 \sum_{\alpha=1}^{\infty} \frac{B_{1\alpha}}{\Gamma_{1\alpha}} (e^{-\Gamma_{1\alpha} z} - R_{b1\alpha} e^{\Gamma_{1\alpha} z}) \Re_\alpha(\rho) \right\} \tag{5.6}$$

The transverse field components at the right hand side of the aperture (inside layer 1) are obtained by setting $z = 0^+$ in (5.6):

$$\vec{E}_t(z=0^+) = \hat{\rho} \left[B_{1o} \frac{1}{\rho} (1 + R_{b1o}) + \sum_{\alpha=1}^{\infty} B_{1\alpha} (1 + R_{b1\alpha}) \Re_\alpha(\rho) \right]$$
$$\vec{H}_t(z=0^+) = \hat{\phi} \left[\frac{B_{1o}}{\eta_1} \frac{1}{\rho} (1 - R_{b1o}) + j\omega\epsilon_1 \sum_{\alpha=1}^{\infty} \frac{B_{1\alpha}}{\Gamma_{1\alpha}} (1 - R_{b1\alpha}) \Re_\alpha(\rho) \right] \tag{5.7}$$

where $R_{b1\alpha}$ and R_{b1o} of layer 1 can be computed from that of neighboring layers.

Matching the tangential E field and H field at z=0 an integral equation can be derived for the unknown aperture E field. Equating (3.14) and (3.15) to (5.7) over the aperture of $a \le \rho \le b$, we have

$$A_o\frac{1}{\rho}(1+R)+\sum_{m=1}^{\infty}A_m\Re_m(\rho)=B_{1o}\frac{1}{\rho}(1+R_{b1o})+\sum_{\alpha=1}^{\infty}B_{1\alpha}(1+R_{b1\alpha})\Re_\alpha(\rho) \tag{5.8}$$

and

$$\begin{aligned}&\frac{A_o}{\eta_1}\frac{1}{\rho}(1-R)-\sum_{m=1}^{\infty}\frac{j\omega\epsilon_1}{\Gamma_m}A_m\Re_m(\rho)\\&=\frac{B_{1o}}{\eta_1}\frac{1}{\rho}(1-R_{b1o})+j\omega\epsilon_1\sum_{\alpha=1}^{\infty}\frac{B_{1\alpha}}{\Gamma_{1\alpha}}(1-R_{b1\alpha})\Re_\alpha(\rho)\end{aligned} \tag{5.9}$$

Equations (5.8) and (5.9) can be cast into an integral equation for aperture electric field via some orthogonality properties. Letting $\mathscr{E}(\rho)$ be the E field at z=0, i.e. $E_\rho(z=0)$, (5.8) becomes

$$A_o\frac{1}{\rho}(1+R)+\sum_{m=1}^{\infty}A_m\Re_m(\rho)=\mathscr{E}(\rho)=B_{1o}\frac{1}{\rho}(1+R_{b1o})+\sum_{\alpha=1}^{\infty}B_{1\alpha}(1+R_{b1\alpha})\Re_\alpha(\rho) \tag{5.10}$$

Applying the following orthogonality properties to (5.10), the unknown amplitudes A_o, A_m , B_{1o} and $B_{1\alpha}$ can be determined:

With

$$\begin{cases}\int_a^b\Re_{m_1}(\rho)\Re_{m_2}(\rho)\rho d\rho=\delta_{m_1m_2}\\ \int_a^c\Re_{\alpha_1}(\rho)\Re_{\alpha_2}(\rho)\rho d\rho=\delta_{\alpha_1\alpha_2}\end{cases} \tag{5.11}$$

and

$$\begin{cases}\int_a^b\Re_m(\rho)d\rho=0\\ \int_a^c\Re_\alpha(\rho)d\rho=0\end{cases} \tag{5.12}$$

we have

$$A_o = \frac{1}{(1+R)\ln(b/a)} \int_a^b \mathcal{E}(\rho) d\rho$$
$$A_m = \int_a^b \mathcal{E}(\rho) \mathcal{R}_m(\rho) \rho d\rho \tag{5.13}$$

and

$$B_{1o} = \frac{1}{(1+R_{b1o})\ln(c/a)} \int_a^c \mathcal{E}(\rho) d\rho = \frac{1}{(1+R_{b1o})\ln(c/a)} \int_a^b \mathcal{E}(\rho) d\rho \tag{5.14}$$

$$B_{1\alpha} = \frac{1}{(1+R_{b1\alpha})} \int_a^c R_\alpha(\rho) \mathcal{E}(\rho) \rho d\rho = \frac{1}{(1+R_{b1\alpha})} \int_a^b R_\alpha(\rho) \mathcal{E}(\rho) \rho d\rho \tag{5.15}$$

Also from A_o we have

$$1+R = \frac{1}{A_o \ln(\frac{b}{a})} \int_a^b \mathcal{E}(\rho) d\rho$$
$$1-R = 2 - \frac{1}{A_o \ln(\frac{b}{a})} \int_a^b \mathcal{E}(\rho) d\rho \tag{5.16}$$

Substituting these amplitude coefficients in (5.9), an integral equation for aperture electric field is derived as follows:

$$A_o \frac{1}{\eta_1} \frac{1}{\rho} \left(2 - \frac{1}{A_o \ln(\frac{b}{a})} \int_a^b \mathcal{E}(\rho') d\rho' \right) - \sum_{m=1}^{\infty} Y_{TM} \mathcal{R}_m(\rho) \int_a^b \mathcal{E}(\rho') \mathcal{R}_m(\rho') \rho' d\rho'$$
$$= \frac{1}{\eta_1} \frac{1}{\rho} \frac{1-R_{b1o}}{1+R_{b1o}} \frac{1}{\ln(\frac{c}{a})} \int_a^b \mathcal{E}(\rho') d\rho' + \sum_{\alpha=1}^{\infty} \frac{j\omega\epsilon_1}{\Gamma_{1\alpha}} \frac{1-R_{b1\alpha}}{1+R_{b1\alpha}} \mathcal{R}_\alpha(\rho) \int_a^b \mathcal{E}(\rho') \mathcal{R}_\alpha(\rho') \rho' d\rho' \tag{5.17}$$

which is rearranged as

$$\frac{2A_o}{\eta_i}\frac{1}{\rho}=\frac{1}{\eta_i}\frac{1}{\rho}\frac{1}{\ln(\frac{b}{a})}\int_a^b \mathcal{E}(\rho')d\rho'$$

$$+\frac{1}{\eta_1}\frac{1}{\rho}\frac{1-R_{b1o}}{1+R_{b1o}}\frac{1}{\ln(\frac{c}{a})}\int_a^b \mathcal{E}(\rho')d\rho' \qquad (5.18)$$

$$+\sum_{m=1}^{\infty} Y_{TM}\mathcal{R}_m(\rho)\int_a^b \mathcal{E}(\rho')\mathcal{R}_m(\rho')\rho'd\rho'$$

$$+\sum_{\alpha=1}^{\infty}\frac{j\omega\epsilon_1}{\Gamma_{1\alpha}}\frac{1-R_{b1\alpha}}{1+R_{b1\alpha}}\mathcal{R}_\alpha(\rho)\int_a^b \mathcal{E}(\rho')\mathcal{R}_\alpha(\rho')\rho'd\rho'$$

where $Y_{TM}=j\omega\epsilon_i/\Gamma_m$.

This integral equation can be solved numerically for the aperture E field using the method of moments as presented in section 5.4. The validity of integral equation (5.18) is verified by an equivalent circuit concept which will be presented in the next section.

5.3 Equivalent Circuit Concept for Discontinuity

In this section, the equivalent circuit for a coaxial line discontinuity is considered, by which the physical meaning of the aperture input impedance of an open-ended coaxial probe is revealed clearly [41,42]. The well known results of the transmission line input impedance are recalled first, then a shunt capacitance is introduced at the discontinuity in addition to the original characteristic impedance to describe the effect of the coaxial discontinuity. The physical reason of the shunt capacitance is also provided.

In fig. 5.2 two segments of coaxial line are considered, where each segment is filled with different material. From transmission theory the reflection coefficient at the interface is

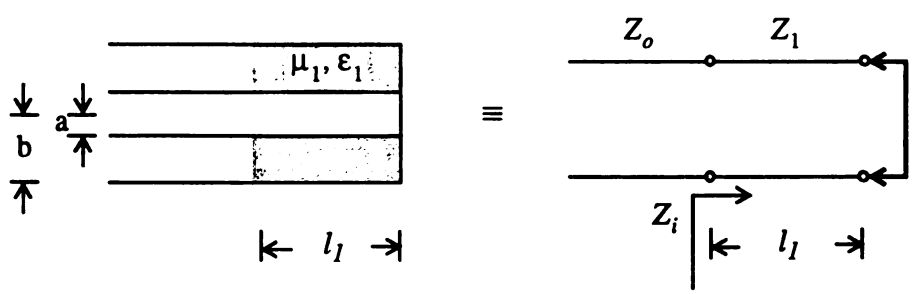

Figure 5.2 Two segments of a coaxial line with a short circuit termination and its equivalent circuit.

$$R = \frac{Z_i - Z_o}{Z_i - Z_o} \tag{5.19}$$

where

$$Z_i = Z_1 j \tan\beta_1 l_1 \tag{5.20}$$

and

$$Z_1 = \sqrt{\frac{\mu_1}{\epsilon_1}} \frac{\ln(b/a)}{2\pi} \quad , Z_o = \sqrt{\frac{\mu_o}{\epsilon_o}} \frac{\ln(b/a)}{2\pi} \tag{5.21}$$

Next, a coaxial structure consisting of two segments of coaxial lines with different outside conductor diameters is studied. In fig. 5.3, Y_d stands for the shunt admittance at the discontinuity, the physical reason for the shunt capacitance is due to the fringing fields (higher-order TM modes) at the discontinuity. Because of the discontinuity at the aperture, the longitudinal component E_z is needed to satisfy the boundary condition, thus higher order TM modes are excited.

If these TM modes are not supported in both coaxial lines, and the shorted end is located sufficiently far away from the discontinuity, then the shorted end has no influence on the TM modes, of which the wave admittance is

$$Y_{TM_\alpha} = \frac{j\omega\epsilon_1}{\Gamma_{1\alpha}} = \frac{j\omega\epsilon_1}{\sqrt{k_{c\alpha}^2 - k_1^2}} \equiv j\omega C_\alpha \tag{5.22}$$

with $C_\alpha = \epsilon_1 / \sqrt{k_{c\alpha}^2 - k_1^2}$.

Thus the wave admittance Y_{TM_α} of each TM mode corresponds to a shunt capacitance. With $Y_i^+ = -jY_1 \cot(\beta_1 l_1)$, the input admittance Y_i is computed by

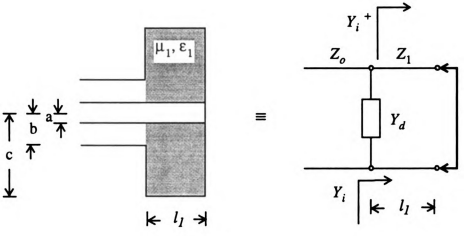

Figure 5.3 Two different segments of coaxial lines with a short circuit termination and its equivalent circuit.

$$
\begin{aligned}
Y_i &= Y_d // Y_i^+ \\
&= j\omega C_d - jY_1 \cot(\beta_1 l_1) \\
&= j(\omega C_d - Y_1 \cot(\beta_1 l_1))
\end{aligned}
\tag{5.23}
$$

where $C_d \equiv Y_d / j\omega = \sum_a C_a$.

And the reflection coefficient is

$$
R = \frac{1 - y_i}{1 + y_i} \tag{5.24}
$$

with

$$
y_i = \frac{Y_i}{Y_o} = j\frac{\omega C_d - Y_1 \cot(\beta_1 l_1)}{Y_o} \equiv j\xi \tag{5.25}
$$

If the material is lossless and the coaxial cavity is made of perfect conductor, then y_i is pure imaginary and $|R|=1$, because no power is carried away and no conducting loss due to the cavity wall exists.

5.4 Numerical Simulation - Method of Moments

In this section the method of moments is applied to solve the EFIE (5.18) [29]. The TM eigenmodes of the coaxial line are chosen to be the basis functions for unknown aperture field and Galerkin's technique is used to convert the integral equation into a set of simultaneous algebraic equations, from which the numerical solution of aperture electric field is obtained and the input admittance at the aperture is resolved. Finally some verifications for the numerical simulation are also given in this section.

The unknown aperture electric field is expanded into a finite sum of the TM eigenmodes of the coaxial line as follows:

$$\mathscr{E}(\rho) = \sum_{i=0}^{S} V_i \Re_i(\rho) \tag{5.26}$$

where

$$\Re_i(\rho) = \begin{cases} C_i[J_1(k_{ci}\rho)Y_0(k_{ci}a) - J_0(k_{ci}a)Y_1(k_{ci}\rho)] & \cdots i \neq 0 \\ \dfrac{1}{\rho} & \cdots i = 0 \end{cases} \tag{5.27}$$

and k_{ci} satisfies the following eigenvalue equation [30]

$$J_o(k_{ci}a)\,Y_o(k_{ci}b) - J_o(k_{ci}b)\,Y_o(k_{ci}a) = 0 \tag{5.28}$$

Substituting (5.26) in (5.18) leads to (from now on assume $\eta_i \rightarrow \eta_0$ for simplicity)

$$\begin{aligned} \frac{2A_o}{\eta_o}\frac{1}{\rho} = & \frac{1}{\eta_o}\frac{1}{\rho}\frac{1}{\ln(\frac{b}{a})}\int_a^b \sum_{i=0}^{S} V_i \Re_i(\rho')d\rho' \\ & + \frac{1}{\eta_1}\frac{1}{\rho}\frac{1-R_{blo}}{1+R_{blo}}\frac{1}{\ln(\frac{c}{a})}\int_a^b \sum_{i=0}^{S} V_i \Re_i(\rho')d\rho' \\ & + \sum_{m=1}^{\infty} Y_{TM}\Re_m(\rho)\int_a^b \sum_{i=0}^{S} V_i \Re_i(\rho')\Re_m(\rho')\rho' d\rho' \\ & + \sum_{\alpha=1}^{\infty} \frac{j\omega\epsilon_1}{\Gamma_{1\alpha}}\frac{1-R_{bl\alpha}}{1+R_{bl\alpha}}\Re_\alpha(\rho)\int_a^b \sum_{i=0}^{S} V_i \Re_i(\rho')\Re_\alpha(\rho')\rho' d\rho' \end{aligned} \tag{5.29}$$

which is rearranged as

$$\frac{2A_o}{\eta_o}\frac{1}{\rho}=\sum_{i=0}^{S}V_i\left(\frac{1}{\eta_o}\frac{1}{\rho}\frac{1}{\ln(\frac{b}{a})}\int_a^b \Re_i(\rho')d\rho'\right)$$
$$+\sum_{i=0}^{S}V_i\left(\frac{1}{\eta_1}\frac{1}{\rho}\frac{1-R_{b1o}}{1+R_{b1o}}\frac{1}{\ln(\frac{c}{a})}\int_a^b \Re_i(\rho')d\rho'\right) \qquad (5.30)$$
$$+\sum_{i=0}^{S}V_i\left(\sum_{m=1}^{\infty}Y_{TM}\Re_m(\rho)\int_a^b \Re_i(\rho')\Re_m(\rho')\rho'd\rho'\right)$$
$$+\sum_{i=0}^{S}V_i\left(\sum_{\alpha=1}^{\infty}\frac{j\omega\varepsilon_1}{\Gamma_{1\alpha}}\frac{1-R_{b1\alpha}}{1+R_{b1\alpha}}\Re_\alpha(\rho)\int_a^b \Re_i(\rho')\Re_\alpha(\rho')\rho'd\rho'\right)$$

Galerkin's method

Galerkin's method suggests using basis functions $\Re_j(\rho)$ as testing functions and does the following operation,

$$\int_a^b (5.30)*\Re_j(\rho)\rho d\rho \quad ,j=0\cdots S$$

such that a system of linear equations is derived as follows:

$$\frac{2A_o}{\eta_o}\int_a^b \Re_j(\rho)d\rho=\sum_{i=0}^{S}V_i\left(\frac{1}{\eta_o}\frac{1}{\ln(\frac{b}{a})}\int_a^b \Re_j(\rho)d\rho\int_a^b \Re_i(\rho')d\rho'\right)$$
$$+\sum_{i=0}^{S}V_i\left(\frac{1}{\eta_1}\frac{1-R_{b1o}}{1+R_{b1o}}\frac{1}{\ln(\frac{c}{a})}\int_a^b \Re_j(\rho)d\rho\int_a^b \Re_i(\rho')d\rho'\right) \qquad (5.31)$$
$$+\sum_{i=0}^{S}V_i\left(\sum_{m=1}^{\infty}Y_{TM}\int_a^b \Re_j(\rho)\Re_m(\rho)d\rho\int_a^b \Re_i(\rho')\Re_m(\rho')\rho'd\rho'\right)$$
$$+\sum_{i=0}^{S}V_i\left(\sum_{\alpha=1}^{\infty}\frac{j\omega\varepsilon_1}{\Gamma_{1\alpha}}\frac{1-R_{b1\alpha}}{1+R_{b1\alpha}}\int_a^b \Re_j(\rho)\Re_\alpha(\rho)d\rho\int_a^b \Re_i(\rho')\Re_\alpha(\rho')\rho'd\rho'\right)$$

Via the orthogonality properties (5.11) and (5.12), (5.31) is simplified to be

$$
\begin{aligned}
A_o \frac{2}{\eta_o} \ln\left(\frac{b}{a}\right) \delta_{jo} = & \sum_{i=0}^{S} V_i \frac{1}{\eta_o} \ln\left(\frac{b}{a}\right) \delta_{jo} \delta_{io} \\
& + \sum_{i=0}^{S} V_i \frac{1}{\eta_1} \frac{1-R_{b1o}}{1+R_{b1o}} \frac{\ln^2(b/a)}{\ln(c/a)} \delta_{jo} \delta_{io} \\
& + \sum_{i=0}^{S} V_i \sum_{m=1}^{\infty} Y_{TM} \delta_{jm} \delta_{im} \\
& + \sum_{i=0}^{S} V_i \left(\sum_{\alpha=1}^{\infty} \frac{j\omega\varepsilon_1}{\Gamma_{1\alpha}} \frac{1-R_{b1\alpha}}{1+R_{b1\alpha}} \int_a^b \Re_j(\rho) \Re_\alpha(\rho) d\rho \int_a^b \Re_i(\rho') \Re_\alpha(\rho') \rho' d\rho' \right)
\end{aligned}
\tag{5.32}
$$

with j = 1,...,S.

These simultaneous algebraic equations can be expressed as

$$
A_o[I] = \{[Y^d]+[Y^c]+[Y^b]+[Y^a]\}[V] \tag{5.33}
$$

with the matrix elements as

$$
\begin{aligned}
I_j &= \frac{2}{\eta_o} \ln\left(\frac{b}{a}\right) \delta_{jo} \\
Y^d_{ji} &= \frac{1}{\eta_o} \ln\left(\frac{b}{a}\right) \delta_{jo} \delta_{io} \\
Y^c_{ji} &= \frac{1}{\eta_1} \frac{1-R_{b1o}}{1+R_{b1o}} \frac{\ln^2(b/a)}{\ln(c/a)} \delta_{jo} \delta_{io} \\
Y^b_{ji} &= \sum_{m=1}^{\infty} Y_{TM} \delta_{jm} \delta_{im} \\
Y^a_{ji} &= \sum_{\alpha=1}^{\infty} \frac{j\omega\varepsilon_1}{\Gamma_{1\alpha}} \frac{1-R_{b1\alpha}}{1+R_{b1\alpha}} \int_a^b \Re_j(\rho) \Re_\alpha(\rho) d\rho \int_a^b \Re_i(\rho') \Re_\alpha(\rho') \rho' d\rho'
\end{aligned}
\tag{5.34}
$$

Equation (5.33) can then be solved by a standard numerical subroutine for linear equations.

After determining $\mathcal{E}(\rho)$ using (5.33), the normalized input admittance can be related

to $\mathcal{E}(\rho)$ with the help of (5.16),

$$y_{in} = \frac{1-R}{1+R} = \frac{2 - \dfrac{1}{A_o \ln(b/a)} \int_a^b \mathcal{E}(\rho)\, d\rho}{\dfrac{1}{A_o \ln(b/a)} \int_a^b \mathcal{E}(\rho)\, d\rho} \tag{5.35}$$

Since $\mathcal{E}(\rho)$ is proportional to A_o, A_o will be canceled in the expression of the normalized input admittance. Setting A_o to 1 leads to

$$y_{in} = \frac{2 - \dfrac{1}{\ln(b/a)} \int_a^b \mathcal{E}(\rho)\, d\rho}{\dfrac{1}{\ln(b/a)} \int_a^b \mathcal{E}(\rho)\, d\rho} = \frac{2\ln(\frac{b}{a}) - \int_a^b \mathcal{E}(\rho)\, d\rho}{\int_a^b \mathcal{E}(\rho)\, d\rho} \tag{5.36}$$

Before presenting the results of the numerical simulation for (5.33), some aspects about the evaluation of the matrix elements are addressed next.

Evaluation of the matrix elements

The computation for the elements of matrices Y^d, Y^c and Y^b is trivial. But the computation for each element of matrix Y^a involves an infinite series which need to be truncated according to some preset accuracy.

Also in (5.34) two integrals need to be computed for each term in the series of Y_{ji}^a, and it is quite time consuming. Fortunately, using the following formula each term in the series of Y_{ji}^a can be converted into a closed form [20],

$$\int Z_\nu(\alpha\rho) Z_\nu(\beta\rho) \rho\, d\rho = \frac{\rho}{\alpha^2 - \beta^2} [\beta Z_\nu(\alpha\rho) Z_{\nu-1}(\beta\rho) - \alpha Z_{\nu-1}(\alpha\rho) Z_\nu(\beta\rho)] \tag{5.37}$$

where $\alpha \neq \beta$ and Z_ν denotes J_ν and Y_ν.

To derive a closed form for each term in the series of Y_{ji}^a, let's consider the following integral,

$$\int_a^b \Re_j(\rho)\,\Re_\alpha(\rho)\,d\rho$$

$$= N_\alpha \left\{ Y_o(k_{c\alpha}a)\int_a^b \Re_j(\rho)\,J_1(k_{c\alpha}\rho)\,d\rho - J_o(k_{c\alpha}a)\int_a^b \Re_j(\rho)\,Y_1(k_{c\alpha}\rho)\,d\rho \right\} \tag{5.38}$$

where $\Re_j(\rho)$ is, from (3.13),

$$\Re_j = C_j[J_1(k_{cj}\rho)Y_0(k_{cj}a) - J_0(k_{cj}a)Y_1(k_{cj}\rho)] \tag{5.39}$$

With (5.37) and after some manipulation the first integral in (5.38) becomes,

$$\int_a^b \Re_j(\rho)J_1(k_{c\alpha}\rho)\rho d\rho$$

$$= C_j\int_a^b [J_1(k_{cj}\rho)Y_0(k_{cj}a) - J_0(k_{cj}a)Y_1(k_{cj}\rho)]J_1(k_{c\alpha}\rho)\rho d\rho \tag{5.40}$$

$$= \frac{C_j k_{c\alpha}}{(k_{cj}^2 - k_{c\alpha}^2)k_{cj}} \frac{2}{\pi}\left[J_o(k_{c\alpha}b)\frac{J_o(k_{cj}a)}{J_o(k_{cj}b)} - J_o(k_{c\alpha}a) \right]$$

Similarly using (5.37) the second integral in (5.38) becomes

$$\int_a^b \Re_j(\rho)\,Y_1(k_{c\alpha}\rho)\rho d\rho$$

$$= C_j\int_a^b [J_1(k_{cj}\rho)Y_0(k_{cj}a) - J_0(k_{cj}a)Y_1(k_{cj}\rho)]\,Y_1(k_{c\alpha}\rho)\rho d\rho \tag{5.41}$$

$$= \frac{C_j k_{c\alpha}}{(k_{cj}^2 - k_{c\alpha}^2)k_{cj}} \frac{2}{\pi}\left[Y_o(k_{c\alpha}b)\frac{J_o(k_{cj}a)}{J_o(k_{cj}b)} - Y_o(k_{c\alpha}a) \right]$$

Substituting (5.40) and (5.41) in (5.38) leads to

$$\int_a^b \Re_j(\rho)\,\Re_\alpha(\rho)\rho d\rho = N_\alpha C_j F_{\alpha j} \tag{5.42}$$

where

$$F_{\alpha j}=\frac{k_{c\alpha}}{(k_{cj}^2-k_{c\alpha}^2)k_{cj}}\frac{2}{\pi}\frac{J_o(k_{cj}a)}{J_o(k_{cj}b)}\left[J_o(k_{c\alpha}b)Y_o(k_{c\alpha}a)-J_o(k_{c\alpha}a)Y_o(k_{c\alpha}b)\right] \tag{5.43}$$

Similarly we have

$$\int_a^b \Re_i(\rho)\,\Re_\alpha(\rho)\rho d\rho = N_\alpha C_i F_{\alpha i} \tag{5.44}$$

where

$$F_{\alpha i}=\frac{k_{c\alpha}}{(k_{ci}^2-k_{c\alpha}^2)k_{ci}}\frac{2}{\pi}\frac{J_o(k_{ci}a)}{J_o(k_{ci}b)}\left[J_o(k_{c\alpha}b)Y_o(k_{c\alpha}a)-J_o(k_{c\alpha}a)Y_o(k_{c\alpha}b)\right] \tag{5.45}$$

With the help of (5.42) and (5.44), Y_{ji}^a in (5.34) becomes

$$Y_{ji}^a=\sum_{\alpha=1}^{\infty}\frac{j\omega\epsilon_1}{\Gamma_{1\alpha}}\frac{1-R_{b1\alpha}}{1+R_{b1\alpha}}N_\alpha^2 C_i C_j F_{\alpha i}F_{\alpha j} \tag{5.46}$$

The above formulation can be numerically evaluated efficiently. After all these considerations about the evaluation of the matrix elements, the simultaneous algebraic equation (5.33) can now be solved by any kind of computer code.

Computer program and numerical results

A fortran computer program was written for the numerical evaluation of (5.33) and (5.34) so that the aperture electric field and other quantities can be calculated when ε and μ of the material are given. The validity of computer program is first verified by computing the impedances of (5.20) for various materials. The second verification is made by comparing the shunt capacitance at the discontinuity with that of the equivalent circuit, which was shown in the work of J. R. Whinnery [42].

The results are shown in fig. 5.4, in which the shunt capacitance per unit length

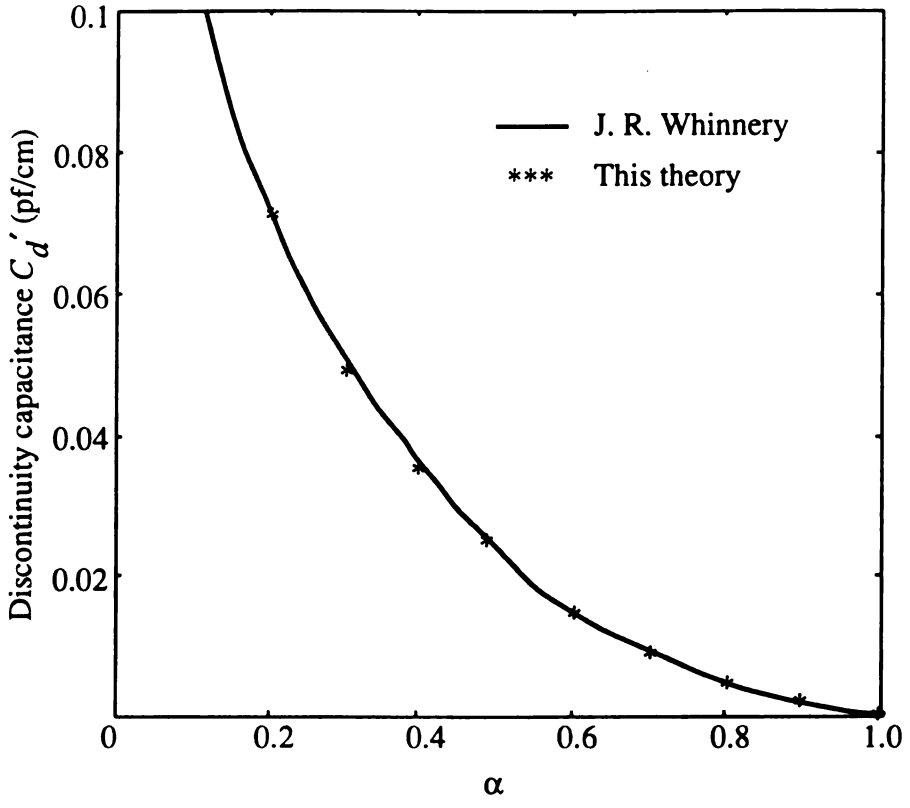

Figure 5.4 Discontinuity capacitance per unit length, C_d', of a coaxial air line v.s. step ratio α.

$C_d'(\alpha)$ is introduced as

$$C_d'(\alpha) = \frac{C_d}{2\pi a \epsilon_{r1}} \tag{5.47}$$

with $\alpha = \frac{b-a}{c-a}$ as the step ratio.

The results of our calculation match well with that of [42] and it shows that the "forward problem" has been correctly solved while the "inverse problem", the final goal, for determining ε and μ of the material via the measurements of input impedance of the coaxial line will be addressed in chapter 6.

5.5 Computation of Metallic Wall Loss for Coaxial Cavity

In this section, the metallic wall loss of the coaxial cavity is studied [27]. The analyses described in previous sections assume perfectly conducting cavity, that is not true in practice. The power loss due to the non-perfectly conducting wall may influence the input impedance and the reflection coefficient, which then, in turn, influences the characterization of the EM parameters of the material filling the cavity. The analysis for metallic wall loss is based on the conservation of energy (Poynting theorem) and perturbation approach.

Let's first recall the complex Poynting theorem for a closed volume V with surface S:

$$P_e = P_d + j2\omega(U_m - U_e) + P_s \tag{5.48}$$

with

$$\begin{aligned} P_e &= \int_V \frac{1}{2}\vec{E}\cdot\vec{J}_e^{\,*}\,dv \\ P_d &= \int_V \frac{\sigma_d}{2}\vec{E}\cdot\vec{E}^{\,*}\,dv \end{aligned} \tag{5.49}$$

and

$$U_m - U_e = \int_V \left(\frac{\mu}{4} \vec{H} \cdot \vec{H}^* - \frac{\epsilon}{4} \vec{E} \cdot \vec{E}^* \right) dv$$
$$P_s = \oint_S \frac{1}{2} (\vec{E} \times \vec{H}^*) \cdot \hat{n} ds \tag{5.50}$$

The notation P_e stands for the power supplied by an active source in V, P_d for the dielectric power loss in V, and U_m and U_e for the stored magnetic and electric energy, respectively. Also P_s stands for the power transfer over boundary surface S. For the structure in fig. 5.5, we have $\vec{J}_e = 0$ beyond the cross section $z=-l_1$, at which all higher order TM modes decay out and only the TEM mode exists. By letting V and I be the voltage and current associated with the TEM wave, the P_s term can be rewritten as

$$\begin{aligned} P_s &= -\frac{1}{2} \int_{C.S.} (\vec{E} \times \vec{H}^*) \cdot \hat{z} ds + \int_{wall} \frac{1}{2} \vec{E} \cdot (-\hat{n} \times \vec{H}^*) ds \\ &= -\frac{1}{2} V I^* + \int_{wall} \frac{1}{2} Z_s \vec{K} \cdot \vec{K}^* ds \\ &= -\frac{1}{2} Z_{in} |I|^2 + (1+j) P_w \end{aligned} \tag{5.51}$$

where

$$P_w = \int_{wall} \frac{R_s}{2} \vec{K} \cdot \vec{K}^* ds$$
$$R_s = \sqrt{\pi f \mu / \sigma_c} \tag{5.52}$$

Hence (5.48) becomes

$$\frac{Z_{in}}{2} |I|^2 = P_d + j2\omega (U_m - U_e) + (1+j) P_w \tag{5.53}$$

In case of perfect conductor, $P_w = 0$, and we have

$$Z_{in} = 2 \frac{P_d + j2\omega (U_m - U_e)}{|I|^2} \tag{5.54}$$

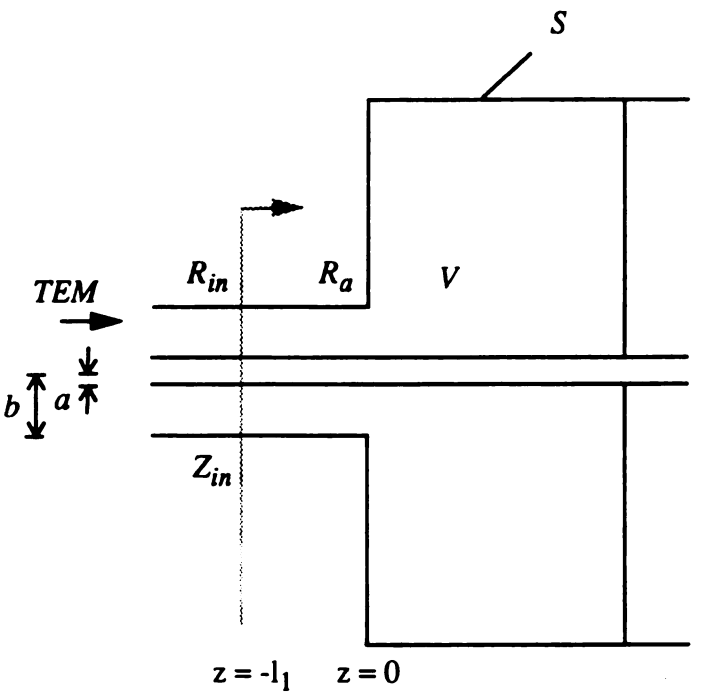

Figure 5.5 Geometry of a coaxial cavity driven by a coaxial line. The complex Poynting theorem is applied to the volume V beyond the cross section $z=-l_1$.

The current I can be derived according to transmission line theory as

$$\begin{aligned} I &= (I^+ + I^-)\big|_{z=-l_1} \\ &= \frac{1}{Z_c}\left(V_o^+ e^{j\beta_1 l_1} - V_o^- e^{-j\beta_1 l_1}\right) \\ &= \frac{V_o^+}{Z_c}\left(e^{j\beta_1 l_1} - R_{in} e^{-j\beta_1 l_1}\right) \end{aligned} \tag{5.55}$$

where R_{in} is the reflection coefficient of the voltage and Z_c is the characteristic impedance of the coaxial line.

Since the transverse dependance of electric field of the incident TEM mode is assumed to be $\mathcal{E}(\rho)=\frac{1}{\rho}$, we have

$$V_o^+ = \int_a^b \mathcal{E}(\rho)d\rho = \ln(b/a) \tag{5.56}$$

Therefore (5.54) leads to the normalized input impedance

$$z_{in} = \frac{Z_{in}}{Z_c} = 2Z_c \frac{P_d + j2\omega(U_m - U_e)}{\ln^2(\frac{b}{a})\left|1 - R_{in} e^{-j2\beta_1 l_1}\right|^2} \tag{5.57}$$

In case of non-perfect conductor, $P_w \neq 0$, a modified input impedance is derived via similar steps. The perturbation approach assumes that the aperture EM fields are not disturbed by P_w so that the current I in (5.55) is unchanged. This leads to

$$\begin{aligned} z'_{in} &= 2Z_c \frac{P_d + j2\omega(U_m - U_e) + (1+j)P_w}{\ln^2(\frac{b}{a})\left|1 - R_{in} e^{-j2\beta_1 l_1}\right|^2} \\ &= z_{in} + 2Z_c \frac{(1+j)P_w}{\ln^2(\frac{b}{a})\left|1 - R_{in} e^{-j2\beta_1 l_1}\right|^2} \end{aligned} \tag{5.58}$$

Also the modified reflection coefficient becomes

$$R'_{in} = \frac{z'_{in} - 1}{z'_{in} + 1} \tag{5.59}$$

The influence of wall loss P_w on the reflection coefficient can then be obtained by the following steps:

1. Transform R_a at the aperture, obtained numerically, to R_{in} at z=-l_1 by

$$R_{in} = R_a e^{-j2\beta_1 l_1} \tag{5.60}$$

and we have

$$z_{in} = \frac{1 + R_{in}}{1 - R_{in}} \tag{5.61}$$

2. Include the influence of P_w on the input impedance and the reflection coefficient by (5.58) and (5.59).

3. Transform R'_{in} back to R'_a by

$$R'_a = R'_{in} e^{j2\beta_1 l_1} \tag{5.62}$$

In these steps the metallic power loss P_w is calculated numerically using (5.52), in which the surface current $\vec{K}$ is related to the unperturbed tangential magnetic field H_ϕ and the value of 1.57X10^7 S/m for the surface resistance R_s is used for the brass cavity wall. That is

$$\vec{K} \cdot \vec{K}^* = |\hat{n} \times \vec{H}|^2 = |H_\phi|^2 \tag{5.63}$$

The component H_ϕ can be expressed in terms of the aperture E field by substituting (5.14) and (5.15) into (5.6). As soon as the aperture E field is solved, H_ϕ and P_w can be computed numerically.

Skipping the computational details, the results of the metallic wall loss P_w normalized by the input power and the dielectric power loss P_d are shown next. Figure 5.6 shows P_w, normalized by the input power, for acrylic and water, where the cavity of length 1" is fully filled with the material and the published value of ε for each material is used for computation. The peaks shown in the figure occur at resonance frequencies. Also fig. 5.7 shows the same P_w as normalized by P_d for acrylic and water. Even though the metallic wall loss is small compared to the input power, it may be large when compared to the dielectric power loss, especially for low-loss material at low frequency range, thus influencing the dielectric constant characterization. Figure 5.8 shows P_w for acetone (ε_r=20, ε_i=0.05) normalized by the input power and dielectric power loss, respectively. It shows that the power loss of metallic wall is important in the EM characterization of the low-loss and high-permittivity materials.

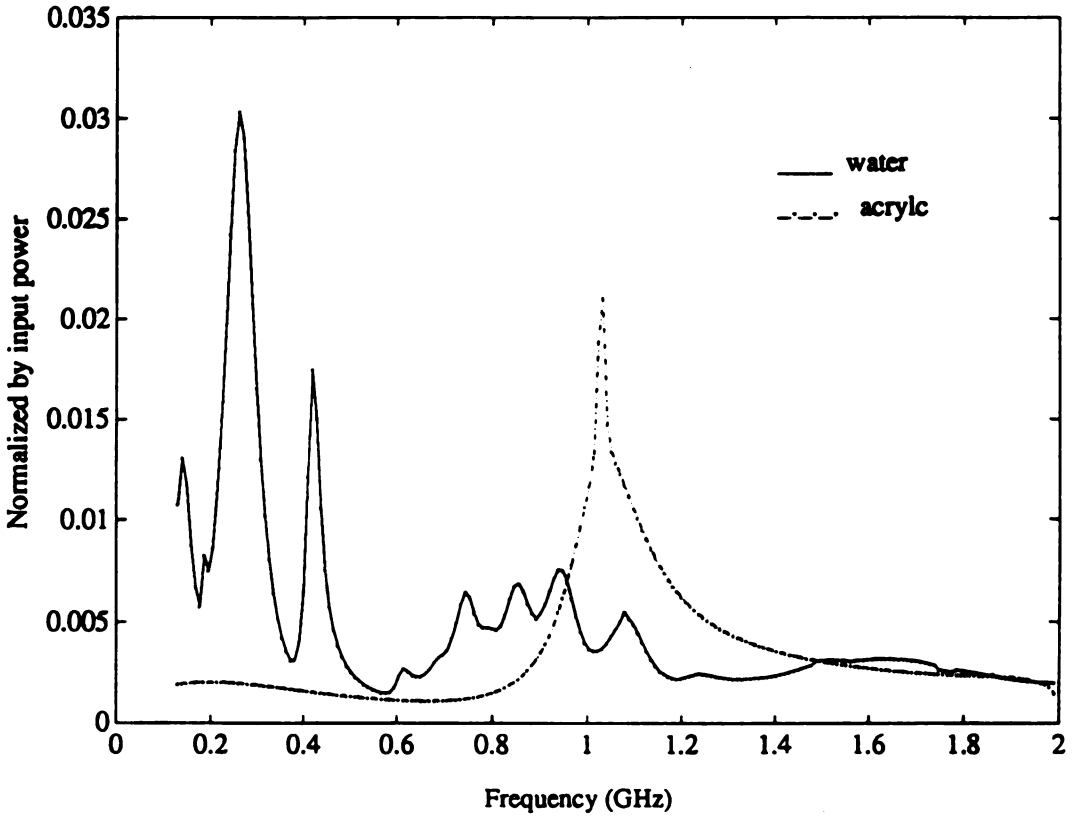

Figure 5.6 The power loss of non-perfectly conducting wall is normalized by the input power, where the filled material is water and acrylic, respectively.

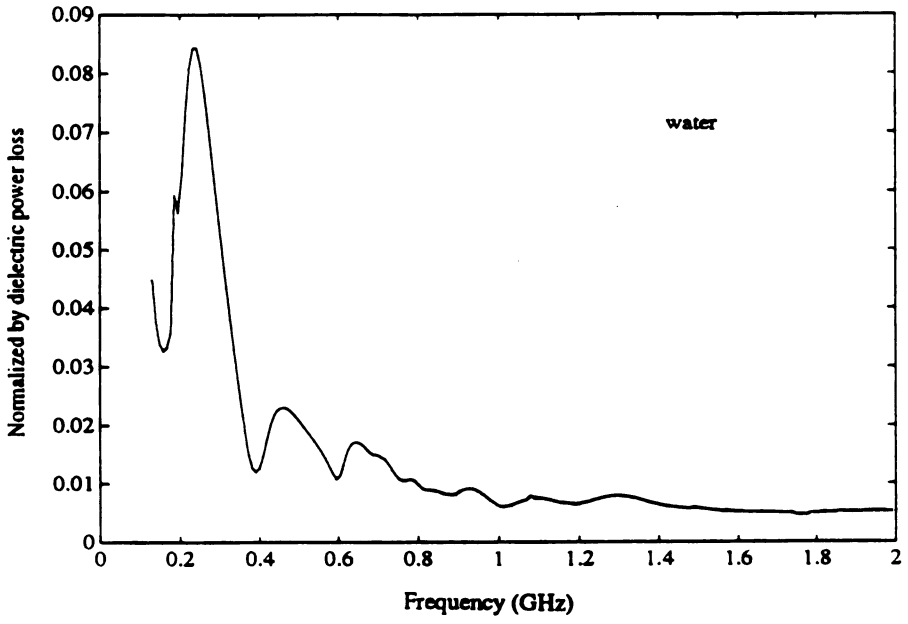

(a)

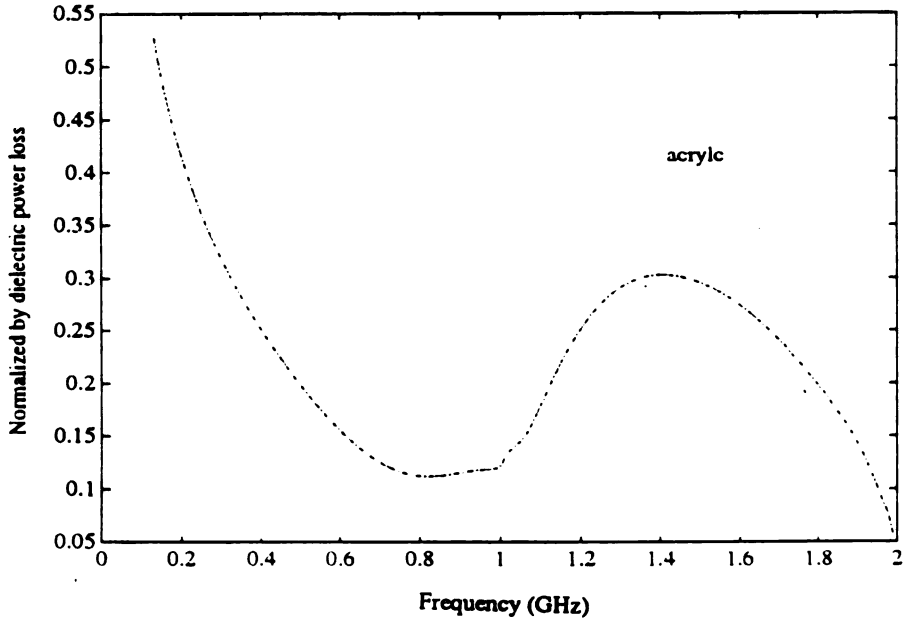

(b)

Figure 5.7 The power loss of non-perfectly conducting wall is normalized by the dielectric power loss, of which the filled material is (a) water, and (b)acrylic, respectively.

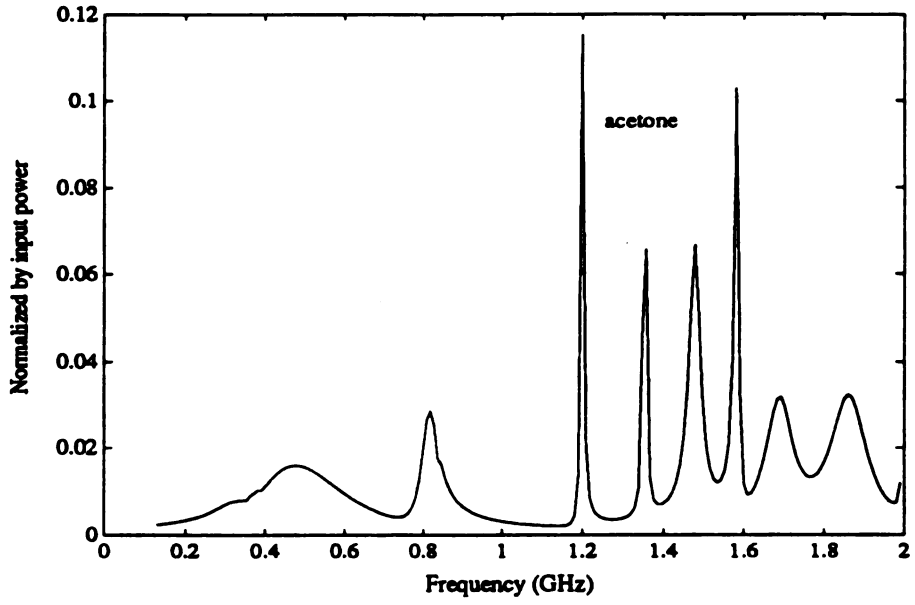

(a)

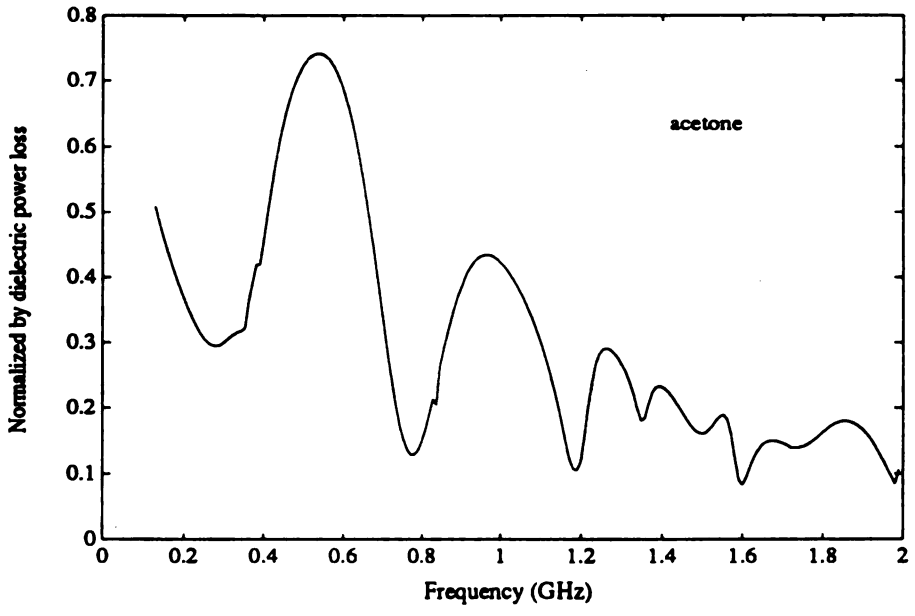

(b)

Figure 5.8 The power loss P_w of non-perfectly conducting wall when the cavity is filled with acetone. P_w is normalized by (a) the input power, and (b) the dielectric power loss, respectively.

CHAPTER 6

EXPERIMENTAL MEASUREMENT FOR VARIOUS MATERIALS

6.1 Introduction

In this chapter, the measurement procedures to obtain the complex permittivity ε and permeability μ of materials are discussed and the results for ε and μ of several materials are presented [44].

Using either the open-ended coaxial line probe or the coaxial cavity system that were analyzed in previous chapters, the complex ε and μ can be measured with a network analyzer connected to the measurement setups as shown in figs. 6.1 and 6.2.

As mentioned before, two measurements of the probe input impedance are needed to determine both ε and μ. For the open-ended coaxial probe, as shown in fig 6.3, this can be achieved by using open-circuit and short-circuit cases, or preparing two samples of the same material with different thickness. Another alternative is to measure an unknown material by inserting some known material (usually air) between the aperture and the unknown material. For the coaxial cavity system, this can be achieved by setting the backwall of the cavity at two different locations.

The results of these two measurements are used for solving the simultaneous equations for ε and μ by numerical inverse scheme. This procedure is then repeated for each frequency of interest.

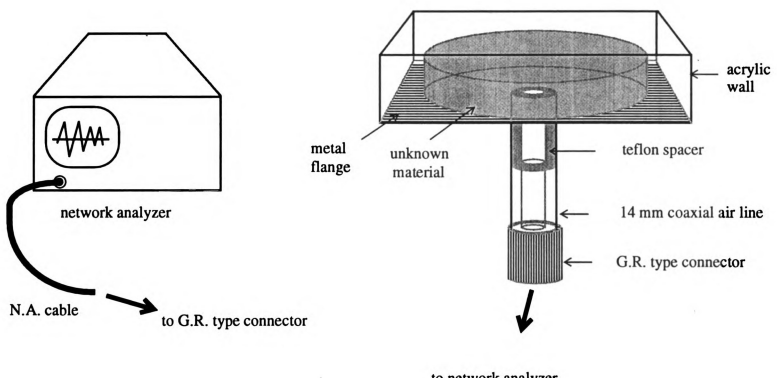

Figure6.1 Experimental setup of an open-ended coaxial probe system to measure the EM parameters of materials.

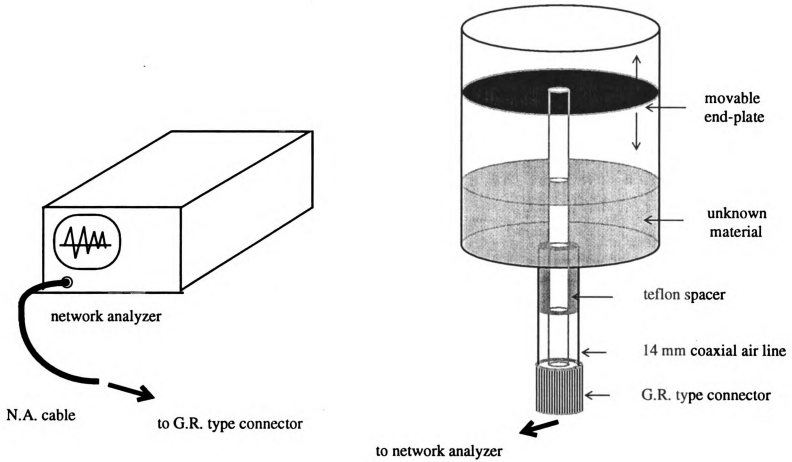

Figure6.2 Experimental setup of a coaxial cavity system to measure the EM parameters of materials.

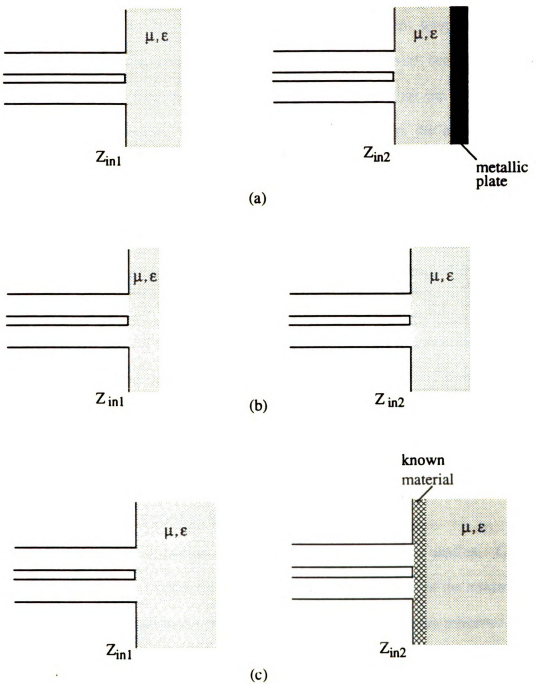

Figure 6.3 Two input impedance measurements are made by (a) using open-circuit and short-circuit cases, (b) preparing two samples of different thicknesses, and (c) inserting some known material for the second one.

In section 6.2 the calibration procedure for the measurement setups is discussed [43,45]. The scattering parameters for the equivalent two-port network between the probe aperture and the measurement reference plane of a network analyzer can be determined via the calibration procedure. With these scattering parameters the measured input impedance at the reference plane can then be converted to the input impedance at the probe aperture.

In section 6.3 the Newton's iterative method is presented [46,47]. Newton's method is used to solve the simultaneous nonlinear equations, which are resulted from the two measured input impedances.

In sections 6.4 and 6.5 the measurement procedures and the measurement results of various materials via the open-ended coaxial probe and the coaxial cavity method, respectively, are presented. The limitations for the use of these probes are also addressed.

6.2 Calibration Procedure for Experimental Setups

In this section, the calibration for the experimental setups is studied. General effects of the G.R. type connector, the teflon bead and the phase shift of the transmission line, which are located between the probe aperture and the measurement reference plane, are described by the scattering parameters of an equivalent two-port network as shown in fig. 6.4.

By determining the scattering parameters of the two-port network, the measured input impedance and reflection coefficient at the reference plane of a network analyzer can be converted to the input impedance and reflection coefficient at the probe aperture, or vice versa, as follows [43]:

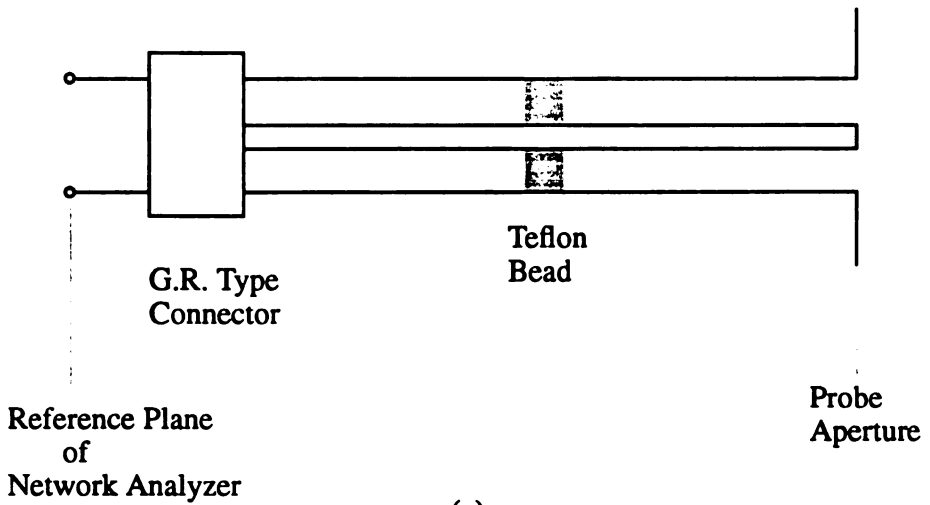

(a)

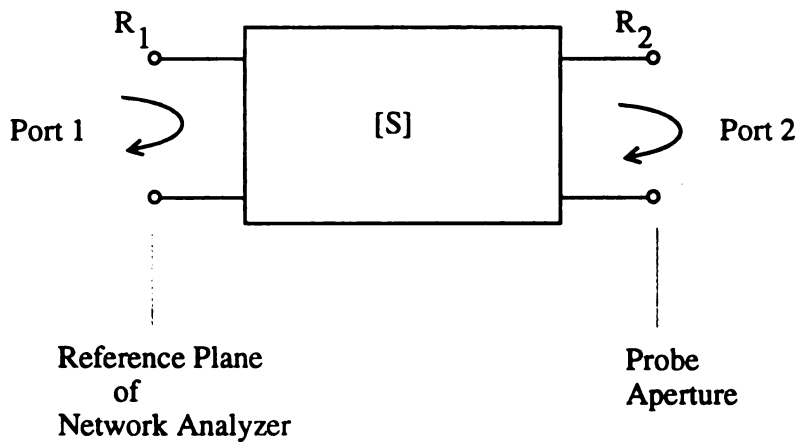

(b)

Figure 6.4 (a) The structure of the coaxial line probe setup. (b) Its equivalent two-port network.

$$R_2 = \frac{R_1 - S_{11}}{(R_1 - S_{11})S_{22} + S_{12}S_{21}} \tag{6.1}$$

or

$$R_1 = \frac{S_{12}S_{21}R_2}{1 - S_{22}R_2} + S_{11} \tag{6.2}$$

From (6.2) it is clear that only three combinations of scattering parameters S_{11}, S_{22} and $S_{12}S_{21}$ need to be determined.

Determination of the scattering parameters using 3 shorting stubs

In order to determine the scattering parameters of the two-port network, three shorting stubs of different lengths l_a, l_b and l_c are fabricated. These shorting stubs are designed to completely fill the space between the inner and outer conductors as shown in fig. 6.5.

The scattering parameters between the terminal plane 1 (the measurement reference plane) and the terminal plane 2 (the shorted end at z'=0) are determined, and the segment of the coaxial line between z'=0 and the probe aperture is treated as a perfect transmission line.

With the help of (6.2), the scattering parameters between the measurement reference plane and z'=0 can be determined experimentally as follows:

With reference to fig. 6.5, R_1^a, R_1^b and R_1^c denote the measured reflection coefficients at the terminal plane 1 with the three shorting stubs filled in the coaxial line. R_2^a, R_2^b and R_2^c denote the theoretical reflection coefficients at terminal plane 2. Then from transmission line theory, we have

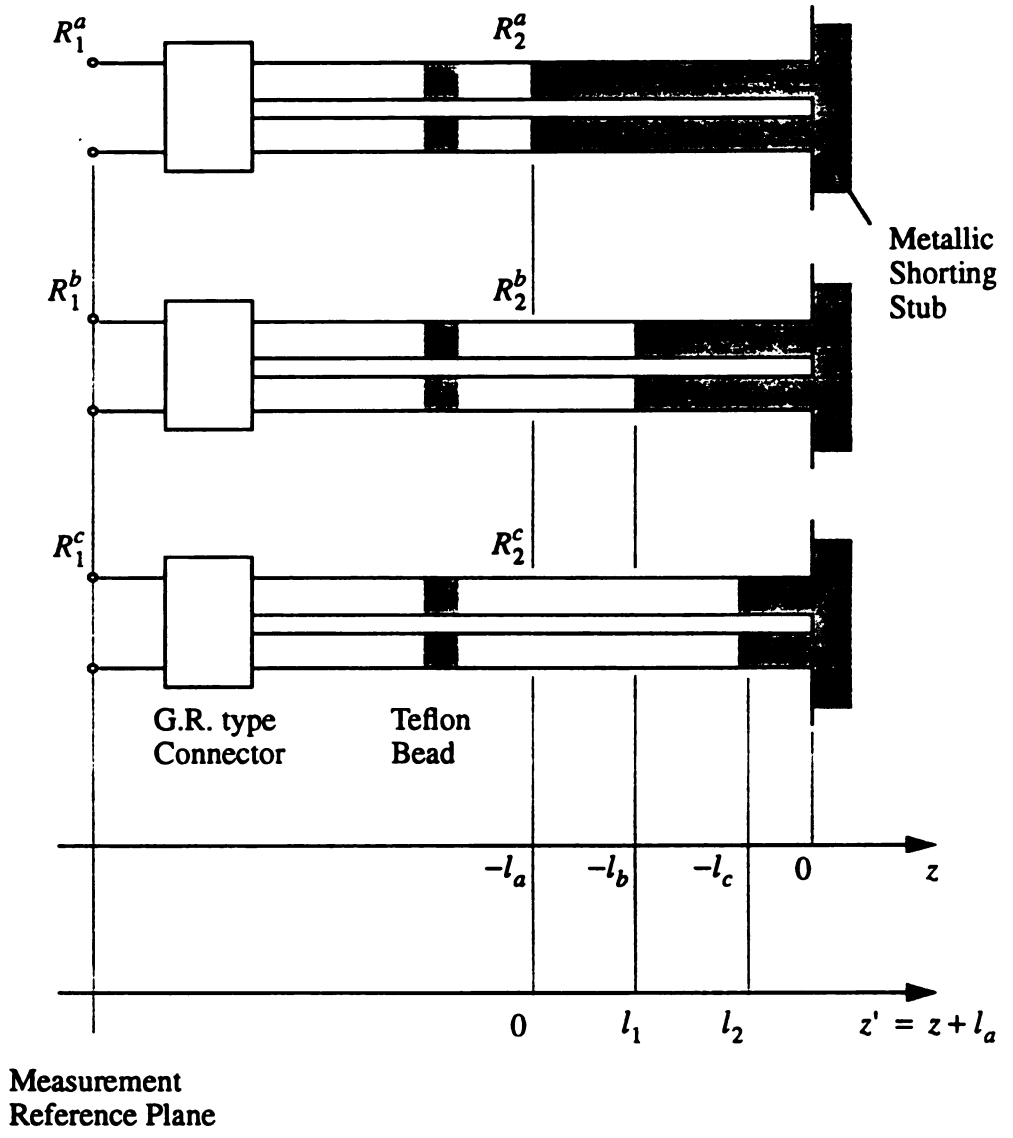

(a)

Figure 6.5 (a) The structure for the calibration of the coaxial line probe using three shorting stubs. (b) Its equivalent circuit is described by the S parameters and one segment of perfect transmission line.

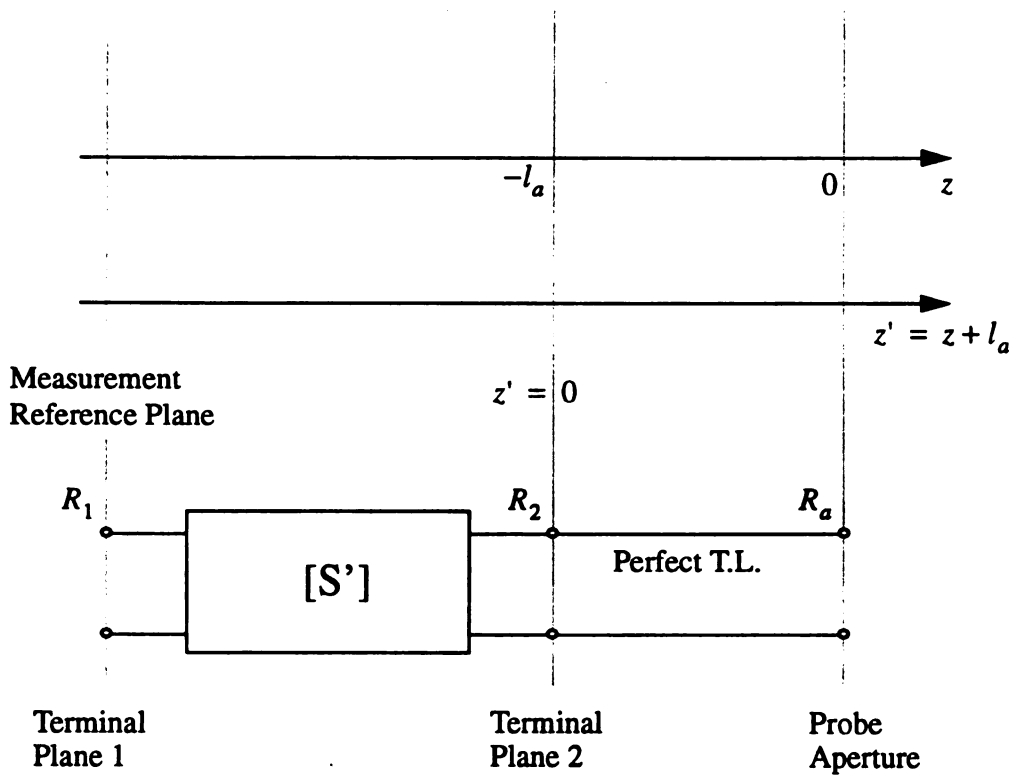

(b)

Figure 6.5 (continued)

$$
\begin{aligned}
R_2^a &= -1 \\
R_2^b &= -e^{-j2\beta l_{ab}} \\
R_2^c &= -e^{-j2\beta l_{ac}}
\end{aligned}
\tag{6.3}
$$

where $\beta = 2\pi/\lambda_o$, $l_{ab} = l_a - l_b$ and $l_{ac} = l_a - l_c$.

Substitution of the measured R_1^a, R_1^b and R_1^c and (6.3) in (6.2) leads to

$$
R_1^\alpha = \frac{S_{12}' S_{21}' R_2^\alpha}{1 - S_{22}' R_2^\alpha} + S_{11}' \tag{6.4}
$$

where α=a, b and c.

If the lengths l_a, l_b and l_c are chosen such that these equations in (6.3) are independent, the scattering parameters can be solved to be

$$
\begin{aligned}
S_{22}' &= \frac{(R_1^c - R_1^b)(R_2^a - R_2^b) - (R_1^a - R_1^b)(R_2^c - R_2^b)}{(R_1^c - R_1^b)(R_2^a - R_2^b)R_2^c - (R_1^a - R_1^b)(R_2^c - R_2^b)R_2^a} \\
S_{12}' S_{21}' &= \frac{R_1^c - R_1^b}{R_2^c - R_2^b}(1 - S_{22}' R_2^c)(1 - S_{22}' R_2^b) \\
S_{11}' &= R_1^c - \frac{S_{12}' S_{21}' R_2^c}{1 - S_{22}' R_2^c}
\end{aligned}
\tag{6.5}
$$

Because the amplitudes of R_1^α, α=a,b and c, are one for all shorting stubs, the measured information is carried by the phases. To assure that the choice of l_a, l_b and l_c does lead to 3 different phases over a wide band of frequencies, it is necessary to make more than 3 measurements with these shorting stubs located at different positions randomly. In practical situation, up to 6 measurements were made to assure a good solution for the scattering parameters.

Since the scattering parameters for the two-port network between the measurement reference plane and $z'=0$ are determined, and the segment of coaxial line from $z'=0$ to the probe aperture can be treated as a perfect transmission line, the transformation of the reflection coefficient from the measurement reference plane of a network analyzer to the probe aperture can be made in 3 steps as follows:

1. Measure R_1 using the network analyzer.

2. Transform R_1 to R_2 at $z'=0$ plane by (6.1)

$$R_2 = \frac{R_1 - S_{11}'}{(R_1 - S_{11}')S_{22}' + S_{12}'S_{21}'} \tag{6.6}$$

3. Transform R_2 to R_a at the probe aperture as

$$R_a = R_2 e^{j2\beta l_a} \tag{6.7}$$

Calibration for the Coaxial Line Probe with a Spacer

In case a liquid material is measured, it's important to prevent the leakage of the liquid into the probe and assure a flat surface of the liquid at the aperture.

To accomplish this, a spacer made of teflon is made to completely fill the space between the inner and outer conductors. It presents a flat surface at the probe aperture as shown in fig. 6.6. The length of the spacer should be large enough that all the higher order TM modes decay out before reaching the $z=-l_d$ interface. Otherwise the reflected higher order modes will complicate the theoretical analysis inside the coaxial line.

It is still possible to do the calibration for this new structure using 3 shorting stubs in a similar manner as before. If the spacer is inserted into the coaxial probe after the reflection coefficient measurements of the 3 shorting stubs are made, then the scattering

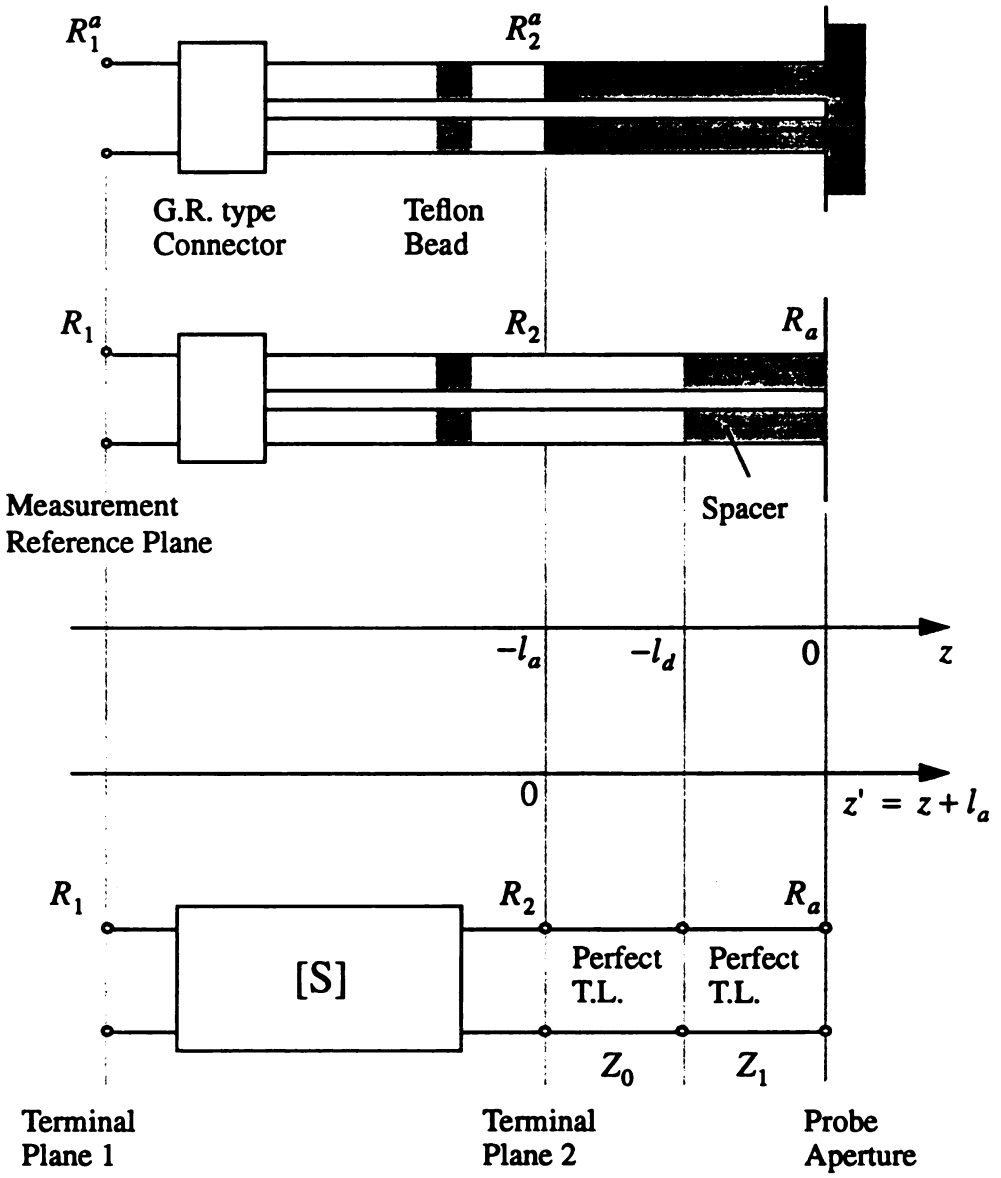

Figure 6.6 The structure of the coaxial line probe with a spacer of length l_d. Its equivalent circuit is described by the S-parameters and two segments of perfect transmission line.

parameters of the two-port network between the measurement reference plane and $z'=0$ can be obtained, and the coaxial line between $z'=0$ and the probe aperture can be treated as a perfect transmission line with two segments filled with different materials (air and teflon). Therefore the transformation of reflection coefficient from the measurement reference to the probe aperture can be achieved.

6.3 Numerical Inverse Algorithm

With the calibration procedure described in previous section, the measured input impedance at the measurement reference plane is transformed to the probe aperture plane. The input impedance at the probe aperture is an implicit function of ϵ and μ as well as the thickness of the material, etc. Conceptually, two equations are needed to solve for two unknowns ϵ and μ. Thus the complex ϵ and μ can be inversely determined by some numerical scheme if two input impedances are measured.

In this section, Newton's iterative method of finding the roots of nonlinear equations is presented for the sake of completeness [46,47]. Let's consider two general equations as

$$\begin{aligned} f(x,y) &= 0 \\ g(x,y) &= 0 \end{aligned} \tag{6.8}$$

At each iterative step of the algorithm, the objective is to find h_1 and h_2 so that (6.8) is satisfied approximately as follows:

$$\begin{aligned} f(x+h_1, y+h_2) &\approx 0 \\ g(x+h_1, y+h_2) &\approx 0 \end{aligned} \tag{6.9}$$

By Taylor's expansion and with the series truncated in 1st-order, (6.9) becomes

$$\begin{aligned} f(x,y)+\frac{\partial f}{\partial x}h_1+\frac{\partial f}{\partial y}h_2=0 \\ g(x,y)+\frac{\partial g}{\partial x}h_1+\frac{\partial g}{\partial y}h_2=0 \end{aligned} \tag{6.10}$$

or

$$\begin{bmatrix} \frac{\partial f}{\partial x} & \frac{\partial f}{\partial y} \\ \frac{\partial g}{\partial x} & \frac{\partial g}{\partial y} \end{bmatrix} \begin{bmatrix} h_1 \\ h_2 \end{bmatrix} = -\begin{bmatrix} f(x,y) \\ g(x,y) \end{bmatrix} \tag{6.11}$$

This leads to the solution for h_1 and h_2 as

$$\begin{bmatrix} h_1 \\ h_2 \end{bmatrix} = -\begin{bmatrix} \frac{\partial f}{\partial x} & \frac{\partial f}{\partial y} \\ \frac{\partial g}{\partial x} & \frac{\partial g}{\partial y} \end{bmatrix}^{-1} \begin{bmatrix} f(x,y) \\ g(x,y) \end{bmatrix} \tag{6.12}$$

If (6.9) is satisfied according to some preset accuracy then the iterative process is stopped and the final values of x and y are the roots of the equations. Otherwise, the searching of new h_1 and h_2 is repeated.

Application of this algorithm to determination of ϵ and μ is as follows. With two measured input impedances, Z_{in1} and Z_{in2}, as shown in fig. 6.3, the values of ϵ and μ are searched so that the theoretical input impedances at the probe aperture, Z_{th1} and Z_{th2}, match the measured ones. Therefore (6.8) becomes

$$\begin{aligned} f(\epsilon,\mu)=Z_{th1}(\epsilon,\mu)-Z_{in1}=0 \\ g(\epsilon,\mu)=Z_{th2}(\epsilon,\mu)-Z_{in2}=0 \end{aligned} \tag{6.13}$$

With the above algorithm, we can determine the correct values of ϵ and μ that lead to the two measured input impedances.

6.4 Experimental Results via Open-Ended Coaxial Line Probe Method

In this section, we'll present the results of complex permittivity ε and permeability μ of various materials measured by an open-ended coaxial probe. With reference to fig. 6.1, a 14mm coaxial air line (a=0.3102cm, b=0.7145cm) is connected to a 16"X16" metallic flange. The metallic flange is surrounded by an acrylic wall in order to accommodate liquid materials. The following procedures are the measurement steps for ε and μ using an HP8720B network analyzer [44]:

1. Set up the network analyzer.
2. Do the calibration for the network analyzer.
3. Do the calibration measurement for the fixture using the shorting stubs.
4. Calculate the S parameters for the equivalent two-port network of the fixture.
5. Put the material inside the fixture.
6. Measure the reflection coefficient.
7. Calculate the reflection coefficient at the probe aperture.
8. Compute ε and μ using numerical inverse algorithm.
9. Plot ε and μ.

Through these steps the EM parameters of four different materials were measured. These include a low permittivity material (acrylic), medium permittivity materials (acetone and Eccosorb-Ls22) and a high permittivity material (water). The frequency range covers from 0.2 GHz to 2 GHz.

It was found that for the open-circuit case the metallic flange is large enough to act as an infinite plate as the theory assumes. But for the short-circuit case, this assumption of infinite plate was valid for high loss material only. For low loss material, the radial guided waves are reflected from the edge of the flange, and a resonant phenomenon

occurs due to the high Q characteristic of the short-circuit structure. This suggests the use of open-circuit case only for low loss materials.

Also it was found that the contact of the measured material with the open-ended coaxial probe is very important. An unintentional air gap may cause considerable inaccuracy in the final results. In addition, a good calibration for the fixture is essential for consecutive measurements. With three calibration stubs of different lengths (l_a=5.84cm, l_b=3.89cm and l_c=1.88cm), a good calibration can be obtained for the frequency above some critical frequency f_c, about 0.5 GHz in our case. For the frequency below f_c, a good calibration is not easy since the wavelength is so large that these shorting stubs do not provide well-separated phases. The critical frequency f_c is then limited by the length of l_a. The difficulty in calibration at low frequency may be overcome if the coaxial feed line and shorting stubs are made longer.

It is observed that there exists an ill-conditioned property in this method at the low frequency range in the determination of EM parameters of materials. That is, a small inaccuracy in the measurement data can lead to a large error in the final results of EM parameters of the materials.

Figures. 6.7(a)-(b) show the measured permittivity ε of acrylic when the permeability $\mu=\mu_o$ is assumed. Two measurements are shown using the setup of fig. 6.3(c): one with an air layer of 2.3mm between the probe and the material and the other without an air gap or a direct contact between the probe and the material. The results from these two measurements are very consistent ($\varepsilon_r \cong 2.6$, and $\varepsilon_i \cong 0$), and the differences are within 4 percent for ε_r over the most part of frequency. Using these two close measurements, the numerical inverse scheme generates simultaneously both ε and μ as shown in figs. 6.8(a)-(b). Figure 6.8(a) shows good results for ε but the results for μ are

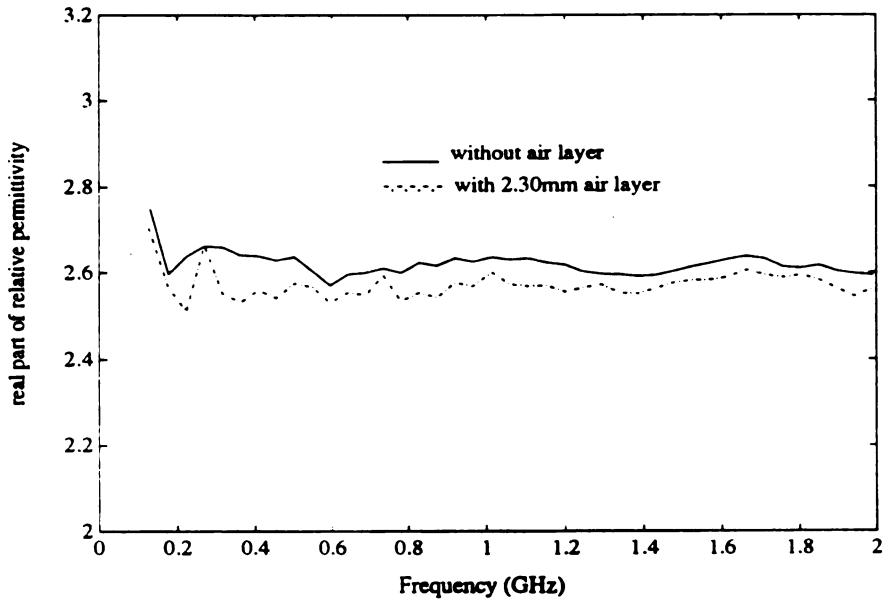

(a)

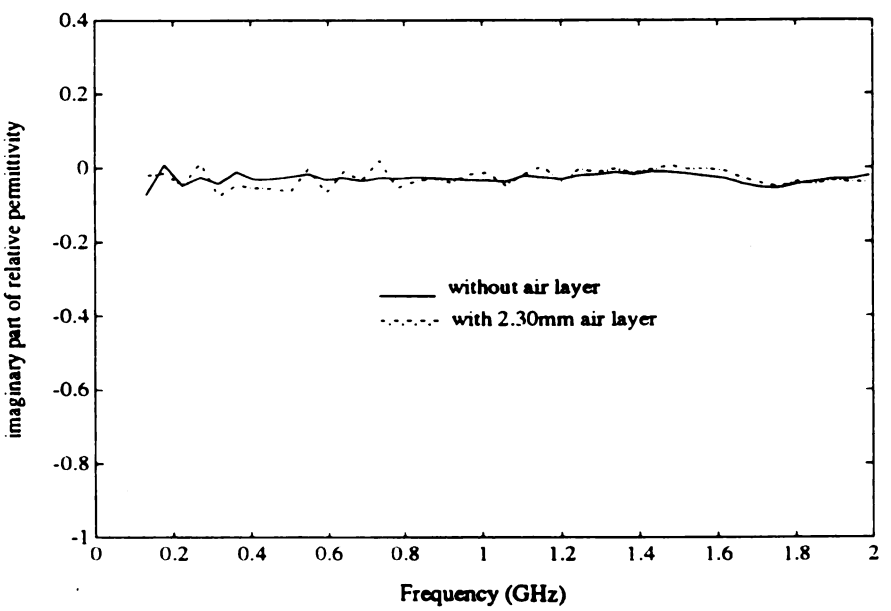

(b)

Figure 6.7 The permittivity ε of acrylic via open-ended coaxial probe ($\mu=\mu_0$ assumed). (a) The real part of relative permittivity. (b) The imaginary part of relative permittivity.

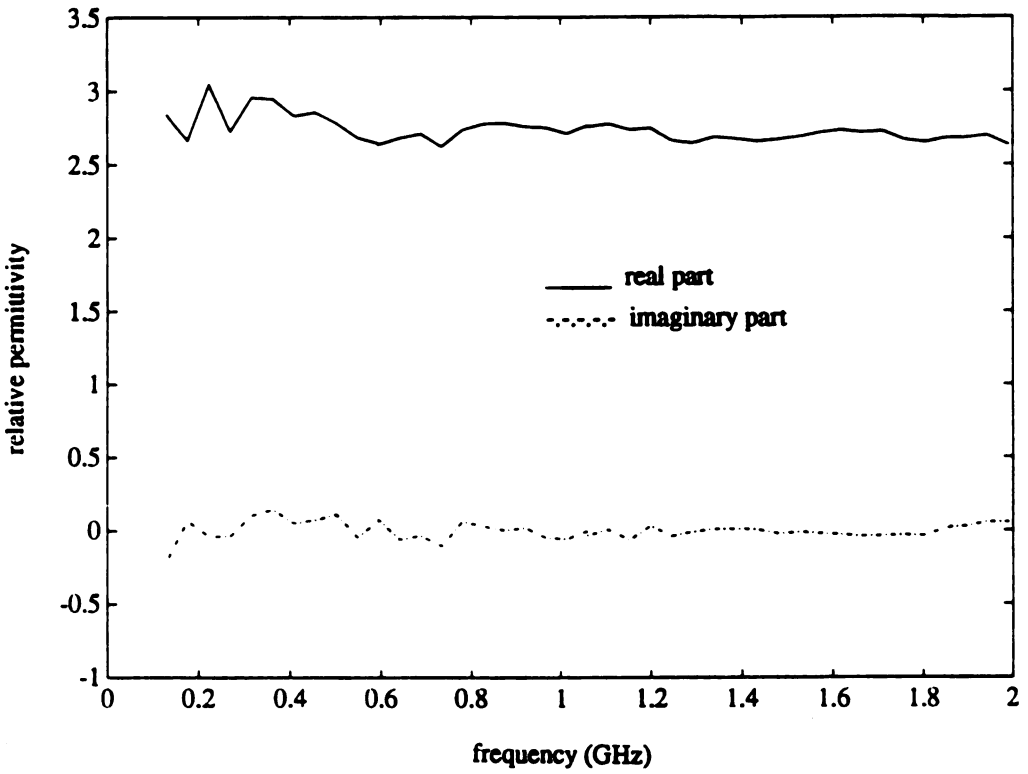

(a)

Figure 6.8 The permittivity ε and permeability μ of acrylic via open-ended coaxial probe. (a) The relative permittivity. (b) The relative permeability.

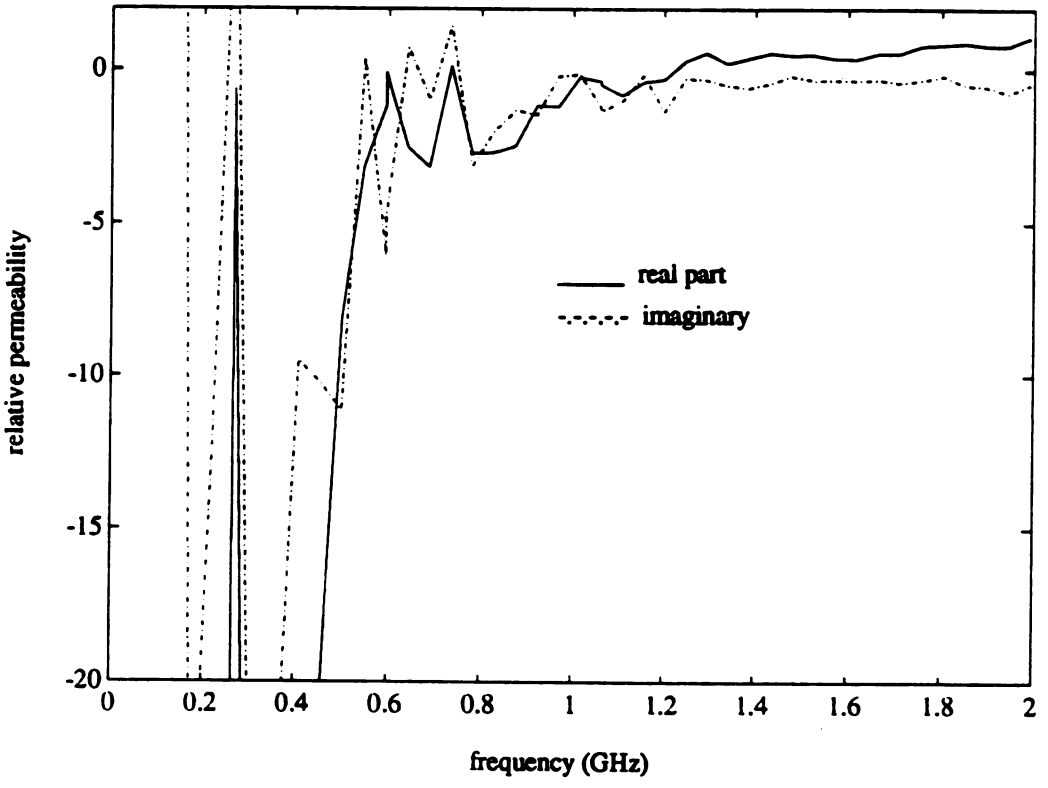

(b)

Figure 6.8(b) (continued)

unstable as shown in fig. 6.8(b). This is probably due to the ill-conditioned property of this method to simultaneously determine ε and μ for low permittivity materials for the low frequency range and difficulty in system calibration for the low frequency range. In addition, fig. 6.9 shows the results of the permittivity of acrylic for the frequencies up to 10 GHz. The values are within a reasonable range for all the frequencies, a slightly larger deviation found in the frequencies above 5 GHz may be due to the use of the GR type connector or the effect due to the excitation of complex waves.

Figures 6.10(a)-(b) show the permittivity and permeability of acetone. The results were obtained from two measurements of two samples of different thicknesses, 1.27mm and 2.54mm, with the setup of fig 6.3(b). The results for complex permittivity are good ($\varepsilon_r \cong 21$, and $\varepsilon_i \cong 0$), but the results for complex permeability again show the ill-conditioned property of this method at low frequency, as $\mu=\mu_o$ is expected. As mentioned earlier, difficulty in system calibration for frequencies below f_c may also contribute to the poor results for complex permeability at low frequency range.

Figures 6.11(a)-(b) show the measured permittivity ε of an absorbing material (Eccosorb-Ls22) when the permeability $\mu=\mu_o$ is assumed. Since Eccosorb is a high loss material, the two measurements were made by using open-circuit and short-circuit setup as shown in fig. 6.3(a). For a sponge-like material as Eccosorb, it is hard to secure a very good contact with the coaxial probe. Especially it was found that the contact with the small center conductor of the probe is very important. Experimentally, a small spot of silver paint was painted on the surface of the Eccosorb to ensure a good contact with the probe. Two set of results generated from the open-circuit and the short-circuit cases are reasonably good (both ε_r and ε_i vary with frequency), but they are not very consistent. During the experiment, it was found that the shape and the EM properties of the material

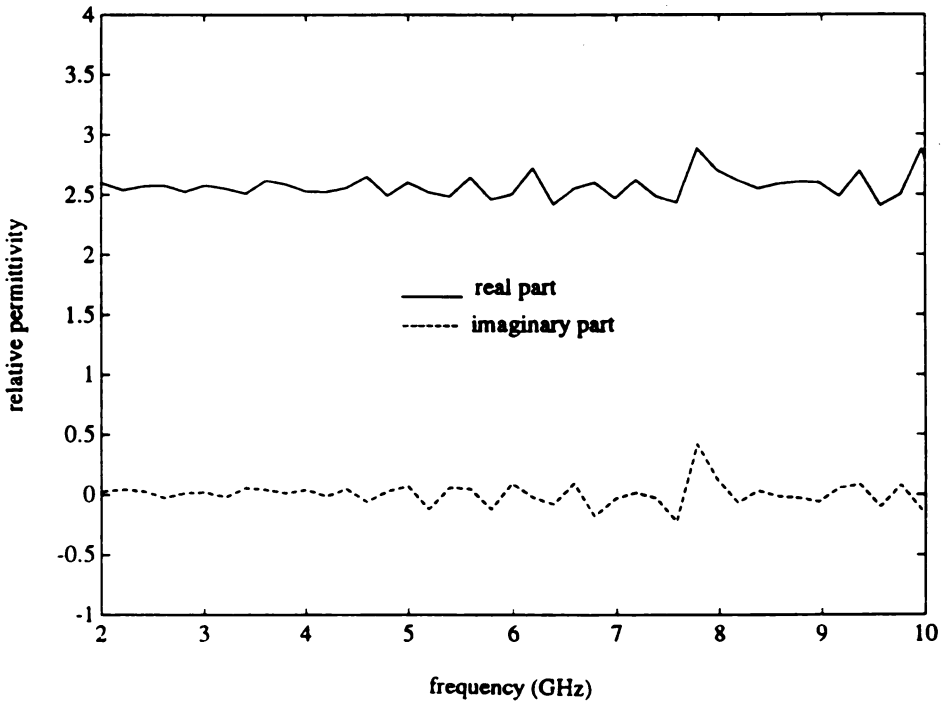

Figure 6.9 The permittivity ε acrylic via open-ended coaxial probe in the frequency range of 2~10 GHz.

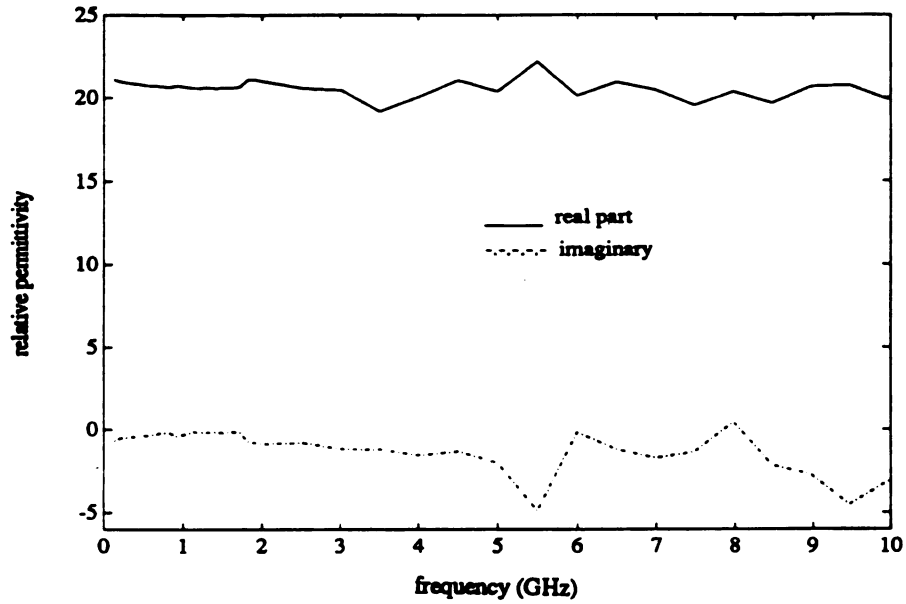

(a)

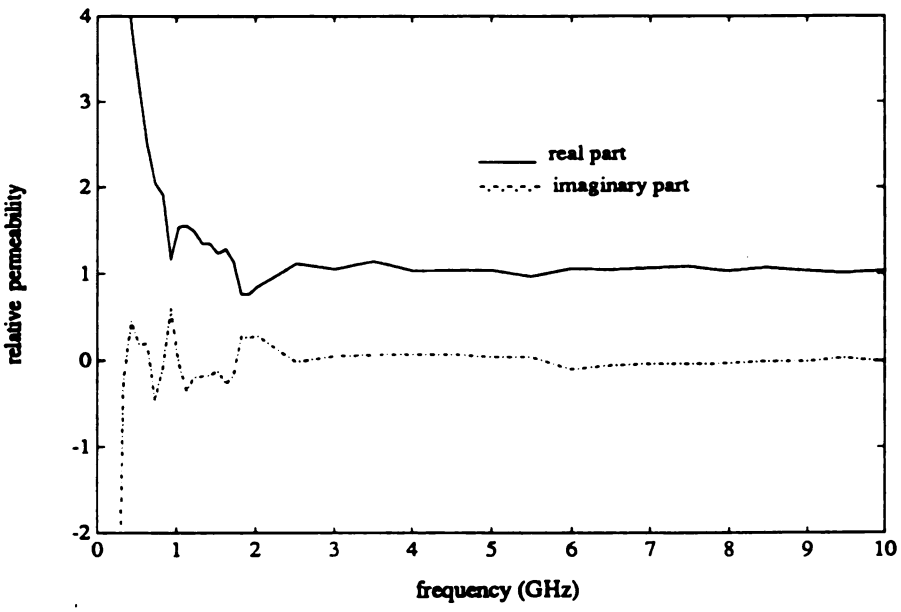

(b)

Figure 6.10 The permittivity ε and permeability μ of acetone via open-ended coaxial probe (a) The relative permittivity. (b) The relative permeability.

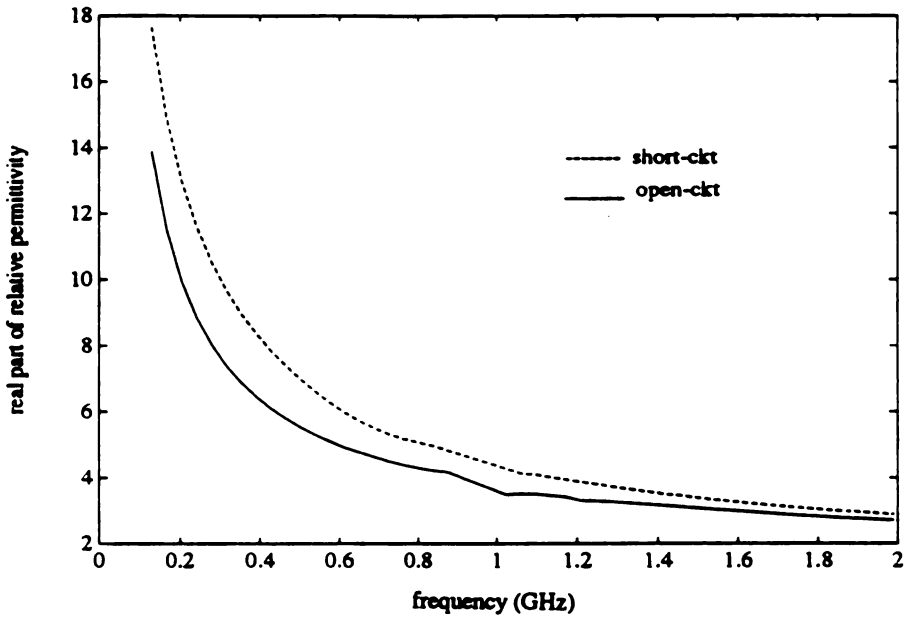

(a)

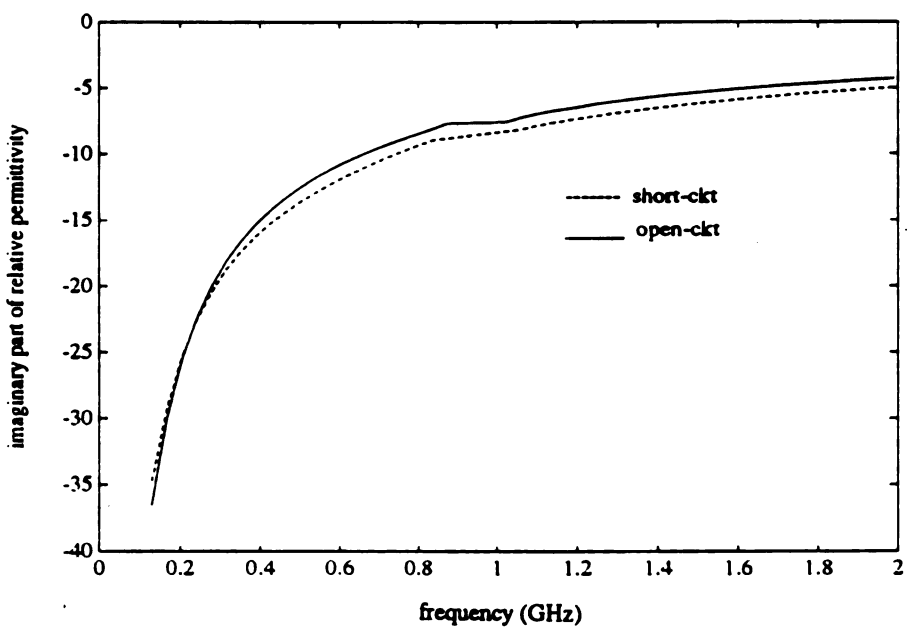

(b)

Figure 6.11 The permittivity ε of Eccosorb-Ls22 via open-ended coaxial probe ($\mu=\mu_0$ assumed). (a) The real part of relative permittivity. (b) The imaginary part of relative permittivity.

change when it is pressed due to its softness. Because of this reason it is difficult to obtain simultaneously ε and μ of this kind of materials.

Figures 6.12(a)-(b) show the permittivity and permeability of distilled water. The results were obtained from two measurements of two samples of different thicknesses, 1.1mm and 2.3mm, with the setup of fig 6.3(b). The measured results are ($\varepsilon_r \cong 78$, and $\varepsilon_i \cong -2 \sim -8$) and ($\mu_r \cong 1$, and $\mu_i \cong 0$) which are considered to be quite satisfactory. It is noted that the ill-conditioned behavior of the method was not observed when the material is of high permittivity type.

6.5 Experimental Results via Coaxial Cavity Method

In this section, the results of EM parameters of various materials measured by a coaxial cavity system are presented. With reference to fig. 6.2, a coaxial cavity (cavity radius 5") driven by a 14mm coaxial air line (a=0.3102cm, b=0.7145cm) was fabricated. The center conductor of the coaxial cavity was made removable in order to facilitate the calibration of the 14mm coaxial line.

The measurement steps in section 6.4 can be applied to the coaxial cavity method as well. Through these steps the EM parameters of three different materials were measured. These include a low permittivity material (acrylic), medium permittivity material (Eccosorb-Ls22) and high permittivity material (water). The frequency range covers from 0.2 GHz to 2 GHz.

It was found that the contact of the movable shorting backwall with the cylindrical wall is very important. In the experiment, aluminum foils were placed between them to achieve a better contact. In addition, a good calibration for the 14mm coaxial line, as

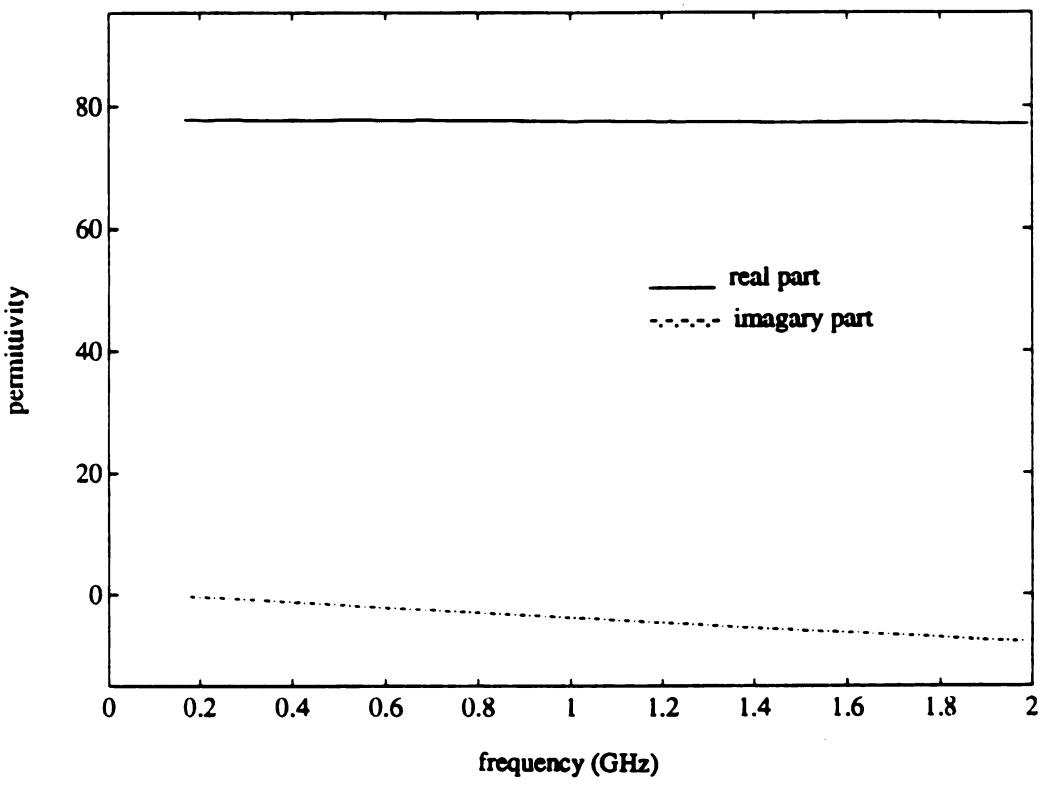

(a)

Figure 6.12 The permittivity ε and permeability μ of distilled water via open-ended coaxial probe. (a) The relative permittivity. (b) The relative permeability.

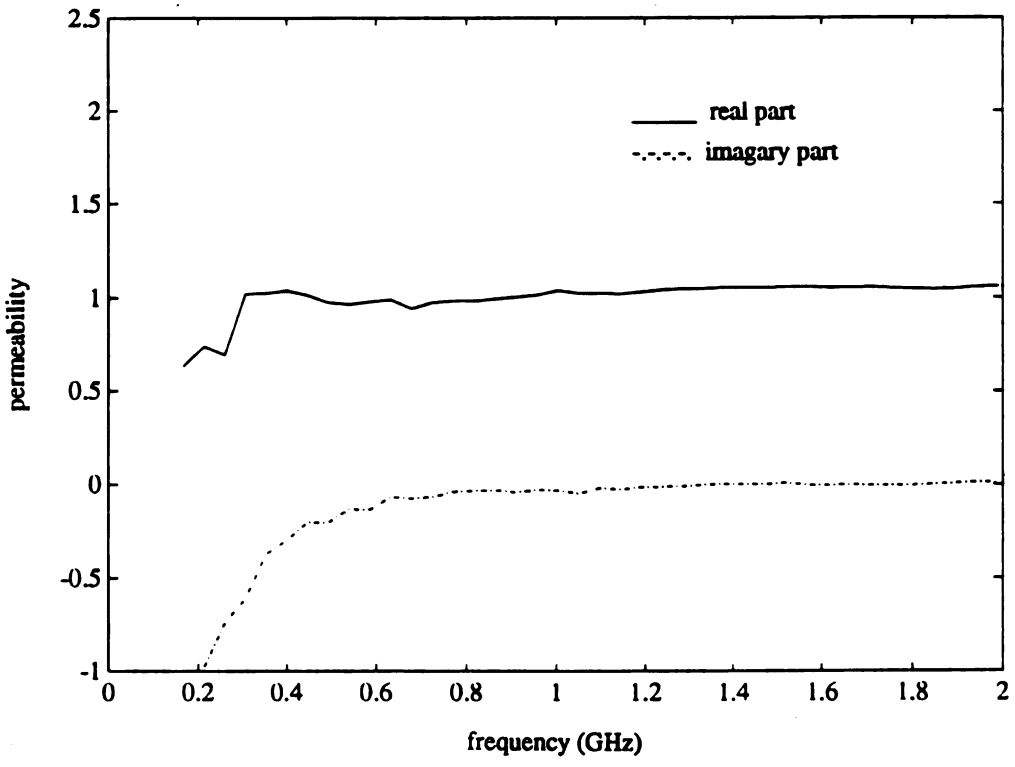

(b)

Figure 6.12(b)(continued).

shown in fig. 6.5, is essential for consecutive measurements. With three shorting stubs of different lengths (l_a=5.84cm, l_b=3.89cm and l_c=1.88cm), the calibration can be made by removing the center conductor of the coaxial cavity. It was found that the calibration was quite good for the frequency above some critical frequency f_c, about 0.5 GHz in our case. For the frequency below f_c, a good calibration is not easy since the wavelength is so large that these shorting stubs do not provide well-separated phases. The critical frequency f_c is then limited by the length of l_a. The difficulty in calibration at low frequency may be overcome if the coaxial feed line and shorting stubs are made longer.

Figures 6.13(a)-(b) show the measured permittivity of acrylic ($\varepsilon_r \cong 2.6$, and $\varepsilon_i \cong 0$) when the permeability $\mu=\mu_o$ is assumed. The effect of metallic wall loss is shown. The effect of the metallic wall loss on the imaginary part of ε was expected to be considerable for low frequency range, but it was not evident because the results at this frequency range are not stable due to the poor calibration for frequencies below f_c.

Figures 6.14(a)-(b) show the measured permittivity of an absorbing material (Eccosorb-Ls22) when the permeability $\mu=\mu_o$ is assumed. The results are compared to that obtained by the open-ended coaxial probe method. The results are reasonably good in the high frequency range, while some inconsistency in the low frequency range may be due to the poor calibration for frequencies below f_c and the ill-conditioned property of this method.

Figures 6.15(a)-(b) show the measured permittivity of distilled water when the permeability $\mu=\mu_o$ is assumed. The results are compared to that obtained by the open-ended coaxial probe method. It was found that the determination of EM parameters is ill-conditioned at the frequencies near cavity resonance even though the effect of metallic wall loss is considered.

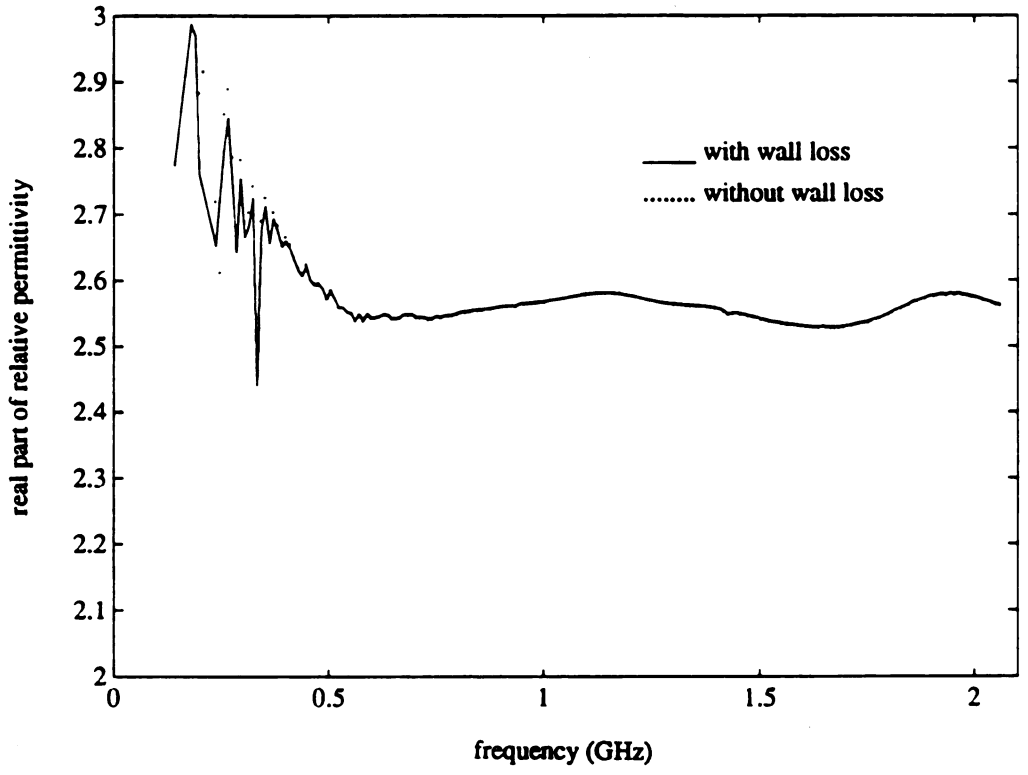

(a)

Figure 6.13 The permittivity ε of acrylic via coaxial cavity method ($\mu=\mu_0$ assumed). The effect of cavity wall loss is shown. (a) The real part of relative permittivity. (b) The imaginary part of relative permittivity.

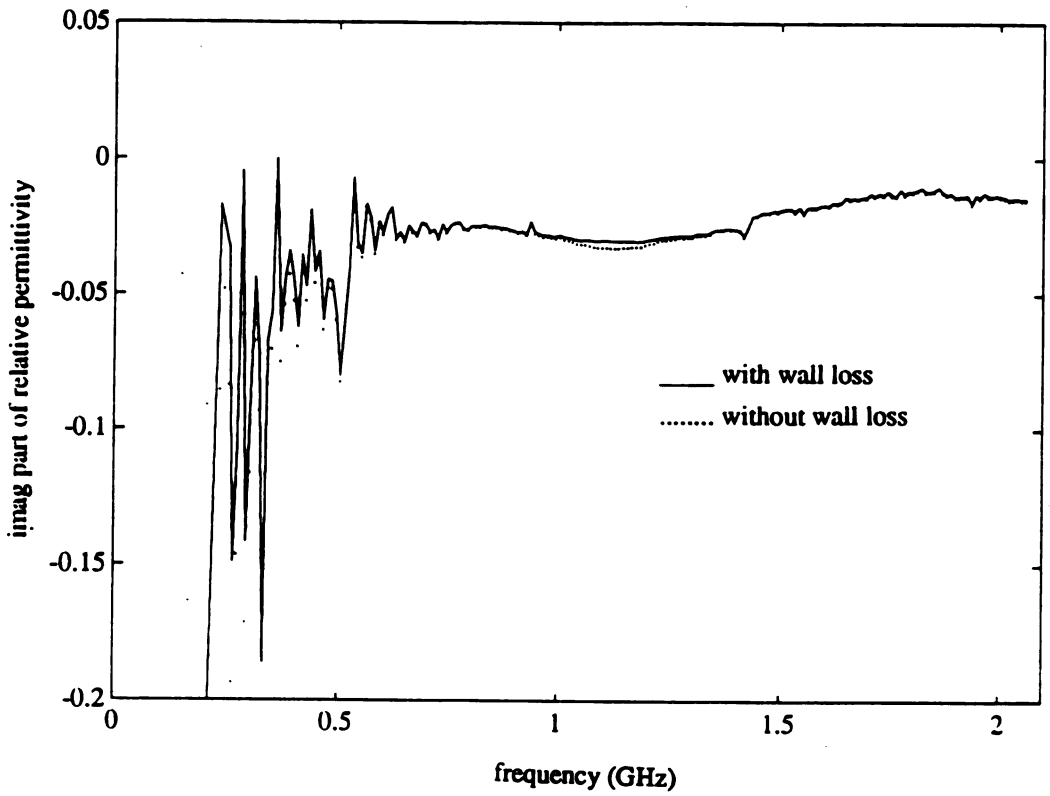

(b)

Figure 6.13(b)(continued).

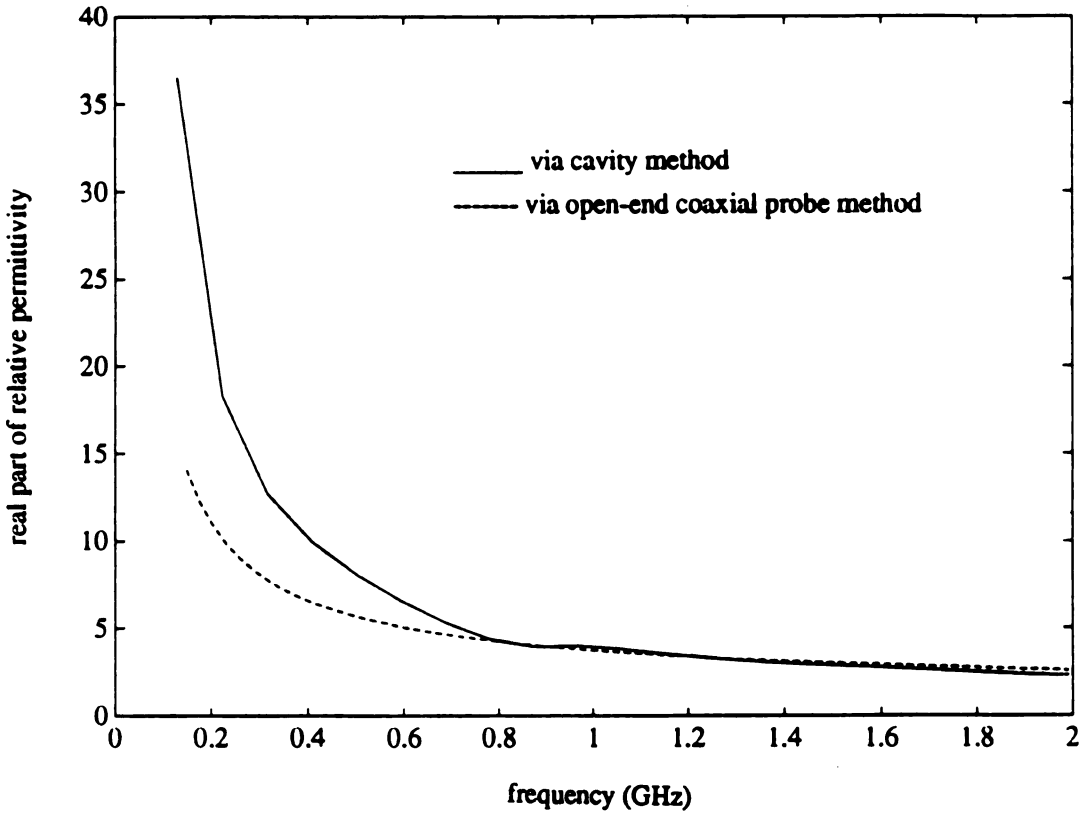

(a)

Figure 6.14 The permittivity ε of Eccosorb-Ls22 via coaxial cavity method ($\mu=\mu_0$ assumed). (a) The real part of relative permittivity. (b) The imaginary part of relative permittivity.

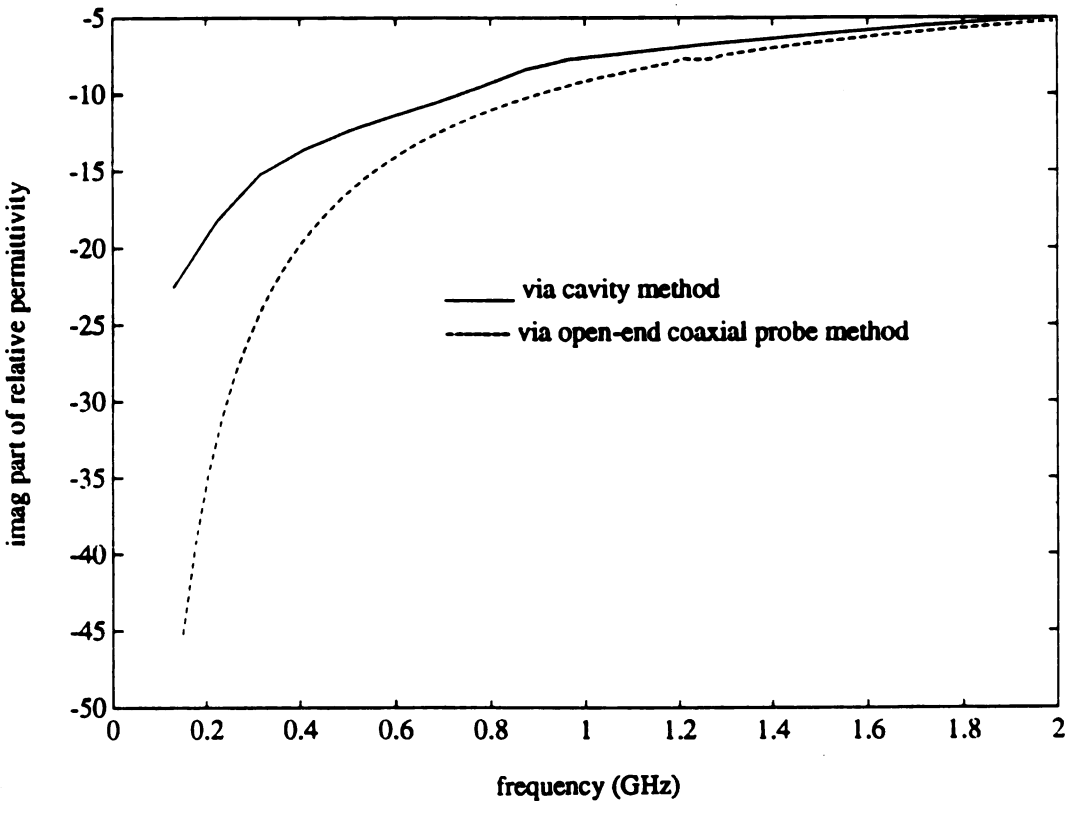

(b)

Figure 6.14(b)(continued).

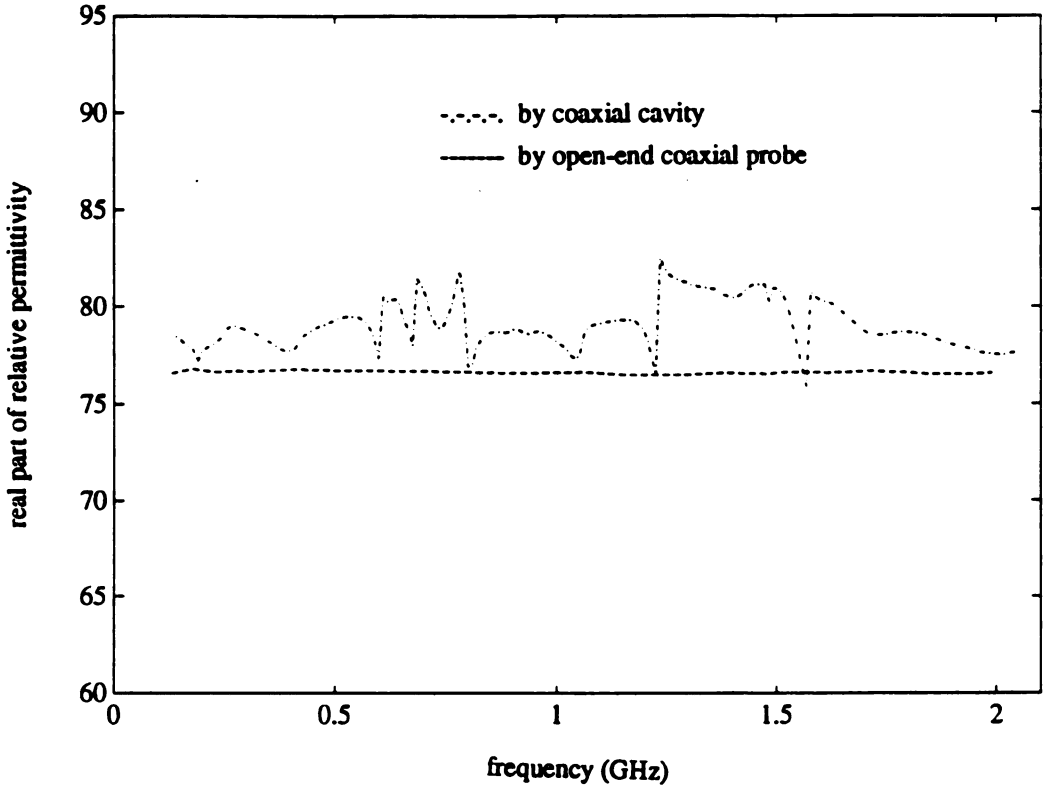

(a)

Figure 6.15 The permittivity ε of distilled water via coaxial cavity method ($\mu=\mu_o$ assumed). (a) The real part of relative permittivity. (b) The imaginary part of relative permittivity.

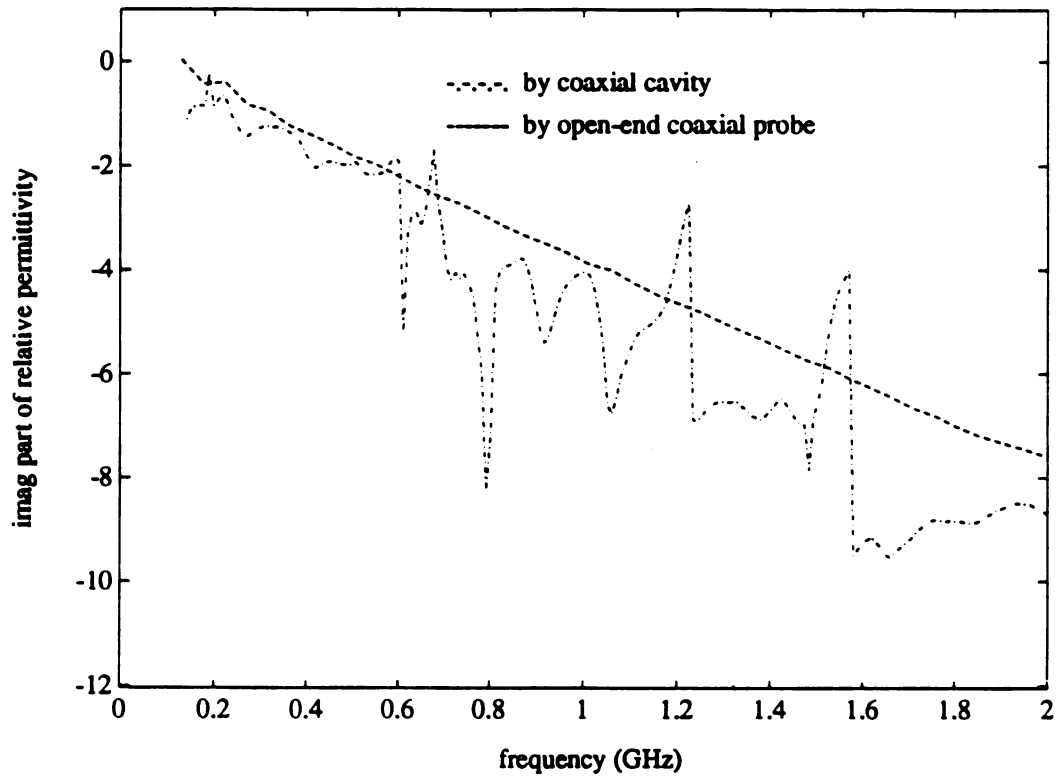

(b)

Figure 6.15(b)(continued).

CHAPTER 7
CONCLUSION

This thesis studied two schemes of measuring the conductivity, permittivity and permeability of various materials using two coaxial probe systems over a wide frequency band (0.2 to 10 Ghz).

The works of this thesis have some contribution to the EM characterization of materials, especially for the theoretical development of the open-ended coaxial line probe technique. The study of the coaxial cavity system also provides a new scheme of EM characterization for materials.

Using an open-ended coaxial probe system, a non-destructive measurement can be achieved easily by simply placing the probe against the material medium. To overcome some weaknesses of the open-ended coaxial probe scheme, a coaxial cavity system was developed to excite EM fields which penetrate into the material medium. This system is suitable for measuring EM properties of liquid materials, but solid material samples need to be machined to fit in the cavity.

Theoretical full wave analyses of these systems lead to an integral equation for the electric field at the aperture of the driving coaxial line. The method of moments was applied to transform the integral equation into a set of simultaneous algebraic equations so that the numerical solution for aperture electric field can be obtained. After the aperture electric field is obtained, other quantities such as the input impedance and the EM fields inside material can be calculated. The input impedance of the coaxial probe

is then used to determine the EM parameters of the material inversely when the input impedance is measured experimentally.

For the open-ended coaxial probe placed against a material layer, the physical pictures are revealed clearly through the analysis of complex waves. For the frequencies at which no power is radiated or carried away by the surface waves, the excited EM field is localized at the aperture, thus, the assumption of an infinite metallic flange employed in the theoretical analysis is justified. This also provides the validity for the quasi-static analysis which has been used by other workers. However, at the frequencies where the radiative power and the surface wave power are significant, the influence of these complex waves on the characterization of EM parameters is important and the effect of finite flange should be investigated in the future. In addition, an efficient way to compute the radiative wave power was derived, and the analysis of the power balance also gave confidence to the evaluation of the radiative power from the open-ended coaxial probe.

In the coaxial cavity system, it is found that at the resonant frequencies, the determination of the EM parameters of materials becomes ill-conditioned. The inclusion of metallic wall loss gives little improvement on the ill-conditioned problem, but it is important on the determination of the EM parameters for low loss materials, especially at the low frequencies.

A series of experiments was conducted to measure the input impedances of the coaxial probe systems for various materials, which included low, medium and high permittivity materials. A good agreement between the experimental results and published data was obtained. Further improvements may be possible with additional investigation, which includes a better calibration technique with longer shorting stubs, minimization of the edge effect due to a finite flange on the radial guided wave excited in the open-ended

coaxial system when the material layer is shorted by a metallic plate. Finally, these systems may be modified and extended to measure EM properties of anisotropic materials.

APPENDIX

FORTRAN COMPUTER PROGRAM

```
ccccccccccccccccccccccccccccccccccccccccccccccccccccccccccccccccccccccccccccccc
c  Program:  EMparameters
c
c  Class :   Main program
c
c  Call to:  calibration, findkcn, cnewton, cjacobian, cnewtonfx, admittance, solveqns,
c            polen, newtr, Bessf0, Bessf1, Romerg, fxvalue, quard, crbnfx, swpower,
c            radialpower.
c
c  Purpose:  To compute the permittivity and permeability of an unknown material,
c            which is placed against an open-ended coaxial line probe with a metallic
c            flange.  Items of interests - input admittance, aperture fields, complex wave
c            power.
c
c  Method:   Newton's method is used to inversely determine the permittivity and
c            permeability of materials so that the theoretical admittances of the probe
c            fit the measured ones.  MOM is used to solve the integral equation for the
c            aperture electric field via coaxial eigenmode expansion and Galerkin's
c            technique.  Cauchy residue theorem and saddle point method are employed
c            to calculate the complex wave power.
c
c  Specifics: All units are in M.K.S. system.
c
c  Program hierarchy for main program:
c            EMparameters
c                calibration
c                findkcn
c                cnewton
c                    cjacobian
c                    cnewtonfx
c                        admittance
c                    solveqns
c
c  Program hierarchy for admittance subroutine:
c            admittance
c                polen
c                    newtr
c                bessf0
c                romerg
c                    fxvalue, fxvalue2, fxvalue3
c                        quard2, crbnfx
c                solveqns
c                swpower
c                radialpower
ccccccccccccccccccccccccccccccccccccccccccccccccccccccccccccccccccccccccccccccc
```

```
ccccccccccccccccccccccccccccccccccccccccccccccccccccc
c      This is the main program, in which the initial
c parameters and options are chosen and the experiment
c data are read.  Newton's method is called to solve
c the EM parameters.
ccccccccccccccccccccccccccccccccccccccccccccccccccccc
       PROGRAM    EMparameters
       PARAMETER  (dim1=201,dim50=50)
       COMPLEX*16 caseepv(2,3),casemuv(2,3)
       COMPLEX*16 epv(65),muv(65),admit0(20)
       COMPLEX*16 zeros(4,dim1),epi,cx(dim50),roots(dim50)
       COMPLEX*16 admitmeasured(dim50),y(2,dim1)
       COMPLEX*16 updateadmit(20),cj
       REAL*8     tolerance,epdelta,datain3,datain4
       REAL*8     a,b,fre,conv,datain1,datain2,pi
       REAL*8     datain0,frequency(dim1),scalefactor
       REAL*8     mu0,ep0,z(65),kcn(100),casez(2,4)
       INTEGER    maxn,openckt,M,layerno,caseopenckt(2)
       REAL*8     x(20),p(20),accuracyr(20),accuracyi(20)
       REAL*8     absf,slope,wei(50,50),xpt(50,50)
       REAL*8     guessptr(2),guesspti(2)
       INTEGER    cntrst5,cntrend5,step,step5
       INTEGER    unknownno,unknownep(20),unknownmu(20)
       INTEGER    functionalmethod,expflag
       INTEGER    asym1version,asym2version,cntr
       INTEGER    versionfx2kntoinfi,cntrst,cntrend
       INTEGER    rx,outputfxno,contourint,i,j,n
       INTEGER    flagbessf,reevaluate,data1,data2
       INTEGER    swcontri,idxf,caseno,kcnflag,kcnno
       CHARACTER*12    file1(2)
       COMMON /paracasez/casez /paracaseno/caseno
       COMMON /paracaseepv/caseepv,casemuv
       COMMON /paracaseopenckt/caseopenckt
       COMMON /paraswcontri/swcontri /paraflagbessf/flagbessf
       COMMON /parareevaluate/reevaluate
       COMMON /para/tolerance,intno /paraabM/a,b,epi,M
       COMMON /parafre/fre,conv /paramuv/muv
       COMMON /para7/layerno /para9/epv,z /paraopen/openckt
       COMMON /parakcn/kcn /paraadmitmeasured/admitmeasured
       COMMON /paraunknownno/unknownno
       COMMON /paraunknownep/unknownep,unknownmu
       COMMON /parap/p /paraepdelta/epdelta /varabsf/absf
       COMMON /parafunctionalmethod/functionalmethod
       COMMON /paraupdateadmit/updateadmit
       COMMON /paraasym1version/asym1version,asym2version
       COMMON /paraaversionfx2kntoinfi/versionfx2kntoinfi
       COMMON /paraoutputfxno/outputfxno
       COMMON  /paracntrst/cntrst,cntrend,step
       COMMON /paracontourint/contourint /paraslope/slope
       COMMON /xandw/xpt,wei
ccccccccccccccccccccccccccccccccccccccccccccccccccccc
c      input the parameters and options
ccccccccccccccccccccccccccccccccccccccccccccccccccccc
```

```
      cj=(0.d0,1.d0)
      pi=atan(1.d0)*4.d0
      mu0=4.d-7*pi
      ep0=1.d-9/pi/36.d0
      WRITE(*,*)'input caseno:'
      READ(*,*)caseno
      WRITE(*,*)'caseno=',caseno
      WRITE(*,*)'input openckt(1/0)? (of case1 case2)'
      READ(*,*)caseopenckt(1),caseopenckt(2)
      openckt=caseopenckt(1)
      WRITE(*,*)'input a,b,M,epi,fre,conv:'
      READ(*,*)a,b,M,datain1,datain2,fre,conv
      epi=datain1+cj*datain2
      WRITE(*,*)'input layerno:'
      READ(*,*)layerno
      DO 10 i=layerno,1,-1
         WRITE(*,*)'input epv(',i,')',' ,muv(',i,')='
         READ(*,*)datain1,datain2,datain3,datain4
     &   ,datain5,datain6,datain7,datain8
         caseepv(1,i)=(datain1+cj*datain2)*ep0
         casemuv(1,i)=(datain3+cj*datain4)*mu0
         epv(i)=caseepv(1,i)
         muv(i)=casemuv(1,i)
         caseepv(2,i)=(datain5+cj*datain6)*ep0
         casemuv(2,i)=(datain7+cj*datain8)*mu0
10    CONTINUE
      casez(1,layerno+1)=0.d0
      casez(2,layerno+1)=0.d0
      DO 20 i=layerno,2,-1
         WRITE(*,*)'input thickness(',i,') (of case1 case2)'
         READ(*,*)datain1,datain2
         casez(1,i)=casez(1,i+1)+datain1
         casez(2,i)=casez(2,i+1)+datain2
         z(i)=casez(1,i)
20    CONTINUE
      WRITE(*,*)'input tolerance,intno'
      READ(*,*)tolerance,intno
      WRITE(*,*)'input epdelta'
      READ(*,*)epdelta
      unknownno=0
      DO 30 i=1,layerno
         READ(*,*)data1,data2
         unknownep(i)=data1
         unknownmu(i)=data2
         unknownno=unknownno+data1+data2
30    CONTINUE
      WRITE(*,*)'input flagbessf,reevaluate:'
      READ(*,*)flagbessf,reevaluate
      WRITE(*,*)'expflag,contourint'
      READ(*,*)expflag,contourint
      WRITE(*,*)'input slope:'
      READ(*,*)slope
      WRITE(*,*)'input kcnflag, no of point'
```

```
      READ(*,*)kcnflag,kcnno
      OPEN(2,FILE='xp.dat')
      OPEN(3,FILE='wp.dat')
      READ(2,*)rx
      READ(3,*)rx
      DO 40 j=2,rx
      DO 40 i=1,j
         READ(2,*)xpt(j,i)
         READ(3,*)wei(j,i)
40    CONTINUE
      CLOSE(2)
      CLOSE(3)
      WRITE(*,*)'input cntrend5,cntrst5, :'
      READ(*,*)cntrend5,cntrst5,step5
      IF (kcnflag.EQ.1) THEN
         CALL findkcn(a,b,kcnno,'kcn.dat')
      ENDIF
      CALL rvectorbin(kcn,maxn,'kcn.dat')
      DO 50 i=1,maxn
         kcn(i)=kcn(i)/a
50    CONTINUE
      IF (expflag.EQ.1) THEN
         CALL calibration()
         DO 60 i=1,unknownno
            WRITE(*,*)'input guess pt'
            READ(*,*)datain1,datain2
            x(2*unknownno-1)=datain1*ep0
            x(2*unknownno)=datain2*ep0
            guessptr(i)=datain1
            guesspti(i)=datain2
60       CONTINUE
         WRITE(*,*)'input filename'
         READ(*,*)file1(1),file1(2)
         WRITE(*,*)'file1(',1,')=',file1(1)
         WRITE(*,*)'file1(',2,')=',file1(2)
         DO 80 i=1,unknownno
            OPEN(i,FILE=file1(i))
            READ(i,*)scalefactor
            DO 70 j=1,dim1
               READ(i,*)datain0,datain1,datain2
               frequency(j)=datain0*scalefactor
               y(i,j)=(datain1+cj*datain2)*scalefactor
70          CONTINUE
            CLOSE(i)
80       CONTINUE
      ELSE
ccccccccccccccccccccccccccccccccccccccccccccc
c     If expflag is zero, then run the default
c data for numerical analysis.
ccccccccccccccccccccccccccccccccccccccccccccc
            CALL admittance(admit0(i))
            STOP
      ENDIF
```

```
      DO 300 cntr=cntrend5,cntrst5,step5
         DO 90 i=1,unknownno
            admitmeasured(i)=y(i,cntr)
90       CONTINUE
         fre=frequency(cntr)
         DO 100 i=1,unknownno
            accuracyr(i)=abs(DBLE(admitmeasured(i)))*1.d-7
            accuracyi(i)=abs(imag(admitmeasured(i)))*1.d-7
100      CONTINUE
         n=unknownno
         cx(1)=guessptr(1)+cj*guesspti(1)
         cx(2)=guessptr(2)+cj*guesspti(2)
         idxf=caseno
         CALL cnewton(cx,roots,n,idxf)
ccccccccccccccccccccccccccccccccccccccccccccccccc
c      Output the results for EM parameters
ccccccccccccccccccccccccccccccccccccccccccccccccc
         WRITE(*,*)'At frequency,',fre,' the zeros are'
         DO 190 i=1,unknownno
            zeros(i,cntr)=roots(i)
            WRITE(*,*)'roots(',i,')=',roots(i)
190      CONTINUE
      DO 200 i=1,unknownno
      WRITE(*,*)'The measured admittance: ',admitmeasured(i)
      WRITE(*,*)'The computed admittance: ',updateadmit(i)
200   CONTINUE
300   CONTINUE
      DO 400 i=1,unknownno
         DO 400 cntr=cntrend5,cntrst5,step5
         WRITE(*,*)frequency(i),zeros(i,cntr)
400   CONTINUE
      STOP
      END



ccccccccccccccccccccccccccccccccccccccccccccccccccccccccccccccccccccc
c      The S-parameters of the setup are computed via 3
c measured reflection coefficients.  To assure the choice of
c these reflection coefficients do lead to well-separated
c phases, it is necessary to make more than 3 measurements.
c From which, 3 reflection coefficients are chosen to
c calculate the S-parameters.  After that the transformation
c of reflection coefficient from the measurement reference to
c the probe aperture can be achieved.
ccccccccccccccccccccccccccccccccccccccccccccccccccccccccccccccccccccc
      SUBROUTINE calibration
      PARAMETER  (shortkitno=9)
      COMPLEX*16 s11(201),s22(201),s1221(201)
      COMPLEX*16 s11m,g1,g2,g3,g(shortkitno,201)
      COMPLEX*16 R1(201),Rap(201),zd,epri,beta1
      COMPLEX*16 rp,r(201),y(201),r3p,r2p,r1p,ya(201),rshort
      COMPLEX*16 rnp(shortkitno),gunknown(201),cj
```

```
      REAL*8      beta,la,lb,lc,lab,lac,pi
      REAL*8      lemda,fre(201),frei,ld,lo
      REAL*8      datain1,datain2,datain0,dssave(3),db,ds
      REAL*8      leng(shortkitno),deltaph(3),dbsave(3)
      REAL*8      dphorig(shortkitno),dph(shortkitno)
      REAL*8      dphp(shortkitno),dphn(shortkitno)
      INTEGER     i,j,k,cntrst,cntrend,step,cntr
      INTEGER     cntrp,cntrn,fileno,idxb,idxs,idxw1,idxw2
      CHARACTER*12  files(shortkitno),fileunknown

      cj=(0.,1.d0)
      pi=atan(1.0d0)*4.0d0
      epri=2.03-cj*1.d-3
ccccccccccccccccccccccccccccc
c Input the initail setting  c
ccccccccccccccccccccccccccccc
      OPEN(1,FILE='expdata.ini')
      OPEN(2,FILE='expdata.out')
      READ(1,*)cntrst,cntrend,step
      READ(1,*)fileno
      WRITE(2,*)'cntrst,cntrend =',cntrst,cntrend,step
      WRITE(2,*)'fileno=',fileno
      DO 6 i=1,fileno
         READ(1,*)files(i),leng(i)
         WRITE(2,*)'files(',i,')=',files(i),leng(i)
6     CONTINUE
      READ(1,*)fileunknown
      WRITE(2,*)'fileunknown=',fileunknown
      READ(1,*)ld
      WRITE(2,*)'ld=',ld
      CLOSE(1)
      CLOSE(2)
      DO 8 i=1,fileno
         OPEN(1,FILE=files(i))
         DO 7 j=1,201
            READ(1,*)datain0,datain1,datain2
            g(i,j)=datain1+(0,1.d0)*datain2
7        CONTINUE
      CLOSE(1)
8     CONTINUE
      OPEN(3,FILE=fileunknown)
      DO 9 i=1,201
         READ(3,*)datain0,datain1,datain2
         gunknown(i)=datain1+(0,1.d0)*datain2
         fre(cntr)=datain0*1.d9
9     CONTINUE
      CLOSE(3)
ccccccccccccccccccccccccccccccccccccccccccccccccccccccccccccccc
c     All the reflection coeffs. are transformed to the
c plane at z=-leng(1). Then the phase difference between
c the first one  and the others is calculated. After that
c three reflection coeffs. are chosed so that they have
c good separation among them and are THEN suitable for
```

```
c determining the S-parameters. By the way, three cases
c are examined in order to accomplish the good separation.
ccccccccccccccccccccccccccccccccccccccccccccccccccccccc
       cntr=0
       DO 70 k=cntrst,cntrend,step
          cntr=cntr+1
          lemda=3.e8/fre(k)
          beta=2.*pi/lemda
          beta1=beta*sqrt(epri)
          lc=leng(fileno)
          rshort=-1.d0
          DO 20 i=1,fileno-1
             rnp(i)=-exp(-2.*cj*beta*(leng(fileno)-leng(i)))
             dphorig(i)=phase(rnp(i))-phase(rshort)
             IF (dphorig(i).GT.180d0) THEN
                dphorig(i)=dphorig(i)-360
             ELSEIF (dphorig(i).LT.-180d0) THEN
                dphorig(i)=dphorig(i)+360
             ENDIF
             dph(i)=dphorig(i)
20        CONTINUE
       CALL directsort(dph,fileno-1)
       cntrp=0
       cntrn=0
       DO 30 i=1,fileno-1
       IF (dph(i).GT.0.d0 .and. dph(i).LT.180d0) THEN
          cntrp=cntrp+1
          dphp(cntrp)=dph(i)
       ELSEIF (dph(i).LT.0.d0 .and. dph(i).GT.-180d0) THEN
          cntrn=cntrn+1
          dphn(cntrn)=dph(i)
          ENDIF
30     CONTINUE

       deltaph(1)=0
       deltaph(2)=0
       deltaph(3)=0
ccccccccccccccccccccccccccccccccccccccccccccccccccccccc
c    Case1 : When the phase differences have both
c      positive and negative signs.
ccccccccccccccccccccccccccccccccccccccccccccccccccccccc
       IF (cntrp*cntrn.NE.0) THEN
          db=dphp(cntrp)
          ds=dphn(1)
          deltaph(1)=db
          IF (db.GT.abs(ds)) THEN
             deltaph(1)=abs(ds)
          ENDIF
          dbsave(1)=db
          dssave(1)=ds
       ENDIF
ccccccccccccccccccccccccccccccccccccccccccccccccccccccc
c    Case2 : When the phase differences have positive signs.
```

```
ccccccccccccccccccccccccccccccccccccccccccccccccccccccccccccccccc
       IF (cntrp.GE.2) THEN
          db=dph(fileno-1)

          ds=dphp(1)
          DO 35 i=2,cntrp
             IF (abs(dphp(i)-db/2.d0).LT.abs(ds-db/2.d0)) THEN
                ds=dphp(i)
             ENDIF
35        CONTINUE
          deltaph(2)=ds
          IF (abs(ds).GT.abs(db-ds)) THEN
             deltaph(2)=abs(db-ds)
          ENDIF
          dbsave(2)=db
          dssave(2)=ds
       ENDIF
ccccccccccccccccccccccccccccccccccccccccccccccccccccccccccccccccc
c    Case3 : When the phase differences have negative signs.
ccccccccccccccccccccccccccccccccccccccccccccccccccccccccccccccccc
       IF (cntrn.GE.2) THEN
          db=dph(1)
          ds=dphn(cntrn)
          DO 40 i=2,cntrn
             IF (abs(dphn(i)-db/2.d0).LT.abs(ds-db/2.d0)) THEN
                ds=dphn(i)
             ENDIF
40        CONTINUE
          deltaph(3)=abs(ds)
          IF (abs(ds).GT.abs(db-ds)) THEN
             deltaph(3)=abs(db-ds)
          ENDIF
          dbsave(3)=db
          dssave(3)=ds
       ENDIF
ccccccccccccccccccccccccccccccccccccccccccccccccccccccccccccccccc
c    choose the one that has best separation from case1,2,3
ccccccccccccccccccccccccccccccccccccccccccccccccccccccccccccccccc
       i=1
       IF (deltaph(2).GT.deltaph(i)) THEN
          i=2
       ENDIF
       IF (deltaph(3).GT.deltaph(i)) THEN
          i=3
       ENDIF
       db=dbsave(i)
       ds=dssave(i)
       DO 50 i=1,fileno-1
          IF (dphorig(i).EQ.db) THEN
             idxb=i
          ENDIF
          IF (dphorig(i).EQ.ds) THEN
             idxs=i
```

```
         ENDIF
50     CONTINUE
       la=leng(idxb)
       lb=leng(idxs)
       idxw1=idxb
       idxw2=idxs
       IF (lb.GT.la) THEN
          la=leng(idxs)
          lb=leng(idxb)
          idxw1=idxs
          idxw2=idxb
       ENDIF
ccccccccccccccccccccccccccccccccccccccccccccccccccccc
c      Compute the S-parameters from three measured
c reflection coeffs.
ccccccccccccccccccccccccccccccccccccccccccccccccccccc
       lab=la-lb
       lac=la-lc
       lo=la-ld
       g3=g(fileno,k)
       g2=g(idxw2,k)
       g1=g(idxw1,k)
       r3p=-exp(-2.*cj*beta*lac)
       r2p=-exp(-2.*cj*beta*lab)
       r1p=-1+cj*0
       s22(k)=((g3-g2)*(r1p-r2p)-(g1-g2)*(r3p-r2p))
     &        /((g3-g2)*(r1p-r2p)*r3p-(g1-g2)*(r3p-r2p)*r1p)
       s1221(k)=(g3-g2)/(r3p-r2p)*(1.-s22(k)*r3p)
     &          *(1.-s22(k)*r2p)
       s11(k)=g3-s1221(k)*r3p/(1.-s22(k)*r3p)
ccccccccccccccccccccccccccccccccccccccccccccccccccccc
c      Transform the reflection coefficient of the unknown
c material to the probe aperture if there is no spacer.
ccccccccccccccccccccccccccccccccccccccccccccccccccccc
       s11m=gunknown(k)
       rp=(s11m-s11(k))/((s11m-s11(k))*s22(k)+s1221(k))
       r(k)=rp*exp(2.*cj*beta*la)
       phaser=phase(r(k))
       y(k)=(1-r(k))/(1+r(k))
ccccccccccccccccccccccccccccccccccccccccccccccccccccc
c      Transform the reflection coefficient of the unknown
c material to the probe aperture if there exists a spacer.
ccccccccccccccccccccccccccccccccccccccccccccccccccccc
       R1(k)=rp*exp(2.*cj*beta*(lo))
       zd=(1+R1(k))/(1-R1(k))
       Rap(k)=-exp(2.*cj*beta1*ld)*(1/sqrt(epri)-zd)
     &    /(1/sqrt(epri)+zd)
       ya(k)=(1-Rap(k))/(1+Rap(k))
70     CONTINUE

ccccccccccccccccccccccccccccccccccccccccccccccccccccc
c    Output the results of reflection coeffs. and the
c admittance at the probe aperture.
```

```
ccccccccccccccccccccccccccccccccccccccccccccccccccccccccccccccc
      OPEN(1,FILE='R.dat')
      OPEN(2,FILE='Y.dat')
      OPEN(3,FILE='Ra.dat')
      OPEN(4,FILE='Ya.dat')
      WRITE(2,*)1.d0
      WRITE(4,*)1.d0
      DO 100 k=cntrst,cntrend,step
         frei=fre(k)
         WRITE(2,*)frei,REAL(y(k)),IMAG(y(k))
         WRITE(4,*)frei,REAL(ya(k)),IMAG(ya(k))
100   CONTINUE
      DO 200 k=cntrst,cntrend,step
         frei=fre(k)
         WRITE(1,*)frei,REAL(r(k)),IMAG(r(k))
         WRITE(3,*)frei,REAL(Rap(k)),IMAG(Rap(k))
200   CONTINUE
      CLOSE(1)
      CLOSE(2)
      CLOSE(3)
      CLOSE(4)
      RETURN
      END


ccccccccccccccccccccccccccccccccccccccccccccccccccccccccccccccc
c     The eigenvalues of the TM modes inside the coaxial
c waveguide are computed.
ccccccccccccccccccccccccccccccccccccccccccccccccccccccccccccccc
      SUBROUTINE findkcn(a,b,number,filekcn)
      PARAMETER  (delta=1.d-7)
      REAL*8     delta,oldx,newx,oldf,newf
      REAL*8     pi,h,kcn(10000),rratio,ptexpect,a,b
      INTEGER    j,number,idx
      CHARACTER*12 filekcn
      COMMON /pararratio/rratio
      pi=atan(1.0)*4.0
      rratio=b/a
5     DO 50 j=1,number
         idx=0
         ptexpect=DBLE(j)*pi/(rratio-1)
         oldx=ptexpect
         newx=oldx-delta
         oldf=eigenfx(oldx)
         newf=eigenfx(newx)
10       idx=idx+1
         h=newf*(newx-oldx)/(newf-oldf)
         oldf=newf
         oldx=newx
20       newx=oldx-h
         newf=eigenfx(newx)
         IF ((newx.LT.(ptexpect-0.4/rratio)).OR.(newx
     &                      .GT.(ptexpect+0.2/rratio))) THEN
```

```
               h=h/2.d0
               goto 20
            ENDIF
            IF (newf.NE.oldf) THEN
               IF (idx.LE.50) THEN
                  GOTO 10
               ELSE
                  WRITE(*,*)'Too many steps in findkcn
     &                     subroutine'
               ENDIF
            ENDIF
            kcn(j)=newx
50       CONTINUE
         OPEN(3,FILE=filekcn,FORM='unformatted')
         WRITE(3)number
         DO 100 j=1,number
            WRITE(3)kcn(j)
100      CONTINUE
         CLOSE(3)
         RETURN
         END

         FUNCTION eigenfx(x)
         REAL*8      x,rratio
         COMPLEX*16 z,j0,j1,y0,y1,h20,h21,j0cx,y0cx
         INTEGER     iprint
         COMMON /pararratio/rratio
         z=x
         CALL bessf0(z,j0,j1,y0,y1,h20,h21,iprint)
         z=rratio*x
         CALL bessf0(z,j0cx,j1,y0cx,y1,h20,h21,iprint)
         eigenfx=j0cx*y0-j0*y0cx
         RETURN
         END


ccccccccccccccccccccccccccccccccccccccccccccccccccccccccccccccccc
c      General Newton's method for n-d complex fuctions with
c complex veriables x.  The variable idxf serves as an index
c for the functions that are to be used.
ccccccccccccccccccccccccccccccccccccccccccccccccccccccccccccccccc
         SUBROUTINE cnewton(x,roots,n,idxf)
         PARAMETER  (dim50=50,interationmax=15)
         COMPLEX*16 x(dim50),f(dim50),W(dim50,dim50)
         COMPLEX*16 p(dim50),roots(dim50)
         REAL*8      convdelta
         INTEGER     i,idxf,n,ra,ca,interation
         convdelta=1.d-3
         ra=n
         ca=n
         CALL cjacobian(x,f,W,n,idxf)
         interation=0
10       DO 11 i=1,ra
```

```
            W(i,n+1)=-f(i)
11        CONTINUE
          CALL solveqns(W,p,ra,ca)
          DO 20 i=1,ra
             x(i)=x(i)+p(i)
20        CONTINUE
          interation=interation+1
ccccccccccccccccccccccccccccccccccccccccccccccccc
c         {get next Jacobian}
ccccccccccccccccccccccccccccccccccccccccccccccccc
          CALL cjacobian(x,f,W,n,idxf)
          DO 80 i=1,n
             IF (( abs(p(i)/x(i)).GE.convdelta).AND.
     &              (interation.LE.interationmax)) THEN
                GOTO 10
             ENDIF
80        CONTINUE
          DO 85 i=1,n
             IF (abs(p(i)/x(i)).GE.convdelta.or.
     &              interation.GT.interationmax) THEN
                WRITE(*,*)'converge error'
             ENDIF
85        CONTINUE
          DO 90 i=1,n
             roots(i)=x(i)
90        CONTINUE
          RETURN
          END


ccccccccccccccccccccccccccccccccccccccccccccccccccccccccccccccccccccccccc
c      This subroutine evaluate both the jacobian and function
c value.  The jacobian is evaluate by difference concept.
ccccccccccccccccccccccccccccccccccccccccccccccccccccccccccccccccccccccccc
          SUBROUTINE cjacobian(x,f,jac,n,idxf)
          PARAMETER  (dim50=50)
          COMPLEX*16 jac(dim50,dim50),x(dim50),f(dim50),xsave
          COMPLEX*16 fsave(dim50)
          REAL*8     jacdelta
          INTEGER    n,i,j,idxf
          jacdelta=1.d-3
          CALL cnewtonfx(x,f,n,idxf)
          DO 10 i=1,n
             fsave(i)=f(i)
10        CONTINUE
          DO 25 j=1,n
             xsave=x(j)
             x(j)=x(j)*(1.d0-jacdelta)
             CALL cnewtonfx(x,f,n,idxf)
             DO 20 i=1,n
                jac(i,j)=fsave(i)/xsave-f(i)/xsave
                jac(i,j)=jac(i,j)/jacdelta
20           CONTINUE
```

```
            x(j)=xsave
25       CONTINUE
         DO 30 i=1,n
            f(i)=fsave(i)
30       CONTINUE
         RETURN
         END

         SUBROUTINE cnewtonfx(x,fx,n,idxf)
         PARAMETER  (dim50=50)
         COMPLEX*16 x(dim50),fx(dim50),epv(65),muv(65)
         COMPLEX*16 admit,admitmeasured(dim50),updateadmit(20)
         COMPLEX*16 caseepv(2,3),casemuv(2,3),reflection
         REAL*8     z(65),ep0,casez(2,4),mu0
         INTEGER    i,idxf,n,caseopenckt(2),openckt
         COMMON /paraupdateadmit/updateadmit
         COMMON /paraadmitmeasured/admitmeasured /para9/epv,z
         COMMON /paracasez/casez /paracaseepv/caseepv,casemuv
         COMMON /paracaseopenckt/caseopenckt /paraopen/openckt
         COMMON /paramuv/muv
         pi=atan(1.d0)*4.d0
         ep0=1.d-9/pi/36.d0
         mu0=4.d-7*pi
         DO 5 i=1,n
            reflection=(1-admitmeasured(i))/(1+admitmeasured(i))
            epv(3)=caseepv(i,3)
            muv(3)=casemuv(i,3)
            epv(2)=caseepv(i,2)
            muv(2)=casemuv(i,2)
            epv(1)=caseepv(i,1)
            muv(1)=casemuv(i,1)
            z(3)=casez(i,3)
            z(2)=casez(i,2)
            openckt=caseopenckt(i)
ccccccccccccccccccccccccccccccccccccccc
c Update unknowns in correct position
ccccccccccccccccccccccccccccccccccccccc
            IF (idxf.EQ.1) THEN
ccccccccccccccccccccccccccccccccccccccccccccccccccccccc
c       2 layer case:
c          This fx always takes ep2 and mu2 as unknowns.
ccccccccccccccccccccccccccccccccccccccccccccccccccccccc
               epv(2)=x(1)*ep0
               IF (n.EQ.2) THEN
                  muv(2)=x(2)*mu0
               ENDIF
            ELSEIF (idxf.EQ.2) THEN
ccccccccccccccccccccccccccccccccccccccccccccccccccccccc
c       2 layer case:
c        This fx always takes ep1 and mu1 as unknowns.
ccccccccccccccccccccccccccccccccccccccccccccccccccccccc
               epv(1)=x(1)*ep0
```

```
            IF (n.EQ.2) THEN
               muv(1)=x(2)*mu0
            ENDIF
         ELSEIF (idxf.EQ.3) THEN
ccccccccccccccccccccccccccccccccccccccccccccccccccccccccccccccc
c      2 layer case:
c         This fx always takes ep1 and mu1 as unknowns
c      first, then it takes ep2 and mu2 as unknowns.
ccccccccccccccccccccccccccccccccccccccccccccccccccccccccccccccc
            epv(i)=x(1)*ep0
            IF (n.EQ.2) THEN
               muv(i)=x(2)*mu0
            ENDIF
         ELSEIF (idxf.EQ.4) THEN
ccccccccccccccccccccccccccccccccccccccccccccccccccccccccccccccc
c      3 layer case:
c         This fx always takes ep2 and mu2 as unknowns
c      first, then it takes ep3 and mu3 as unknowns.
ccccccccccccccccccccccccccccccccccccccccccccccccccccccccccccccc
            epv(i+1)=x(1)*ep0
            IF (n.EQ.2) THEN
               muv(i+1)=x(2)*mu0
            ENDIF

         ELSEIF (idxf.EQ.5) THEN
ccccccccccccccccccccccccccccccccccccccccccccccccccccccccccccccc
c      3 layer case:
c this fx always took the ep3 and mu3 as unknowns first
c         THEN took the ep3 and mu3 as unknowns second
ccccccccccccccccccccccccccccccccccccccccccccccccccccccccccccccc
            epv(3)=x(1)*ep0
            IF (n.EQ.2) THEN
               muv(3)=x(2)*mu0
            ENDIF
         ELSE
            WRITE(*,*)'idxf no error in cnewton.f'
         ENDIF
         CALL admittance(admit)
         fx(i)=(1+admit)/(1-admit)-1./reflection
         updateadmit(i)=admit
5      CONTINUE
       RETURN
       END


ccccccccccccccccccccccccccccccccccccccccccccccccccccccccccccccc
c      The admittance of the coaxial at the probe aperture
c is calculated in this subroutine.  Some other quantities
c such as the complex wave power and the aperture electric
c field is also solved.
ccccccccccccccccccccccccccccccccccccccccccccccccccccccccccccccc
       SUBROUTINE admittance(admit)
       PARAMETER  (dim1=50)
```

```
PARAMETER  (dim2=201)
COMPLEX*16 sum,w,zarg,j1,y0,y1,h20,h21,kN
COMPLEX*16 jwep0,jwepN,epN,epv(65),muv(65)
COMPLEX*16 epipass,epi,itai,jwepi,k(65),total
COMPLEX*16 cj,Yb(0:50,0:50),Ya(0:50,0:50),c(50,50)
COMPLEX*16 input(0:50),sol(50),admit,R,sol1(50)
COMPLEX*16 tem6,savetotal,cn2(0:50)
COMPLEX*16 cj0kciab,cj0kcjab,cj0kca,cj0kcb,Er
COMPLEX*16 cj1kcx,cy1kcx,cy0kca
COMPLEX*16 sum0to2knf,eps1,eps2,thpi(0:10)
COMPLEX*16 pt1,pt2,pt3,pt4
REAL*8     froma,tob,kmax,kmin,kw(0:65)
REAL*8     ratio,dummy,interv,kleft,kright
REAL*8     ita0,mu0,ep0,z(65),pi,conv,omega
REAL*8     kcn(100),kcj,kci,waveno,waveno2,fre
REAL*8     a,b,realM,kc,radiusa,radiusb
REAL*8     tolerance,accur,kmilestone(65)
REAL*8     kthird,slope,asym1dat(0:50,0:50)
REAL*8     kmaxpass,kminpass,fromapass,tobpass
REAL*8     j0kcb,j0kca,x,kc0array(65),t,kcpi
REAL*8     toalp1op2,powerin,swp,ploss,losstan
INTEGER    iprint,i,j,idx,layerno,index1,M,test2
INTEGER    ctr,intno,step,cntrend,cntrst,no3,openckt
INTEGER    index1,u,no512,ctrmax,ctr2max
INTEGER    contourint,opentoair,u,asymYes
INTEGER    Mmax,reevaluate,swcontri,kc0zerono,nc
COMMON /parakcpi/kcpi /parakc0array/kc0array,kc0zerono
COMMON /paracn2/cn2 /paraswcontri/swcontri
COMMON /parareevaluate/reevaluate
COMMON /varcj0kciab/cj0kciab,cj0kcjab
COMMON /paraasymYes/asymYes /para1/total,ctr
COMMON /paractr2max/ctr2max /varkcij/kcj,kci
COMMON /para5/kmaxpass,kminpass /parajw/jwepN /para6/kw
COMMON /parakmilestone/kmilestone  /para7/layerno
COMMON /para11/k /para8/kN /para9/epv,z
COMMON /paraopen/openckt /para4/no3,branchptflag
COMMON /para/tolerance,intno /paractrmax/ctrmax
COMMON /parano512/no512 /para10/accur
COMMON /paratest2/test2 /paraabM/a,b,epi,M
COMMON /pararadiusab/radiusa,radiusb /parafre/fre,conv
COMMON /paramuv/muv /parakcn/kcn /varindex1/index1
COMMON /varratio/ratio,dummy /varfatb/fromapass,tobpass
COMMON /varkc/kc /paraopentoair/opentoair
COMMON /paracontourint/contourint /paraslope/slope
COMMON /paracntrst/cntrst,cntrend,step /parasol/sol1
accur=0.d0
test2=1
radiusa=a
radiusb=b
pi=atan(1.0d0)*4.0d0
cj=(0.0d0,1.0d0)
mu0=4.d-7*pi
ep0=1.d-9/pi/36.d0
```

```
      omega=fre*2.d0*pi
      epipass=epi
      realM=M
      ita0=sqrt(mu0/ep0)
      itai=ita0/sqrt(epi)
      waveno=omega*sqrt(mu0*ep0)
      waveno2=waveno**2*epi
      jwep0=cj*omega*ep0
      jwepi=jwep0*epi
      epN=epv(layerno)
      jwepN=cj*omega*epN
      DO 10 i=1,layerno
         k(i)=omega*cdsqrt(muv(i)*epv(i))
10    CONTINUE
      kN=k(layerno)
      losstan=IMAG(epv(layerno))/REAL(epv(layerno))
      DO 20 i=0,M
         input(i)=0
      DO 20 j=0,M
         Yb(j,i)=(0.0d0,0.0d0)
         Ya(j,i)=(0.0d0,0.0d0)
20    CONTINUE

      DO 30 i=1,M+1
      DO 30 j=1,M+1
         c(j,i)=(0.0d0,0.0d0)
30    CONTINUE
      DO 40 j=1,M
         kcj=kcn(j)
         Yb(j,j)=jwepi/sqrt(kcj*kcj-waveno2)
         zarg=kcj*a
         CALL bessf0(zarg,cj0kca,j1,y0,y1,h20,h21,iprint)
         zarg=kcj*b
         CALL bessf0(zarg,cj0kcb,j1,y0,y1,h20,h21,iprint)
         j0kca=DBLE(cj0kca)
         j0kcb=DBLE(cj0kcb)
         tem6=2.d0*((j0kca/j0kcb)**2-1.d0)
         cn2(j)=pi*kcj/sqrt(tem6)
40    CONTINUE
      cn2(0)=1.d0
      input(0)=2.d0/itai*log(b/a)
      Yb(0,0)=1.d0/itai*log(b/a)
      kmin=DBLE(k(1))
      kmax=DBLE(k(1))
      kmaxpass=kmax
      kminpass=kmin
      DO 50 i=2,layerno
         kmin=DMIN1(DBLE(k(i)),kmin)
         kmax=DMAX1(DBLE(k(i)),kmax)
50    CONTINUE
      IF (reevaluate.EQ.0 ) THEN
         OPEN(3,FILE='asym1.dat',FORM='unformatted')
         READ(3)Mmax
```

```
            DO 60 j=0,Mmax
            DO 60 i=0,Mmax
               READ(3)asym1dat(j,i)
60          CONTINUE
            CLOSE(3)
         ENDIF
         eps1=epv(1)/ep0
         eps2=epv(2)/ep0
         t=z(2)/(2*pi/waveno)
         CALL polen(eps1,eps2,t,thpi,nc)
         kc0zerono=nc/2+1
         DO 70 i=1,kc0zerono
            kc0array(i)=thpi(2*i-2)*waveno
70       CONTINUE
ccccccccccccccccccccccccccccccccccccccccccccccccccccc
c        Filling the matrix element
ccccccccccccccccccccccccccccccccccccccccccccccccccccc
42       DO 1100 j=0,M
         DO 1000 i=0,j
            IF ((j+i).EQ.0) THEN
               u=0
            ELSEIF (j.EQ.0 .and. i.NE.0) THEN
               u=1
            ELSEIF (j.NE.0 .and. i.EQ.0) THEN
               u=2
            ELSEIF (j.NE.0 .and. i.NE.0) THEN
               u=3
            ENDIF
            kcj=kcn(j)
            kci=kcn(i)
            IF (i.NE.0) THEN
               zarg=kci*a
               CALL bessf0(zarg,cj0kca,j1,y0,y1,h20,h21,iprint)
               zarg=kci*b
               CALL bessf0(zarg,cj0kcb,j1,y0,y1,h20,h21,iprint)
               cj0kciab=cj0kca/cj0kcb
            ENDIF
            IF (j.NE.0) THEN
               zarg=kcj*a
               CALL bessf0(zarg,cj0kca,j1,y0,y1,h20,h21,iprint)
               zarg=kcj*b
               CALL bessf0(zarg,cj0kcb,j1,y0,y1,h20,h21,iprint)
               cj0kcjab=cj0kca/cj0kcb
            ENDIF
ccccccccccccccccccccccccccccccccccccccccccccccccccccc
c        Asymtotic term evaluation
ccccccccccccccccccccccccccccccccccccccccccccccccccccc
            IF (reevaluate.EQ.1) THEN
               asymYes=1
               ctr=0
               total=0.d0
               CALL cromerg(DCMPLX(sqrt(2.d0)*a),
     &                           DCMPLX((a+b)/sqrt(2.d0)),u)
```

```
               Ya(j,i)=Ya(j,i)+total*4.d0/pi*jwepN
               asym1dat(j,i)=total*4.d0/pi
               asymYes=2
               ctr=0
               total=0.d0
               CALL cromerg(DCMPLX((a+b)/sqrt(2.d0)),
     &                                 DCMPLX(sqrt(2.d0)*b),u)
               Ya(j,i)=Ya(j,i)+total*4.d0/pi*jwepN
               asym1dat(j,i)=asym1dat(j,i)+total*4.d0/pi
            ELSE
               Ya(j,i)=Ya(j,i)+asym1dat(j,i)*jwepN
            ENDIF
            asymYes=0
ccccccccccccccccccccccccccccccccccccccccccccccccccccccccccc
c       Evaluation from 2*kmax to a large number(infinite)
ccccccccccccccccccccccccccccccccccccccccccccccccccccccccccc
            dblflag=0
            interv=pi/a
            sum=0.d0
            idx=1
            kleft=2.d0*kmax+(idx-1.d0)*interv
            kright=2.d0*kmax+idx*interv
            ctr=0
            total=0.d0
            CALL cromerg(DCMPLX(kleft),DCMPLX(kright),u)
            sum=total
c begin whileloop
1230    idx=idx+1
            kleft=2.d0*kmax+(idx-1.d0)*interv
            kright=2.d0*kmax+idx*interv
            ctr=0
            total=0.d0
            CALL cromerg(DCMPLX(kleft),DCMPLX(kright),u)
            IF (abs(total)/abs(sum).GT.conv) THEN
               sum=sum+total
               GOTO 1230
            ELSE
               kthird=(2.d0*kleft+kright)/3.d0
               ctr=0
               total=0.d0
               CALL cromerg(DCMPLX(kleft),DCMPLX(kthird),u)
               savetotal=total
               ctr=0
               total=0.d0
               CALL cromerg(DCMPLX(kthird),DCMPLX(kright),u)
               sum=sum+savetotal+total
               IF ((abs(total/sum).GT.conv).OR.
     &                     (abs(savetotal/sum).GT.conv)) THEN
                  GOTO 1230
               ELSE
                  dblflag=dblflag+1
                  IF (dblflag.LT.2) THEN
                    GOTO 1230
```

```
                ENDIF
             ENDIF
          ENDIF
c END whileloop
          Ya(j,i)=Ya(j,i)+sum*jwepN
ccccccccccccccccccccccccccccccccccccccccccccccccccccccccccccccccccccc
c      Integration from 0 to 2*kmax. The contour off the real
c axis is chosen in this subroutine.
ccccccccccccccccccccccccccccccccccccccccccccccccccccccccccccccccccccc
          sum0to2knf=0.
          froma=0.d0
          IF (openckt.EQ.1) THEN
             tob=kmin/2.d0
          ELSE
             tob=0.d0
          ENDIF
          ctr=0
          total=0.d0
          CALL cromerg(DCMPLX(froma),DCMPLX(tob),u)
          Ya(j,i)=Ya(j,i)+total*jwepN
          sum0to2knf=sum0to2knf+total
          pt1=tob
          pt2=kmax*slope*cj+kmin/2.d0
          pt3=kmax*2.d0+kmax*slope*cj
          pt4=2.d0*kmax
          ctr=0
          total=0.d0
          CALL cromerg(pt1,pt2,u+4)
          Ya(j,i)=Ya(j,i)+total*jwepN
          ctr=0
          total=0.d0
          CALL cromerg(pt2,pt3,u+4)
          Ya(j,i)=Ya(j,i)+total*jwepN
          ctr=0
          total=0.d0
          CALL cromerg(pt3,pt4,u+4)
          Ya(j,i)=Ya(j,i)+total*jwepN
          Ya(j,i)=Ya(j,i)*cn2(j)*cn2(i)
1000    CONTINUE
1100    CONTINUE
        IF (reevaluate.EQ.1) THEN
           Mmax=M
           OPEN(3,FILE='asym1.dat',FORM='unformatted')
           WRITE(3)Mmax
           DO 1150 j=0,Mmax
           DO 1150 i=0,Mmax
              WRITE(3)asym1dat(j,i)
1150       CONTINUE
           CLOSE(3)
        ENDIF
        DO 1700 j=0,M
           c(j+1,M+2)=input(j)
           DO 1700 i=0,M
```

```
            c(j+1,i+1)=Yb(j,i)+Ya(j,i)
1700    CONTINUE

        DO 1750 j=1,M+1
        DO 1750 i=1,j
           c(i,j)=c(j,i)
1750    CONTINUE
        CALL solveqns(c,sol,M+1,M+1)
        DO 1800 i=1,M+1
           sol1(i)=sol(i)
1800     CONTINUE
ccccccccccccccccccccccccccccccccccccccccccccccccccccccccccccccc
c       Compute and output the complex wave power and the
c aperture electric field.
ccccccccccccccccccccccccccccccccccccccccccccccccccccccccccccccc
        OPEN(1,FILE='F&P.dat')
        IF (openckt.EQ.1 .AND. losstan.LT.1.d-3) THEN
           CALL swpower(sol,swp,toalplop2,w)
           u=10
           ctr=0
           total=0.d0
           CALL cromerg(DCMPLX(0.d0),DCMPLX(pi/2.d0),u)
           radpw=DBLE(total*4.d0*pi*omega*
     &           abs(epv(2)**2/epv(1))*k(1)**2)
        ELSEIF (openckt.EQ.0 .AND. losstan.LT.1.d-3) THEN
           CALL radialpw(sol,radpw)
        ENDIF
        R=sol(1)-1.d0
        admit=(1.d0-R)/(1.d0+R)
        ploss=1.d0-R*conjg(R)
        powerin=log(b/a)/120.
        WRITE(1,*)'R=',R
        WRITE(1,*)'swp,radpw=',swp/powerin,radpw/powerin
        WRITE(1,*)'ploss=',ploss
        WRITE(1,*)'E field:'
        DO 2200 i=0,100
           h=(b-a)/100.d0
           x=a+i*h
           Er=0
           DO 2300 j=1,M
              zarg=kcn(j)*x
              CALL bessf0(zarg,j0,cj1kcx,y0,cy1kcx,h20
     &                                          ,h21,iprint)
              zarg=kcn(j)*a
              CALL bessf0(zarg,cj0kca,j1,cy0kca,y1,h20
     &                                          ,h21,iprint)

Er=Er+sol(j+1)*cn2(j)*(cj1kcx*cy0kca-cj0kca*cy1kcx)
2300       CONTINUE
           Er=Er+sol(1)*1.d0/x
           WRITE(1,*)Er
2200    CONTINUE
        CLOSE(1)
```

```
      RETURN
      END


ccccccccccccccccccccccccccccccccccccccccccccccccccccccccccccccccccccc
c      Subroutine for finding surface wave poles.  Inputs are
c eps1, eps2, and t (thickness normalized by lamda0.  The
c results in thpi are normalized by k0.
ccccccccccccccccccccccccccccccccccccccccccccccccccccccccccccccccccccc
      SUBROUTINE polen(eps1,eps2,t,thpi,nc)
      IMPLICIT REAL*8         (a-h,o-z)
      COMPLEX*16 thp(0:10),thpi(0:10),eps1,eps2,thi,th
      tc1=.25/SQRT(abs(eps2)-abs(eps1))
      nc=INT(t/tc1)
      do 10 it=0,nc,2
      tc=DBLE(it)*tc1
      th=1.
      thi=1.00005
      nmin=MIN(10,1+INT((t-tc)/0.01))
      Do 20 i=1,nmin
      tt=tc+(t-tc)*dble(i)/DBLE(nmin)
      CALL newtr(eps1,eps2,tt,thi,th)
      thi=th
   20 CONTINUE
      thp(it)=th
   10  CONTINUE
      DO 30 i=0,nc,2
      ig=2*int(nc/2)-i
      thpi(i)=thp(ig)
   30  CONTINUE
      RETURN
      END
c
      SUBROUTINE newtr(eps1,eps2,t,thi,th)
      IMPLICIT REAL*8   (a-h,o-z)
      COMPLEX*16 p1,q2,p1t,q2t,d,dd,term
      COMPLEX*16 eps1,eps2,thi,th,k1,k2
      REAL*8     kot
      pai=3.14159265358979
      pai2=pai*2.
      k1=SQRT(eps1)
      k2=SQRT(eps2)
      th=thi
      kot=pai2*t
      DO 10 i=1,100
         p1=SQRT((th+k1)*(th-k1))
         q2=SQRT((k2+th)*(k2-th))
         p1t=kot*p1
         q2t=kot*q2
         IF (abs(q2t).Le.1.D-6) THEN
            d =cos(q2t)-eps1/eps2*q2/p1*sin(q2t)
            dd=th*(kot*kot+eps1/eps2*kot/p1*((k2-k1)
     &                  *(k2+k1)/p1**2+cos(q2t)))
```

```
            ELSE
               d =cos(q2t)-eps1/eps2*q2/p1*sin(q2t)
               dd=th*(kot*sin(q2t)/q2+eps1/eps2*q2/p1*(sin(q2t)
     &           *(k2-k1)*(k2+k1)/(p1*q2)**2+kot*cos(q2t)/q2))
            ENDIF
            term=d/dd
            aterm=abs(term)
            IF (aterm.Gt.1.D-12) THEN
               th=th-term
            ELSE
               GO TO 20
            ENDIF
10       CONTINUE
         write(*,*) 'too many steps in newtr, t=',t
20       RETURN
         END

ccccccccccccccccccccccccccccccccccccccccccccccccccccccccccccccccc
c        Subroutine to compute the Bessel function of the
c first and second kinds with orders 1 or 2.  The input
c arguments are complex.
ccccccccccccccccccccccccccccccccccccccccccccccccccccccccccccccccc
         SUBROUTINE bessf0(zp,j0,j1,y0,y1,h20,h21,iprint)
         IMPLICIT INTEGER*4 (i-n)
         IMPLICIT REAL*8    (a-h,o-z)
         COMPLEX*16 zpsq,zpfact,j0add,j1add,fact
         COMPLEX*16 zphalf,fach,cosp,sinp,ezp,p,q
         COMPLEX*16 zp,j0,j1,y0,y1,h20,h21,wronsk,ihulp
         ihulp=DCMPLX(0d0,1d0)
         IF (abs(zp).LT.1d1) THEN
            j0=1d0
            j0add=1d0
            j1=1d0
            j1add=1d0
            y1=1d0
            y0=0d0
            fk=1d0
            fkfact=1d0
            zpsq=-zp*zp/4d0
            zpfact=1d0
            skinv=1d0
100         zpfact=zpfact*zpsq
            fact=zpfact/fkfact
            j0add=fact/fkfact
            j0=j0+j0add
            fk=fk+1d0
            fkfact=fkfact*fk
            j1add=fact/fkfact
            j1=j1+j1add
            y0=y0+j0add*skinv
            skinvh=skinv+1d0/fk
            y1=y1+j1add*(skinv+skinvh)
            skinv=skinvh
```

```
      IF (MAX(ABS(j0add/j0),ABS(j1add/j1)).GT.1d-14)
     &                                              GOTO 100
      zphalf=5d-1*zp
      fach=LOG(zphalf)+0.5772156649015330d0
      j1=zphalf*j1
      y0=(fach*j0-y0)/1.5707963267949d0
      y1=(fach*j1-(1e0-zpsq*y1)/zp)/1.5707963267949d0
      h20=j0-ihulp*y0
      h21=j1-ihulp*y1
    ELSE
      fact=sqrt(3.14159265358979d0*zp)
      cosp=cos(zp)/fact
      sinp=sin(zp)/fact
      zpfact=dcmplx(1d0,1d0)*exp(-ihulp*zp)/fact
      ezp=8d0*zp
      u=0d0
      DO 300 iu=1,2
        fn=1d0
        fk=1d0
        p=1d0
        q=(u-1d0)/ezp
        fact=q
        DO 200 j=1,13
          fn=fn+2d0
          fk=fk+1d0
          fact=-fact*(u-fn*fn)/(ezp*fk)
          p=p+fact
          fn=fn+2d0
          fk=fk+1d0
          fact=fact*(u-fn*fn)/(ezp*fk)
          q=q+fact
          IF (abs(fact/q).lt.1d-8) goto 210
200     CONTINUE
210     IF (iu.eq.1) THEN
          j0=(p+q)*cosp+(p-q)*sinp
          y0=(p+q)*sinp-(p-q)*cosp
          h20=zpfact*(p-ihulp*q)
        ELSE
          j1=(p+q)*sinp-(p-q)*cosp
          y1=-(p+q)*cosp-(p-q)*sinp
          h21=zpfact*(q+ihulp*p)
        ENDIF
        u=4d0
300   CONTINUE
    ENDIF
    IF (iprint.eq.1) THEN
      const=2d0/(3.14159265358979d0*zp)
      p=j1*y0
      q=j0*y1+const
      wronsk=p/q
      diff=abs(1d0-wronsk)
      IF (diff.gt.1d-6) WRITE(*,400) zp,diff
    ENDIF
```

```
400    format(1h0,'wronskian check failed in bessf0 for zp= ',
     &              2e9.2,', difference is ',e8.1,'.')
       RETURN
       END


ccccccccccccccccccccccccccccccccccccccccccccccccccccccccccccccccc
c      A recursive,adaptive and iterative scheme based on
c Romerg integration.
ccccccccccccccccccccccccccccccccccccccccccccccccccccccccccccccccc
       SUBROUTINE cromerg(a,b,fxnumber)
       PARAMETER  (ppno=9,depthno=50)
       COMPLEX*16 temp,fa,fb,y(21),ynew,save,fx,diff
       COMPLEX*16 total,tolerance,h,xbar,a,b
       COMPLEX*16 a1(100),b1(100),anew(100),bnew(100)
       REAL*8     relativetolerance,k,accuracy,kipass,shift
       REAL*8     diffr,diffi,tolerancer,tolerancei
       INTEGER    k1,m,j,n9,intno,ctr,n,fxnumber,fxno,idx
       COMMON /varindex1/idx /para/relativetolerance,intno
       COMMON /para10/accuracy /para1/total,ctr
       COMMON /para3/fxno /varkipass/kipass
       fxno=fxnumber
       ctr=ctr+1
       IF (ctr.GT.depthno) THEN
          WRITE(*,*)'The recursive depth in cromerg subroutine
     &                          is too large for fxno=,',fxno
          STOP
       ENDIF
       k=1/3.0d0
       m=1
       a1(ctr)=a
       b1(ctr)=b
       xbar=(b+a)/2.d0
       h=(b-a)/2.d0
       CALL fxvalue(a1(ctr),fa)
       CALL fxvalue(xbar,fx)
       CALL fxvalue(b1(ctr),fb)
       y(1)=(fa+4.d0*fx+fb)*h/3.d0
c begin a while loop
4100   save=y(m)
       m=m+1
       k=k*3.d0
       h=h/3.d0
       temp=0
       k1=int(k)
       shift=0.d0
       DO 4200 j=1,k1
          xbar=a1(ctr)+(shift+1.d0)*h
          CALL fxvalue(xbar,fx)
          temp=temp+4.d0*fx
          xbar=a1(ctr)+(shift+2.d0)*h
          CALL fxvalue(xbar,fx)
          temp=temp+2.d0*fx
```

```
            xbar=a1(ctr)+(shift+4.d0)*h
            CALL fxvalue(xbar,fx)
            temp=temp+2.d0*fx
            xbar=a1(ctr)+(shift+5.d0)*h
            CALL fxvalue(xbar,fx)
            temp=temp+4.d0*fx
            shift=shift+6.d0
4200     CONTINUE
         ynew=y(1)/3.0d0+temp*h/3.d0
         n9=9
         DO 4300 n=2,m
            n9=n9*9
            temp=ynew+(ynew-y(n-1))/(n9-1)
            y(n-1)=ynew
            ynew=temp
4300     CONTINUE
         y(m)=ynew
         diff=y(m)-y(m-1)
         tolerance=relativetolerance*ynew
         diffi=abs((-diff+conjg(diff))*(0.d0,0.5d0))
         diffr=abs((diff+conjg(diff))*0.5d0)
         tolerancei=abs((-tolerance+conjg(tolerance))
     &                                      *(0.d0,0.5d0))
         tolerancer=abs((tolerance+conjg(tolerance))*0.5d0)
         IF (tolerancei.LT.1.d-14) THEN
            tolerancei=1.d-14
         ENDIF
         IF (tolerancer.LT.1.d-14) THEN
            tolerancer=1.d-14
         ENDIF
         IF (m.LT.ppno.AND.(diffi.GT.tolerancei.OR.
     &                          diffr.GT.tolerancer)) THEN
            GOTO 4100
         ENDIF
c end of while loop
         IF (diffi.GT.tolerancei.OR.diffr.GT.tolerancer) THEN
ccccccccccccccccccccccc
c        Recursive call
ccccccccccccccccccccccc
            anew(ctr)=a1(ctr)+(b1(ctr)-a1(ctr))/2.0d0
            bnew(ctr)=anew(ctr)
            CALL cromerg(a1(ctr),bnew(ctr),fxnumber)
            ctr=ctr-1
            CALL cromerg(anew(ctr),b1(ctr),fxnumber)
            ctr=ctr-1
         ELSE
            total=total+y(m)
         ENDIF
         RETURN
         END


ccccccccccccccccccccccccccccccccccccccccccccccccccccccccccccccccc
```

```
c      The subroutines for cromerg2 and cromerg3 are omitted
c here since they are essentially the same as cromerg with the
c following variable change:
c      ctr   -> ctr3
c      total -> total3
c      fxno  -> fxno3
c      These two subtoutines are called only when a triple
c integration is encountered.
ccccccccccccccccccccccccccccccccccccccccccccccccccccccccccc


ccccccccccccccccccccccccccccccccccccccccccccccccccccccccccc
c      A subroutine describing the integrand of a integral
c which is done by cromerg subroutine.
ccccccccccccccccccccccccccccccccccccccccccccccccccccccccccc
      SUBROUTINE fxvalue(cx,y)
      COMPLEX*16 y,kN,rbn,cx,total2,ckc,ckcpass,yc
      COMPLEX*16 zarg,j1,y0,y1,h20,h21,W,epv(65),epidummy
      COMPLEX*16 cj0kciab,cj0kcjab,cj0kca,cj0kcb
      COMPLEX*16 k(65),cn2(0:50),gama1,gama2,sol(50)
      REAL*8     kcn(100),kc,beta1,beta2,j0kcab(65)
      REAL*8    zdummy(65),kcpass,a,b,xlevel,ylevel,x,upper
      REAL*8     kci,kcj,kcjpass,kcipass
      INTEGER    fxno2pass,ctr2,fxno,fxno2,iprint,asymYes,M
      COMMON /para2/total2,ctr2 /varxylevel/xlevel,ylevel
      COMMON /para3/fxno /para31/fxno2pass
      COMMON /paraasymYes/asymYes /para8/kN
      COMMON /varkcij/kcjpass,kcipass /varckc/ckcpass,kcpass
      COMMON /varcj0kciab/cj0kciab,cj0kcjab
      COMMON /paraabM/a,b,epidummy,M /para11/k
      COMMON /parakcn/kcn /paracn2/cn2 /parasol/sol
      COMMON /para9/epv,zdummy
      pi=atan(1.0d0)*4.0d0
      fxno2=fxno2pass
ccccccccccccccccccccccccccccccccccc
c      Asymptotic term evaluation
ccccccccccccccccccccccccccccccccccc
      IF (asymYes.NE.0) THEN
         x=DBLE(cx)
         IF (asymYes.EQ.1) THEN
            upper=x-sqrt(2.d0)*a
         ELSEIF (asymYes.EQ.2) THEN
            upper=-x+sqrt(2.d0)*b
         ENDIF
         IF (upper.LT.1.d-14) THEN
               y=0.d0
         ELSE
            xlevel=DBLE(cx)
            ctr2=0
            total2=0.d0
            fxno2=3
            CALL quard2(0.d0,upper,fxno2)
            y=total2
```

```
            ENDIF
            GOTO 100
         ENDIF
         kc=DBLE(cx)
         ckc=cx
         kcpass=DBLE(cx)
         ckcpass=cx
         kcj=kcjpass
         kci=kcipass
         CALL crbnfx(ckc,rbn)
         IF (abs(ckc).NE.0.d0) THEN
            y=(1.d0-rbn)/(1.d0+rbn)/sqrt(ckc*ckc-kN*kN)*ckc-1.d0
            zarg=ckc*a
            CALL bessf0(zarg,cj0kca,j1,y0,y1,h20,h21,iprint)
            zarg=ckc*b
         CALL bessf0(zarg,cj0kcb,j1,y0,y1,h20,h21,iprint)
         ENDIF
         IF (abs(ckc).LE.1.d-10) THEN
            y=0.d0
            GOTO 100
         ELSEIF (fxno.EQ.0 .or. fxno.EQ.4) THEN
            GOTO 4
         ELSEIF (fxno.EQ.1 .or. fxno.EQ.5) THEN
            GOTO 5
         ELSEIF (fxno.EQ.2 .or. fxno.EQ.6) THEN
            GOTO 6
         ELSEIF (fxno.EQ.3 .or. fxno.EQ.7) THEN
            GOTO 7
         ELSEIF (fxno.EQ.10) THEN
            GOTO 10
         ELSE
            WRITE(*,*)'report fxno error;fxno=',fxno
         ENDIF
4        yc=(cj0kca-cj0kcb)/ckc
         y=y*yc**2
         GOTO 100
5        yc=(cj0kca-cj0kcb)/ckc
         y=y*yc*2.d0/pi*ckc/(kci*(kci*kci-ckc*ckc))
     &                   *(cj0kcb*cj0kciab-cj0kca)
         GOTO 100
6        yc=(cj0kca-cj0kcb)/ckc
         y=y*yc*2.d0/pi*ckc/(kcj*(kcj*kcj-ckc*ckc))
     &                   *(cj0kcb*cj0kcjab-cj0kca)
         GOTO 100
7        yc=2.d0/pi*ckc/(kcj*(kcj*kcj-ckc*ckc))
     &                   *(cj0kcb*cj0kcjab-cj0kca)
         y=y*yc*2.d0/pi*ckc/(kci*(kci*kci-ckc*ckc))
     &                   *(cj0kcb*cj0kciab-cj0kca)
         GOTO 100
ccccccccccccccccccccccccccccccccccccccccccccc
c        Radiation wave power evaluation
ccccccccccccccccccccccccccccccccccccccccccccc
10       x=cx
```

```
      DO 50 i=1,M
         zarg=kcn(i)*a
         CALL bessf0(zarg,cj0kca,j1,y0,y1,h20,h21,iprint)
         zarg=kcn(i)*b
         CALL bessf0(zarg,cj0kcb,j1,y0,y1,h20,h21,iprint)
         j0kcab(i)=cj0kca/cj0kcb
50    CONTINUE
      kc=DBLE(k(1))*sin(x)
      ckc=kc
      beta1=DBLE(k(1))*cos(x)
      beta2=sqrt(abs(k(2))**2-kc**2)
      gama2=(0.d0,1.d0)*beta2
      gama1=(0.d0,1.d0)*beta1
      IF (abs(x-pi/2.d0).LE.1.d-6) THEN
         rbn=0.d0
      ELSE
         CALL crbnfx(ckc,rbn)
      ENDIF
      zarg=kc*a
      CALL bessf0(zarg,cj0kca,j1,y0,y1,h20,h21,iprint)
      zarg=kc*b
      CALL bessf0(zarg,cj0kcb,j1,y0,y1,h20,h21,iprint)
      W=0.d0
      DO 200 i=1,M
      W=W+cn2(i)*sol(i+1)*kc/(kcn(i)**2-kc**2)/kcn(i)
     &               *(cj0kcb*j0kcab(i)-cj0kca)
200   CONTINUE
      W=W*2./pi
      W=W+(cj0kca-cj0kcb)/kc*sol(1)
ccccccccccccccccccccccccccccccccccccccccccccccccccccccccccccccc
c     The following if is to take care of the end pt,
c x=pi/2.d0, for which theta=90 deg s.t. beta2->0.d0  and
c cos(x) -> 0.d0
ccccccccccccccccccccccccccccccccccccccccccccccccccccccccccccccc
      IF (abs((epv(2)-epv(1))/epv(1)).LT.1.d-3 .and.
     &                          abs(x-pi/2).LT.1.d-6 ) THEN
         y=1.d0/abs(k(2))**2
         y=y*(sin(x)**3*abs(k(1))+sin(x)*cos(x)*beta1)
         y=y*abs( W/(1.d0+rbn)/2.d0 )**2
      ELSE
         y=cos(x)**2/beta2**2
         y=y*(sin(x)**3*abs(k(1))+sin(x)*cos(x)*beta1)
         y=y*abs( W/(1.d0+rbn)/(1.d0+gama1*epv(2)
     &                              /(gama2*epv(1))) )**2
      ENDIF
100   RETURN
      END


ccccccccccccccccccccccccccccccccccccccccccccccccccccccccccccccc
c     A subroutine describing the integrand of a integral
c which is done by quard2 subroutine.
ccccccccccccccccccccccccccccccccccccccccccccccccccccccccccccccc
```

```
      SUBROUTINE fxvalue2(x,y)
      COMPLEX*16 y,ckc,total3,zarg,j0,j1,y0,y1,h20,h21
      COMPLEX*16 yc1,yc2,yc3,yc4
      COMPLEX*16 j1kcrp,y1kcrp,j0kca,y0kca,j1kcr,y1kcr
      REAL*8     yreal,x,r,rp,ratio,dumm
      REAL*8     kc,a,b,kci,kcj,xlevel,ylevel
      INTEGER    fxno2,iprint,fxno,ptr,ctr3,dummy
      COMMON /varxylevel/xlevel,ylevel
      COMMON /paratotal3/total3,ctr3 /para31/fxno2
      COMMON /para3/fxno /varkcij/kcj,kci
      COMMON /varratio/ratio,dumm /pararadiusab/a,b
      ptr=fxno*10+fxno2
      kc=kcpass
      ckc=ckcpass
3     ylevel=x
      rp=(xlevel+ylevel)/sqrt(2.d0)
      r=(xlevel-ylevel)/sqrt(2.d0)
      yreal=r/(rp*rp)
      ctr3=0
      total3=0.d0
      dummy=0
      ratio=r/rp
      CALL romerg3(0.d0,1.d0,dummy)
      y=yreal*total3
      IF (ptr.EQ.3) THEN
         y=y*2.d0
         GOTO 100
      ELSEIF (ptr.EQ.13) THEN
         GOTO 113
      ELSEIF (ptr.EQ.23) THEN
         GOTO 123
      ELSEIF (ptr.EQ.33) THEN
         GOTO 133
      ELSE
         WRITE(*,*)'report fxno error fxvalue2 subroutine'
      ENDIF
113   zarg= kci*rp
      CALL bessf0(zarg,j0,j1kcrp,y0,y1kcrp,h20,h21,iprint)
      zarg= kci*a
      CALL bessf0(zarg,j0kca,j1,y0kca,y1,h20,h21,iprint)
      zarg= kci*r
      CALL bessf0(zarg,j0,j1kcr,y0,y1kcr,h20,h21,iprint)
      yc1=(j1kcrp*y0kca-j0kca*y1kcrp)*rp
      yc2=(j1kcr*y0kca-j0kca*y1kcr)*r
      y=y*(yc1+yc2)
      GOTO 100
123   zarg= kcj*rp
      CALL bessf0(zarg,j0,j1kcrp,y0,y1kcrp,h20,h21,iprint)
      zarg= kcj*a
      CALL bessf0(zarg,j0kca,j1,y0kca,y1,h20,h21,iprint)
      zarg= kcj*r
      CALL bessf0(zarg,j0,j1kcr,y0,y1kcr,h20,h21,iprint)
      yc1=(j1kcrp*y0kca-j0kca*y1kcrp)*rp
```

```
      yc2=(j1kcr*y0kca-j0kca*y1kcr)*r
      y=y*(yc1+yc2)
      GOTO 100
133   zarg= kci*rp
      CALL bessf0(zarg,j0,j1kcrp,y0,y1kcrp,h20,h21,iprint)
      zarg= kci*a
      CALL bessf0(zarg,j0kca,j1,y0kca,y1,h20,h21,iprint)
      zarg= kci*r
      CALL bessf0(zarg,j0,j1kcr,y0,y1kcr,h20,h21,iprint)
      yc1=(j1kcrp*y0kca-j0kca*y1kcrp)
      yc2=(j1kcr*y0kca-j0kca*y1kcr)
      zarg= kcj*rp
      CALL bessf0(zarg,j0,j1kcrp,y0,y1kcrp,h20,h21,iprint)
      zarg= kcj*a
      CALL bessf0(zarg,j0kca,j1,y0kca,y1,h20,h21,iprint)
      zarg= kcj*r
      CALL bessf0(zarg,j0,j1kcr,y0,y1kcr,h20,h21,iprint)
      yc3=(j1kcrp*y0kca-j0kca*y1kcrp)
      yc4=(j1kcr*y0kca-j0kca*y1kcr)
      y=y*(yc4*yc1+yc2*yc3)*r*rp
100   RETURN
      END


ccccccccccccccccccccccccccccccccccccccccccccccccccccccccccccccccc
c     A subroutine describing the integrand of a integral
c which is done by cromerg3 subroutine.
ccccccccccccccccccccccccccccccccccccccccccccccccccccccccccccccccc
      SUBROUTINE fxvalue3(cx,y)
      COMPLEX*16 cx,y
      REAL*8     u,u2,ratio,dummy
      COMMON /varratio/ratio,dummy
      u=cx
      u2=u*u
      y=(1.d0-u2)**2/sqrt(2.d0-u2)
      y=y/sqrt(1.d0-(ratio*(1.d0-u2))**2)
      RETURN
      END


ccccccccccccccccccccccccccccccccccccccccccccccccccccccccccccccccc
c     A integration subroutine using quardrature scheme.
ccccccccccccccccccccccccccccccccccccccccccccccccccccccccccccccccc
      SUBROUTINE quard2(a,b,fxnumber)
      COMPLEX*16 save,fx,total2,sum
      REAL*8     a,b,xx(50,50),ww(50,50)
      REAL*8     x(50,50),w(50,50),diffi,reltolerance,kc
      INTEGER    j,intno,ctr2,maxidx
      INTEGER    fxnumber,fxno2,idx,initialidx,idxmax
      COMMON /para/reltolerance,intno /xandw/x,w
      COMMON /para2/total2,ctr2 /paraidxmax/idxmax
      COMMON /para31/fxno2 /varkc/kc
      fxno2=fxnumber
```

```
      maxidx=11
      initialidx=4
      idx=initialidx
      DO 10 j=1,idx
         xx(idx,j)=x(idx,j)*(b-a)/2.d0+(b+a)/2.d0
         ww(idx,j)=w(idx,j)*(b-a)/2.d0
10    CONTINUE
      sum=0.d0
      DO 20 j=1,idx
         CALL fxvalue2(xx(idx,j),fx)
         sum=sum+ww(idx,j)*fx
20    CONTINUE
30    save=sum
      idx=idx+2
      DO 35 j=1,idx
         xx(idx,j)=x(idx,j)*(b-a)/2.d0+(b+a)/2.d0
         ww(idx,j)=w(idx,j)*(b-a)/2.d0
35    CONTINUE
      sum=0.d0
      DO 40 i=1,idx
         CALL fxvalue2(xx(idx,i),fx)
         sum=sum+ww(idx,i)*fx
40    CONTINUE
      diffi=2.d0*abs(sum-save)/abs(sum+save)
      IF ((diff.GT.reltolerance).AND.(idx.LT.maxidx)) THEN
         GOTO 30
      ENDIF
      total2=sum
      RETURN
      END


ccccccccccccccccccccccccccccccccccccccccccccccccccccccccccccccccc
c     A subtoutine for computing the coefficient of Rbn
ccccccccccccccccccccccccccccccccccccccccccccccccccccccccccccccccc
      SUBROUTINE crbnfx(ckc,rbn)
      COMPLEX*16 rbn,epv(65),ga(65),k(65),kratio2,Rb2
      COMPLEX*16 expterm,tem1,tem2,Rbj,Rbjm1,muv(65),ckc,tem3
      REAL*8     z(65),epvre,epvim
      INTEGER    layerno,openckt,opentoair,i,j
      COMMON /paramuv/muv /para9/epv,z /paraopen/openckt
      COMMON /paraopentoair/opentoair /para7/layerno
      COMMON /para11/k
      DO 10 i=1,layerno
         epvre=DBLE(epv(i))
         epvim=imag(epv(i))
         ga(i)=cdsqrt(ckc**2-k(i)**2)
10    CONTINUE
      Rb2=cdexp(-2.d0*ga(2)*z(2))
      IF (openckt.EQ.1) THEN
         kratio2=epv(1)/epv(2)
         Rb2=Rb2*(ga(1)-kratio2*ga(2))/(ga(1)+kratio2*ga(2))
      ELSE
```

```
            Rb2=-Rb2
         ENDIF
         Rbjm1=Rb2
         IF (layerno.GE.3) THEN
            DO 20 j=3,layerno
               kratio2=epv(j-1)/epv(j)
               expterm=cdexp(-2.d0*ga(j-1)*z(j))
               tem1=ga(j-1)*(expterm+Rbjm1)
               tem2=kratio2*(expterm-Rbjm1)*ga(j)
               tem3=cdexp(-2.d0*ga(j)*z(j))
               Rbj=tem3*(tem1-tem2)/(tem1+tem2)
               Rbjm1=Rbj
20          CONTINUE
         ENDIF
         rbn=Rbjm1
         RETURN
         END


ccccccccccccccccccccccccccccccccccccccccccccccccccccccccccccccc
c       A subroutine for computing the surface wave power
ccccccccccccccccccccccccccccccccccccccccccccccccccccccccccccccc
         SUBROUTINE swpower(sol,totalprho,toalp1op2,wsave)
         COMPLEX*16 sol(*),epv(65),W,L,prho2,prho1,wsave
         COMPLEX*16 fz2,kr2,gama2,gar,k(65),cn2(0:50),epidummy
         COMPLEX*16 zarg,cj0kca,cj0kcb,j1,y0,y1,h20,h21
         REAL*8     p1op2(20),toalp1op2,fre,dummyconv
         REAL*8     totalprho,totalprho1,totalprho2
         REAL*8     pi,z(65),omega,kcp(65),j0kcab(65),temp,a,b
         REAL*8     beta2,gama1,v,bz2,kcn(100)
         INTEGER    i,I1,kc0zerono,iprint
         COMMON /parafre/fre,dummyconv /para9/epv,z
         COMMON /paracn2/cn2 /parakc0array/kcp,kc0zerono
         COMMON /parakcn/kcn /paraabM/a,b,epidummy,I1
         COMMON /para11/k
         DO 100 i=1,I1
            zarg=kcn(i)*a
            CALL bessf0(zarg,cj0kca,j1,y0,y1,h20,h21,iprint)
            zarg=kcn(i)*b
            CALL bessf0(zarg,cj0kcb,j1,y0,y1,h20,h21,iprint)
            j0kcab(i)=cj0kca/cj0kcb
100      CONTINUE
         totalprho=0.d0
         totalprho1=0.d0
         totalprho2=0.d0
         DO 300 m=1,kc0zerono
            pi=4.d0*atan(1.d0)
            omega=2.d0*pi*fre
            beta2=sqrt(DBLE(k(2))**2-kcp(m)**2)
            gama1=sqrt(-DBLE(k(1))**2+kcp(m)**2)
            gama2=(0.d0,1.d0)*beta2
            gar=gama1/gama2
            bz2=beta2*z(2)
```

```
            v=gama1/beta2
            kr2=epv(1)/epv(2)
            temp=cos(bz2)*sin(bz2)/bz2
            IF (beta2.LT.1.d-15) THEN
               fz2=kr2**2*z(2)
            ELSE
               fz2=(kr2**2*(1.+temp)+v**2*(1.-temp))*z(2)/2.d0
               fz2=fz2+kr2*v*(1.-cos(2*bz2))/(2.d0*beta2)
            ENDIF
            zarg=kcp(m)*a
            CALL bessf0(zarg,cj0kca,j1,y0,y1,h20,h21,iprint)
            zarg=kcp(m)*b
            CALL bessf0(zarg,cj0kcb,j1,y0,y1,h20,h21,iprint)
            W=0.d0
            DO 200 i=1,I1
               W=W+cn2(i)*sol(i+1)*kcp(m)/(kcn(i)**2-kcp(m)**2)
     &              /kcn(i)*(cj0kcb*j0kcab(i) -cj0kca)
200         CONTINUE
            W=W*2./pi
            W=W+(cj0kca-cj0kcb)/kcp(m)*sol(1)
            L=exp(-2.*gama2*z(2))*( (gar-kr2)/(gar+kr2)
     &        *(-2.*z(2))*kcp(m)/gama2+ 2.*kcp(m)*kr2
     &        *(1./gar-gar)/(gama1+kr2*gama2)**2  )
            L=1.d0/L
            prho2=8.d0*pi*pi*omega*epv(2)*kcp(m)**2
     &        *fz2/(v**2+kr2**2)/(beta2**2)*(abs(W*L))**2
            prho1=4.d0*pi*pi/gama1/beta2**2*omega*epv(2)**2
     &             /epv(1)*kcp(m)**2*(abs(W*L))**2
     &             /(1.d0+(gama1*epv(2)/epv(1)/beta2)**2)
            totalprho=totalprho+DBLE(prho1+prho2)
            totalprho1=totalprho1+DBLE(prho1)
            totalprho2=totalprho2+DBLE(prho2)
            p1op2(m)=DBLE(prho1)/DBLE(prho2)
300      CONTINUE
         IF (kc0zerono.NE.0) THEN
            toalp1op2=totalprho1/totalprho2
         ENDIF
         RETURN
         END


ccccccccccccccccccccccccccccccccccccccccccccccccccccccccccccccccc
c     A subroutine for computing the radial guided wave power
ccccccccccccccccccccccccccccccccccccccccccccccccccccccccccccccccc
         SUBROUTINE radialpw(sol,totalprho)
         COMPLEX*16 sol(*),epv(65),W,L,prho2,epidummy
         COMPLEX*16 cn2(0:50),gz2,kr2,gama2,k(65)
         COMPLEX*16 zarg,cj0kca,cj0kcb,j1,y0,y1,h20,h21
         REAL*8     fre,dummyconv
         REAL*8     totalprho
         REAL*8     pi,omega,kcp(65),z(65)
         REAL*8     beta2,bz2,kcn(100)
         REAL*8     j0kcab(65),a,b
```

```
      INTEGER    i,I1,kc0zerono,kc0zeronodummy,iprint
      COMMON /parafre/fre,dummyconv /para9/epv,z
      COMMON /paracn2/cn2 /parakc0array/kcp,kc0zeronodummy
      COMMON /parakcn/kcn /paraabM/a,b,epidummy,I1
      COMMON /para11/k
      pi=4.d0*atan(1.d0)
ccccccccccccccccccccccccccccccccc
c     find the zeros
ccccccccccccccccccccccccccccccccc
      kc0zerono=int(abs(k(2)*z(2))/pi)
      kcp(1)=abs(k(2))
      DO 50 i=1,kc0zerono-1
         kcp(i+1)=sqrt(abs(k(2))**2-((i)*pi/z(2))**2)
50    CONTINUE
      kc0zerono=kc0zerono+1
      DO 100 i=1,I1
         zarg=kcn(i)*a
         CALL bessf0(zarg,cj0kca,j1,y0,y1,h20,h21,iprint)
         zarg=kcn(i)*b
         CALL bessf0(zarg,cj0kcb,j1,y0,y1,h20,h21,iprint)
         j0kcab(i)=cj0kca/cj0kcb
100   CONTINUE
      totalprho=0.d0
      DO 300 m=1,kc0zerono
         pi=4.d0*atan(1.d0)
         omega=2.d0*pi*fre
         beta2=sqrt(abs(k(2))**2-kcp(m)**2)
         gama2=(0.d0,1.d0)*beta2
         bz2=beta2*z(2)
         kr2=epv(1)/epv(2)
         IF (bz2.LT.1.d-16) THEN
            gz2=z(2)
         ELSE
            gz2=z(2)/2.d0
         ENDIF
         zarg=kcp(m)*a
         CALL bessf0(zarg,cj0kca,j1,y0,y1,h20,h21,iprint)
         zarg=kcp(m)*b
         CALL bessf0(zarg,cj0kcb,j1,y0,y1,h20,h21,iprint)
         W=0.d0
         DO 200 i=1,I1
            W=W+cn2(i)*sol(i+1)*kcp(m)/(kcn(i)**2-kcp(m)**2)
     &                  /kcn(i)*(cj0kcb*j0kcab(i) -cj0kca)
200      CONTINUE
         W=W*2./pi
         W=W+(cj0kca-cj0kcb)/kcp(m)*sol(1)
         IF (kcp(m).LT.1.d-10) THEN
            L=0.d0
         ELSEIF (abs(kcp(m)-k(2)).LT.1.d-10) THEN
            L=1.d0/(4.d0*k(2)*z(2))
         ELSE
            L=1.d0/(exp(-2.*gama2*z(2))*kcp(m)*2.*z(2))
         ENDIF
```

```
          prho2=8.d0*pi*pi*omega*epv(2)
          prho2=prho2*(abs(W*L))**2*kcp(m)**2*gz2
300     CONTINUE
        RETURN
        END


ccccccccccccccccccccccccccccccccccccccccccccccccccccccccccccccccc
c       A function for computing the phase of a complex number
ccccccccccccccccccccccccccccccccccccccccccccccccccccccccccccccccc
        FUNCTION phase(x)
        COMPLEX*16   x
        REAL*8      r,i,pi,ph
        pi=ATAN(1.0d0)*4.d0
        r=(x+CONJG(x))/2.d0
        i=(CONJG(x)-x)/2.d0*(0.d0,1.d0)
        IF ((r.EQ.0.d0).AND.(i.EQ.0.d0)) THEN
             ph=0.d0
         ELSEIF(r.EQ.0.d0) THEN
             IF (i.GT.0) THEN
                 phase=90.d0
              ELSEIF (i.LT.0) THEN
                 phase=-90.d0
              ENDIF
        ELSE

            ph=ATAN(i/r)*4.d0/pi*45.d0
            IF (r.LT.0) THEN
               IF (i.GT.0) THEN
                  phase=180.d0+ph
               ELSEIF (i.LT.0) THEN
                  phase=-180.d0+ph
                ELSE
                  phase=-180.d0
               ENDIF
            ELSE
              phase=ph
             ENDIF
        ENDIF
        RETURN
        END


ccccccccccccccccccccccccccccccccccccccc
c       A subroutine for reading an array
ccccccccccccccccccccccccccccccccccccccc
        SUBROUTINE rvectorbin (v,r,nameread)
        REAL*8      v(*)
        INTEGER     r,i1
        CHARACTER*12 nameread
        OPEN(3,FILE=nameread,FORM='unformatted')
        READ(3)r
        DO 420 i1=1,r
```

```
         READ(3)v(i1)
420     CONTINUE
        CLOSE(3)
        RETURN
        END

ccccccccccccccccccccccccccccccccccccccc
c       A subroutine for sorting an array
ccccccccccccccccccccccccccccccccccccccc
        SUBROUTINE directsort(arr,n)
        REAL*8      arr(*),act
        INTEGER     i,j,n
        DO 2000 j=2,n
           act=arr(j)
           i=j-1
1700       IF (arr(i).GT.act) THEN
              arr(i+1)=arr(i)
              arr(i)=act
           ENDIF
           i=i-1
           IF ((i.GT.0).AND.(arr(i).GT.act)) THEN
              GOTO 1700
           ENDIF
2000    CONTINUE
        RETURN
        END


ccccccccccccccccccccccccccccccccccccccccccccccccccccccccccccccc
c       The last subroutines are  for solving a system of
c linear equation using Householder scheme
ccccccccccccccccccccccccccccccccccccccccccccccccccccccccccccccc
        SUBROUTINE solveqns(W,sol,ra,ca)
        COMPLEX*16 W(50,50),sol(50),x(50),y(50)
        INTEGER    i,m,loop,ra,ca
        loop=ca
        IF (ra.EQ.ca) THEN
           loop=ca-1
        END IF
        DO 790 m=1,loop
           DO 770 i=1,ra
              x(i)=W(i,m)
770        CONTINUE
           CALL hvec(x,y,ra,m)
           CALL Htrans(y,W,ra,ra+1,m)
790     CONTINUE
        CALL trisolve(W,sol,ca)
        RETURN
        END


        SUBROUTINE hvec (x1,y1,ra,m1)
        COMPLEX*16 x1(50),y1(50),zm
```

```
      REAL*8      zmr,ab
      INTEGER     m1,k1,ra
      zm=0
      zmr=0
      DO 660 k1=1,m1-1
         y1(k1)=0
660   CONTINUE
      DO 670 k1=m1+1,ra
         y1(k1)=x1(k1)
         zmr=zmr+abs(x1(k1))*abs(x1(k1))
         x1(k1)=0
670   CONTINUE
      ab=abs(x1(m1))
      IF (ab.NE.0) THEN
         zmr=zmr+ab*ab
         zm=x1(m1)/ab*sqrt(zmr)
      ELSE
         zm=sqrt(zmr)
      END IF
      y1(m1)=x1(m1)-zm
      x1(m1)=zm
      RETURN
      END


      SUBROUTINE Htrans (y1,A1,r,c,m1)
      COMPLEX*16 y1(50),A1(50,50),u1(50),vt1(50)
      REAL*8      yty1
      INTEGER     m1,i1,j1,r,c
      yty1=0
      DO 675 i1=1,r
         yty1=yty1+y1(i1)*conjg(y1(i1))
675   CONTINUE
      IF (yty1.NE.0) THEN
         DO 680 i1=m1,r
            u1(i1)=y1(i1)/yty1*2
680      CONTINUE
         DO 690 i1=m1,c
            vt1(i1)=0
            DO 690 j1=m1,r
               vt1(i1)=vt1(i1)+conjg(y1(j1))*A1(j1,i1)
690      CONTINUE
         DO 700 j1=m1,c
         DO 700 i1=m1,r
            A1(i1,j1)=A1(i1,j1)-u1(i1)*vt1(j1)
            IF (i1.EQ.j1) THEN
               IF (abs(A1(i1,j1)).LT.1.d-15) THEN
                 WRITE(*,*)'in Htrans: A1(',i1,',',j1,')
     &                                              is 0 item'
               ENDIF
            ENDIF
700      CONTINUE
      END IF
```

```
      RETURN
      END


      SUBROUTINE trisolve(W1,x1,n)
      COMPLEX*16 W1(50,50),x1(50),temp
      INTEGER    n,i1,j1,k1
      x1(n)=W1(n,n+1)/W1(n,n)
      DO 760 k1=2,n
         i1=n+1-k1
         temp=0
         DO 750 j1=1,k1-1
            temp=temp+W1(i1,i1+j1)*x1(i1+j1)
750      CONTINUE
         x1(i1)=(W1(i1,n+1)-temp)/W1(i1,i1)
760   CONTINUE
      RETURN
      END
```

BIBLOGRAPHY

BIBLIOGRAPHY

1. M. N. Afsar, J. Birch, and R. Clarke, "The measurement of properties of materials," Proc. IEEE, vol. 74, pp. 183-199, Jan. 1986.

2. E. Tanabe and W. T. Joines, "A nondestructive method for measuring the complex permittivity of dielectric materials at microwave frequencies using an open transmission line resonator," IEEE Trans. Instrum. Meas., vol. IM-25, pp. 222-226, Sept. 1976.

3. J. R. Mosig et al., "Reflection of an open-ended coaxial line and application to non-destructive measurement of material," IEEE Trans. Instrum. Meas., vol. IM-30 pp. 46-51, 1981.

4. D. K. Misra et al., "Noninvasive electrical characterization of materials at microwave frequencies using an open-ended coaxial line: Test of an improved calibration technique," IEEE Trans. Microwave Theory Tech., vol. 38, pp. 8-14, Jan. 1990.

5. W. B. Wier, "Automatic measurement of complex dielectric constant and permeability at microwave frequencies," Proc. IEEE, vol. 62, no. 1, pp. 33-36, Jan. 1974.

6. W. Barry, "A broad-band, automated, stripline technique for the simultaneous measurement of complex permittivity and permeability," IEEE Trans. Microwave Theory Tech., vol. MTT-34, 80-84, Jan. 1986.

7. Belhadj-Tahar, N. E., and A. Fourrier-Lamer, and H. de Chanterac, "Broad-band simultaneous measurement of complex permittivity and permeability using a coaxial discontinuity," IEEE Trans. Microwave Theory Tech., vol. MTT-38, pp. 1-7, Jan. 1990.

8. R. J. Cook and C. B. Rosenberg, "Measurement of the complex refractive index of isotropic and anisotropic materials at 35 Ghz using a free space microwave bridge," J. Phys. D: Appl. Phys., vol. 12, pp. 1643-1652, 1979.

9. F. I. Shimabukuro et al., "A quasi-optical method for measuring the complex permittivity of materials," IEEE Trans. Microwave Theory Tech., vol. MTT-32, no. 7, pp. 659-665, July 1984.

10. M. A. Stuchly and S. S. Stuchly, " Coaxial line reflection method for measuring dielectric properties of biological substances at radio and microwave frequencies-A review, " A Trans. Instrum. Meas., vol. IM-29, pp. 176-183, 1980.

11. R. M. Pannell and B. W. Jervis, "Two simple methods for the measurement of dielectric permittivity of low-loss microstrip substrates," IEEE Trans. Microwave Theory Tech., vol. MTT-29, no. 4, pp. 383-386, Apr. 1981.

12. B. Terselius and B. Ranby, "Cavity perturbation measurements of the dielectric properties of vulcanizing rubber and polyethylene compounds," J. Microwave Power, vol. 13, pp. 327-335, 1978.

13. L. L. Li, N. H. Ismail, L. S. Taylor and C. C. Davis, " Flanged coaxial microwave probes for measuring thin moisture layers " IEEE Trans. Biomedical eng., vol. 39, pp. 49-57, Jan 1992.

14. Hongming Zheng and C. E. Smith, "Permittivity measurements using a short open-ended coaxial line probe," IEEE microwave and guided wave lett., vol. 1 no. 11, Nov. 1991.

15. S Fan, K Staebell, and D Misra, "Static analysis of an open-ended coaxial line terminated by layered media," IEEE Trans. Instrum., vol. 39, no. 2, Apr. 1990.

16. G. B. Gajda and S. S. Stuchly, "Numerical analysis of open-ended coaxial lines," IEEE Trans. Microwave Theory Tech., vol. MTT-31, pp. 380-384, May 1983.

17. S. Fan and D. Misra, "A study on the metal-flanged open-ended coaxial line terminating in a conductor-backed dielectric layer," 1990 IEEE Instrumentation and Measurement Technology Conference Record, 43-46.

18. A. Parkash, J. K. Vaid, and A. Mansingh, "Measurement of dielectric parameters at microwave frequencies by cavity perturbation technique," IEEE Trans. Microwave Theory Tech., vol. MTT-27, pp. 791-795, 1979.

19. C. B. Rosenberg, N. A. Hermiz, and R. J. Cook, "Cavity resonator measurements of the complex permittivity of low-loss liquids," Proc. IEE, pt. H, vol. 129, pp. 71-76, 1982.

20. S. Ramo, J. R. Whinnery and T. V. Duzer, Fields and Waves in Communication Electronics. New York: John Wiley & Sons, 1984, pp. 364-371.

21. R. E. Collin, Field Theory of Guided Waves, 2nd ed., IEEE Press, 1991, Chap. 3,5,11.

22. A. Ishimaru, Electromagnetic Wave Propagation, Radiation, and Scattering. NJ: Prentice-Hall, 1991, pp. 20-22,46-57,76-85, 586-601.

23. J. Galejs, Antennas in Inhomogeneous Media. Oxford: Pergamon, 1969, pp. 39-44, 105-109.

24. H. Levine and C. H. Papas, "Theory of the circular diffraction antenna," J. Appl. Phys., vol. 22, no. 1, pp. 29-43, Jan. 1951.

25. C. W. Harrison, Jr., and D. C. Chang, "Theory of the annular slot antenna based on duality," IEEE Trans. Electromagn. Compat., vol. EMC-11, pp. 8-14, Feb, 1971.

26. T. P. Marsland and S. Evans, "Dielectric measurements with an open-ended coaxial probe," Proc. Inst. Elec. Ecg., vol. 134, pt. H, no. 4, pp. 341-349, Aug. 1987.

27. H. A. Atwater, Introduction to Microwave Theory. New York: McGraw-Hill, 1962, pp. 70-78.

28. A. Sommerfeld, Partial Differential Equations in Physics, Academic Press, New York, 1965.

29. R. F. Harrington, Field Computation by Moment Methods. New York: Macmillan, 1968.

30. H. B. Dwight, "Table of roots for natural frequencies in coaxial type cavities," J. Math. and Phys. vol 27, no. 1, pp. 84-89, 1948.

31. W. Press, et. al., Numerical Recipes: The Art of Scientific Computing, Cambridge University Press, New York, 1986.

32. R. D. Nevels, C. M. Butler and W. Yablon, "The annular slot antenna in a lossy biological medium," IEEE Trans. Microwave Theory and Tech., vol. MTT-33, pp. 314-319, 1985.

33. E. P. Irzinski, "The input admittance of a TEM excited annular slot antenna", IEEE Trans. Antennas Propagat., vol. Ap-23, pp. 829-834, Nov. 1975.

34. W.A. Johnson, "Real axis integration of Sommerfeld integrals: Source and observation points in air," Radio Science, vol. 18, pp. 175-186, Nov. 1983.

35. D. K. Misra, "A quasi-static analysis of open-ended coaxial lines," IEEE Trans. Microwave Theory Tech., vol. MTT-35, pp. 925-928, 1987.

36. J. R. Mosig et al., "Reflection of an open-ended coaxial line and application to non-destructive measurement of material," IEEE Trans. Instrum. Meas., vol. IM-30 pp. 46-51, 1981.

37. D. P. Nyquist, D. R. Johnson and S. V. Hsu, "Orthogonality and amplitude spectrum of radiation modes along open-boundary waveguides," J. Opt. Soc. Am. **71**, 49-54, 1981.

38. C. P. Wu, "Integral equation solutions for the radiation from a waveguide through dielectric slab," IEEE Trans. Antennas Propagat., vol. Ap-17, pp. 733-739, Nov. 1969.

39. E. V. Jull, Aperture Antennas and Diffraction Theory. London: IEE, 1981, pp. 154-155.

40. J. Song, S. Ohnuki, D.P. Nyquist, K.M. Chen and E. Rothwell, "Technical Report No. 5: Scattering of TE polarized EM waves by a discontinuity in a grounded dielectric sheet," Boeing Defence and Space Group, 1991.

41. G. L. Ragan, Microwave Transmission Circuits. New York: McGraw-Hill, 1948, pp. 184-188.

42. J. R. Whinnery, H. W. Jamieson and T. E. Robbins, "Coaxial line discontinuities," Proc. I.R.E., pp. 695-709, Nov. 1944.

43. E. F. da Silva, and M. K. McPhun, "Calibration techniques for one prot measurement," Microwave J., pp. 97-100, June 1978.

44. Hewlett-Packard, "Measuring dielectric constants with the H.P. 8510 Network Analyzer," Hewlett-Packard Product Note 8510-3.

45. A. E. Bailey, Microwave Measurements. 2nd ed., London: IEE, 1989, pp. 59-73.

46. J. H. Mathews, Numerical Methods. New Jersey: Prentice-Hall, 1987, pp. 59-70.

47. C. T. H. Baker and C. Phillips, The Numerical Solution of Nonlinear Problems. Oxford: Clarendon Press, 1981.

48. M. Abramowitz and I. T. Stegun, Eds., Handbook of Mathematical Functions. New York: Dover, 1965.